Spring 4-2021

Ultra-High Performance Concrete (UHPC) Deck-To-Girder Connection For Accelerated Bridge Construction

Mostafa Abo El-Khier
University of Nebraska-Lincoln

ULTRA-HIGH PERFORMANCE CONCRETE (UHPC) DECK-TO-GIRDER CONNECTION FOR ACCELERATED BRIDGE CONSTRUCTION

by

Mostafa Abo El-Khier

A DISSERTATION

Presented to the Faculty of

The Graduate College at the University of Nebraska

In Partial Fulfilment of Requirements

For the Degree of Doctor of Philosophy

Major: Engineering

(Construction Engineering)

Under the Supervision of Professor George Morcous

Lincoln, Nebraska

May, 2021

ULTRA-HIGH PERFORMANCE CONCRETE (UHPC) DECK-TO-GIRDER CONNECTION FOR ACCELERATED BRIDGE CONSTRUCTION

Mostafa Abo El-Khier, Ph.D.

University of Nebraska, 2021

Advisor: George Morcous

Precast concrete deck systems have been successfully used for Accelerated Bridge Construction. In most systems, special deck-to-girder connections are designed to achieve structurally composite sections. These connections require tight production/erection tolerances that complicate deck and girder fabrication and compromise the economics of these systems. This study presents a new precast concrete deck-to-girder connection that takes advantage of the excellent mechanical, workability, and durability properties of ultra-high performance concrete (UHPC) to simplify precast concrete deck and girder fabrication and erection. Typical girder shear reinforcement is terminated below the soffit of deck panels to eliminate any conflicts with deck reinforcement and relax production and erection tolerances. Shear pockets with loose bars are filled with UHPC to provide shear transfer mechanism between concrete deck panels and girders.

To evaluate the performance of the new connection, a non-proprietary UHPC mix was developed using local materials at approximately one-third the cost of commercial mixes. Two interface shear planes were identified in the proposed connection: in the monolithic UHPC shear pocket at deck soffit; and between fresh UHPC and hardened conventional concrete (CC-UHPC) at the top of the precast concrete girder. Current code provisions do not provide guidance on either of the two planes. Therefore, experimental

investigation was conducted to evaluate these interface planes using slant shear, direct shear, L-shape push-off, and double shear testing. Then, finite element analysis was conducted to perform a parametric study on the shear pocket diameter and reinforcement size. Full-scale push-off tests were conducted to evaluate the constructability and structural performance of the new connection.

Test and analysis results indicated that the interface shear resistance of CC-UHPC with surface roughening of 1/4 in. can be predicted using cohesion and friction factors of 0.63 ksi and 1.23 respectively. Interface shear resistance of monolithic UHPC can be predicted using cohesion and friction factors of $0.49\sqrt{f'_{UHPC}}$ (ksi) and $0.85\sqrt{f'_{UHPC}}$, respectively. The UHPC mix stability was found to significantly affect the structural performance of the new connection. Cost analysis indicated that the proposed connection is 21% more cost effective than existing connections.

Advisory Committee:

Professor George Morcous, Chair

Durham School of Architectural Engineering & Construction, University of Nebraska-Lincoln

Professor Ece Erdogmus

Durham School of Architectural Engineering & Construction, University of Nebraska-Lincoln

Professor James Goedert

Durham School of Architectural Engineering & Construction, University of Nebraska-Lincoln

Associate Professor Jiong Hu

Department of Civil Engineering, University of Nebraska-Lincoln

To My Parents, My Beloved Wife, My Beautiful Sons

(Yousef and Yaseen), and My Brother and Sisters

ACKNOWLEDGEMENT

First and foremost praise to ALLAH, my creator, almighty to whom, I owe all the success I have been achieving in my life.

I would like to express my gratitude to Professor George Morcous for his immense support and encouragement throughout my research. I cannot thank him enough for the opportunities he provided me during my PhD journey and his profound belief in my work. I would like to declare my special appreciation and gratefulness to members of the advisory committee: Prof. James Goedert, Prof. Ece Erdogmus, and Prof. Jiong Hu, for serving on the committee as well as for their invaluable comments and suggestions on this research.

I wish to thank the Nebraska Department of Transportation (NDOT) for their financial support of the experimental part of this research and LafargeHolicm, Chryso, GCP, Ash Grove, Central Plains Cement Company for material donation. I also appreciate the assistance of the fellow students and lab technicians who helped with the experimental phase of this research: Antony Kodsey, Flavia Mendonca, Jacob Greenleaf, and Jose Lopez.

This journey would not have been possible and more meaningful without endless love and untiring support of my wife, Aya Allam. I cannot begin to express my thanks to my mother; Aml Aboelroos and my father; Prof. Mahmoud Aboelkhier, having a precious place in my heart that words are not enough to describe my feelings. Finally, I take this opportunity to thank my dear brother, sisters, and friends who were always there when I needed them the most from all around the world.

TABLE OF CONTENTS

LIST OF FIGURES

LIST OF TABLES

CHAPTER 1: INTRODUCTION

1.1. Accelerated Bridge Construction (ABC)

Accelerated Bridge Construction (ABC) is the bridge construction that uses innovative planning, design, materials, and construction methods in a safe and cost-effective manner to reduce the onsite construction time when building new bridges or replacing/rehabilitating existing bridges (Culmo et al, 2011). FHWA works with state Departments of Transportation (DOTs) to identify and implement innovations for ABC. Examples of these innovations are:

- Geosynthetic Reinforced Soil-Integrated Bridge System (GRS-IBS)
- **Prefabricated Bridge Elements and Systems (PBES)**
- Slide-in Bridge Construction (SIBC)
- **Ultra-High Performance Concrete (UHPC) for Connections**

One of ABC innovations is the implementation of prefabricated bridge elements in construction. Recently, precast concrete deck panels have been successfully used in bridge projects in various forms and systems. Casting concrete deck panels off-site in a high-quality controlled environment reduces deck cracking and provides more durable elements. Also, transporting and installing precast concrete deck panels, then, connecting them to the supporting girders at the construction site reduce construction duration and traffic disruption. These advantages make the precast concrete deck panels system more attractive alternative to the conventional cast-in-place (CIP) concrete deck system.

Another ABC innovation is using Ultra-High Performance Concrete (UHPC) in bridge connections. UHPC is a new generation of cementitious materials that has exceptional mechanical properties, durability, and workability. The low water-to-binder ratio, high binder content, use of supplemental cementitious material, high particle-packing density, and use of steel fibers significantly enhance the fresh and hardened UHPC properties compared to conventional concrete (CC). According to ASTM C1856-17, UHPC is characterized by a minimum specified compressive strength of 17 ksi, maximum aggregate size of 1/4 in. and flow between 8-10 in. UHPC became commercially available in the U.S. through several proprietary sources as early as year 2000. Since its introduction to the commercial market, the use of UHPC in various applications has been the focus of multiple research endeavors. The exceptional durability and mechanical properties make UHPC an ideal grouting material for field casting bridge connections that reduces cracks and leakage.

1.2. Problem Statement

Although precast concrete deck systems is a promising ABC technique, it is not commonly used in the US. According to the 2016 national bridge inventory (NBI) data, CIP concrete deck is the most common bridge deck type as shown Figure 1.1. This is despite the fact that CIP deck system requires a long construction duration leading to traffic closures and detouring. In addition, the inconsistent quality of CIP concrete decks due to variability in environmental conditions and labor quality results in excessive early-age shrinkage cracking, decreased deck durability and increased life-cycle cost.

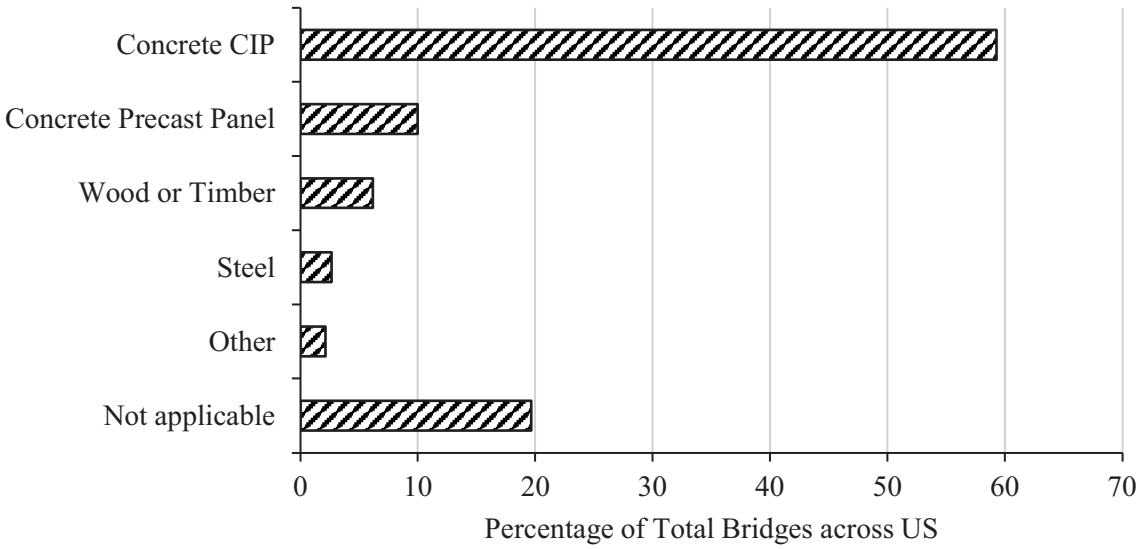

Figure 1.1. National Bridge Inventory (NBI) by Deck Structure Type in 2016.

One of the reasons for the unpopularity of precast concrete deck systems compared to CIP concrete bridge decks is the large number of panels to be produced, transported, and erected, which requires many longitudinal and transverse field-cast joints. Also, the connections between precast concrete deck panels and supporting girders to achieve composite action are often complex and lead to challenges in panel and girder production/erection and high construction cost.

A recent development of precast concrete deck-to-girder connections was made by Nebraska Department of Transportation (NDOT) and University of Nebraska-Lincoln (UNL) as shown in Figure 1.2. In these connections, shear connectors (i.e., threaded rods) are embedded in the concrete girders and extended into Hollow Structural Section (HSS) steel-formed shear pockets in the deck panels, that are filled later with flowable material (i.e., self-consolidating concrete) to achieve composite action. These connections were

implemented successfully in two highway bridges in Nebraska: Kearney East Bypass and Belden-Laurel bridges.

Figure 1.2. Precast Concrete Deck-to-Girder Connections using threaded rods and HSS-formed shear pockets used in Kearney East Bypass Project (top) and Belden-Laurel Bridge Project (bottom)

Despite the satisfactory performance of these connections, they required high levels of quality control/quality assurance (QA/QC) in spacing the shear connectors

during girder fabrication as well as shear pockets during panel fabrication to avoid any conflict between them during erection (tight tolerances). Also, the shear connectors are required to have a minimum embedment length in the shear pockets to achieve the composite action, which varied the connector length based on girder camber and had to be field adjusted. The complexity, tight tolerances, and high cost of current precast concrete deck-to-girder connections limited the implementation of precast concrete deck systems in ABC. Therefore, there is a need for simplified and economical alternatives to encourage owners to specify and choose precast concrete deck systems over CIP concrete deck systems and benefit from their enhanced durability and speed of construction.

1.3. Research Objectives

The main objective of this research is to develop a simplified yet economical precast concrete deck-to-girder connection that addresses the complexity and tolerance concerns of the current connections. To achieve that, UHPC was proposed to be the grouting material of the new connection due to its workability, durability, and strength characteristics. The specific objectives of this research were defined as follows:

1. Develop deck-to-girder connection that eliminates any changes to girder design/production and avoid conflicts between deck and girder reinforcement during erection.
2. Develop a non-proprietary UHPC mix for field-cast connections between precast concrete deck panels and precast/prestressed concrete girders.

3. Investigate the interface shear resistance of fresh UHPC cast on hardened conventional concrete.
4. Investigate the interface shear resistance of monolithic UHPC.
5. Evaluate the constructability and structural performance of the new connection through full-scale push-off testing.
6. Conduct a parametric study using Finite Element Analysis (FEA) to evaluate the impact of connection design parameters.
7. Provide design procedures, design aids, and cost analysis for the proposed connection.

1.4. Dissertation Overview

This dissertation consists of eight chapters as follows.

Chapter 1 - Introduction

Chapter 2 - Literature Review: Chapter 2 presents a literature review on the existing deck-to-girder connections using UHPC and all the previous experimental work conducted to evaluate the interface shear resistance of UHPC. Several test methods were presented and interface shear prediction methods according to different codes and standards were discussed.

Chapter 3 – Proposed Deck-To-Girder Connection: Chapter 3 presents the new UHPC connection between precast concrete deck panels and precast/prestressed concrete girders. This connection eliminates any changes to girder design/production and any possible conflict between deck and girder reinforcement. Two different interface

shear planes are controlling the proposed connection: (a) at the soffit of the precast deck panels and (b) at the top of the precast/prestressed concrete girder. A study methodology is proposed to evaluate both interface shear planes. Also, a construction sequence of the new connection is illustrated using the current bridge construction practices.

Chapter 4 – Development of Non-Proprietary UHPC Mix: Chapter 4 presents the development of a non-proprietary UHPC mix based on mechanical properties testing of three non-proprietary mixes using local materials. The mechanical properties testing includes compressive strength, modulus of elasticity and Poisson's ratio, flexural strength, splitting tensile strength, and rebar development length. The obtained properties were compared to those obtained for a commercial UHPC mix. The non-proprietary mix the had the best performance was named UNL-UHPC and was used in the experimental investigation.

Chapter 5 – Interface Shear Resistance of UHPC Cast on Hardened Conventional Concrete: Chapter 5 presents the slant shear, and L-shape push-off tests conducted to evaluate the interface shear resistance of fresh UHPC cast on hardened conventional concrete (CC-UHPC). The obtained results and collected data from the literature were utilized to propose cohesion and friction factors for predicting the interface shear resistance for three different interface surface texture: sandblasted, low roughening, and high roughening. These results and factors were compared to different current codes provision including, ACI 318-19, AASHTO LRFD (2020), Eurocode-2 (2004), and CSA A23.3-14. Also, the exposed aggregate interface shear associated with the shear key was studied for the purpose of designing the connection between precast deck panels.

Chapter 6 – Interface Shear Resistance of Monolithic UHPC:

Chapter 6 presents the direct shear, L-shape push-off, and double shear push-off tests conducted to evaluate the interface shear resistance of monolithic UHPC with and without reinforcement. The obtained results and collected data from the literature were utilized to propose cohesion and friction factors. These factors were compared to current code provisions including ACI 318-19, AASHTO LRFD (2020), Eurocode-2 (2004), and CSA A23.3-14. A finite element model (FEM) was developed using ANSYS 20 R2 software to perform a parametric study on the effect of shear pocket diameter, interface reinforcement size, and grade. Finally, a full-scale push-off test for the proposed connection was conducted to evaluate the constructability and structural performance, especially the effect of UHPC stability on the connection performance.

Chapter 7 – Design Procedures and Design Aids: Chapter 7 presents the design procedure and design aids of the proposed connection based on test results and the parametric study. An example bridge from PCI Bridge Design Manual 2014 (PCI BDM Ex. 9.1a) was used to present the design procedure and the advantage of using UHPC over CC. Finally, cost analysis was conducted to illustrate the benefits of using the proposed connection.

Chapter 8 – Summary and Conclusions: Chapter 8 presents the design, detailing, and production recommendations for a new precast concrete deck-to-girder connection using UHPC. These recommendations were developed based on the test results and the experience gained from the experimental and numerical investigation.

CHAPTER 2: LITERATURE REVIEW

Chapter 2 presents the literature review of the existing deck-to-girder connections using UHPC and previous experimental work conducted to evaluate the interface shear resistance of UHPC. The interface shear of UHPC is presented for the following three cases: monolithic UHPC, between fresh UHPC and hardened conventional concrete (CC-UHPC) and between fresh and hardened UHPCs (UHPC-UHPC).

2.1. Deck-To-Girder Bridge Connections Using UHPC

This section summarizes the literature review conducted on UHPC used for deck-to-girder connections. Typically, this connection is made of shear connectors, such as bent rebars or threaded rods in concrete girders, and shear studs in steel girders, that are embedded into discrete shear pockets or continuous troughs in the precast concrete deck panels. Then, a flowable concrete or grout is used to fill these pockets or troughs to establish the connection. One of the disadvantages of these systems is that shear connectors are required to have minimum embedment into the shear pockets/troughs to develop the design capacity, which necessitates high level of QA/QC and complicates girder and panel production.

UHPC connections were developed to eliminate this problem and simplify production and erection procedure, which consequently improve construction speed and economy. A series of interstate highway bridges near Syracuse, NY were constructed using UHPC deck-to-girder connections developed by NYSDOT (Graybeal 2014). These connections consist of panel-to-panel longitudinal shear key with lap spliced transverse reinforcing rebars over the girder lines. Conventional shear studs (¾ in. x 3 ¼ in.) are

welded to the top flange of the steel I-girder as shown in Figure 2.1. The V-shaped shear keys have roughened/exposed aggregate finish to properly bond with the field-cast UHPC that connects the adjacent panels to each other and to the supporting girders. Dimensions of the longitudinal joint is typically 7 in. at the top and bottom of the deck slab and 10 in. at the middle of deck slab. Length and spacing of lap splices depend on bar size and type.

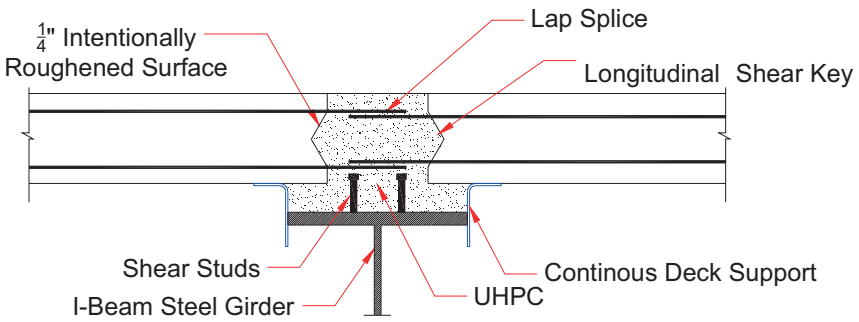

Figure 2.1. Panel-to-Panel Connection over Steel Girder (Graybeal 2014)

Another precast concrete deck-to-steel girder connection was recently developed and tested using UHPC (Graybeal 2014). In this connection, ¾ in. x 3 ¼ in. shear studs are installed on the girder top flange similar to CIP deck construction (i.e. similar spacing requirements). A 10.5 in. wide and 4.5 in. deep trough with exposed aggregate finish is formed in precast concrete deck slab with 2 in. grouting holes every 24 in. over each girder line as shown in Figure 2.2a. Shear studs are kept below the bottom mat of deck reinforcement without embedment in the deck panels to simplify panel and girder production and eliminate any conflicts during panel installation. An interstate highway bridge near Syracuse, NY was constructed using this connection concept with single field casting of UHPC through grouting holes for each girder line to hide the connection and eliminate the need for deck overlay. The same concept can be used with concrete girders by replacing the shear studs with conventional shear reinforcement (i.e. U bars) that are

extended above the top flange and below the bottom mat of deck reinforcement (Graybeal 2014) as shown in Figure 2.2b. This connection has been tested but not implemented yet.

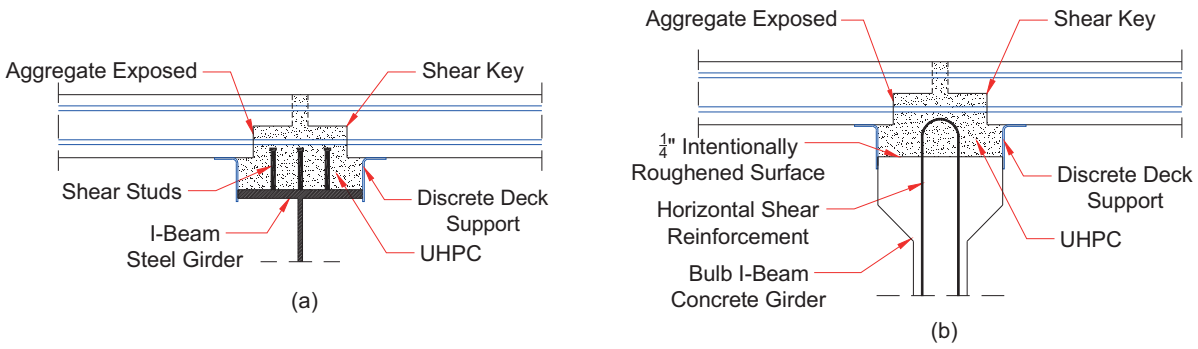

Figure 2.2. Hidden UHPC Deck-to-Girder Connection in Steel Girder (a) and Concrete Girder (b) (Graybeal 2014)

Recently, a study was conducted on implementing UHPC as a grout for deck-to-steel girder composite connection using two new concepts (Haber et al. 2017): a) using shear lugs through deck slab with different areas, and b) using vertical rebar dowels from the deck slab to connection without lugs as shown in Figure 2.3. The second concept was investigated for different haunch thicknesses 5 in. and 3.5 in. and different distributions of shear studs. Push-off specimens were fabricated by having a symmetric layout with W10x60 steel beam at the middle connected to two 20 in. x 24 in. precast slabs through a grouted UHPC connection. The push-off test was performed by applying the shear force on the steel stub and evaluate the connection performance at the shear interface surface. The UHPC shear lugs have shown to be effective in transferring shear forces and the location and number of shear studs have an effect of the capacity of the connection. Adding rebar dowels to the connection increases the shear resistance, develops better anchorage, and achieves ductile failure behavior due to rebar dowel action.

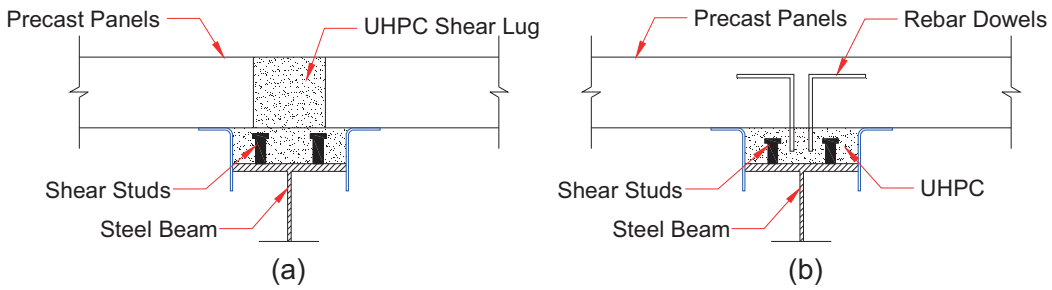

Figure 2.3. New Haunch-to-Deck Connection Using UHPC through Shear Lug (a) and Rebar Dowels (b) (Haber et al. 2017)

2.2. Interface Shear Resistance of UHPC

The interface shear resistance is the maximum shear stress that prevents the relative slide between two different concrete layers. The shear friction theory was first presented by Birkeland and Birkeland (1966) as presented schematically in Figure 2.4. In this theory, a crack was assumed to develop at the interface plane creating a roughened surface that is simulated by fine sawtooth pattern. The mechanism of resisting shear force (V) relies on the friction force produced by the normal force (i.e. clamping force) to the interface, which is either: externally applied compression load; or internal tension in the shear reinforcement crossing the interface (T). When the two layers of concrete start to move away from each other at the interface, a displacement (δ) normal to interface plane occurs, which generates a tension force in interface shear reinforcement up to yield. In this case, the interface shear resistance (v_{ni}) can be predicted using the following equation:

$$v_{ni} = \rho . f_y . \tan(\phi) = \rho . f_y . \mu \leq 0.80\ ksi \qquad (2.1)$$

where, ρ is the interface shear reinforcement ratio (A_{vf} / A_{cv}) and is limited to 1.5%; A_{cv} is the area of concrete engaged in interface shear transfer (in.^{2}); A_{vf} is the area of

reinforcement crossing interface shear plane (in.^{2}); f_y is the yield strength of the interface shear reinforcement and is limited to 60 ksi, and tan(Φ) is the slope of sawtooth ramps, which is also called shear friction factor (μ). Concrete compressive strength is assumed to be greater than 4.0 ksi.

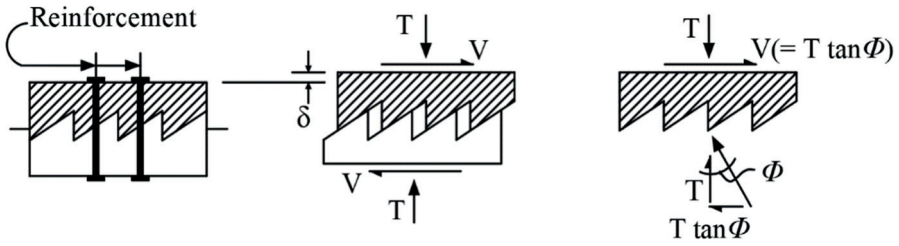

Figure 2.4. Shear friction theory by Birkeland and Birkeland (1966) for the case roughened interface surface.

Based on experimental testing results, the friction factor (μ) was found to be 1.70, 1.40, 0.80, and 1.0 for monolithic concrete, intentionally roughened concrete surfaces, smooth concrete surfaces, and concrete to steel interfaces, respectively (Birkeland and Birkeland 1966). Many researchers studied the interface shear behavior between two concrete layers for different cases and different interface surface textures over the last few decades (Hofbeck et al. 1969; Mattock and Hawkins 1972; Paulay et al. 1974; Mattock et al. 1976; Walraven et al. 1987; Loov and Patnaik 1994; Mattock 2001). Concrete cohesion factor (c) was added later to shear friction theory, known as "Modified shear-friction theory", to represent the chemical bond between the concrete particles at the interface plane adding to the initial interface shear resistance (Mattock and Hawkins 1972).

In the following subsections, the interface shear resistance of UHPC is presented for the three cases that are relevant to the design of deck-to-girder connections:

1. Interface shear resistance between hardened conventional concrete and fresh UHPC (CC-UHPC),
2. Interface shear resistance of monolithic UHPC, and
3. Interface shear resistance between hardened conventional concrete and fresh UHPC (UHPC-UHPC).

2.2.1. Interface Shear Resistance between Fresh UHPC cast on Hardened Conventional Concrete (CC-UHPC)

Slant shear test and L-shape push-off tests are the most common testing techniques to evaluate the interface shear resistance between UHPC cast on hardened conventional concrete (CC-UHPC) with and without interface reinforcement. Slant shear testing is conducted to evaluate the bond resistance over the interface plane between two materials. The type and dimensions of slant shear specimens and interface angle varies according to the standard as shown in Table 2.1. British and French standards use prism specimens while ASTM C882 uses cylindrical specimen. Interface plane angle with the horizontal axis is 60˚ in all standards.

Table 2.1

Slant Shear Composite Specimen Dimensions in Different Standards

Standard	Type of Specimen	Dimensions	Interface Plane Angle with Horizontal Axis
ASTM C882/C882M-13a	Cylinder	3x6 in.	60˚
BS EN 12615:1999	Prism	3.9x3.9x15.7 in. or 1.6x1.6x6.3 in	60˚
French standard NFP 18-872	Prism	3.9x3.9x11.8 in	60˚

ASTM C882/C882M-13a is used mainly for determining the bond resistance of a layer of epoxy-resin-base material between either two hardened or between hardened and fresh Portland-cement concrete. The slant shear test is performed on 3 in. by 6 in. specimens with an interface plane angle of 60° with horizontal axis as shown in Figure 2.5. The specimen sections are prepared by placing Portland-cement mortar in the mold in two layers of approximately equal volume which are uniformly rodded 25 time per each layer. The compressive strength of the concrete section should have at least 4,500 psi at 28 days after being cured. Based on 60° angle inclined interface plane, the area of the elliptical interface plane is twice the area of the specimen base. The specimens shall be tested at 73 ± 2 °F in compression after capping in accordance with test method C39/C39M. A minimum of three composite specimens are required for each test type.

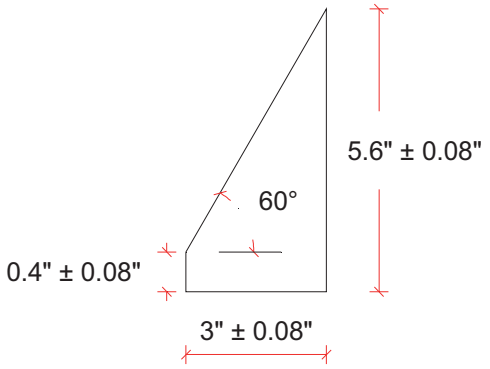

Figure 2.5. Portland-Cement Concrete Section Dimensions (ASTM C882)

The interface shear resistance between a UHPC overlay and hardened normal concrete substrate with different textures was investigated in the literature by three different test procedures: slant shear test, flexural test, and split prism test (Harris et al. 2011). The slant shear test was performed according to ASTM C882/C882M to evaluate the interface shear resistance using 3×6 in. composite cylinders. A total of twenty-seven

composite cylinders were fabricated and tested. The hardened section composed of type III cement mortar that had compressive strength of 5000 psi at 28 days with moist curing (f'_m). Three different surface textures were applied to the interface shear plane; smooth (no surface preparation), low roughened (average depth of 0.1 in.), and high roughened (0.20 in. transverse grooves) surfaces as shown in Figure 2.6(a). Wire brush treatment and handheld metal grinder were used to obtain the low and high roughened surfaces respectively. Also, trapezoidal shear key (fluted), with 0.50 in. depth and 0.63 in.^{2} area, was prepared as a precast scenario for using UHPC as a protective overlay. The hardened concrete mortar sections were placed back inside the molds and filled with UHPC. The composite specimens were cured under ambient conditions for 10 days until the UHPC and normal concrete gained compressive strength of 15 ksi and 5 ksi, respectively. The composite specimens were loaded in compression as shown in Figure 2.6(b) until failure in the interface plane or crashing of concrete happened. The interface shear resistance was calculated by dividing the peak load by the interface surface area.

(a) (b)

Figure 2.6. Slant Shear Test; (a) Mortar Different Roughened Surfaces and Trapezoidal Shear Key, (b) Test Setup (Harris et al. 2011)

The composite specimens with smooth interface exhibited failure along interface plane, however, the roughened interface specimens had a normal concrete compression failure as shown in Figure 2.7. The average interface shear resistance for smooth surface was 1.6 ksi and it increased with 28%, 56%, and 57% with applying low roughened, high roughened surfaces, and shear key, respectively, as shown in Figure 2.8.

(a) (b)

Figure 2.7. Failure Modes; (a) Failure along Interface Plane, (b) Normal Concrete Failure (Harris et al. 2011)

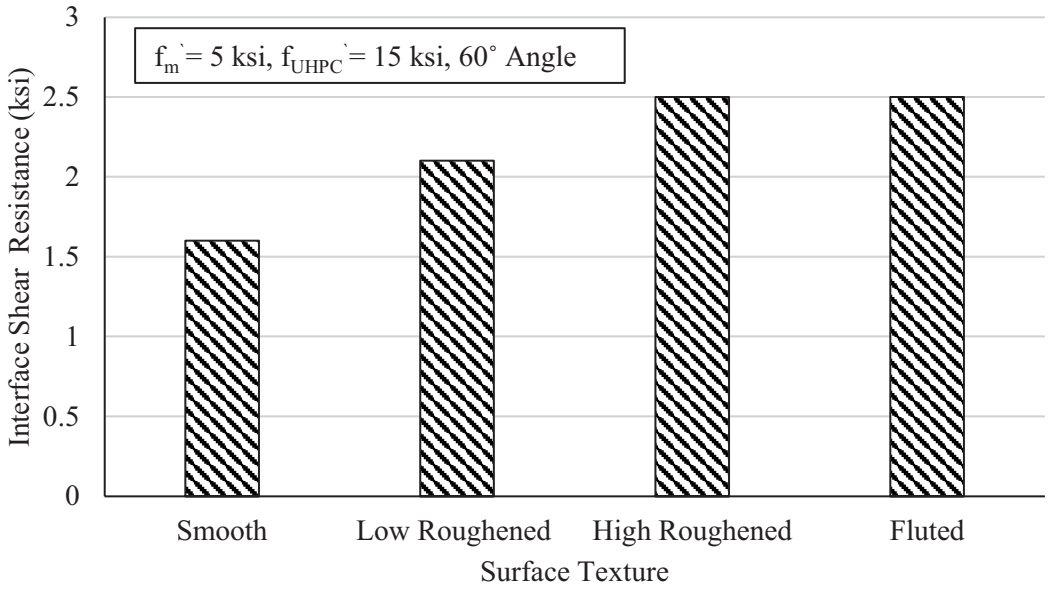

Figure 2.8. Interface Shear Resistance of Cement Type III Mortar with Different Surface Textures (Harris et al. 2011)

Tayeh et al. (2012) investigated the mechanical and permeability properties of interface between normal concrete (NC) substrate, which represents old concrete, and an overlay of ultra-high performance fiber concrete (UHPFC) as a repair material. The interface shear resistance and influence of different surface roughening were evaluated through performing slant shear test and splitting tensile test. The mix proportions of UHPFC and NC are shown in Figure 2.9(a). The slant shear composite specimens were fabricated using prism of 3.9x3.9x11.8 in. with interface angle with vertical of 30°. The interface plane was prepared with five different surface textures: as cut, sand blasted, wire brushed, drilled holes (0.4 in. diameter and 0.2 depth), and grooved (0.4 in. width and 0.2 in. depth) as shown in Figure 2.9(b). The compressive strength of NC and UHPFC at 28 days were 6.53 and 24.66 ksi, respectively. The test was conducted according to ASTM C288 and the test setup is shown in Figure 2.9(c).

Four different failure modes were observed: pure interfacial failure, interfacial failure with minor NC cracking, interfacial failure with NC fracture, and substrata failure. The interface shear resistance was calculated by dividing the maximum applied load by the interface contact area. The sand-blasted texture specimens give the highest interface shear resistance of 2.58 ksi. The surface texture clearly influences the interface shear resistance, as compared to surface without preparation, the interface shear resistance increases with 105%, 60%, 47%, and 41% for sand blasted, grooved, wire brushed, and drilled holes surfaces as shown in Figure 2.10.

Table 1
Mix proportions for NC substrate and UHPFC.

Concrete type (kg/m^3)	NC substrate	UHPFC
OPC (Type 1, 42.5R)	400	768
Coarse aggregate (max. 12.5 mm)	930	–
River sand (F.M. = 2.4)	873	–
Mining sand (<1180 μm)	–	1140
Silica fume (23.7 m^2/g)	–	192
Steel fiber (L_f = 10 mm, d_f = 0.2 mm)	–	157
Superplasticizer (PCE-based)	4	40
Water	200	144
Total	2407	2441
W/B	0.5	0.15
Cube strength, $f_{cc,28d}$	45 MPa	170 MPa
Split cylinder tension strength, $f_{sp,28d}$	2.75 MPa	15.3 MPa

(a)

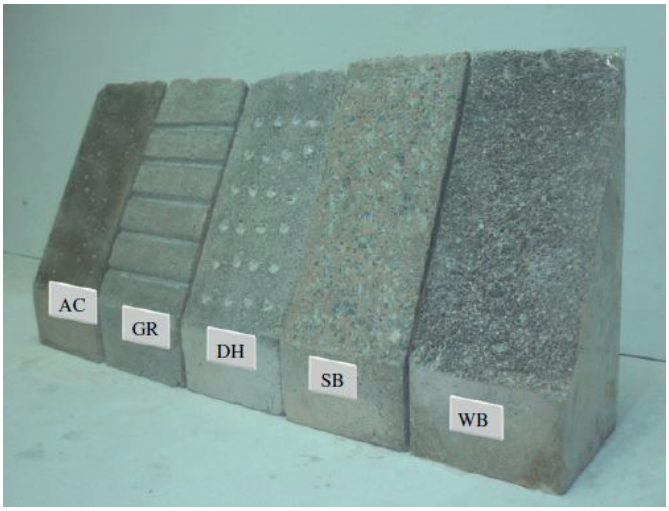

(b)

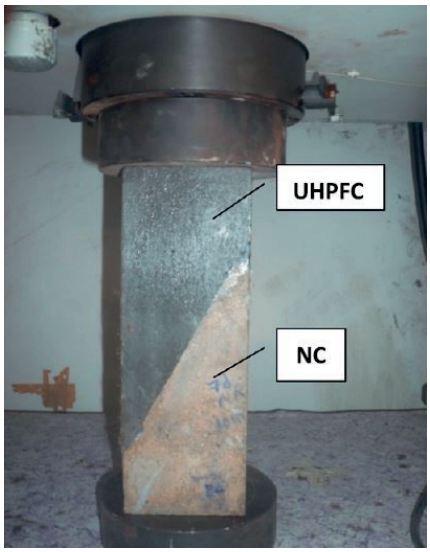

(c)

Figure 2.9. (a) Mix Proportions of UHPFC and NC, (b) Surface Textures, and (c) Test Configuration (Tayeh et al. 2012)

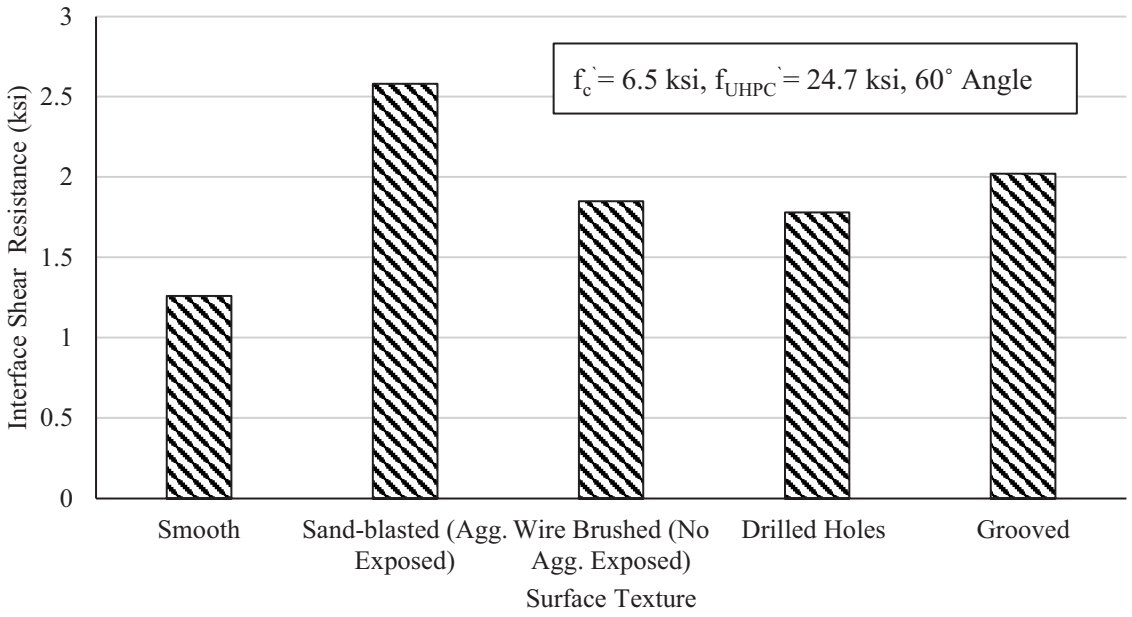

Figure 2.10. Different Surface Texture Effect on Interface Shear Resistance of NC-UHPC (Tayeh et al. 2012)

Muñnoz (2012) conducted a study on using UHPC as a repair material by investigating the interface shear resistance between UHPC and normal strength concrete (NSC). The interface shear resistance was evaluated by three different test methods: slant shear test, splitting prism test, and pull-off test. The slant shear test was conducted to obtain the interface shear resistance of different surface preparation treatment and interface angles. The slant shear composite specimens were 3.5x3.5x14 in prism to allow casting concrete substrate contrasting ASTM C 882 that uses mortar substrate as shown in Figure 2.11. This study focused on four different surface textures: brushed, sandblasted, grooved, and roughened (exposed aggregate), and two different interface angles with horizontal axis, 60° and 70°. The normal concrete sections were casted in wooden forms and cured in two stages: 24 hours in moist cure before demolding and, then, in a lime water tank for 28 days. The compressive strength of NSC mixes was 6.46

ksi, 6.61 ksi, and 8.11 ksi for grooved and brushed, roughened, and sandblasted surface texture specimens respectively. A steel brush and drill-bit, sandblasting equipment, wet saw, and concrete retarder were used to obtain the brushed, sandblasted, grooved, and roughened interface surface textures respectively. Two different methods were used to evaluate the roughening degree, the macrotexture depth test and the concrete surface preparation index given by International Concrete Repair Institute (ICRI) guide. Figure 2.12 and Table 2.2 show the different surface textures and the degree of roughening measurement.

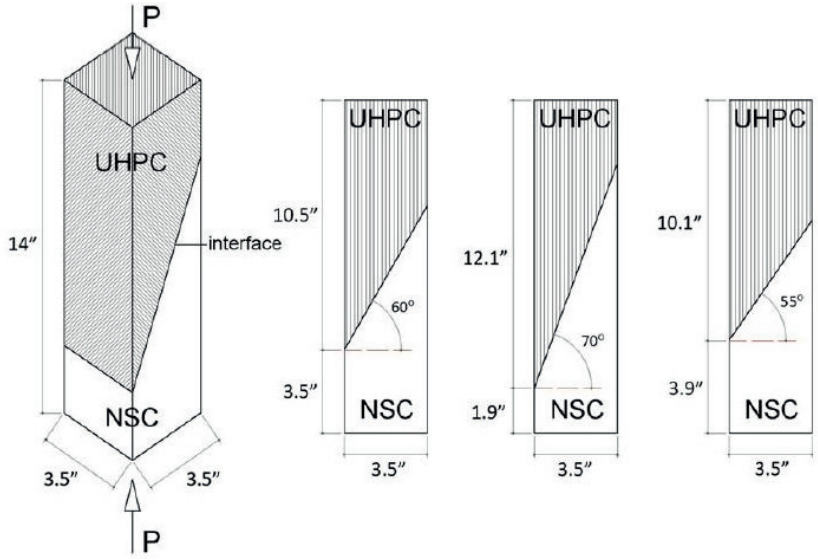

Figure 2.11. Slant Shear Composite Specimen Dimensions (Carbonell Muñoz 2012).

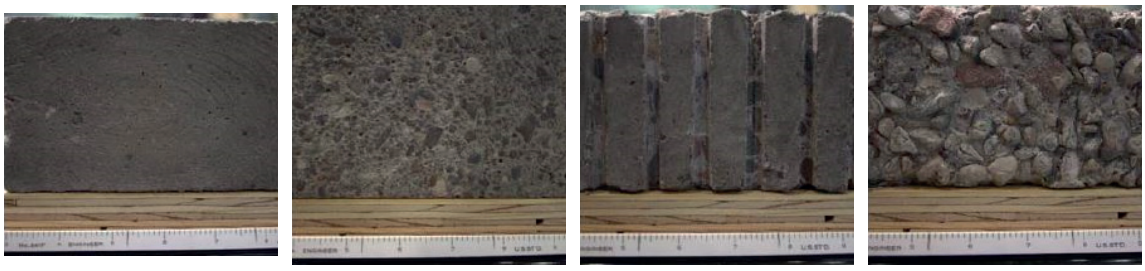

(a) Brushed (b) Sandblasted (c) Grooved (d) Roughened

Figure 2.12. Different Surface Textures (Carbonell Muñoz 2012).

Table 2.2

The Macrotexture Depths of Prepared Surfaces (Carbonell Muñnoz 2012)

Surface	ICRI Profile	Macrotexture Depth (in)
Brushed	1,3	0.03
Sandblasted	4,5	0.03
Grooved	Not applicable	Not applicable
Roughed	Aggregate exposure >8,9	0.09

The composite specimens consisted of hardened NSC blocks with prepared interface surface texture after curing in a water tank and Ductal®JS1000 UHPC poured on the blocks. Four composite specimens were tested at 8 days for each texture. A load rate of 35 psi/second was used to apply load using compression machine until failure as shown in Figure 2.13. The tested specimens exhibited different failure modes. The slant shear specimens with 60° interface angle and 8 days of UHPC exhibited NSC failure. However, the 70° interface angle brushed surface specimens had interface failure, the other surface textures expressed NSC failure. Figure 2.14 shows the effect of interface angle on the interface shear resistance for different surface texture at 8 days of UHPC. The interface shear resistance was calculated by dividing the maximum applied load by the interface contact area. The interface shear resistance of sandblasted specimens is the highest compared to the other surface texture specimens. The higher compressive strength of sandblasted NSC section might give a wrong conclusion as mentioned by the authors. Failure modes and interface shear resistance are affected by the change of the interface angles. The interface shear resistance at 8 days for all surface preparations exceeded the

requirements specified by ACI 546.3R-06 at 7 days and satisfied the minimum bond requirements for 28 days.

Figure 2.13. Slant Shear Test Configuration (Carbonell Muñnoz 2012).

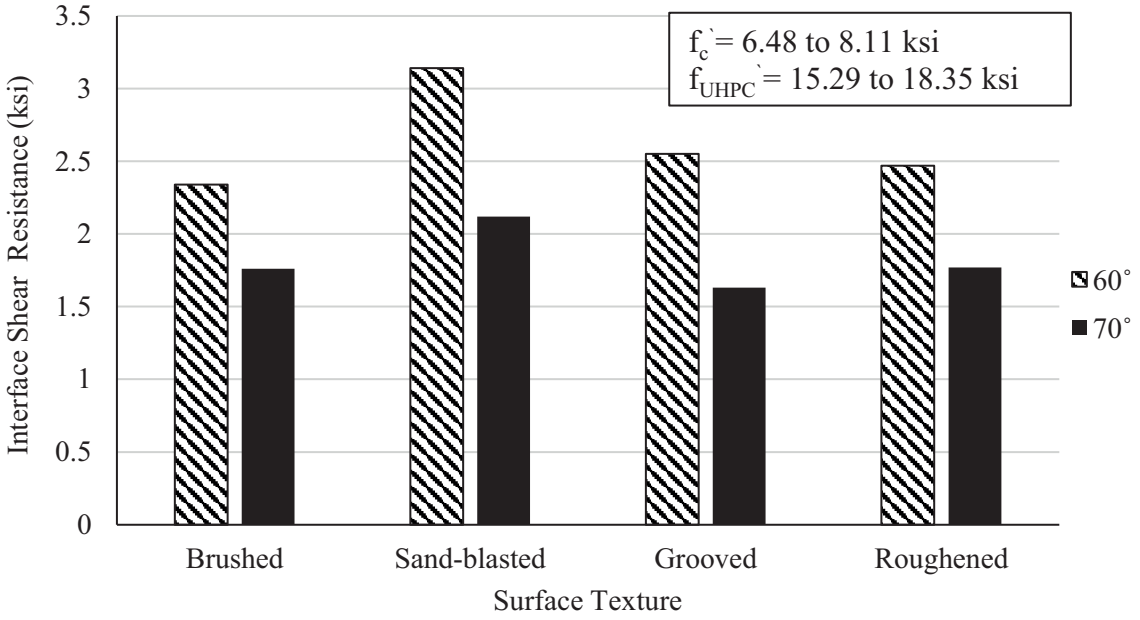

Figure 2.14. Effect of Interface Angle on Interface Shear Resistance at 8 Days of UHPC (Carbonell Muñnoz 2012).

Rangaraju et al. (2013) performed a study on developing local UHPC using available materials in South Carolina and evaluating its performance as shear key grout for

bridge systems. Slant shear test was conducted to evaluate the interface shear resistance of the local UHPC as a part of determining the local UHPC mix properties. The developed mixes proportions are shown in Table 2.3. The slant test was performed according to ASTM C882 with modifications, using normal concrete representing bridge deck instead of concrete mortar. The normal concrete was cast in 3x6 in. cylinders and moist-cured for a 28-day period. The range of normal concrete compressive strength was from 5.92 to 7.61 ksi. The interface surface was then treated by sand-blasting to obtain a roughened surface. Four different UHPC mixes were poured on the top of normal concrete section, demolded after 1 day, and moist-cured for 6 days. The composite specimens were tested at 7 and 28 days under compression rate according to ASTM C39. Most of the specimens failed in the normal concrete portion, one specimen exhibited interface failure. The maximum applied loads and failure modes are shown in Table 2.4.

Table 2.3

Different Mix Proportions Used in Evaluating Local UHPC Properties, Ib/yd3 (Rangaraju et al. 2013)

UHPC ID	Cement	Sand	Silica fume (SF)	Water	SP, %	Steel microfiber**
UHPC 1	1601	2002	-	320	RQ	-
UHPC 2	1300	1949	260	312	RQ	-
UHPC 3	1273	1909	255	305	RQ	270
UHPC 4	1249	1873	250	300	RQ	270

**SP quantity is expressed in terms of percentage by weight of the total cementitious material (cement + silica fume)*

***microfiber dosage is expressed in terms of percentage by volume of the non-microfiber mixture*

RQ indicates required quantity to obtain a full flow of 150%

Table 2.4

Slant Shear Test Results and Failure Modes (Rangaraju et al. 2013)

UHPC ID	Maximum Applied Force					
	7-days			28-days		
	Average, kips	COV, %	Failure Location	Average, kips	COV, %	Failure Location
UHPC 1	28.3	2.0	Concrete	46.2	4.7	Concrete
UHPC 2	32.7	8.4	Concrete	56.2	5.2	Concrete & UHPC
UHPC 3	64.6	6.6	Interface & Concrete	58.5	9.6	Concrete
UHPC 4	62.7	11.2	Concrete	66.9	10.5	Concrete

The shear transfer behavior across the interface plane between UHPC and normal concrete (NC) was investigated analytically and experimentally by conducting slant shear test and flexural test (Aaleti and Sritharan 2017). The slant shear testing was performed to evaluate the effect of NC compressive strength, interface roughness, curing condition, and pouring sequence on the direct shear transfer behavior. Prismatic specimens consist of normal concrete with five different texture along the interface plane and UHPC were used for performing the slant shear test. The composite specimen dimensions were 4.5 in. × 6 in. in cross-section and 24 in. long and interface angle of 53.1° with the horizontal axis as shown in Figure 2.15.

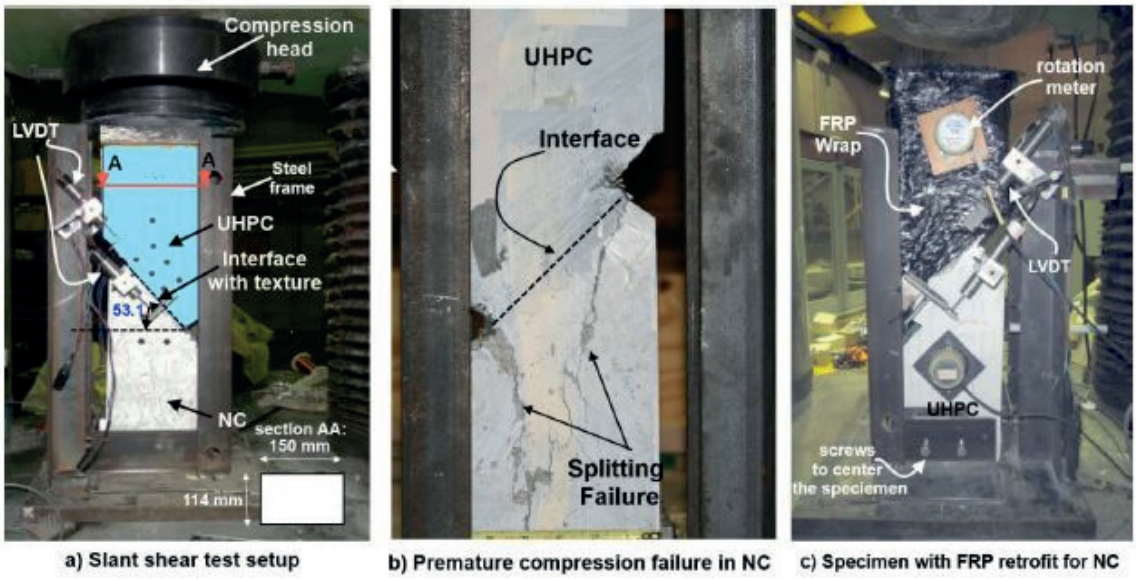

Figure 2.15. Test Setup and Instrumentation of Large Prism Slant Shear Test (Aaleti and Sritharan 2017)

A total of sixty specimens were fabricated with three normal concrete compressive strength, five different textures, and four different curing conditions as shown in Table 2.5. The surface textures were obtained by adding form liners to the interface shear plane. The five surface textures represented low roughness (< 0.06 in.), medium roughness (0.12 in.), and high roughness (0.2 in. to 0.25 in.). The NC sections of composite specimens were cast vertically, and their compressive strength were obtained at 28 days and at the time of slant shear specimen testing. Then, UHPC was used to cast the second section of composite specimens. The texture depth of composite section was measured before pouring the second half. Based on ASTM C882, a uniaxial compression load was applied at the end of the composite slant shear specimens using a universal testing machine as shown in Figure 2.15. Four linear variable differential transducers (LVDTs) were used to capture the slip at the interface shear plane. Two rotation meters were used to capture any rotation induced by possible eccentricity of loading.

Table 2.5

Summary of NC-UHPC Interface Test Matrix (Aaleti and Sritharan 2017)

Specimen Type	Texture (# of specimens)	Casting Sequence	Target NC Strength
UHPCw-NC5	5 textures (3 per texture)	Wet UHPC over cured NC	5 ksi
UHPCw-NC7	5 textures (3 per texture)	Wet UHPC over cured NC	7 ksi
UHPCw-NC10	5 textures (3 per texture)	Wet UHPC over cured NC	10 ksi
UHPCh-NC5	5 textures (3 per texture)	Wet NC on heat-treated UHPC	5 ksi

Two failure modes were noticed: interface failure or NC failure, as shown in Figure 2.16. The authors did fiber-reinforced polymer (FRP) retrofitting to NC section of some specimens that did not experience significant sliding due to splitting cracks in NC. The interface shear resistance was calculated by dividing the maximum load along the inclined plane by the interface contact area. Figure 2.17 shows average interface shear resistance of three specimens for different surface texture depths and concrete compressive strength. The interface shear resistance generally increased with the increase of texture roughness and concrete strength. Average interface shear resistance of textures deeper than 0.08 in. satisfied the ACI 546.3R-06 limits. Also, interface shear capacity calculated based on AASHTO (2010) equations was conservative in predicting NC-UHPC interface shear resistance.

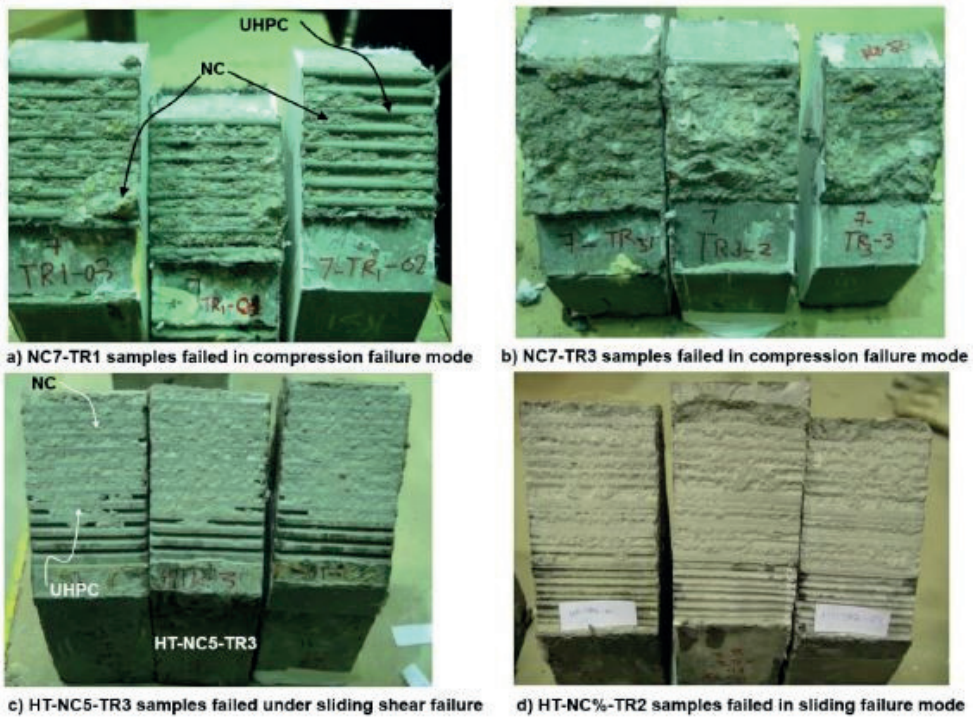

Figure 2.16. Samples of NC-UHPC Interfaces of Specimen with Different Failure Modes (Aaleti and Sritharan 2017)

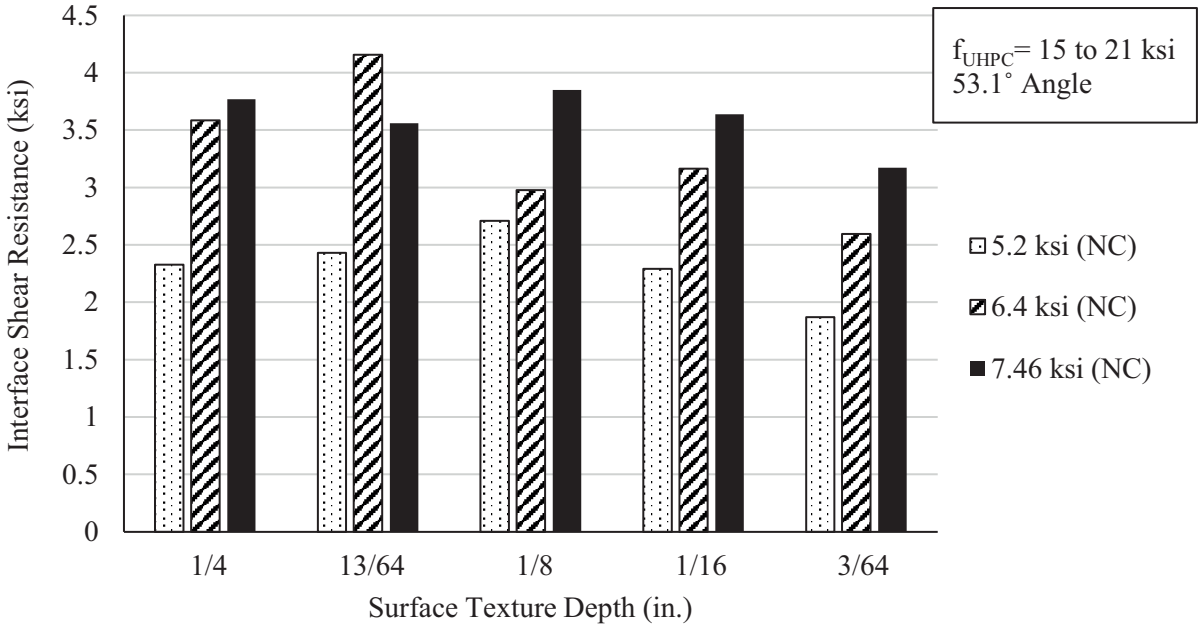

Figure 2.17. Effect of Surface Texture Depth and NC Compressive Strength on Interface Shear Resistance of NC-UHPC (Aaleti and Sritharan 2017)

Jang et al. (2017) conducted vertical shear test on L-shape push-off specimen to evaluate the interface shear resistance between UHPC and normal strength concrete (NSC) without interface reinforcement as shown in Figure 2.18. The L-shape specimen dimensions are 5.9 x 11.8 x 25.2 in. with interface shear area of 5.9 x 7.9 in. Five different surface treatments were applied to the CC sections: smooth, water jet, grooved (0.4 in.), grooved (0.8 in.), and grooved (1.2 in.) as shown in Figure 2.18. The UHPC matrix consists of water-to-binder ratio (w/b) of 0.14, type I/II Portland cement, Australian silica sand, and silica with a fiber content of 1.5% of volume. The CC and UHPC achieved 5.2 and 29.08 ksi respectively. A vertical load was applied to the specimen with a rate of 0.024 in./min. until failure. Four LVDTs were used to measure the horizontal and relative vertical displacement in the L-shape specimen. Figure 2.19 shows the average interface shear resistance of NSC-UHPC with different surface treatments. Based on the results, the interface shear resistance of NSC-UHPC without interface reinforcement increases with the increase of the surface roughening.

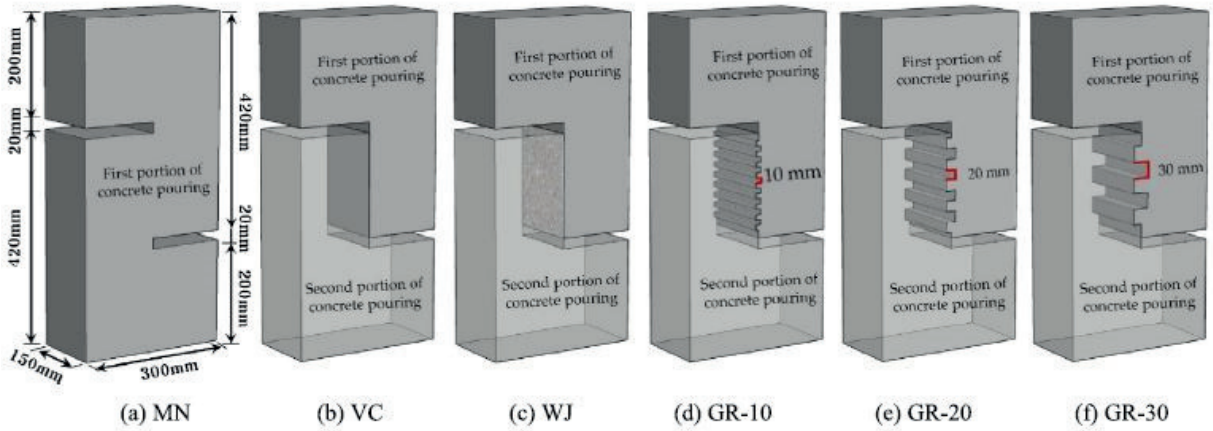

Figure 2.18. L-Shape Specimen Dimensions and Different Surface Treatment of NSC-UHPC (Jang et al. 2017)

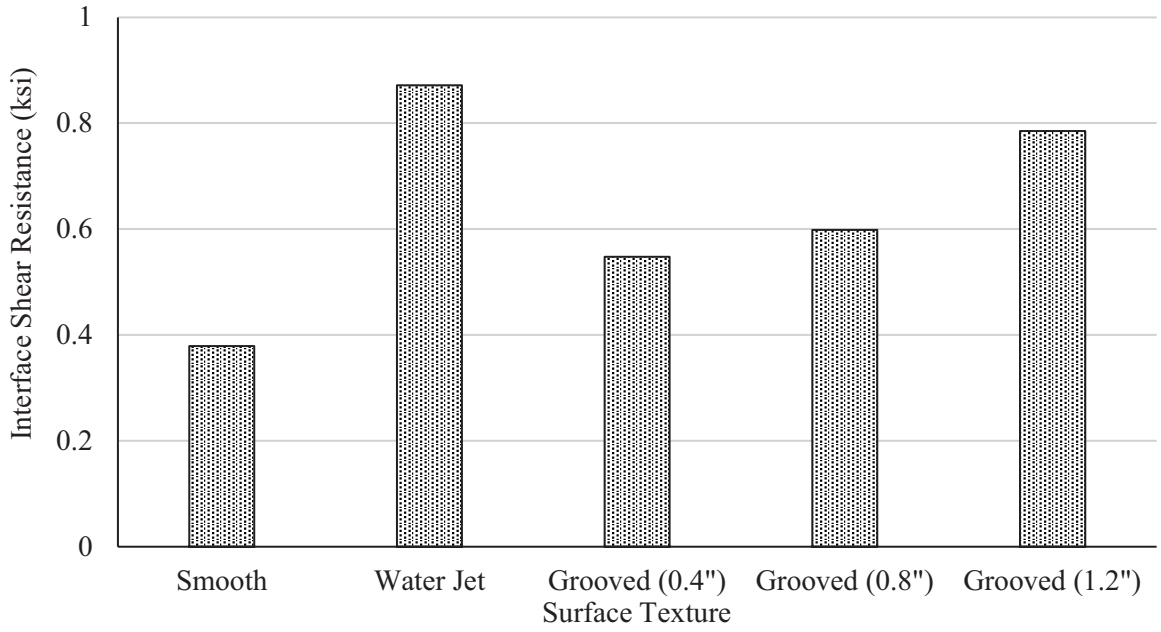

Figure 2.19. L-Shape Test Results of NSC-UHPC Specimens (Jang et al. 2017)

2.2.2. Interface Shear Resistance of Monolithic UHPC

Crane (2010) performed vertical interface shear push-off tests of monolithic UHPC specimens to determine whether ACI 318 (2008) and AASHTO LRFD (2007) equations of interface shear are applicable to monolithic UHPC. UHPC specimens with un-cracked and pre-cracked interfaces, and with reinforcement ratios of 0 and 0.5% were tested. Three identical push-off specimens were tested for each combination of interface type and reinforcement ratio as shown in Figure 2.20. Test results indicated that the ultimate interface shear resistance was significantly higher than that predicted for monolithic concrete in all cases. Regression analysis was performed to estimate UHPC cohesion and friction coefficients (c and μ). For un-cracked UHPC, $\mu = 4.5$, and $c = 2$ ksi were proposed, and for cracked monolithic UHPC, $\mu = 4.0$, and $c = 0.65$ ksi were proposed. These high values were attributed to the contribution of the steel fibers

distributed across pre-existing cracks even when no mild shear reinforcement is used. Also as expected, the specimens with reinforced UHPC exhibited more ductile behavior than those with unreinforced UHPC. The average interface shear resistance of un-cracked monolithic UHPC increases by 48% with the increase of interface reinforcement ratio from 0 to 0.5% as shown in Figure 2.21.

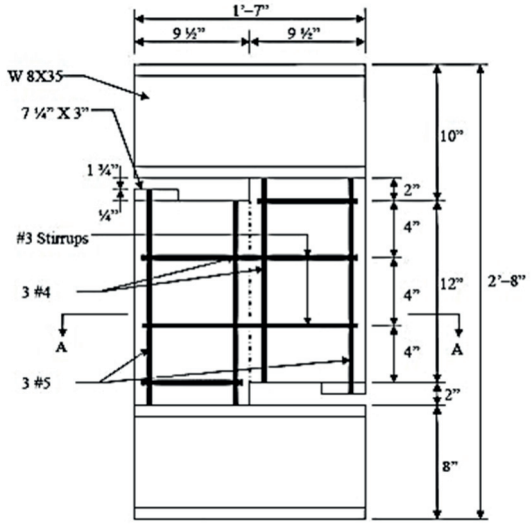

Figure 2.20. Vertical Interface Shear Push-off specimen of Monolithic UHPC (Crane 2010)

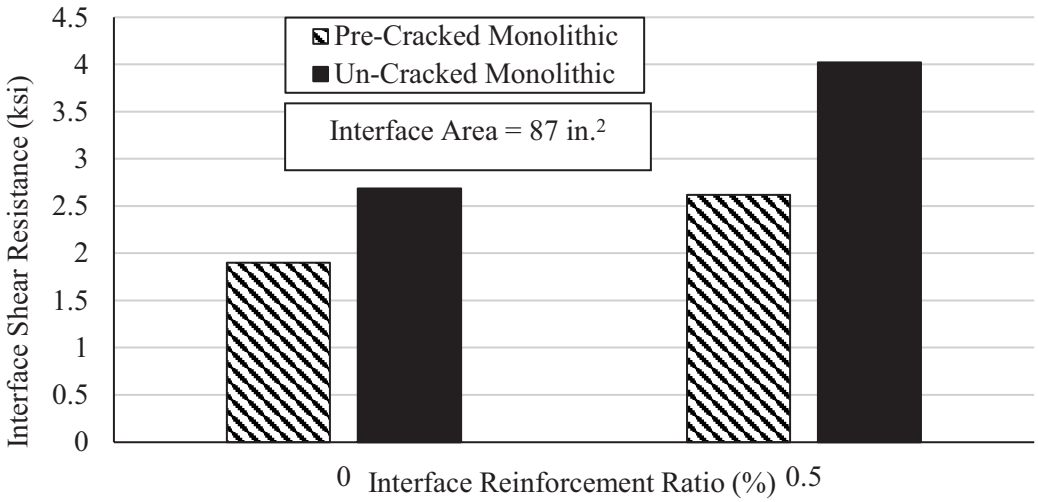

Figure 2.21. Average Interface Shear Resistance of Monolithic UHPC with and without Interface reinforcement (Crane 2010)

Maroliya (2012) investigated the behavior of reactive powder concrete (which is another term for UHPC) in direct interface shear. A series of direct shear specimens having inverted "L" shape in shear failure plane were tested using monolithic UHPC with different percentages of steel fibers as shown in Figure 2.22. Test results showed that plain UHPC samples failed in a brittle manner at the first-crack load, which happens to be the maximum load taken by the specimen. On the other hand, samples having 2.5% fibers indicated multiple visible cracks, while samples having 2% fibers resulted in a maximum load much higher than the first-crack load, which clearly reflects failure after the strain hardening of the material. These results helped concluding that UHPC exhibits a ductile failure mode depending on the percentage of fibers. Figure 2.23 shows the effect of different fiber content and curing methods on the direct shear strength of monolithic UHPC. Results also indicated an average value of direct shear strength for normal cured monolithic UHPC with 2% fiber volume fraction of about 2 ksi.

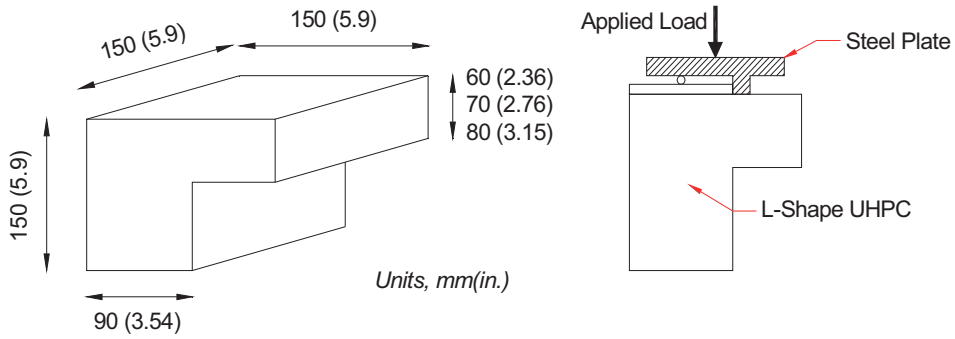

Figure 2.22. Shear Testing on Inverted L-Shape UHPC Specimen (Maroliya 2012)

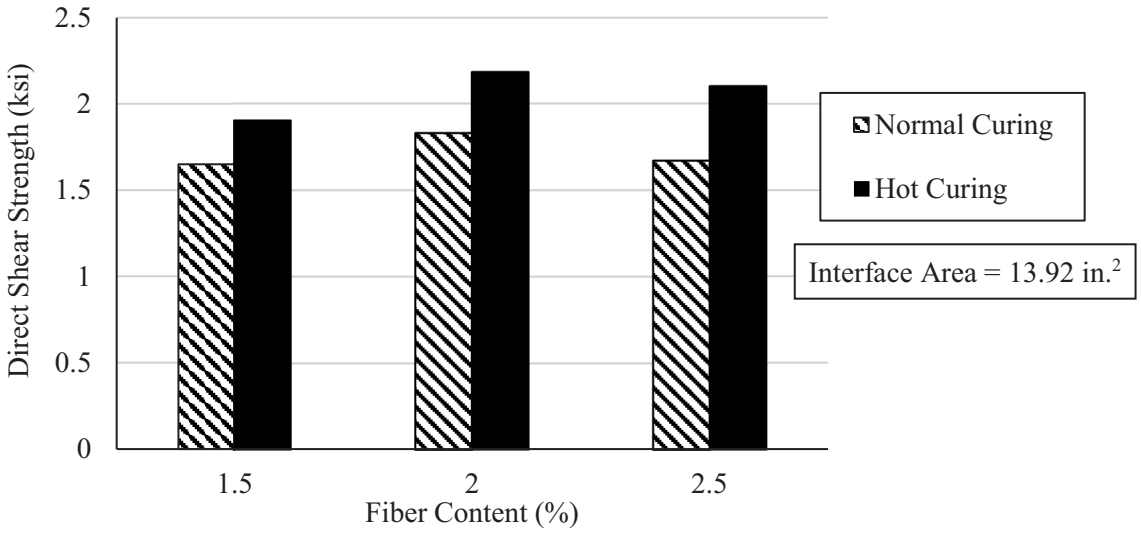

Figure 2.23. Effect of Fiber Content and Curing Methods on Direct Shear Strength of Monolithic UHPC without Interface reinforcement (Maroliya 2012)

Jang et al. (2017) conducted vertical shear test on L-shape specimen to evaluate the monolithic interface shear resistance of UHPC without interface reinforcement as shown in Figure 2.24. The UHPC matrix consists of water-to-binder ratio (w/b) of 0.14, type I/II Portland cement, Australian silica sand, and silica with a fiber content of 1.5% of volume. The UHPC achieved 29.08 ksi at 91 days. A vertical load was applied on the specimen with a rate of 0.024 in./min. until failure. Four LVDTs were used to capture the horizontal and relative vertical displacement in the L-shape specimen. The interface shear resistance of monolithic UHPC without interface reinforcement was 2.72 ksi with interface shear area of 46.50 $in.^2$.

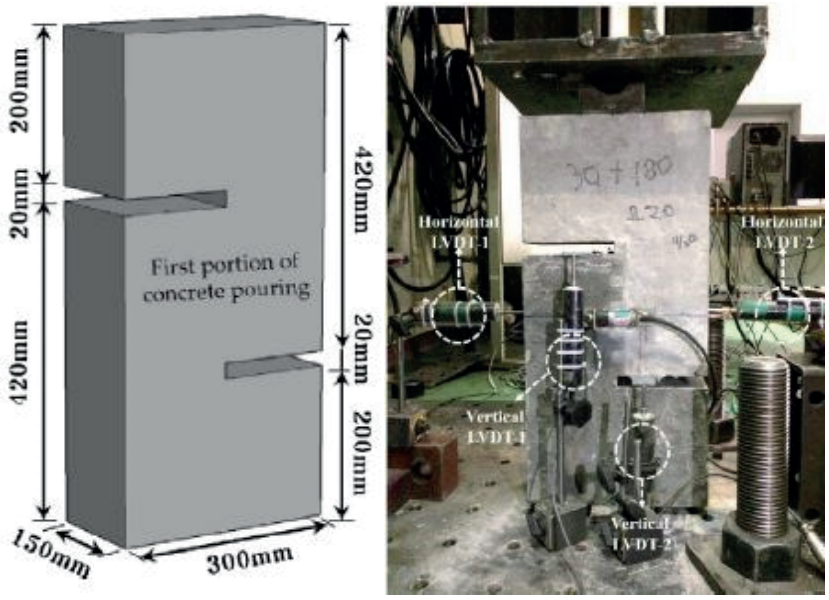

Figure 2.24. Monolithic L-Shape UHPC Specimen Test Setup and Specimen Dimensions (Jang et al. 2017)

Small and large scale push-off tests were performed to obtain the direct shear capacity of UHPC (Haber et al. 2017). Three small specimens composed of 6 in. long with 2 in. square cross section beams were tested by applying vertical load on the beam that was fixed by square supports from both ends. The UHPC were poured from one end to ensure the fiber orientation was perpendicular to the applied loads. Fourteen inches by twenty-four inches two precast concrete slabs with lug pockets were prefabricated and the lugs were filled with UHPC with a stub. A vertical load was applied on the UHPC stub to investigate the shear capacity of the proposed UHPC shear lugs. The direct shear testing for the small and large specimens are shown in Figure 2.25. The specimens exhibited a double shear failure, and the test results are summarized in Figure 2.26. A range of 4 ksi to 8 ksi UHPC direct shear capacity were achieved according to the tested specimens.

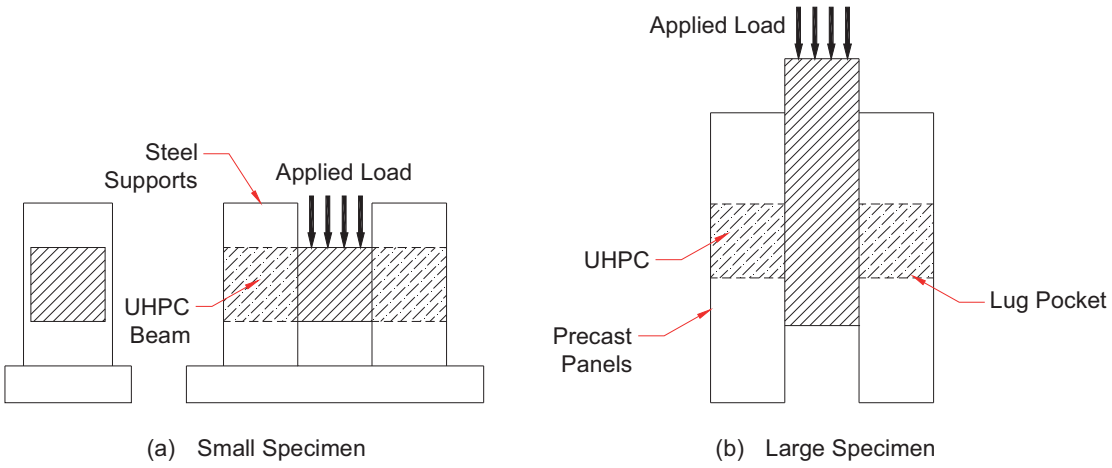

Figure 2.25. Small and Large Scale Push-off Test of Monolithic UHPC without Interface reinforcement (Haber et al. 2017)

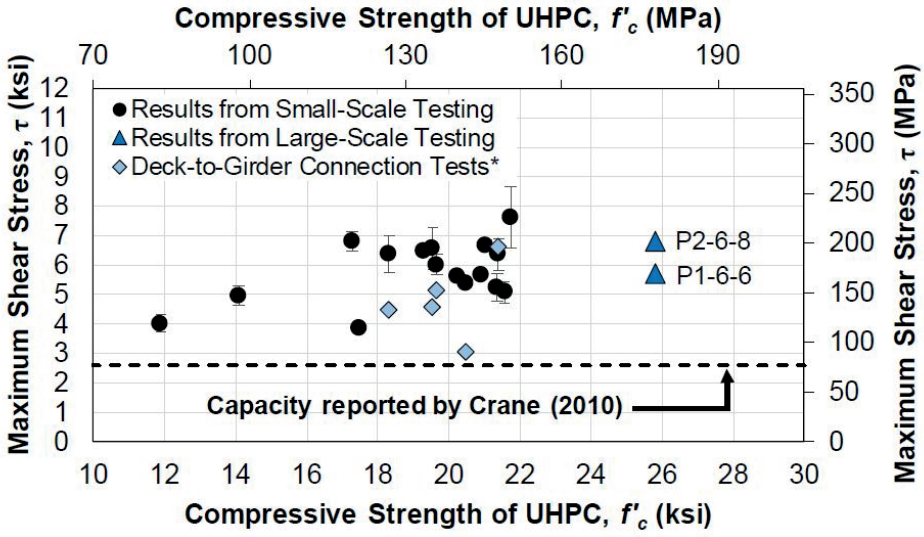

Figure 2.26. Small and Large Scale Push-off Test of Monolithic UHPC without Interface reinforcement (Haber et al. 2017)

2.2.3. Interface Shear Resistance between Fresh UHPC cast on Hardened UHPC (UHPC-UHPC)

Crane (2010) performed vertical interface shear push-off tests of high-performance concrete (HPC) casted on hardened UHPC specimens to determine whether

ACI 318 (2008) and AASHTO LRFD (2007) equations of interface shear are applicable to UHPC interface resistance. The compressive strengths of hardened and fresh UHPC were 28.9 ksi. Smooth interface surface texture was investigated with two transverse reinforcement ratios: 0%, 0.5%. A load rate of 500 Ib/sec was applied vertically on the specimens and instrumentation of two LVDTs was installed to capture the relative displacement between hardened and fresh UHPC as shown in Figure 2.27. The interface shear resistance of UHPC-UHPC was 0.21 and 0.56 ksi for 0%, 0.5% reinforcement ratios.

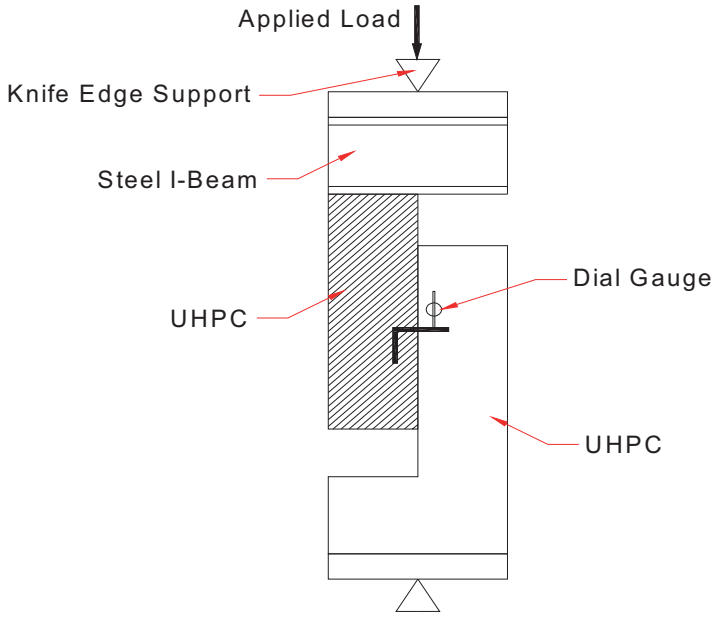

Figure 2.27. Vertical Interface Shear Push-Off Tests of UHPC-UHPC Specimens (Crane 2010)

Jang et al. (2017) conducted vertical shear test on L-shape specimen to evaluate the interface shear resistance of UHPC-UHPC without transverse reinforcement as shown in Figure 2.28. The L-shape specimen dimensions are 5.9 x 11.8 x 25.2 in. with interface

shear area of 5.9 in. x 7.9 in. Five different surface treatments were applied to the UHPC sections; smooth, water jet, grooved (0.4 in.), grooved (0.8 in.), and grooved (1.2 in.) as shown in Figure 2.28. The UHPC matrix consists of water-to-binder ratio (W/B) of 0.14, type I/II portland cement, Australian silica sand, and silica with a fiber content of 1.5% of volume. The hardened UHPC compressive strength ranged from 29 to 33 ksi and the fresh UHPC compressive strength is 29 ksi after 91 days.

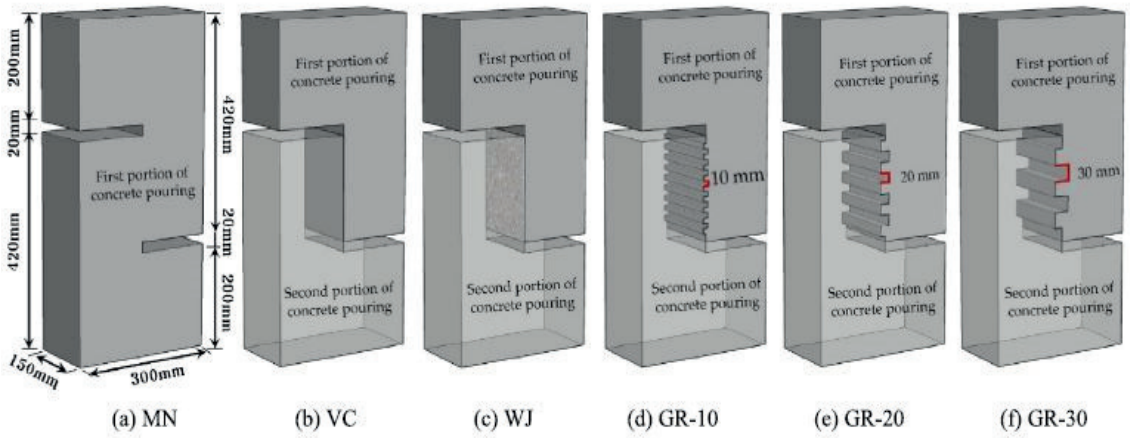

Figure 2.28. L-Shape Specimen Dimensions and Different Surface Treatment of UHPC-UHPC (Jang et al. 2017)

A vertical load was applied on the specimen with a rate of 0.024 in./min. until failure. Four LVDTs were used to capture the horizontal and relative vertical displacement in the L-shape specimen. Figure 2.29 shows the average interface shear resistance of UHPC-UHPC with different surface treatment. Based on the results, the interface shear resistance of UHPC-UHPC without transverse reinforcement increases with the increase of the surface roughening.

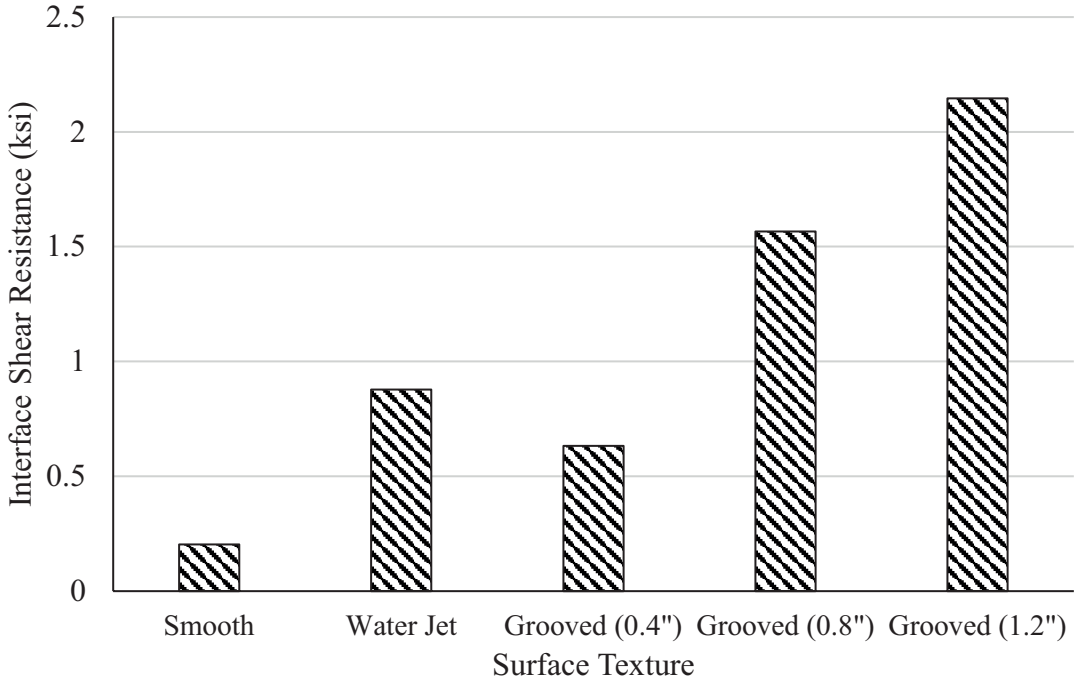

Figure 2.29. L-Shape Test Results of UHPC-UHPC Specimens (Jang et al. 2017)

Kim et al (2018) performed double shear tests to evaluate the interface shear resistance of UHPC joints between UHPC segmental bridges; dry joint with epoxy and cast-in-place UHPC joint as shown in Figure 2.30. Several parameters were studied including shear key height and number, treatment temperature, and effect of compressive stress on interface shear plane. Also, in the case of UHPC-UHPC, mortar and normal concrete joints were tested using the same shear key dimensions for comparison. Figure 2.31 shows the double shear test setup with lateral loading applied to the specimens during the test to simulate the prestressing force generated by strands in segmental bridges. A vertical load was applied on the middle section of the specimens with a load rate of 0.016 in./min. Concrete strain and displacement gauges were placed at the interface planes to capture the behavior. The test results were compared to the AASHTO and Japanese recommendation for conventional concrete to indicate the applicability of

recommendations in case of using UHPC. The AASHTO equations underestimate the interface shear capacity of UHP-UHPC, however, the Japanese recommendation overestimates the interface shear resistance for the same case.

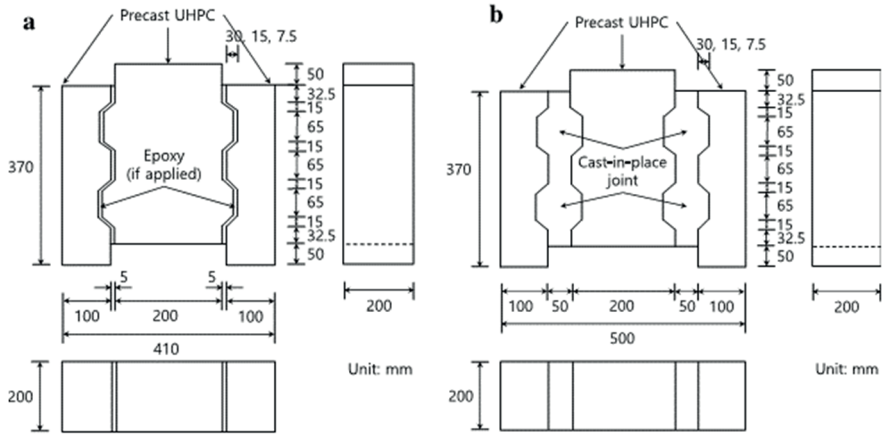

Figure 2.30. Double Shear Test Specimens Dimensions by Kim et al. (2018); (a) Dry Joint with Epoxy and (b) Cast-in-Place UHPC Joint (25 mm = 1 in.)

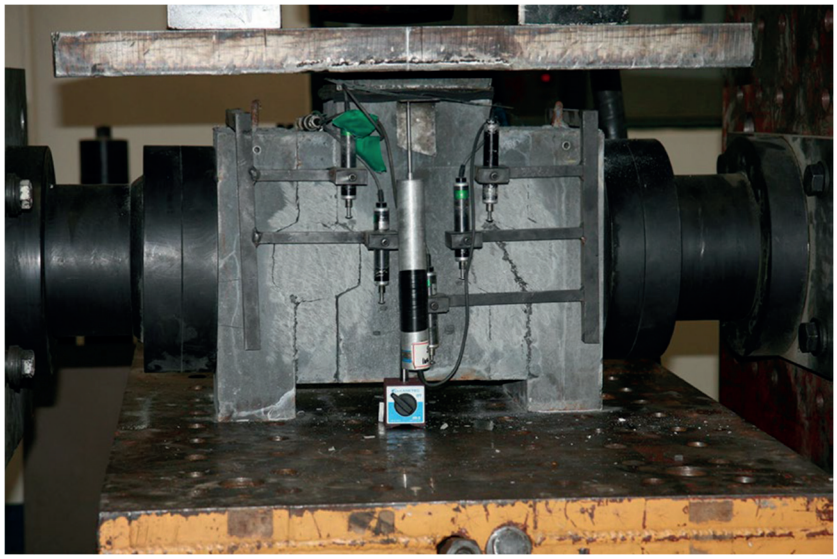

Figure 2.31. Double Shear Test Setup (Kim et al 2018)

According to the French Standards (NF-P-18-710 (2016)), the interface shear resistance of UHPC can be predicted using a modified interface shear provisions based

on Eurocode 2 to count for UHPC interface texture. The concrete cohesion portion of the interface shear resistance in Eurocode 2 is a function of the tensile properties of concrete multiplied by a factor (c) which is different than AASHTO LRFD that has constant values for the same factor. The French standard stated two cases for the interface texture of hardened UHPC as following:

1. Very smooth: when no data is available for the interface texture, the interface factors are taken as c= 0.025 to 0.10 and μ=0.50
2. Formed flutes as shown in Figure 2.32: the interface factors are taken as c= 0.5 and μ=1.4

The flutes dimensions and requirements are adopted from Eurocode which specifies it for construction joint and modified based on the length of the fibers as shown in Figure 2.32. The dimensions of the flutes, *b*, h_1, and h_2, should be greater than twice the length of the fiber and the depth of the flutes should be equal to or higher than half of the fiber length. The spacing between the flutes, h_1 and h_2, should be greater than 10 times the depth of the flutes. Thus, the flutes dimension mainly rely on the length of the fiber used in UHPC. For very smooth surface, Eq. 2.2 is used to obtain the interface shear capacity. However, when using flutes, a new term is added to the equation to count for the fibers crossing the interface as shown in Eq. 2.3. The maximum nominal interface shear resistance of UHPC is limited to $\mathbf{1.15}{f_{ck}}^{2/3}$ according to NF-P-18-710 (2016) provisions.

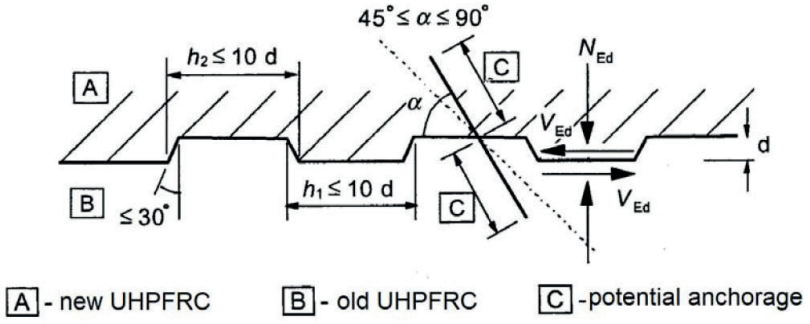

Figure 2.32. Fluted Joint Details as Specified by NF-P-18-710 (2016)

For interface with unroughened interface:

$$V_{ni} = c\frac{f_{clk,el}}{\gamma_c} + \mu\sigma_n + \rho f_{yd}(\mu sin\alpha + cos\alpha) \leq 1.15\alpha_{cc}\frac{{f_{ck}}^{2/3}}{\gamma_c} \quad (2.2)$$

For interface with roughened (fluted) interface:

$$V_{Rdi} = c\frac{f_{clk,el}}{\gamma_c} + \mu\sigma_n + \rho f_{yd}(\mu sin\alpha + cos\alpha) + (0.35\mu + 0.3)\frac{f_{clfk}}{K\gamma_{cf}} \leq 1.15\alpha_{cc}\frac{{f_{ck}}^{2/3}}{\gamma_c} \quad (2.3)$$

where:

$f_{clk,el}$ = characteristic value of the tensile limit of elasticity (MPa)

f_{clfk} = characteristic value of the post-cracking strength (MPa)

f_{ck} = characteristic value of compressive strength (MPa)

K = fiber orientation factor, determined by testing

c = cohesion factor

μ = friction factor

σ_n = the stress caused by the minimum external axial force across the interface (MPa)

ρ = transverse reinforcement ratio across the interface plane

α = angle of fiber indentation with the interface shear surface of the hardened UHPC as shown in Figure 2.32; 45°< α<90°.

γ_c = partial factor for compressed UHPC

2.3. Summary

Shear friction and cohesion are the main mechanisms that control the interface shear resistance between two concrete surfaces. The interface shear resistance of monolithic UHPC without transverse reinforcement was investigated in two different methods: single plane direct shear test (L-shape and Inverted L-shape) and double plane direct shear test. The L-shape specimens had a maximum shear resistance of 2.72 ksi (Jang et al. 2017), the small-scale prism (2x2x6 in.) and large-scale specimens done by Harber et al. 2017 exhibited double shear failure and had a higher direct shear resistance varied between 4 to 8 ksi. The specimen size and fiber alignment of small-scale prism influenced the results which led to high results variations. The average interface shear resistance of un-cracked monolithic UHPC increases by 48% with the increase of transverse reinforcement ratio from 0 to 0.5% (Crane 2010).

Slant shear test is the most common test to evaluate the interface shear resistance of CC-UHPC without transverse reinforcement. Rangaraju et al. (2013) and Harris et al. (2011) followed the ASTM C882/C882M composite specimen dimensions. Different prismatic slant shear specimen dimensions were tested by Tayeh et al. (2012), Muñoz (2012), Aaleti and Sritharan (2017). Different interface plane angles with horizontal axis were investigated; 55°, 60°, and 70° (Muñoz 2012) and 53.1° (Aaleti and Sritharan 2017). Of those tests, the sand-blasted interface texture usually gives the highest interface shear resistance.

L-shape push-off test is the most common method for determining the interface shear resistance between two layers of concrete. L-shape push-off tests were conducted using 11.8x25.2x5.9 in. specimens without interface shear reinforcement. Five different surface treatments were applied to CC sections: smooth, water jet, grooved with 0.4 in. depth, grooved with 0.8 in. depth, and grooved with 1.2 in. depth. The CC and UHPC achieved compressive strength of 5.2 ksi and 29.08 ksi, respectively. Based on the results, the interface shear resistance of CC-UHPC increased with the increase of the grooved interface surface texture depth. Banta (2005) and Crane (2010) also conducted push-off testing to evaluate the interface shear resistance of normal weight and lightweight CC cast on hardened UHPC, which is different from the case of CC-UHPC as the surface of UHPC is almost impermeable and much harder to roughen compared to that of CC.

Limited research was done to evaluate the interface shear resistance of UHPC-UHPC. The interface shear resistance of UHPC-UHPC without reinforcement were 0.20 to 0.63 ksi for smooth and 0.4 in. grooved interface surface respectively (Jang et al. 2017). The interface shear resistance of UHPC-UHPC with transverse reinforcement were 0.21 and 0.56 ksi for 0%, 0.5% transverse reinforcement ratios respectively (Crane 2010). The interface shear resistance of UHPC-UHPC without transverse reinforcement increased with the increase of the surface roughening. The AASHTO equations underestimate the interface shear resistance of UHPC-UHPC, however, the Japanese recommendations overestimate it (kim et al 2018). The French Standard (NF-P-18-710 (2016)) has cohesion and friction factors for interface shear resistance of UHPC-UHPC.

CHAPTER 3: PROPOSED DECK-TO-GIRDER CONNECTION

This chapter presents a new UHPC connection between precast concrete deck panels and precast/prestressed concrete girders. This connection eliminates any changes to girder design/production and any possible conflict between deck and girder reinforcement. Two different interface shear planes are controlling the proposed connection: (a) at the soffit of the precast deck panels and (b) at the top of the precast/prestressed concrete girder. A study methodology is proposed to evaluate both interface shear planes. Also, a construction sequence of the new connection is illustrated using current bridge construction practices.

3.1. Connection Design and Detailing

Based on the literature review, the current precast concrete deck-to-girder connections using UHPC consist of open longitudinal joints or covered longitudinal troughs with exposed aggregate finish and grouting holes every 24 in. over each girder line. These two systems consume large quantities of UHPC to fill the joints and haunches that significantly impact the system economics due to the high price of UHPC. Also, using opened/covered longitudinal joints prevent transverse prestressing of concrete deck panels, which limits the use of full-width precast concrete deck panels.

To simplify the connection, the longitudinal joints and covered longitudinal troughs are eliminated and replaced with discrete round shear pockets. Figure 3.1 shows the proposed precast concrete deck-to-girder connection using UHPC shear pockets supported by precast/prestressed concrete girders. In this connection, discrete round shear pockets, 4 – 8 in. in diameter, are formed in the deck panels every 2 - 4 ft. over each

girder line. The diameter and spacing of these pockets are determined based on the interface shear demand. Girder shear reinforcement is the same as it is in case of CIP concrete bridge decks but terminated below the soffit of deck panels. Once all panels are installed at the desired elevation using support angles or leveling bolts, a loop bar is inserted in each shear pocket to cross the interface between the two components. The shear pockets and haunches are, then, filled with UHPC cast from the shear pocket openings to connect the two components and achieve the composite section. The side surface of the shear pockets should be roughened using either form liner or exposed aggregate to provide adequate bond between UHPC and the deck panel concrete. Also, blocks of compressible material are recommended as shown in Figure 3.1 to form the haunch area and reduce the quantity of field-cast UHPC. The same concept can be used to connect precast concrete deck panels to steel girders with conventional shear studs as shown in Figure 3.2, which is not the focus of this study. Figure 3.3 shows a rendered view of the proposed precast concrete deck-to-girder connections.

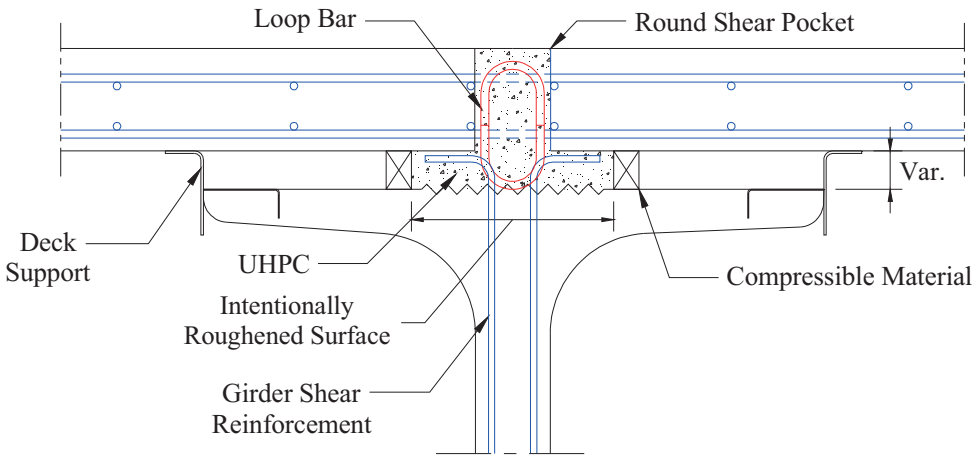

Figure 3.1. Proposed Precast Concrete Deck-To-Concrete Girder Connection

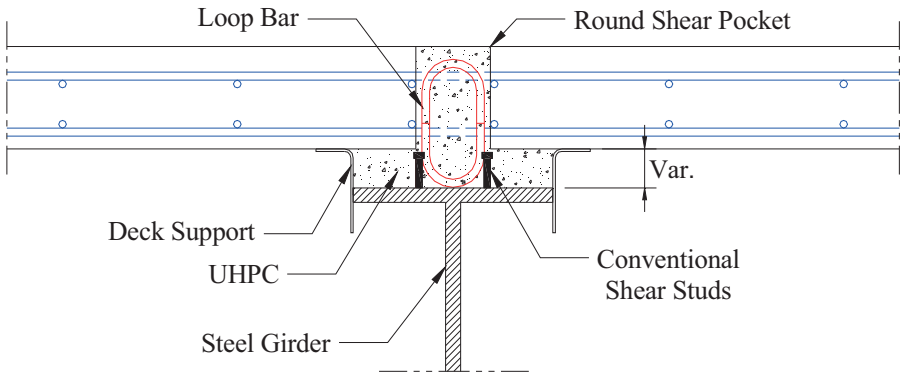

Figure 3.2. Proposed Precast Concrete Deck-To-Steel Girder Connection

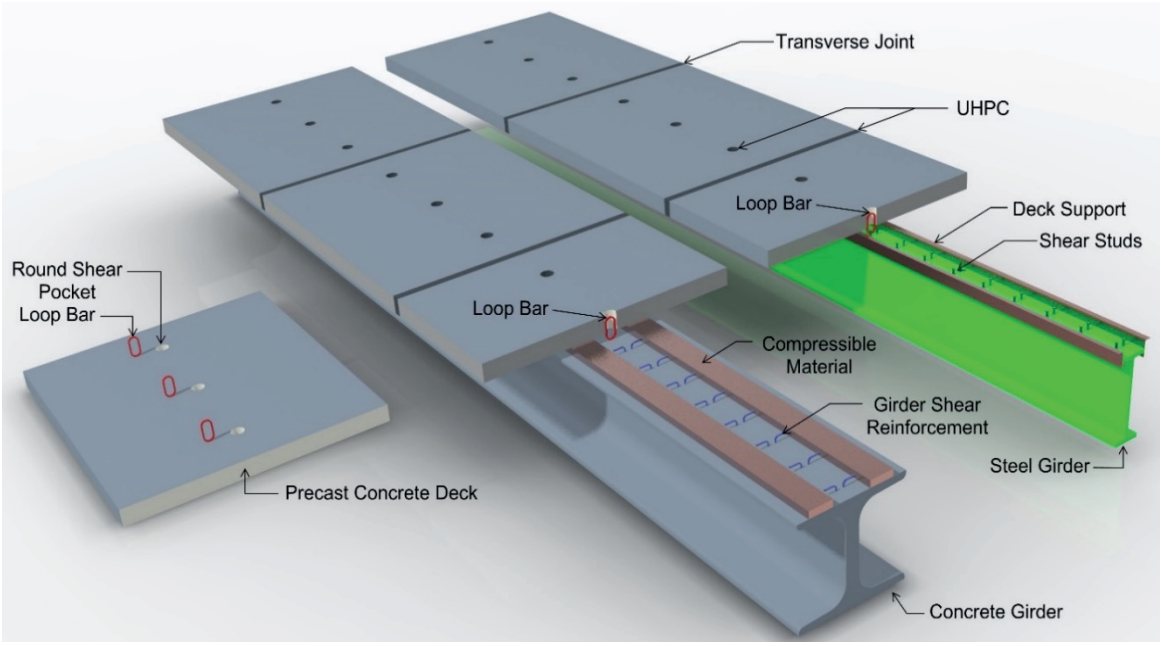

Figure 3.3. Rendered View for Proposed Precast Concrete Deck-To-Girder Connection

The proposed connection allows transverse prestressing of precast deck panels as shown in Figure 3.4. Prestressing the deck panels significantly decreases the deck reinforcement besides eliminating the need for forming the overhangs. Also, prestressing deck panels allows using large panels that reduce the construction time and minimize the

number of open joints that need to be ground for leveling the surface. The round shape of proposed shear pocket eliminates any tolerance limits for adding the loop bar and keep it in position as shown in Figure 3.2.

While the cost of UHPC is much higher than the cost of grout/flowable concrete, the advantages of using the proposed connection compared to existing systems are as following:

1. **Unchanged Girder Reinforcement**

One of the main goals of the proposed connection is keeping the girders design the same as conventional systems without any special requirement for interface shear reinforcement such as threaded rods. In addition, using UHPC as a grouting material reduces the amount of interface shear reinforcement needed for the connection resulting in less rebar congestion.

2. **Simple Construction**

The proposed connection offers an easy construction system that has no conflict between the interface shear reinforcement, loop bar, and the deck slab reinforcement. This enormously reduces the time of construction and eliminates any need of fitting the interface shear reinforcement inside the shear pocket at similar systems.

3. **Easy installation of interface shear reinforcement**

The unique design of round shear pocket and the associated loop bar which is added from the top of precast deck slab eliminate any conflict between the interface reinforcement. Also, adding the loop bar from the top allows adjustments based on the haunch thickness.

4. **Less reinforcement needed at shear pocket**

The proposed connection does not need any special reinforcement for the shear pockets at precast deck slab to achieve composite action. Similar systems require having heavy HSS at shear pockets with studs around the perimeter to anchor it to the precast deck panel. This requirement adds cost to the prefabrication of the precast deck panels which is eliminated by the proposed connection.

5. **Reducing the traffic closure and detouring period**

The proposed connection allows the bridge to open for traffic after just 3 days from casting UHPC. The UHPC gains around 12 ksi compressive strength in the first three days which is enough to achieve the composite action between precast deck slab and precast girder. Compared to conventional cast-in-place concrete deck, the proposed connection cuts down the project duration significantly. In addition, the excellent durability of UHPC eliminates the need for an overlay or other protection systems.

Based on the current experience of dealing with UHPC, there are some challenges in using UHPC, which are associated with being a new material. Examples are limited contractor experience in mixing and placing UHPC, which increases the total cost of UHPC. In addition, UHPC requires special mixers to be used on site. UHPC is highly thixotropic, which means it quickly forms a stiff layer (i.e. elephant skin) when casting is interrupted. Therefore, continuous casting or agitation is required to avoid forming cold joints. Also, the QC/QA of UHPC requires special training as its performance is very sensitive to material qualities, batching sequence, temperature, and water/superplasticizer content. These issues will be addressed in the following chapters.

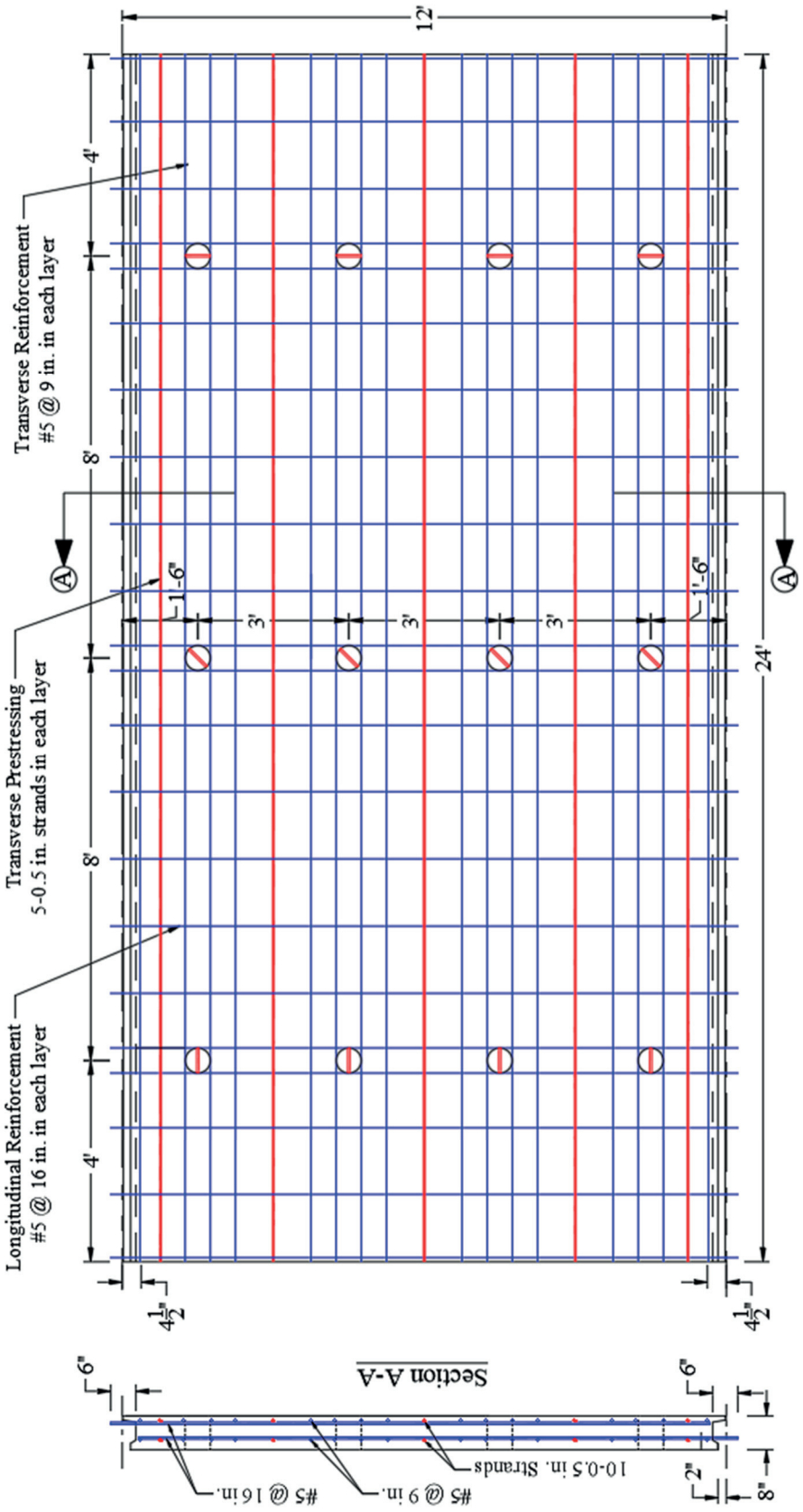

Figure 3.4. Reinforcement and Pre-Tensioning of the Panel with Proposed Connection.

3.2. Critical Interface Shear Planes

Two critical interface shear planes exist in the proposed connection as shown in Figure 3.5. The first plane is at the girder top surface between fresh UHPC and hardened conventional concrete (CC-UHPC), which is intentionally roughened surface as a common practice. The second plane is at the soffit of the deck panels across the monolithic UHPC. The loop bar placed in each pocket crosses the second plane to enhance its interface shear resistance. Also, the roughened side surface of the shear pocket prevents pocket pull-out from the deck panel concrete. Since the current code provisions do not provide concrete cohesion and shear-friction factors for predicting the interface shear resistance of either monolithic UHPC or CC-UHPC, experimental investigations are conducted to understand the new connection behavior and predict the interface shear resistance of connections.

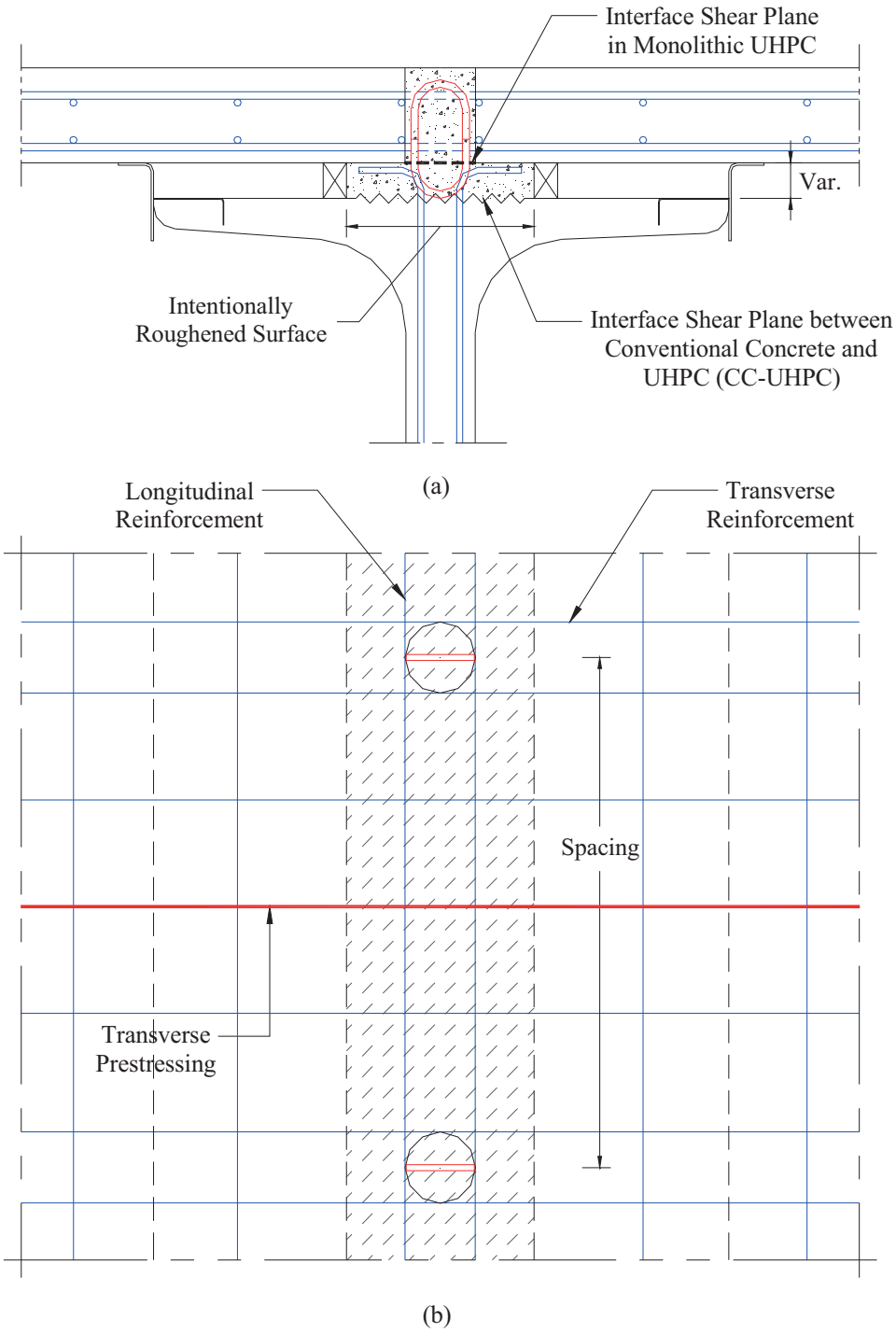

Figure 3.5. Interface Shear Resisting Area; (a) at the Top of the Concrete Girder and (b) at the Soffit of the Deck Panels

3.3. Construction Sequence of New Connection

The construction sequence of the new precast concrete deck-to-concrete girder using UHPC is presented in the following steps as shown in Figure 3.6:

1. Fabricate precast/prestressed concrete girders with conventional shear reinforcement and roughen the girder top flange according to the common practice.
2. Fabricate precast/prestressed concrete deck panels with discrete round shear pockets at designed spacing. Roughen side surface of the shear pockets using either form liner or exposed aggregate.
3. Erect all girders as shown in Figure 3.6.1a
4. Form, reinforce, and pour end diaphragms up to the girder top flange as shown in Figure 3.6.1b.
5. Conduct shim shots on the edges and center of each girder line to determine the actual profile of the cambered girders prior to panel erection.
6. Place blocks of compressible material to form the haunch area and use leveling bolts or shelf angles to achieve the desired deck elevation as shown in Figure 3.6.2a.
7. Attach extruded polystyrene panels to the top of concrete diaphragms between girders to fill the gap underneath the deck panels.
8. Place deck panels on the girders as shown in Figure 3.6.2b.

9. Fill the gaps between adjacent deck panels using backer rod and clean/moist the joint surface prior to casting UHPC as shown in Figure 3.6.3a.
10. Place loop bars in the shear pockets as shown in Figure 3.6.3b.
11. Pour UHPC to fill haunch, round shear pockets, and transverse joints between deck panels as shown in Figure 3.6.4. Pouring should continue until the UHPC overflows from every pocket.
12. Grind the top surface of UHPC to achieved leveled deck top surface.

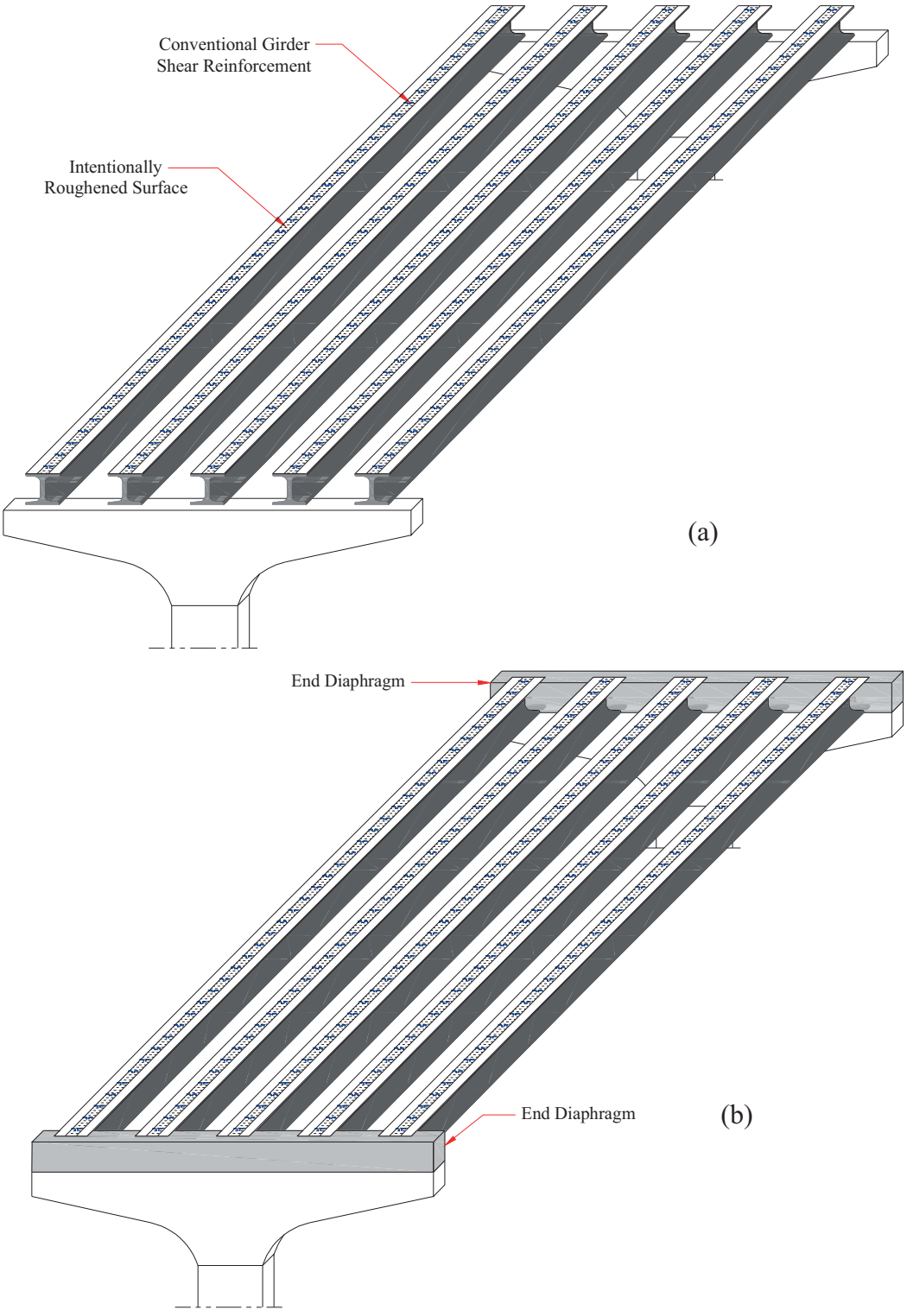

Figure 3.6.1. Construction Sequence of the Proposed Precast Concrete Deck-to-Concrete Girder Connection Using UHPC

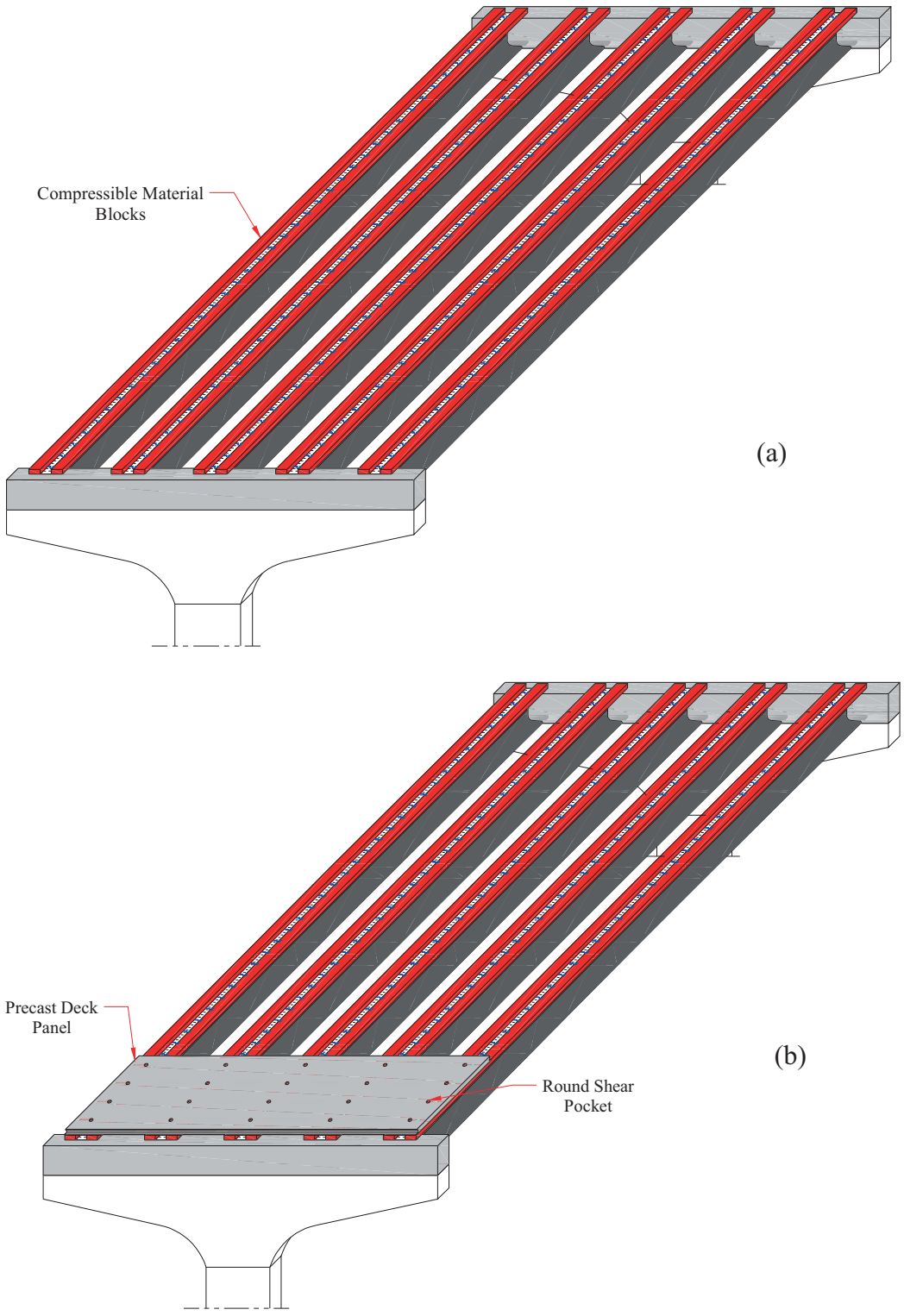

Figure 3.6.2. Construction Sequence of the Proposed Precast Concrete Deck-to-Concrete Girder Connection Using UHPC

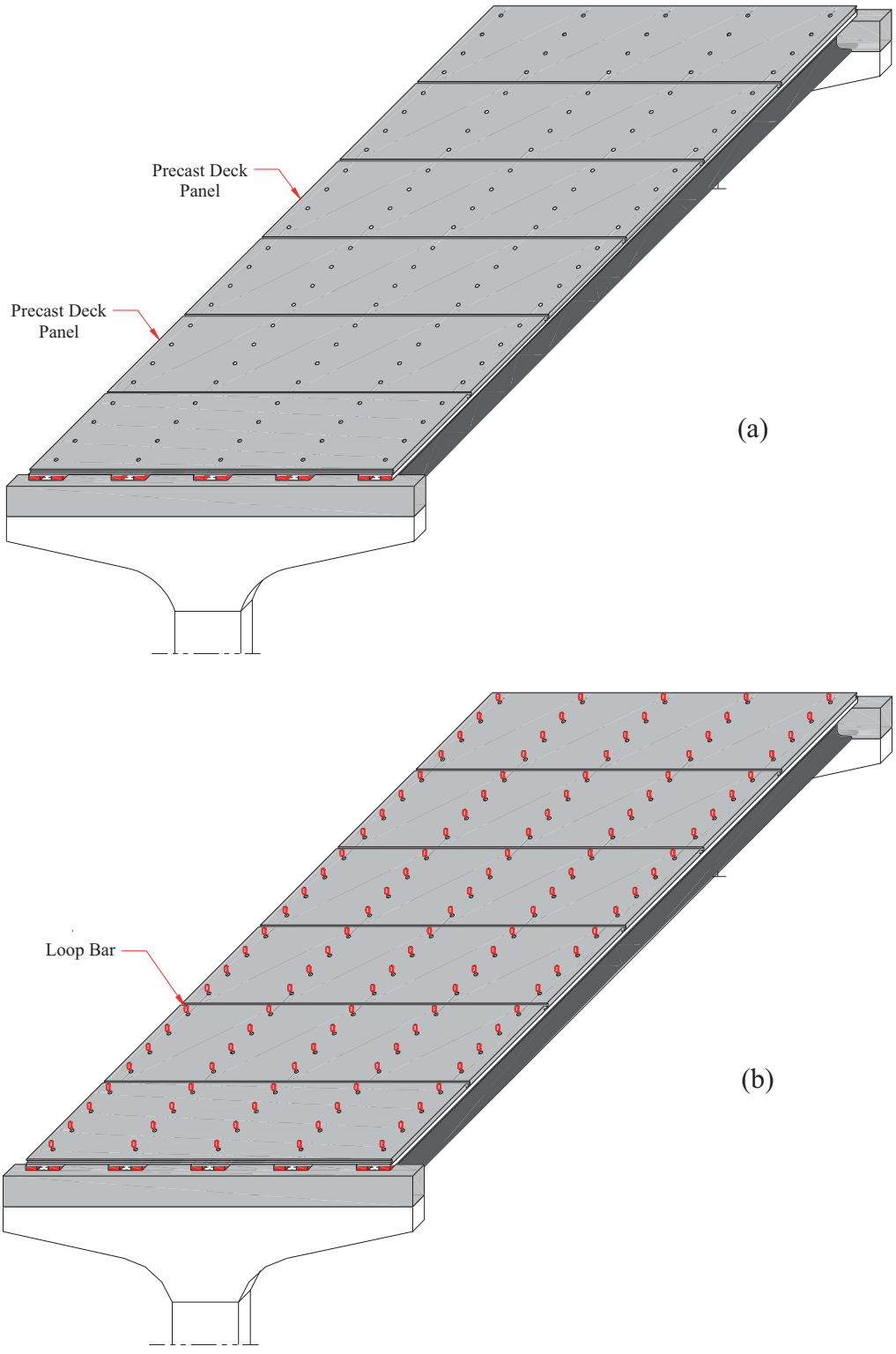

Figure 3.6.3. Construction Sequence of the Proposed Precast Concrete Deck-to-Concrete Girder Connection Using UHPC

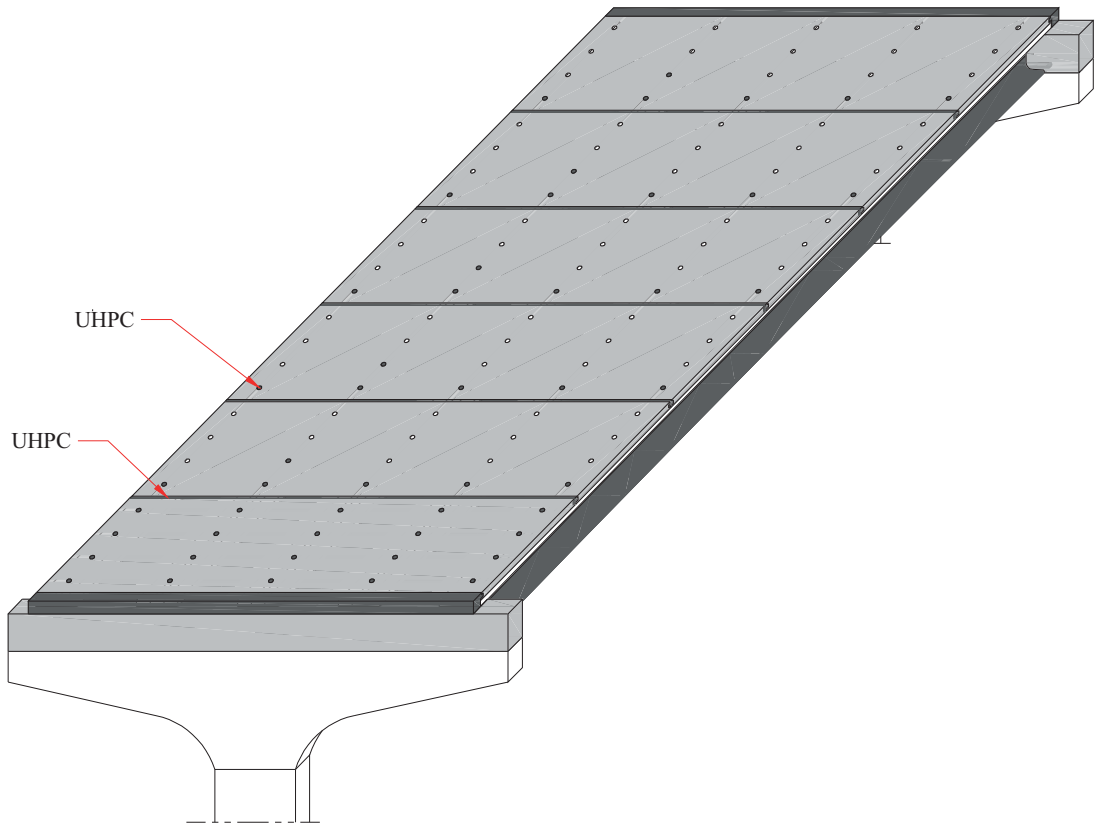

Figure 3.6.4. Construction Sequence of the Proposed Precast Concrete Deck-to-Concrete Girder Connection Using UHPC

3.4. Design Example

The PCI Bridge Design Manual (2014) design example 9.1a was adopted to be redesigned using the proposed connection. The design example is a 120 ft. single span AASHTO bulb-tee beam bridge with no skew. The width of the bridge is 51 ft. with 3 ft. overhang. Six precast/prestressed girders were used at 9 ft. spacing and made composite with an 8 in. thick cast-in-place CC slab as shown in Figure 3.7. The design loads used were ½ in. wearing surface and live load of HL-93 with impact besides the dead loads from girder, haunch, slab weight.

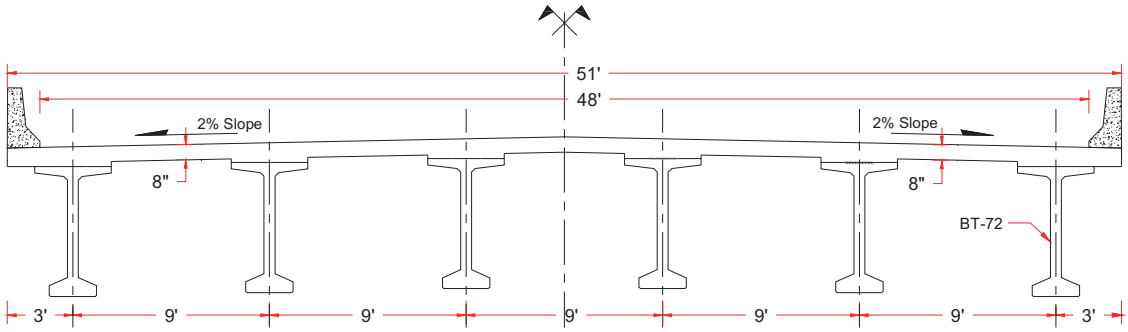

Figure 3.7. Designed PCI BDM Ex. 9.1a Bridge Layout.

The same input data were used with replacing the CIP deck slab with precast CC deck panels having the same thickness (8 in.) and using UHPC as a grouting material instead of CC through round shear pockets spaced at 4 ft as shown in Figure 3.8. The initial connection design is 6 in. diameter round shear pockets with #5 loop bar and minimum haunch of 4 in. to develop the #5 bar. The input from the PCI BDM design example 9.1a is used to calculate the interface shear demand as following:

1) Factored interface shear due to DW and LL at h/2 (DC does not apply to the composite section)

$$V_u = 1.50 * 10.8\ kip + 1.75 * 104.4\ kip = 198.9\ kip$$

2) Shear Depth "d_v" which is the distance from the center of tension steel to the middle of deck slab (AASHTO LRFD 2020)

$$d_e = 75.78\ in. \qquad \text{(PCI BDM Example 9.1a)}$$

$$d_v = d_e - \frac{t_s}{2} = 75.78\ in. - \frac{7.5}{2} = 72.03\ in.$$

3) Ultimate interface shear at critical section (V_{ui})

$$V_{ui} = V_u / d_v \qquad \text{(AASHTO LRFD Eq. C5.7.4.5-7)}$$

$$V_{ui} = \frac{198.9}{72.03} = 2.76\ kip/in.$$

4) Strength reduction factor (φ)

$$\varphi = 0.9 \qquad \text{(AASHTO LRFD Art. 5.5.4.2)}$$

5) Nominal interface shear at critical section (V_{ni})

$$V_{ni} = \frac{V_{ui}}{\varphi} = \frac{2.76}{0.9} = 3.07\ kip/in.$$

Therefore, the nominal interface shear resistance for the proposed connection is $3.07\ kip/in. x4\ ft. x12 = 147.36\ kip/4\ ft.$ which is the spacing between the shear pockets.

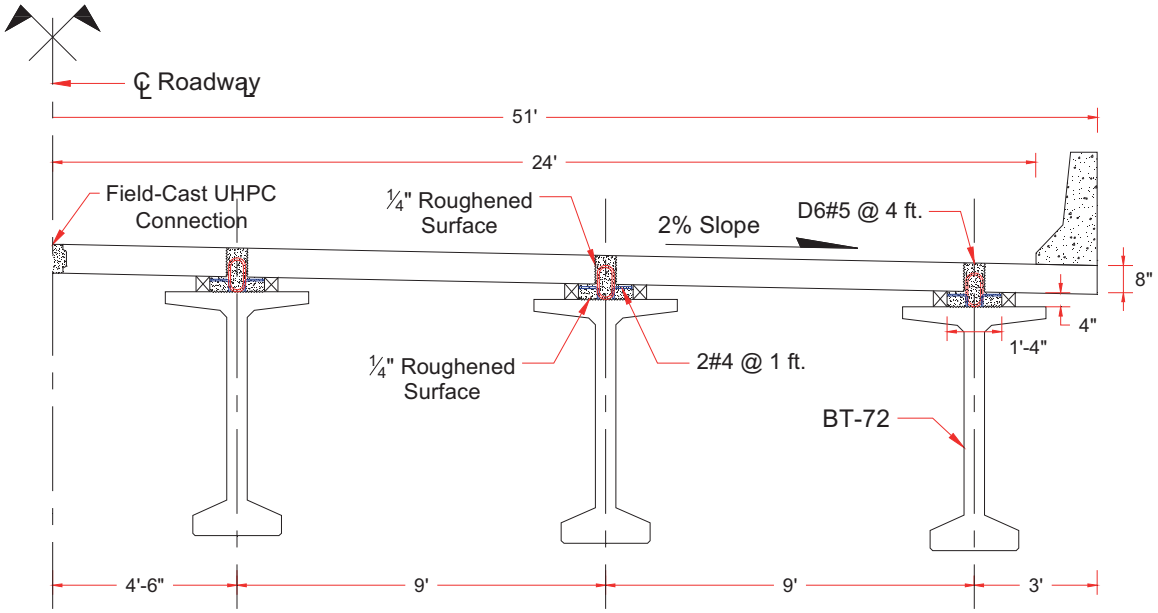

Figure 3.8. Designed PCI BDM Ex. 9.1a Bridge Cross-Section Using Proposed Connection

As mentioned previously, the current code provisions do not have a prediction interface shear factors for cases including UHPC. So, a study methodology including three stages; experimental investigation, numerical analysis, and design procedure, is

conducted to evaluate these factors. The experimental investigation started with obtaining the mechanical properties of three non-proprietary UHPC mixes developed by University of Nebraska-Lincoln (UNL) using local materials. These properties were compared to those of commercial UHPC mix obtained from the same test setups to promote the best mix (UNL UHPC). Then, small-scale testing was conducted to evaluate the interface shear resistance of the connection critical sections using slant shear and L-shape push-off tests for CC-UHPC interface; and direct shear, L-shape, and double shear push-off tests for monolithic UHPC. Concrete cohesion and friction factors for interface shear resistance of UHPC were proposed based on the experimental testing findings. A finite element model (FEM) was created using ANSYS 2020 R2 software to conduct a parametric study on the shear pocket diameter, interface shear reinforcement, and reinforcement grade. Full-scale push-off specimens simulating the actual connection were designed and tested to evaluate the structural performance and constructability of the new connection. Finally, an example bridge is presented to demonstrate connection design using the proposed factors and perform cost analysis. Figure 3.9 shows a chart that illustrates the study methodology.

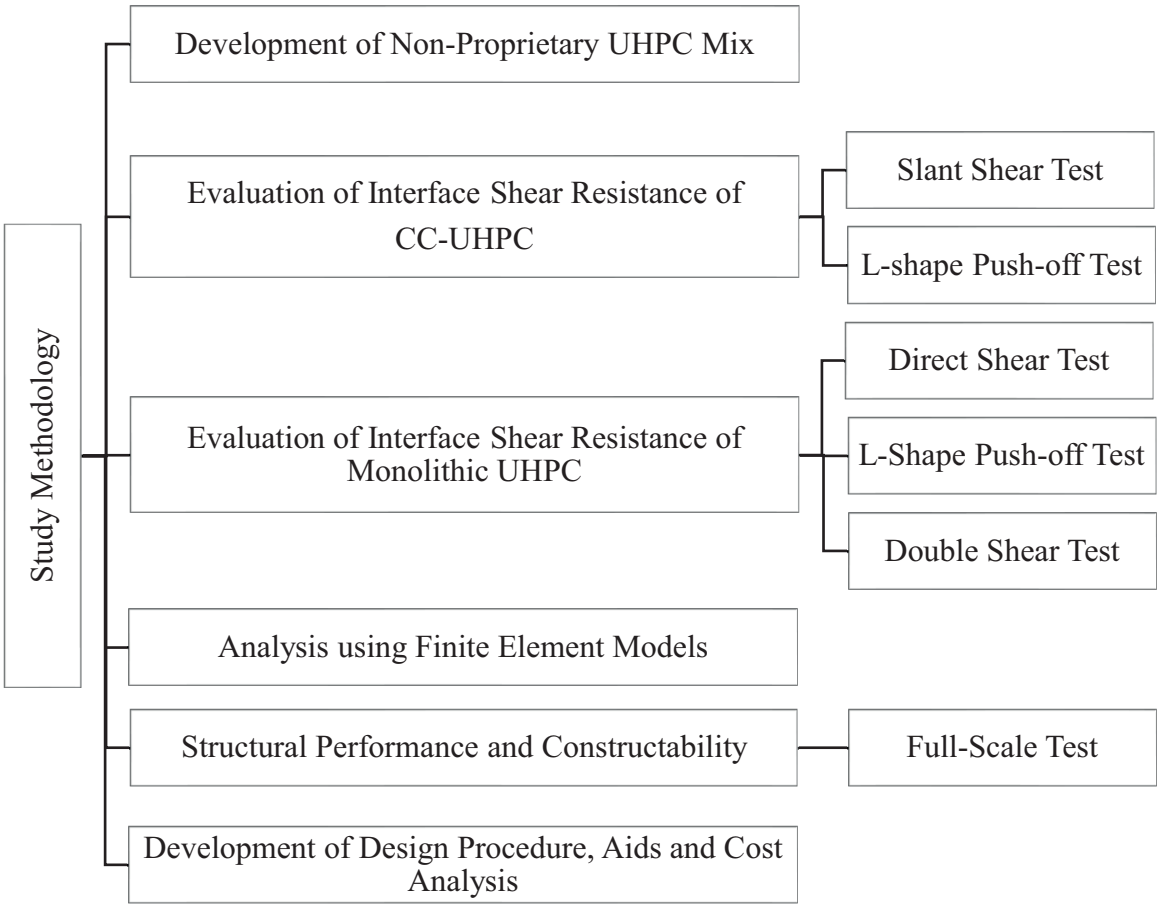

Figure 3.9. Study Methodology

CHAPTER 4: DEVELOPMENT OF NON- PROPRIETARY ULTRA-HIGH PERFORMANCE CONCRETE(UHPC) MIX

This chapter presents the development of non-proprietary UHPC mix using local materials. Three non-proprietary UHPC mixes developed by University of Nebraska-Lincoln (UNL) were tested to determine the best mix based on mechanical properties. The evaluated mechanical properties are: compressive strength, modulus of elasticity and Poisson's ratio, flexural strength, splitting tensile strength, and rebar development length. The obtained properties were compared to those of a commercial UHPC mix. The selected non-proprietary mix was named UNL-UHPC and was used in the experimental investigation.

4.1. UHPC Mix Design Requirements

Different organizations have different requirements that characterize UHPC. ASTM C1856 (ASTM, 2017) specifies a minimum compressive strength of 17,000 psi (120 MPa), maximum aggregate nominal size of aggregate of 1/4 in (5 mm), and flow between 8 and 10 inches (200 and 250 mm) measured using the flow table test. On the other hand, Federal Highway Administration (FHWA) (Haber et al., 2018), and American Concrete Institute ACI 239 (ACI 239R-18, 2018) define UHPC as a cementitious composite material composed of an optimized gradation of granular constituents, w/b less than 0.25, and a high percentage of discontinuous internal fibers reinforcement. The mechanical properties of UHPC include compressive strength greater than 21,700psi (150MPa) and sustained post-cracking tensile strength greater than 720 psi (5 MPa). Besides, other state agencies such as the New York State Department of

Transportation (NYDOT, 2013), Georgia Department of Transportation (GADOT, 2015), and District Department of Transportation (DCDOT, 2014) require UHPC to have a minimum 28-day compressive strength of 21,000psi (145MPa). Montana Department of Transportation (Berry et al. 2017) and California Department of Transportation (CALTRANS, 2016), require a minimum 28-day compressive strength of 20,000psi (137MPa). Some other state agencies such as Iowa Department of Transportation (IADOT, 2011) and Michigan Department of Transportation (El-Tawil et al. 2018) requirements include the minimum 4-day compressive strength, with which Iowa requires 10,000 psi (68MPa) and Michigan requires 12,000psi (83MPa).

According to ACI 239 (ACI 239R-18, 2018), the high performance of UHPC is due to its discontinuous pore structure and the reduced void space in the matrix. It is implied that the level of stress transferred between particles is reduced when the contact points between particles are increased. Thus, the proper selection of materials is very important. The reduction of the level of stress improves the mechanical properties because it alleviates the formation of microcracks. Also, UHPC is expected to have a discontinuous pore structure, which reduces the ingress of liquids and significantly enhances its durability compared to conventional concrete.

The flexural strength properties are evaluated based on ASTM C1609 test and the minimum requirements for steel fiber-reinforced concrete stated by ACI-318-19 Section 26.12.7 and Sim et al (2020). These requirements are as following:

1. The minimum flexural strength at first crack and peak flexural strength are 1.50 ksi and 2 ksi, respectively and the peak flexural strength is greater

than 125% of the measured first-crack strength obtained from a flexural test.

2. The residual strength obtained from flexural testing in accordance with ASTM C1609 at a midspan deflection of 1/300 of the span length is greater than 90% of the measured first-peak strength obtained from a flexural test.
3. The residual strength obtained from flexural testing in accordance with ASTM C1609 at a midspan deflection of 1/150 of the span length is greater than 75% of the measured first-peak strength obtained from a flexural test.

4.2. Non-proprietary UHPC Mix Design

The current use of UHPC in the U.S. is limited mostly to proprietary, pre-packed products provided by international suppliers because of the highly-sophisticated design of the mixture, the mixing procedure, and in some cases, the limited availability of raw materials. The high costs associated with these products, which can be as much as $2,000 per cubic yard plus the costs associated with batching, placing, and curing, have been a major impediment for the extended use of UHPC. Therefore, Nebraska Department of Transportation (NDOT) funded a project (SPR-P1(18) M072) conducted by University of Nebraska-Lincoln (UNL) to develop a non-proprietary UHPC mix using local materials available in Nebraska. This developed mix needs to meet the same performance of commercially available mixes while being cost competitive.

Figure 4.1 shows a schematic depiction of the difference between the matrix structure of conventional concrete and UHPC. The UHPC structure is packed densely with minimum voids between the particles, while the structure of conventional concrete is loosely packed. To achieve a high particle packing, Table 4.1 shows the materials used in developing the non- proprietary mixes. These materials were selected based on extensive investigation that can be found in Mendonca et al. (2020).

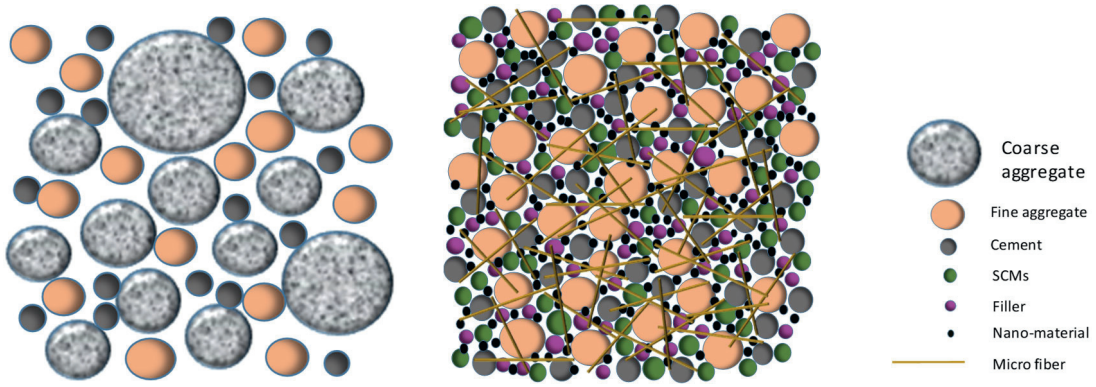

(a) Conventional concrete (b) UHPC

Figure 4.1. Schematic difference between particle packing in conventional concrete and UHPC (Mendonca et al. 2020).

Table 4.1

The materials Used in Developing the Non- proprietary Mixes (Mendonca et al. 2020).

Sand	No.10 silica sand
Cement	Type I/II
Slag	Grade 100 Slag
Silica fume	Force10,000 densified microsilica
Fiber	13/.20 mm micro steel fiber
HRWR	Premia 150

Table 4.2 lists the final non-proprietary and commercial UHPC mixes proportion. The mechanical properties of three non-proprietary UHPC mixes, UHPC 1450, UHPC 1700, and UNL-UHPC are investigated and their comparison to a commercially available UHPC mix. The mechanical properties results include compressive strength, modulus of elasticity and Poisson's ratio, flexural strength, splitting tensile strength, direct tension strength and rebar development length. All UHPC mixes listed in Table 4.2 were developed in large quantities (2.5 ft^3) to allow making the specimens required for the tests listed in Table 4.3. Most of mechanical properties testing was performed based on the corresponding ASTM as shown in Table 4.3 otherwise FHWA reports, and previous research were used. All the mechanical properties testing was conducted at 28 days except for UHPC 1450 at 56 days.

Table 4.2

Mix Proportions of Non-proprietary and Commercial UHPC (Mendonca et al. 2020)

Constituent	Weight (Ib/yd^3)			
	UHPC 1450	UHPC 1700	UHPC 1900	Commercial
Cement I/II	878	1070	1178	
Silica Fume	117	143	152.7	
Slag	425	518	570	Pre-bagged
Powder Content	1420	1731	1900.7	
#10 Sand	2119	1925	1663.7	
Water + Ice	241	289	317	219
HRWRA[a]	55	61	61	34
WRA[b]	-	-	-	17
Fiber	267	283	263	263
w/b	0.196	0.192	0.189	-

[a] High Range Water Reducer Admixture (Chryso Premia 150)
[b] Workability Retaining Admixture (RheoTech Z-60)

Table 4.3

UHPC Mechanical Properties Testing Matrix

Test	Reference	Specimen	Number
Compressive Strength	ASTM C1856	Cylinders 3″x6″	9
Modulus of Elasticity & Poisson's Ratio	ASTM C469/C469M	Cylinders 4″x8″	3
Flexural Strength	ASTM C1856 & ASTM C1609/C1609M	Prism 3″x3″x14″	3
Splitting Tensile Strength	ASTM C496	Cylinders 4″x8″	3
Rebar Development Length	Roy, et al. (2017)	Prism 8″x9″x3″	3

4.3. Mixing Procedure and Curing Process

The mixing procedure for the presented non-proprietary mixes was developed by UNL research team after several iterations and depending on engineering judgment. A mortar mixer, as shown in Figure 4.2, was utilized to mix the UHPC components in steps to achieve good UHPC quality and avoid any fiber clumping and forming raw materials balls. The mixing procedure is explained briefly as follows and mainly relies on engineering judgment at the time of mixing, extensively explained in Mendonca et al. (2020):

1. The sand is air-dried for several days before mixing and its moisture content is measured prior to storage until the day of mixing. The moisture content of sand is a part of the UHPC water-content and must be considered.

2. The air-dried sand and silica fume are first loaded into the mixer and mixed for three minutes.
3. Add cement and slag and mix for another three minutes.
4. Add approximately 75 % of the premixed liquids (water and HRWR) into the mixer. Adding ice as a portion of the water content or using chill water rely on the temperature at the day of mixing which can vary from 25% to 75%. The main idea of adding ice or using chill water is reducing the mix temperature and avoiding low flowable UHPC because of early hydration reaction.
5. After approximately five minutes of mixing, the mix starts to be wet and some flowability can be observed.
6. Add the remaining 25% of the premixed liquids (water and HRWR) into the mixer and mix for 5 more minutes or until consistency and flowability are observed.
7. When the mix starts to be flowable and consistency is observed, add the fibers and mix for additional 3 minutes.

Figure 4.2. Mortar Mixer Used for Mixing UHPC

The mixer should be working during the mixing procedure without stopping to add the materials. Again, the mixing procedure depends on the engineering judgment and several conditions can change the mixing duration such as mixing quantities, type of mixer and materials. The mix is considered acceptable when it achieves 8 in. to 10 in. flowability measured using a 10 in. diameter flow test table for mortar.

The mechanical properties test specimens were prepared as following:

1. The cylinders were cast on 45° and then tapped on the side to minimize the entrapped air.
2. The prisms were cast from one and allow the UHPC to flow to the other end to help align the fibers.

The specimens were stripped out of the forms after 24 hours and subjected to standard curing procedure until the day of testing. The standard curing procedure is submerging the specimens in lime-saturated water at temperature of 73º F (room temperature).

4.4. Compressive Strength

According to ASTM C1856-17, 3 in. x 6 in. cylinders were used to determine the compressive strength of UHPC mixes and were tested at 4, 7, 28, and 56 days. The cylinders were cast on an angle of 45º and then tapped on the side to minimize the entrapped air inside the specimens. The cylinders were stripped out of the molds after 24 hours and had standard curing procedure. Cylinder ends were ground mechanically using cylinder end grinder manufactured by Marui Co., LTD., as shown in Figure 4.3, to ensure flat and level surface at both ends and the consistency of test results.

According to ASTM C1856, a load rate of 150 psi/sec. was applied on the ground cylinders using axial loaded compression machine until failure. A minimum of three specimens were tested from each mix at a specific age. Figure 4.4 shows the average compressive strength versus age of UHPC for each mix. However, UHPC 1900 mix achieved a compressive strength of 17.77 ksi at 28 days UHPC age. UHPC 1700 achieved 17.2 ksi at 56 days which both satisfies the ASTM C1856 requirement of 17 ksi. UHPC 1900 mix showed good agreement with the FHWA (2018) report as it reached 19.93 ksi at 56 days with standard curing. Testing results are available in Appendix A.

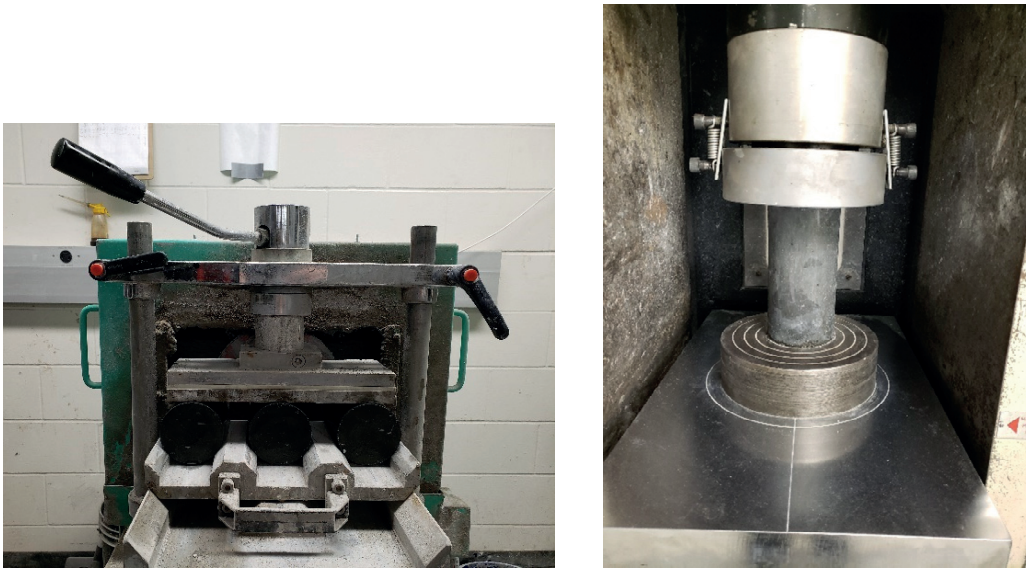

Figure 4.3. Cylinder End Grinding and Testing

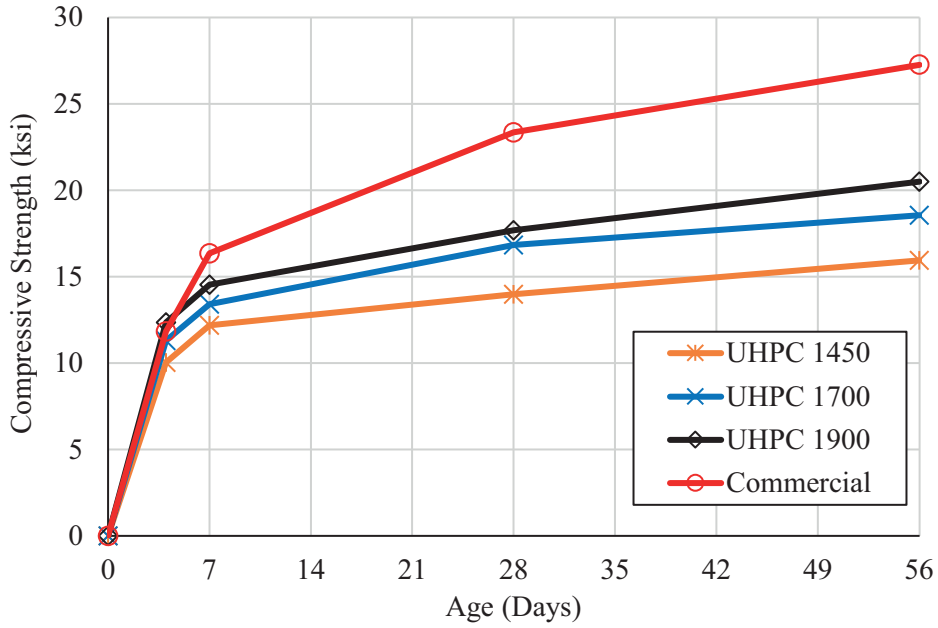

Figure 4.4. Average Compressive Strength Versus Age of Non-Proprietary and Commercial UHPC Mixes

Since the concrete compressive strength is dependent on the type of curing used, the effect of two different curing procedures was evaluated for UHPC 1900 mix. Two accelerated curing procedures were investigated: oven curing method, and hot bath method.

Oven curing method was conducted on nine cylinders and according to the PCI Architectural Quality Control Manual. The specimens were cast in plastic molds and immediately covered and left at the room temperature for 6 hours to allow initial set. Cylinders were then moved to an oven whose temperature was set at 90º F. After one hour, the temperature was increased by 15º F per hour for three hours until the oven temperature reaches 135º F. The specimens were left at 135º F for 9 hours. Then, the temperature was reduced in intervals of 10º F per hour until the oven temperature reached 90ºF. After one hour at 90ºF, the cylinders were removed from the oven, stripped out, and placed in lime saturated water until day of testing.

Following steam curing procedure presented on report No. FHWA-HRT-13-060, hot bath method was conducted on nine cylinders. The cylinders were cast in plastic molds and immediately covered and left at the room temperature for 6 hours to allow initial set. Cylinders were then carefully moved out of the molds and submerged in hot water bath with constant water temperature of 182º F. After 58 hours, the cylinders were removed out water and left to cool down in air then placed in lime saturated water until day of testing. Figure 4.5 shows the temperature setting profile for oven and hot bath accelerated curing methods.

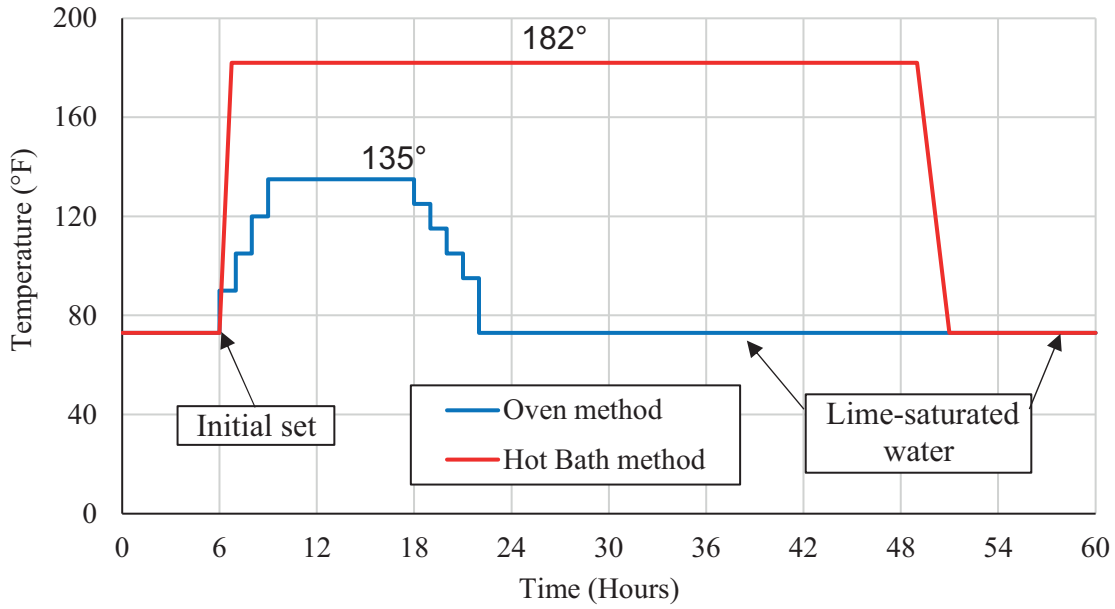

Figure 4.5. Temperature Setting Profile for Oven and Hot Bath Accelerated Curing Methods.

The cylinders of UHPC 1900 mix which were cured using the above-mentioned accelerated curing procedures and those that were standard cured were tested at 1, 4, 7, and 28 days. The average compressive strength was plotted as shown in Figure 4.6. This figure indicates that the accelerated curing procedures result in approximately 68% and 119%

higher 1-day compressive strength than standard curing procedure for oven and hot bath curing procedures, respectively. The hot bath method cylinders achieved 21.25 ksi which is 20% higher than standard cured.

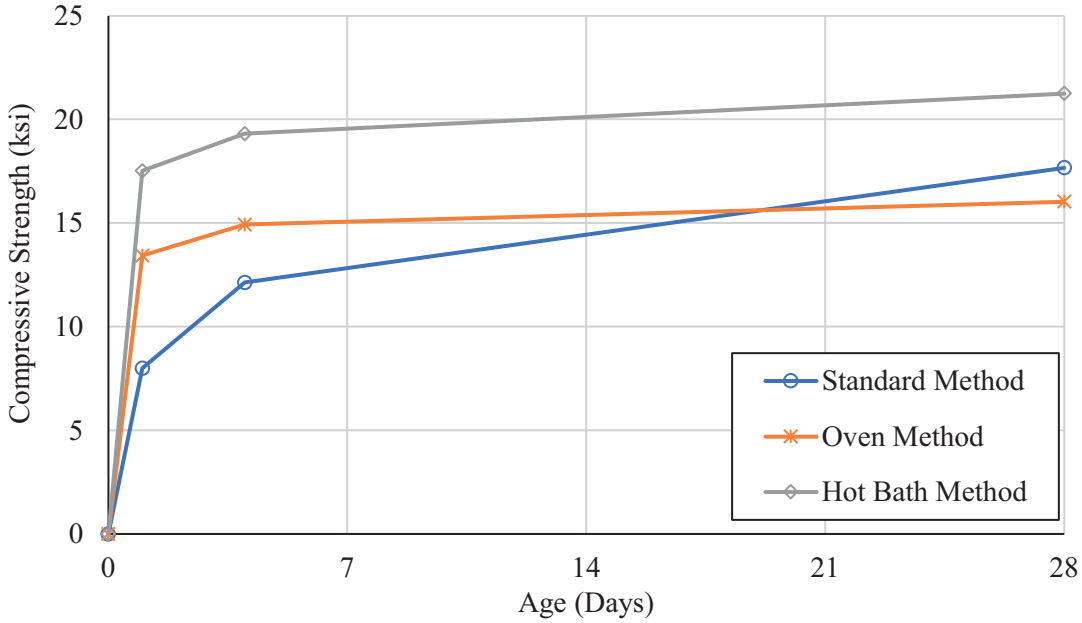

Figure 4.6. Accelerated and Standard Curing Procedures Average Compressive Strength.

Several separate batches were conducted to evaluate the repetition of UHPC 1900 mix and its mixing procedure in large batches (from 2.0 $ft.^3$ to 3.20 $ft.^3$). Figure 4.7 shows the compressive strength of a minimum of three cylinders at different ages of UHPC 1900 mix. The high coefficient of determination (R^2) of the trendline model shows strong correlations with the recorded compressive strength and indicates adequate repeatability of mixing procedures.

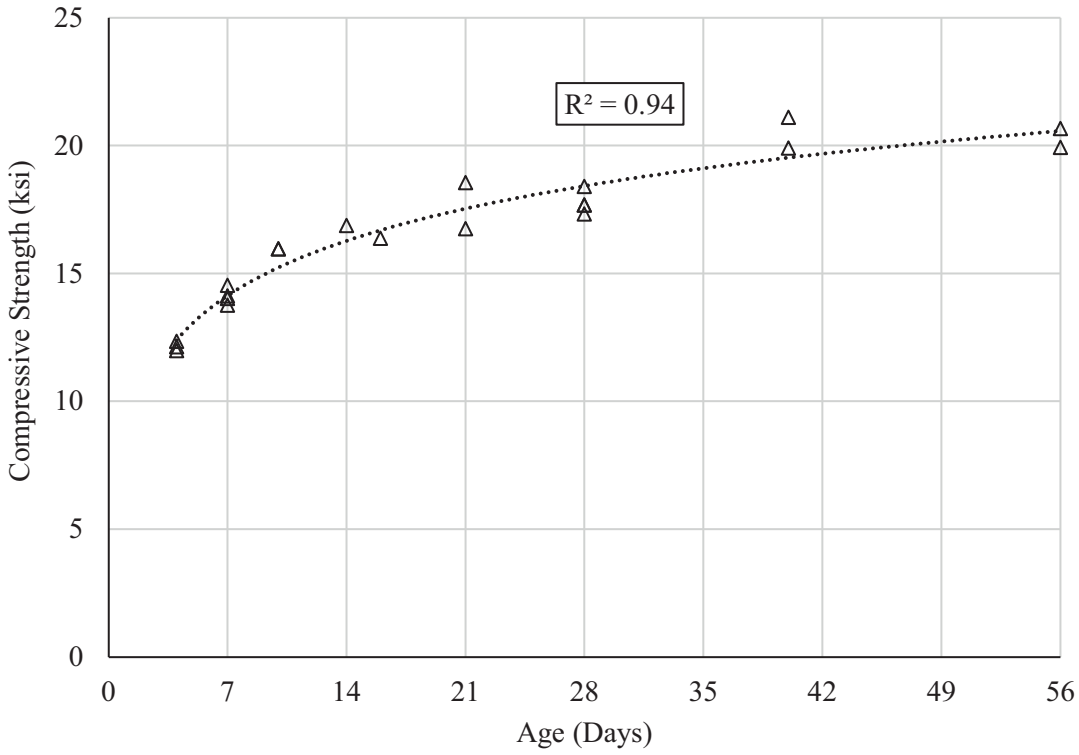

Figure 4.7. Compressive Strength versus Age for Several Batches of UHPC 1900 Mix.

4.5. Modulus of Elasticity & Poisson's Ratio

Three 4 in. x 8 in. cylinders from each UHPC mix were tested for modulus of elasticity (MoE) and Poisson's ratio according to ASTM C469, specified by ASTM C1856-17. The cylinder ends were ground to insure flat and level surface using end grinder machine. A uniaxial compression machine was used to test the cylinders while measuring the concrete strain using attached Compressometer/Extensometer cage as shown in Figure 4.8. Each cylinder was loaded to approximately 40% of its compressive strength. The average MoE and Poisson's ratio obtained from three tested cylinders for non-proprietary and commercial UHPC mixes are plotted in Figures 4.9 and 4.10. For comparison purposes, the MoE and Poisson's ratio of a 6 ksi conventional concrete is

presented to show the superior properties of UHPC. No significant difference was observed in the modulus of elasticity for non-proprietary mixes. The measured MoE was lower than the commercial UHPC as it depends mainly on the compressive strength value. Also, the Poisson's ratio of UHPC 1900 was lower than other two non-proprietary mixes and close to the commercial mix.

Figure 4.8. Modulus of Elasticity Test Setup.

According to AASHTO LRFD Bridge Design Specification (2020), the modulus of elasticity can be calculated with the following equation for normal concrete with design compressive strength up to 15 ksi and unit weight between 0.090 to 0.155 kcf.

$$E_c = 120000 K_1 w_c^{2.0} f_c'^{\,0.33} \quad (4.1)$$

Where:

E_c = modulus of elasticity (ksi)

K_1 = correction factor for source of aggregate to be taken as 1.0 unless determined by physical test, and as approved by the owner.

wc = unit weight of concrete (kcf)

fc' =compressive strength of concrete for use in design (ksi)

Based on Report No. *FHWA-HRT-18-036*, the modulus of elasticity can be calculated with the following equation.

$$E_c = 1430\sqrt{f_c'} \quad (4.2)$$

The obtained modulus of elasticity for the non-proprietary mixes were compared to predicted values by AASHTO LRFD 2020 and report No. FHWA-HRT-18-036 as shown in Figure 4.9. However, the measured MoE showed good agreement with FHWA-HRT-18-036 predicted values, the AASHTO LRFD 2020 predicted values gave higher MoE as the prediction equation was designed for conventional concrete. Testing results are available in Appendix A.

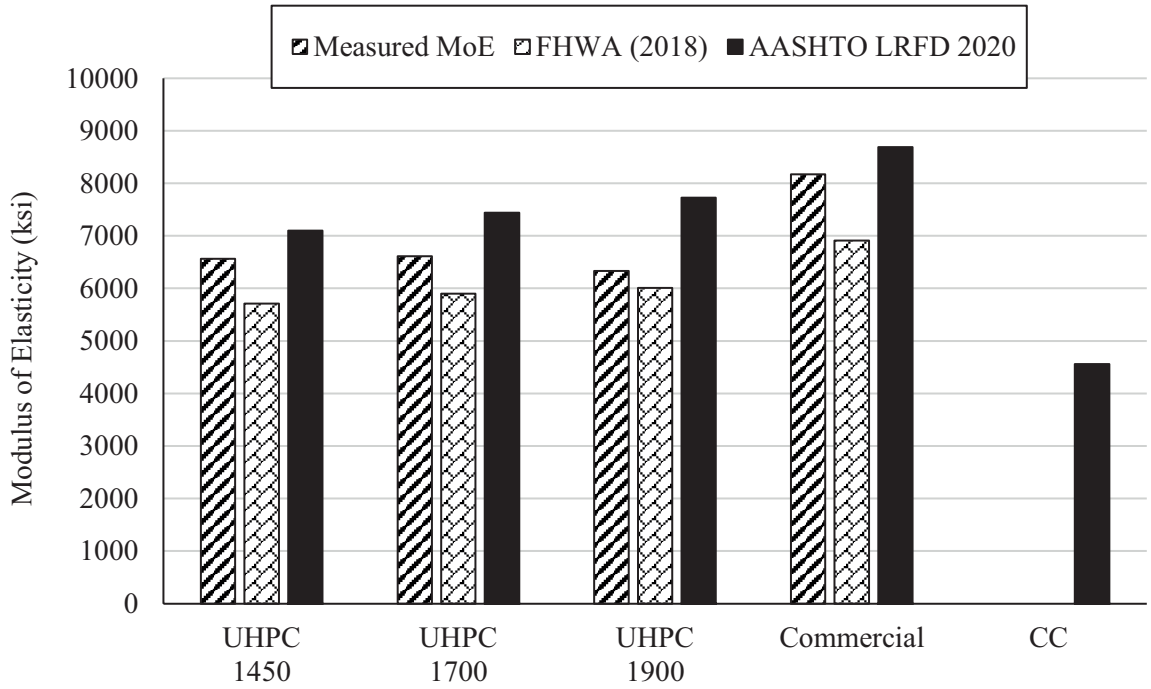

Figure 4.9. Average Modulus of Elasticity for the Non-proprietary and Commercial UHPC Mixes and Comparison to Predicted Values.

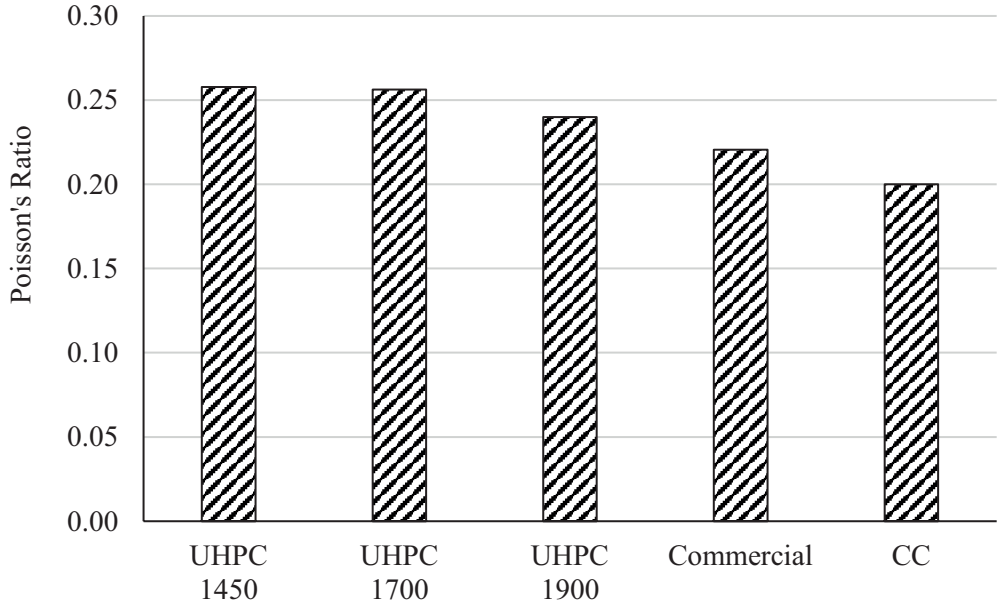

Figure 4.10. Average Poisson's Ratio for the Non-proprietary and Commercial UHPC Mixes

4.6. Stress-Strain Behavior

Three 4×8in. cylinders of UHPC 1900 mix were cast and used for obtaining the stress-strain behavior. Two strain gauges, 2 in. long each, were attached vertically to the side of each specimen at the middle section to measure longitudinal strains. Figure 4.11 shows the specimen placed in the compression machine and loaded according to ASTM C1856 (ASTM, 2017), with a load rate of 150 psi/sec. until failure. The measured compressive stress and corresponding strain were plotted as shown in Figure 4.12. The modulus of elasticity was calculated based on the slope of the secant at 40% of the ultimate load according to ASTM C469 (ASTM, 2014). The average modulus of elasticity was found to be 6920 ksi. The average peak compressive stress and strain were 21.07 ksi and 0.0035. It should be mentioned that the top steel plate used to apply the

load was bent at 16 ksi in the first specimen and, therefore, the ultimate stress and strain of this test were aborted, and a thicker plate was used with the remaining two specimens.

Figure 4.11. Test Setup for Obtaining Stress-Strain Behavior.

Based on *FHWA-HRT-18-036*, the stress-strain curve can be predicted using the following equations:

$$f_c = \varepsilon_c E(1 - \alpha) \tag{4.3}$$

Where, ε_c is the compressive strain, f_c is the compressive stress (ksi) corresponding to ε_c, E is the modulus of elasticity (ksi), and α is the linearity deviation parameter which is calculated as following:

$$\alpha = a\left(\frac{\varepsilon_c E}{f_c'}\right)^b \tag{4.4}$$

Where, ε_c is the peak compressive strain, f_c' peak compressive stress (ksi), and a and b are curve fitting parameters depending on the UHPC mix. According to *FHWA-*

HRT-18-036, average values for *a* and *b* are 0.106 and 2.754, respectively. Figure 4.12 shows the measured and predicted stress-strain curve for UHPC 1900 mix. The predicted stress-strain curve using these fitting parameters shows good agreement with the measured values.

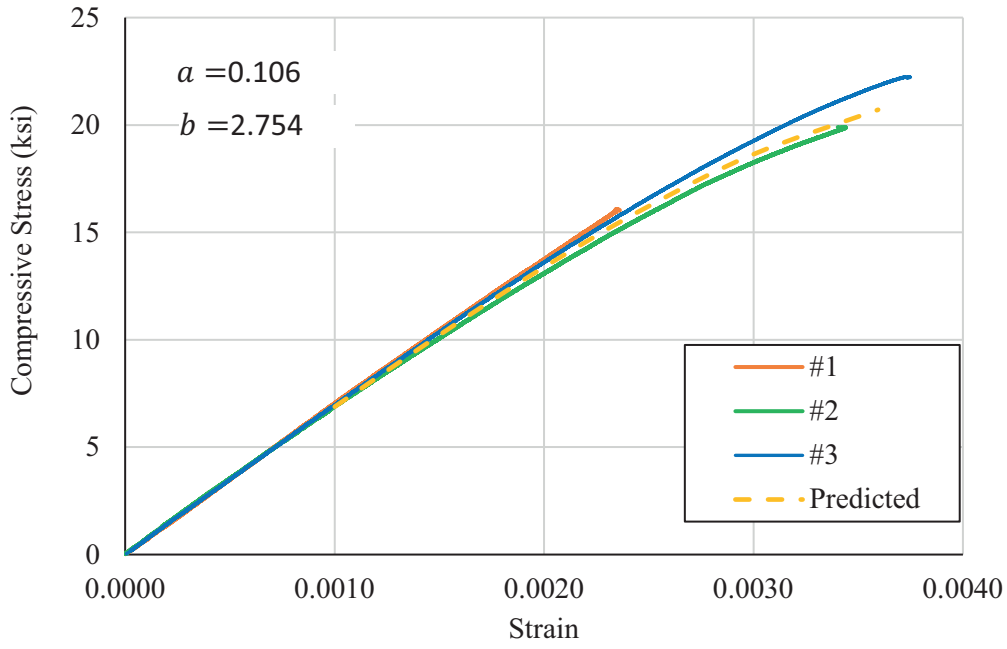

Figure 4.12. Stress-Strain Behavior Obtained for UHPC 1900 Mix and Its Comparison with the Prediction Equations

4.7. Flexural Strength

According to ASTM C1856-17, the flexural strength test of UHPC follows the ASTM C1609/C1609M for flexural performance of fiber-reinforced concrete and size of specimen changes according to fiber length. The steel fibers used had a length of 0.5 in. which allows a minimum cross section for flexure specimen of 3 in. x 3 in. According to ASTM C78, the minimum effective length (L) of the flexural specimen is three times the depth of the specimen which should not be less than 12 in. Three 3x3x14 in. prisms from

each mix were tested for flexure strength according to ASTM C1609/C1609M using four-point loading as shown in Figure 4.13. A Tinius Olson testing machine was used to apply compression load on the specimens to failure. According to ASTM C1609/C1609M, a displacement rate up to 0.003 in./min was applied until a mid-span deflection of (L/900) and then increased gradually up to 0.008 in./min. until a mid-span deflection of (L/150). The specimen mid-span deflection was captured using two LVDTs connected to the steel base and pointing to a steel frame attached to the specimen top at middle section. The width and depth of each prism was measured to accurately calculate the flexural strength. All beams exhibited cracks at the middle third of the span as shown in Figure 4.14; therefore, all results are valid.

Figure 4.13. Flexure Strength Test Setup.

(a) (b) (c)

Figure 4.14. Flexure Specimen Failure. (a) UHPC 1450, (b) UHPC 1700, and (c) UHPC 1900

The flexural strength was calculated using bending theory for linear elastic materials and gross (uncracked) section properties according to ASTM C1609/C1609M. Figure 4.15 and Figure 4.16 show the calculated flexural strength versus midspan deflection for UHPC mixes. The flexural test results were compared to the ACI-318-19 limits for flexural strength of fiber reinforced concrete. Figure 4.17 shows the flexural test results of the UHPC mixes and their comparison to ACI limits. Table 4.4 and Figure 4.17 show that all the mixes satisfy the ACI limits including UHPC 1700 which shows the lowest values because of fiber segregation as shown in Figure 4.15(b). The UHPC 1900 mix flexural curve showed agreement with the commercial UHPC mix and satisfied ACI-318-19 limits.

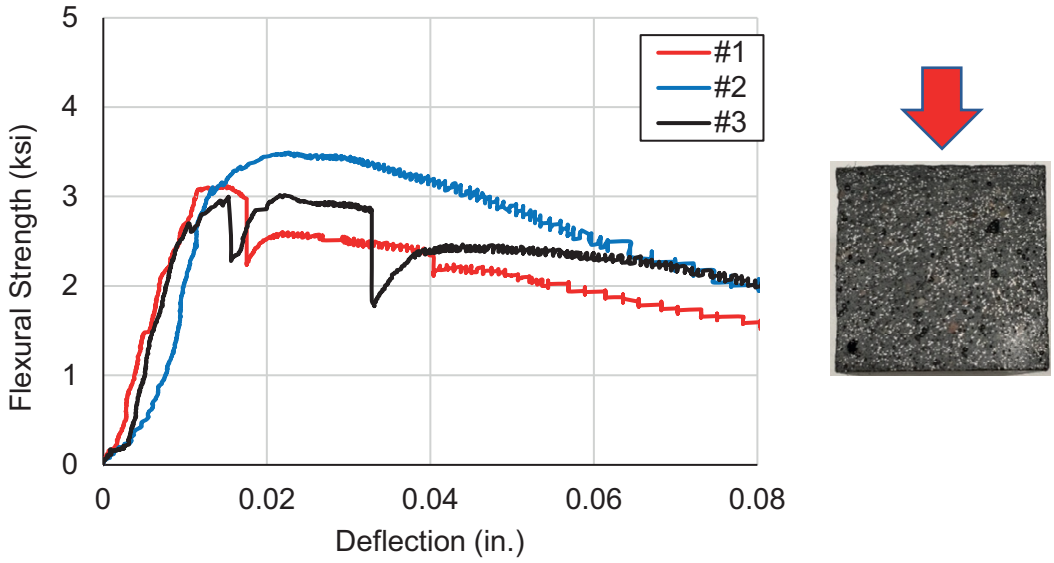

(a)

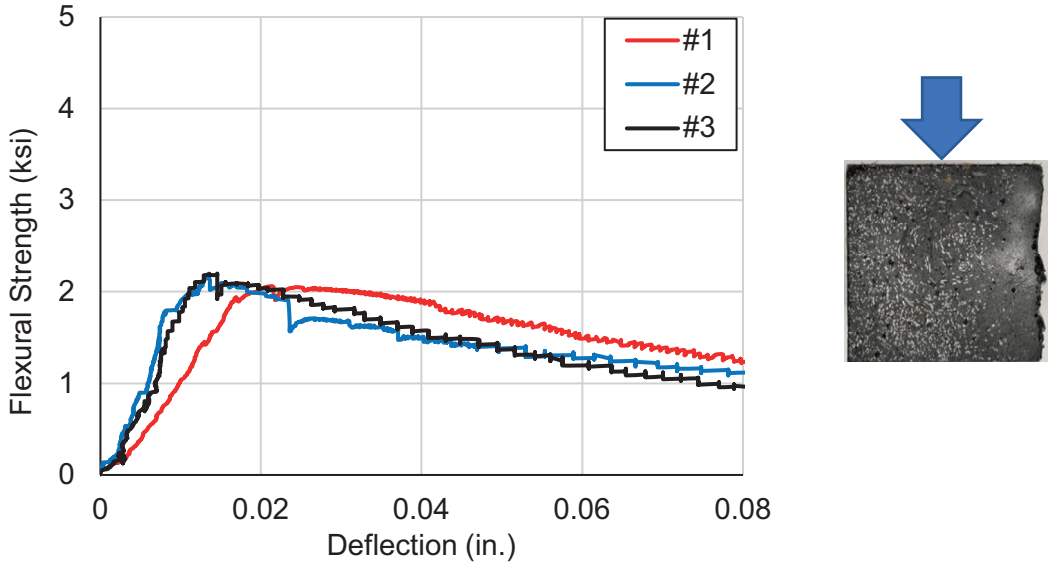

(b)

Figure 4.15. Flexural Test Results of UHPC Mixes; (a) UHPC 1450 and (b) UHPC 1700.

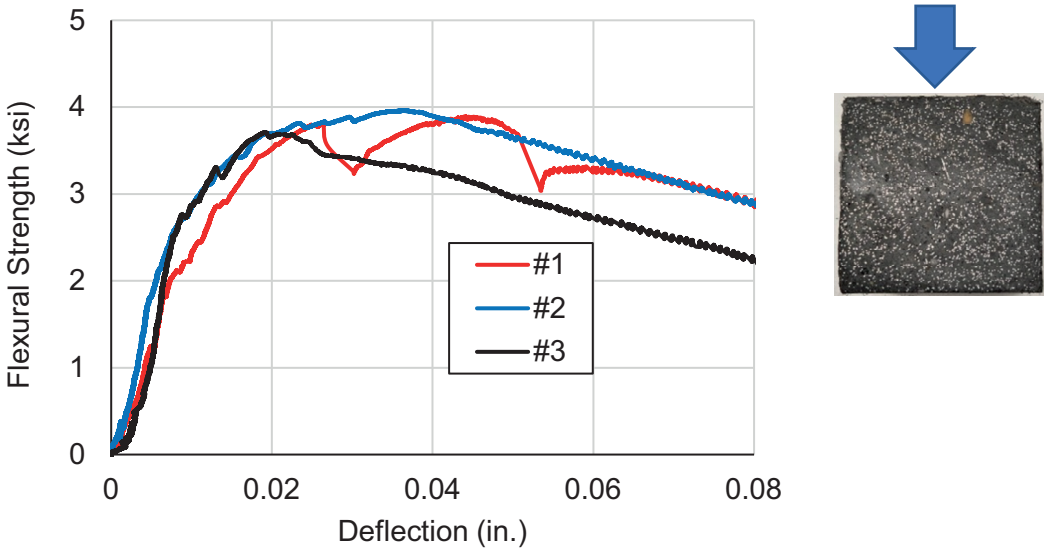

(a)

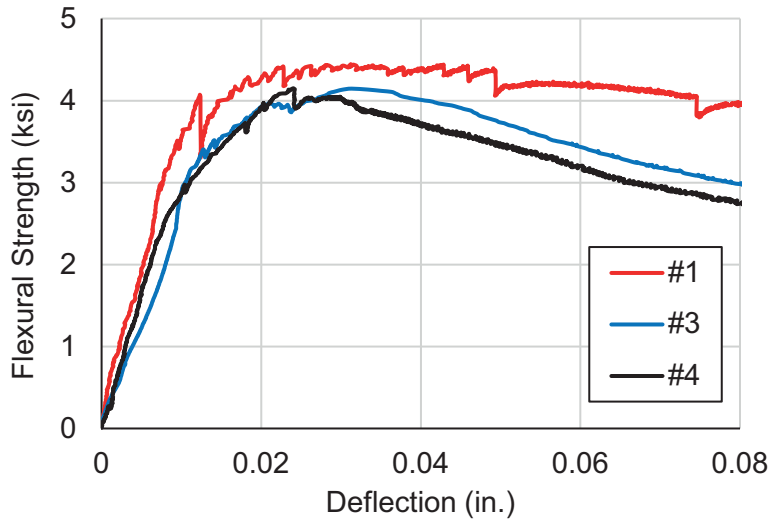

(b)

Figure 4.16. Flexural Test Results of UHPC Mixes; (a) UHPC 1900, and (b) Commercial UHPC.

Table 4.4

Flexural Test Results of the Non-proprietary and Commercial UHPC Mixes and their Comparison to ACI-318-19 Limits.

Property	**Design Criteria**	**UHPC 1450**	**UHPC 1700**	**UHPC 1900**	**Commercial**
Flexural Strength at First Crack, psi	**1500**	2320	1470	2810	2970
Peak Flexural Strength, psi	**2000**	3210	2150	3886	4250
Peak Flexural Strength, % of First	**125%**	138%	147%	137%	143%
Residual at L/300, % of First Crack	**90%**	113%	113%	130%	136%
Residual at L/150, % of First Crack	**75%**	81%	75%	92%	97%

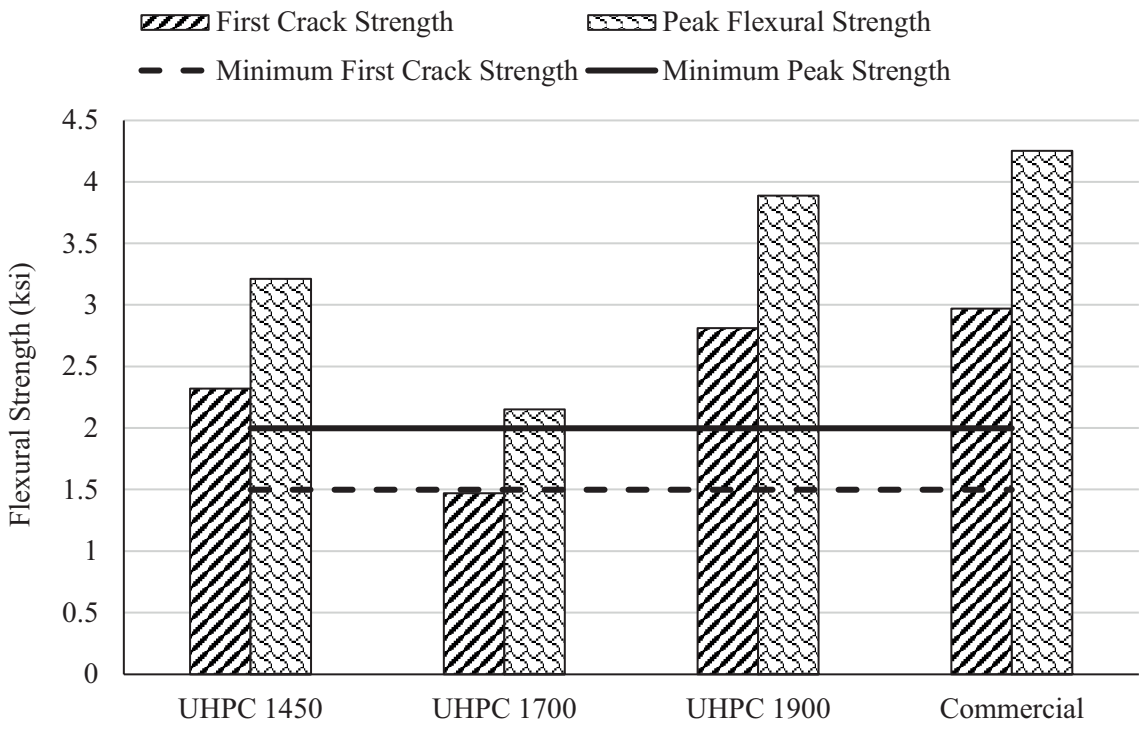

Figure 4.17. Flexural Test Results of the Non-proprietary and Commercial UHPC Mixes and their Comparison to ACI-318-19 Limits.

4.8. Splitting Tensile

The splitting tensile strength test was performed according to ASTM C496 to determine the split tensile strength of each mix. Three 4 in. x 8 in. cylinders were used to conduct the splitting tensile test instead of 6 in. x 12 in. cylinders as UHPC has high compressive strength. A load rate of 300 lb/sec. was applied using a compression machine until failure as shown in Figure 4.18(a). According to ASTM C496, the splitting tensile strength was obtained using the following equation:

$$T = 2P/\pi ld \tag{4.5}$$

Where:

T = splitting tensile strength *(psi)*

P = maximum applied load indicated by the testing machine (Ibf).

l = cylinder length (in.)

d = cylinder diameter (in.)

According to AASHTO LRFD 2020, the direct tensile strength may be determined by splitting tensile strength test and may be estimated by the following equation for normal concrete with design compressive strength up to 10 ksi.

$$f_t = 0.23\sqrt{f_c'} \tag{4.6}$$

Where:

f_t = direct tensile strength *(ksi)*

f_c' = compressive strength of concrete for use in design (ksi)

Figure 4.18(b) shows the failure mode of non-proprietary and commercial mixes. The average splitting tensile strength of each non-propriety and commercial UHPC mixes

and their comparison to AASHTO LRFD 2020 are plotted in Figure 4.19. Detailed testing results are available in Appendix A. However, the obtained splitting tensile strength of UHPC mixes showed no significant difference, it was lower than the commercial one as it depends mainly on the compressive strength value and fiber content. The high variance of the splitting test results might conclude that splitting tensile test is not adequate for predicting tensile strength of UHPC. Testing results are available in Appendix A.

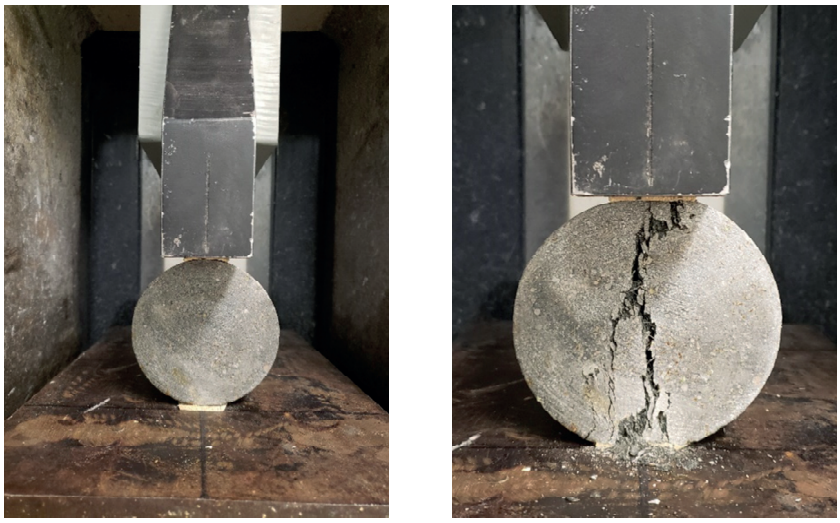

(a) (b)

Figure 4.18. Splitting Tensile Strength Test; a) Test Setup, and b) Failure Mode.

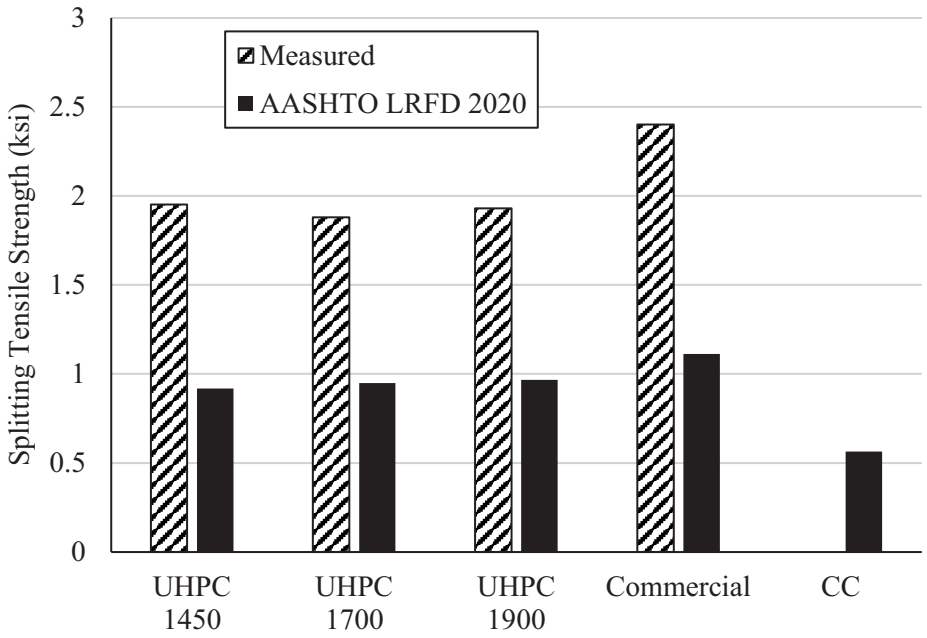

Figure 4.19. Average Splitting Strength for the Non-proprietary and Commercial UHPC Mixes and their Comparison to Predictions Using AASHTO LRFD 2020.

4.9. Rebar Development Length

The FHWA-HRT-14-090 report recommended a minimum embedment length of $8d_b$ and minimum side cover of $3d_b$ to attain deformed bar by achieving the lesser of the bar yield strength or 75 ksi before bond failure. The rebar development length test was conducting using UHPC blocks with two embedded steel bars aligned along the same axis as shown in Figure 4.20 (Roy, et al. 2017). The longer embedded bar (support bar) has a larger diameter (No. 6) compared to the pullout bar (anchorage bar No. 4) to ensure the failure will happen first at the pullout bar side. The two No. 4 bars at the sides prevent the concrete block from monolithic tensile failure at the mid-section. Three concrete blocks, with dimensions of 8 in. x 9 in. x 3 in. that meet the minimum FHWA report recommendations, were cast using commercial and UHPC 1900 mixes. The commercial

UHPC mix specimens were tested under an axial tension load rate of 1500 lb/min. until failure using a 400 kips Tinius Olsen testing machine as shown in Figure 4.21. The UHPC 1900 mix specimens were tested using steel frame and applying tension load using a hydraulic ram attached to pullout bar (#4). The anchorage bar (#6) was fixed using a coupler resting on steel plate against the frame as shown in Figure 4.22. Two LVDTs were attached to the pullout bar to capture the bar slippage after subtracting the bar elongation as shown in Figures 4.21 and 4.22. Figures 4.23 and 4.24 show the test results of commercial and UHPC 1900 mix specimens. All specimens exhibited splitting failure mode in the UHPC block as shown in Figure 4.25(a); except the first UHPC 1900 specimen as it was tested twice for anchorage bar slippage out of the coupler. No failure happened at the anchorage bar (#6) as shown in Figure 4.25(b). All the specimens achieved maximum bar tensile strength higher than 60 ksi before exhibiting bond failure and before 0.1 in. bar slippage. The UHPC 1900 mix satisfied the recommendations of FHWA-HRT-14-090.

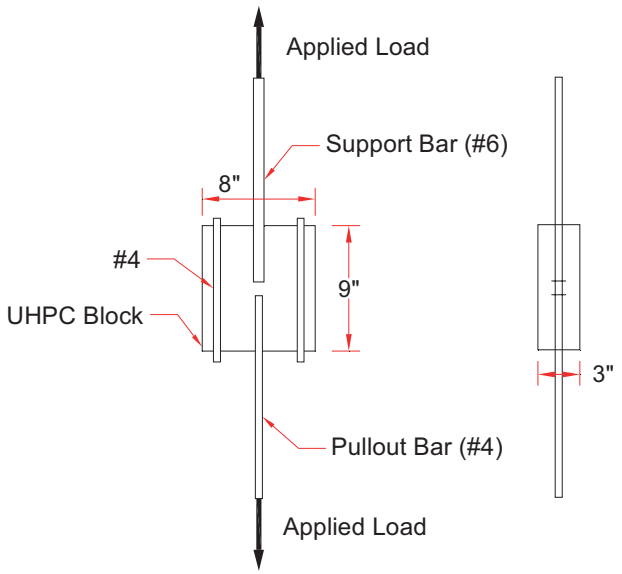

Figure 4.20. Rebar Pullout Specimen Dimensions.

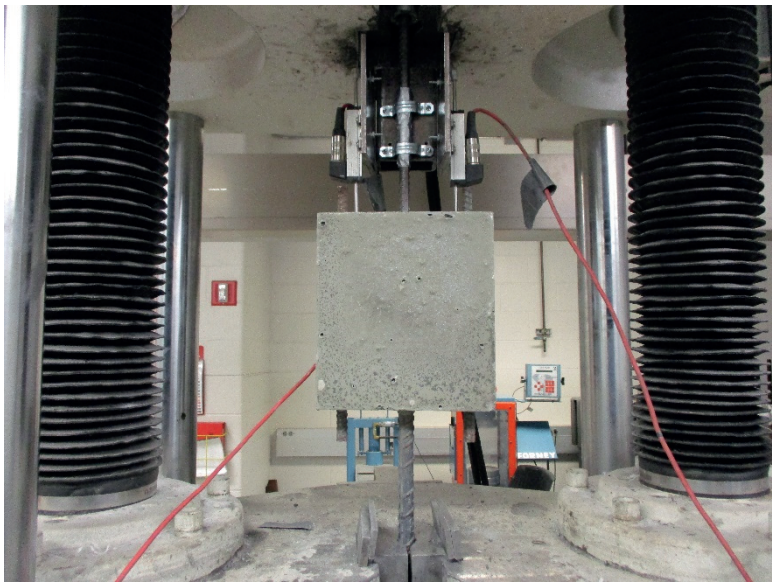

Figure 4.21. Rebar Pullout Test Setup of Commercial UHPC Mix.

Figure 4.22. Rebar Pullout Test Setup of UHPC 1900 Mix.

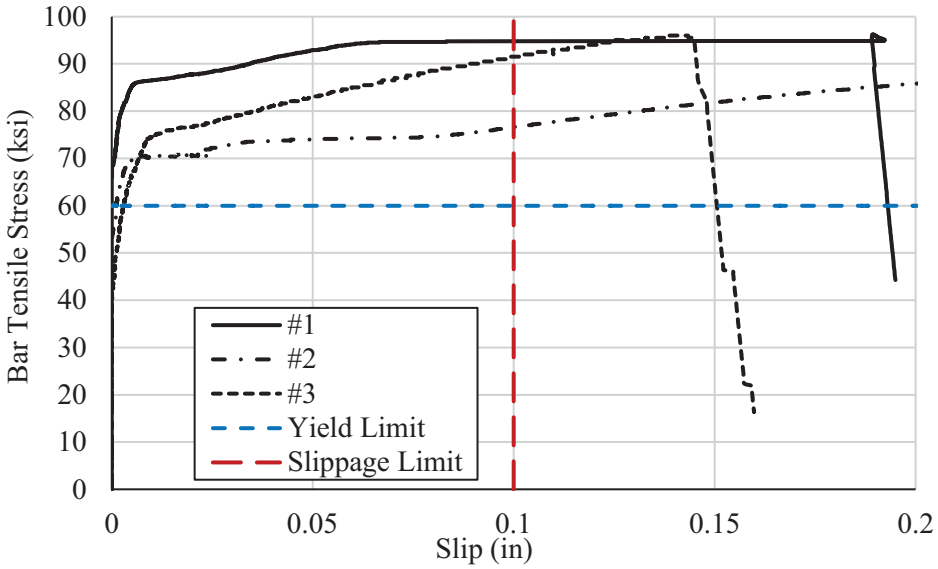

Figure 4.23. Rebar Pullout Test Results of Commercial UHPC Mix.

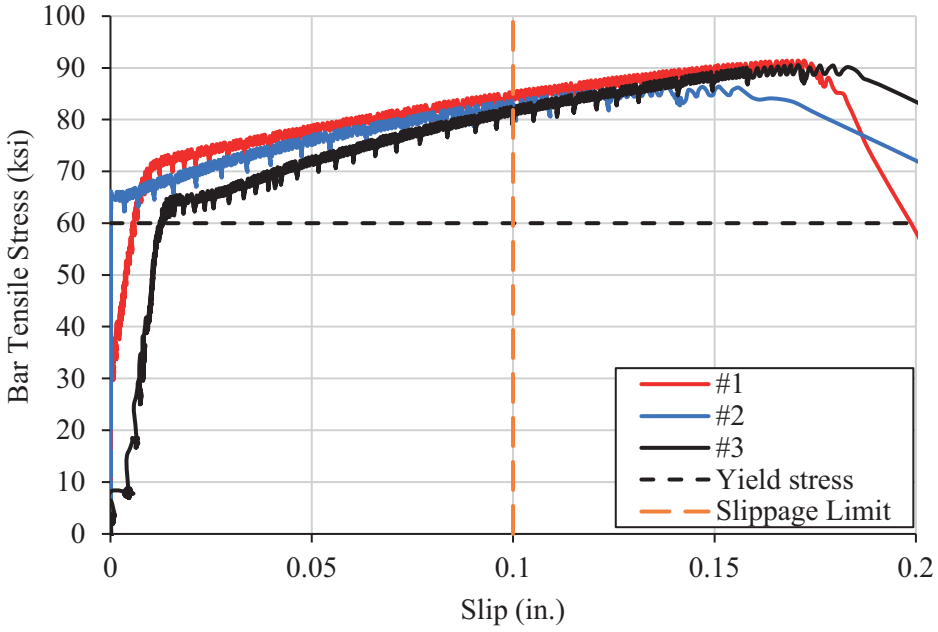

Figure 4.24. Rebar Pullout Test Results of UHPC 1900 mix

(a) (b)

Figure 4.25. Rebar Pullout Test Splitting Failure Mode; (a) splitting cracking failure at #4 bar and (b) No failure at #6 bar.

4.10. Effect of Specimen Orientation on Flexural Strength

Six-3x3x14 inches flexural prisms cast using UHPC 1900 mix were tested with two different specimen orientations. The first three specimens were tested according to ASTM C78 by turning the test specimen on its side relative to molding position. The other three specimens were tested as cast. The flexural test was conducted following the same procedure in section 4.7. Figure 4.26 shows the flexural strength versus mid-span deflection for the two specimen orientations. There is no significant difference in first cracking and peak flexural strengths as shown in Table 4.5. It worth mentioning that the UHPC 1900 mix was low flowability which had better fiber distribution. The conclusion may differ if the UHPC mix has low stability.

Table 4.5

Effect of Specimen Orientation on Flexural Strength of UHPC 1900 mix.

Specimen Orientation	Flexural Strength at First Crack (ksi)	Peak Flexural Strength (ksi)
Side	3.04	4.88
As-Cast	3.39	4.90

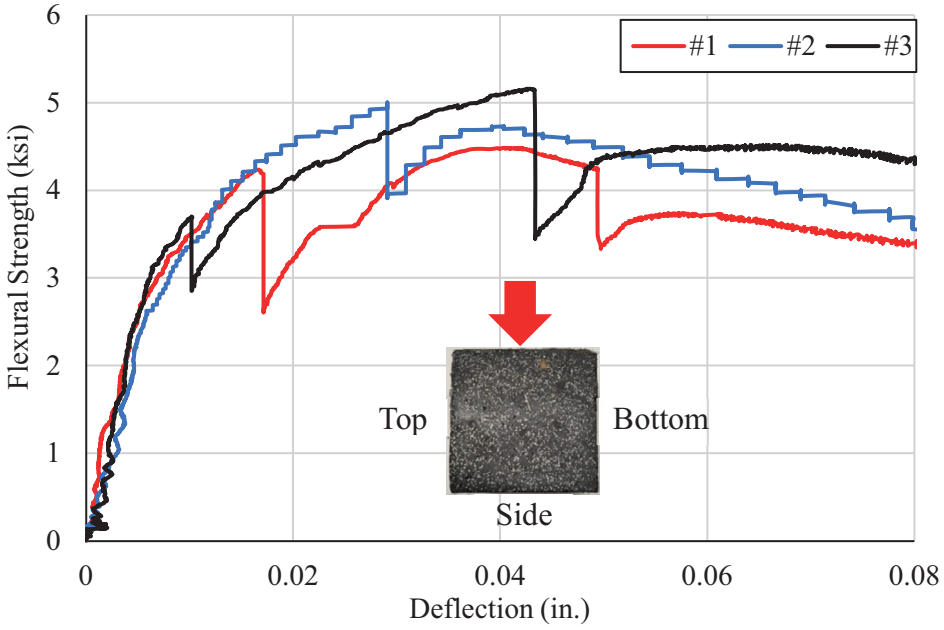

(a)

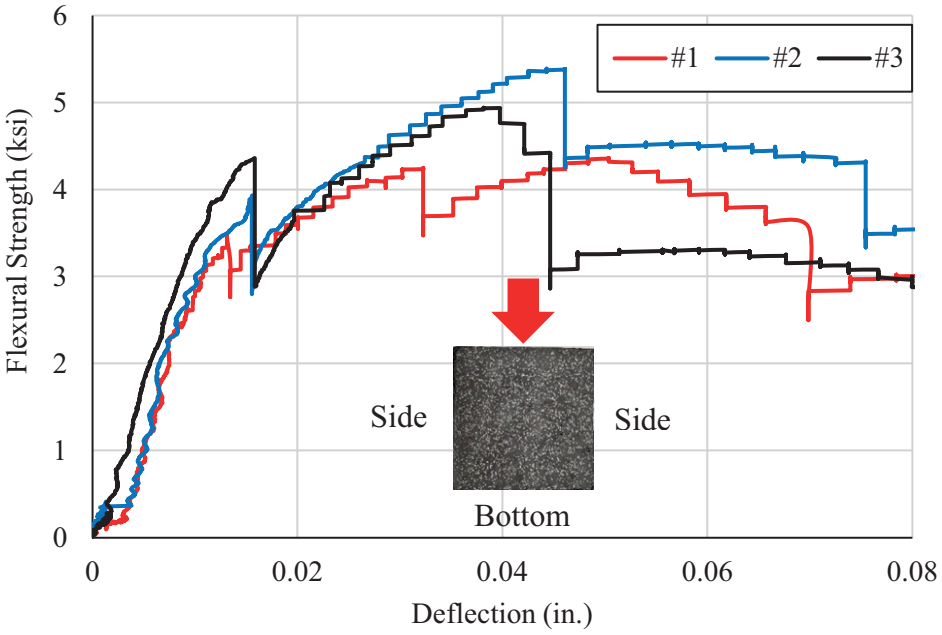

(b)

Figure 4.26. Flexural Strength Results of Different Specimen Orientation; (a) Side, and (B) As Cast.

4.11. Effect of Stability on Mechanical properties

The effect of stability on compressive strength and flexural strength was studied using UHPC 1900 mix. Figure 4.27 shows the fiber distribution in low and high stability of UHPC 1900 mixes. The compressive strength for low stability mix was 17.76 ksi, which is higher than the high stability mix (16.16 ksi) at day of testing. Six-3x3x14 inches flexural prisms were tested with the same previously discussed procedures. Figure 4.28 shows the flexural strength versus mid-span deflection for a low stability UHPC 1900 mix. The third flexural specimen is not plotted due to equipment malfunction. Table 4.6 shows that the first crack and peak strengths of low stability mix are 37% and 54% lower than those of the high stability mix, respectively, as a result of fiber segregation.

However, the low stability mix satisfied the minimum first crack and peak strengths of 1.5 ksi and 2 ksi.

Table 4.6

Effect of Stability on Flexural Strength of UHPC 1900 mix.

Stability	f'_{UHPC} (ksi)	Flexural Strength at First Crack (ksi)	Peak Flexural Strength (ksi)
Low	17.67	1.91	2.26
High	16.16	3.04	4.88

(a) (b)

Figure 4.27. Cross-section of UHPC 1900 Non-proprietary Mix; (a) Low Stability, and (b) High Stability.

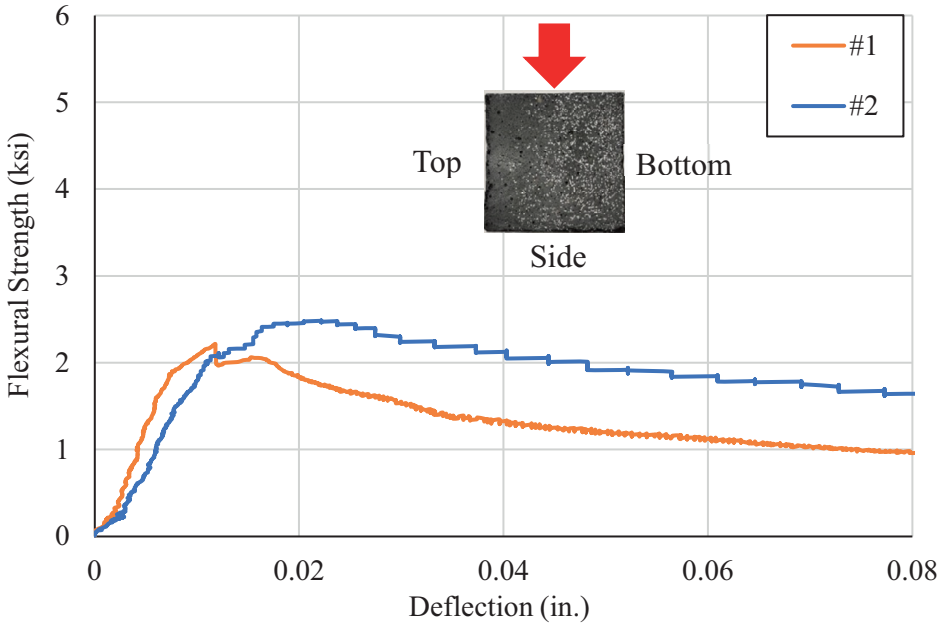

Figure 4.28. Flexural Strength Results of UHPC 1900 Mix with Low Stability

4.12. UNL-UHPC Mix

The UHPC 1900 mix, named later as UNL-UHPC, showed the highest mechanical properties and good agreement with the mechanical properties of commercial mix as shown in Table 4.7. The current material cost of the commercial UHPC mix is over $2000/cy, which is very high compared to CC. This significant difference highly impacts the implementation of UHPC in the bridge construction. Using a locally developed UHPC mix will reduce the cost of the UHPC raw materials. Tables 4.8 and 4.9 lists the raw materials sources and unit cost for UNL-UHPC, which show a total cost of $723.4/cy.

Table 4.7

Summary of Mechanical Properties Testing of UHPC

Property	Requirements from ASTM C1856	FHWA Acceptance Criteria (2014)	FHWA Results U-A, (2018)	Commercial	UNL-UHPC
Compressive Strength, 28d (psi)	17,000	21,000	18,000	23,300	17,670
Modulus of Elasticity, 28d (ksi)	n/a	7	6 : 8	8.17	6.33
Poisson's Ratio, 28d	n/a	n/a	0.15	0.22	0.24
Flexural Strength at First Crack, 28d (ksi)	n/a	1.3	n/a	2.97	2.81
Peak Flexural Strength, 28d (ksi)	n/a	n/a	n/a	4.25	3.90
Splitting Tensile Strength, 28d (ksi)	n/a	1.3 (Cracking Strength)	2.57*	2.4	1.93
Rebar Development Length	Satisfied the FHWA-HRT-14-090 recommendation ($L_d=8d_b$ and Cover= $3d_b$) Bar Yield before Bond Failure				

**29 days with 3% fiber content*

Table 4.8

Unit Cost of Raw Materials for locally developed UHPC Mixes (Mendonca et al. 2020)

	Materials	Source and location	Unit cost $/ton
Sand	No.10 sand	Lyman-Richey Corporation Omaha, NE	10
Cement	Type I/II	Ash Grove Cement Company Louisville, NE	105
Slag	Grade 100 Slag	Central Plains Cement Company Omaha, NE	123
Silica fume	Force10,000 densified microsilica	GCP Grace Construction Products	1080
Fiber	13/.20 mm micro steel fiber	US Domestic Source	3000
HRWR	Premia 150	Chryso	18.5*

* in $/gallon

Table 4.9 shows the cost of UNL-UHPC mix based on the available raw material unit cost. The UNL-UHPC mix costs approximately \$723.4/yd^3 which is 36.2% of commercially available mix. This significant reduction makes UHPC attractive to bridge construction community.

Table 4.9

UNL-UHPC Raw Material Cost

Constituent	Weight (Ib/yd^3)	Unit cost \$/ton	Cost (\$/yd^3)
Cement I/II	1178	\$105	\$61.9
Silica Fume	152.7	\$1080	\$82.5
Slag	570	\$123	\$35.1
#10 Sand	1663.7	\$10	\$8.3
Fibers	263	\$3000	\$394.5
HRWRA[a]	61	\$18.5*	\$141.1
		Sum	\$723.4

* in \$/gallon

CHAPTER 5: INTERFACE SHEAR RESISTANCE OF UHPC CAST ON HARDENED CONVENTIONAL CONCRETE

This chapter presents the experimental and analytical investigations conducted to develop friction and cohesion factors of the shear friction theory for UHPC cast on hardened CC in composite sections. Slant shear and L-shape push-off tests were conducted to evaluate the effect of interface surface texture, interface reinforcement ratio, CC and UHPC compressive strength, and fiber presence. Cohesion and friction factors of UHPC were found to be significantly higher than those of CC in current design.

5.1. Code Provisions

The current provisions of ACI 318-19, AASHTO LRFD (2020), Eurocode-2 (2004), and CSA A23.3-14 adopt the shear friction theory, but they do not address the interface shear resistance of CC-UHPC. Only the French standard for UHPC (NF-P-18-710-UHPC) indicates that normal concrete interface shear equations of the Eurocode 2 (EN 1992-1-1:2004) can be used to predict the interface shear resistance of CC-UHPC.

5.2.1. ACI 318-19

The Building Code Requirements for Structural Concrete (ACI 318-19) Section 22.9.4 provide a shear friction equation for predicting the shear transfer across a given plane, such as existing or potential crack, interface between dissimilar materials, or interface between two concretes cast at different times. The ACI 318-19 provisions only consider the friction portion generated by the interface plane texture and interface shear reinforcement to transfer the shear forces. The nominal shear strength is calculated using

Eq. 5.1 where α is the interface shear reinforcement inclination angle to the interface plane. Also, ACI 318-19 stated that permanent net compression across the shear plane shall be permitted to be added to $A_{vf}.f_y$. The upper bound for resistance are stated in Eq. 5.2 and Eq. 5.3 for roughened surface with amplitude of 1/4 in. and smooth, respectively.

$$V_n = A_{vf}.f_y.(\mu \sin\alpha + \cos\alpha) \quad (5.1)$$

$$V_n \leq (480 + 0.08f_c').A_{cv} \leq 0.20\, f_c'.A_c \leq 1600\, A_c \quad (5.2)$$

$$V_{ni} \leq 0.20\, f_c'.A_c \leq 800\, A_c \quad (5.3)$$

Where:

V_n = nominal shear strength, lb

A_{vf} = area of shear-friction reinforcement, in.2

A_c = area of concrete section resisting shear transfer, in.^{2}

f_y = interface reinforcement yield stress, which is limited to 60000 psi, psi

α = acute angle between shear-friction reinforcement and assumed shear plane

f_c' = the lesser concrete compressive strength out of the two layers, psi

5.2.2. AASHTO LRFD (2020)

AASHTO LRFD Bridge Design Specifications (2020) Section 5.7.4 provides prediction equation for obtaining the interface shear resistance between two concrete layers either cast monolithically or fresh and at different times with different interface plane textures. The equation consists of two sections; the first section calculates the contribution of concrete cohesion and the second section calculates the friction contribution as shown in Eq. 5.4.

$$V_{ni} = c.A_{cv} + \mu.\left(A_{vf}.f_y + P_c\right) \leq K_1.f_c'.A_{cv} \leq K_2.A_{cv} \quad (5.4)$$

Where:

V_{ni} = nominal interface shear resistance, kip

c = cohesion factor, ksi

μ = friction factor

A_{vf} = area of the interface shear reinforcement crossing the shear plane, in.^{2}

A_{cv} = area of concrete considered to be engaged in interface shear transfer ($b_{vi}.L_{vi}$), in.^{2}

f_y = interface reinforcement yield stress, which is limited to 60 ksi, ksi

P_c = normal force applied to the shear plane, kip

b_{vi} = interface width considered to be engaged in shear transfer, in.

L_{vi} = interface length considered to be engaged in shear transfer, in.

K_1 = fraction of concrete strength available to resist interface shear which is 0.2 and 0.25 for smooth and roughened surface with amplitude of 1/4 in., respectively.

K_2 = limiting interface shear resistance which is 0.8 ksi and 1.5 ksi for smooth and roughened surface with amplitude of 1/4 in., respectively.

f_c' = the lesser concrete compressive strength out of the two layers, ksi

5.2.3. Eurocode 2 (EN 1992-1-1:2004)

Eurocode 2 considered the cohesion and friction to resist the interface shear force in section 6.2.5. The interface shear resistance between concrete cast at different time is calculated using Eq. 5.5 which is stress-based. The cohesion portion of the equation is a

function of the concrete tensile strength which results in a unitless "c" factor. Also, the inclination of interface shear reinforcement is included in Eq. 5.6.

$$V_{Rdi} = c.f_{ctd} + \mu.\sigma_n + \rho.f_{yd}(\mu \sin\alpha + \cos\alpha) \leq 0.5\upsilon f_{cd} \quad (5.5)$$

$$\upsilon = 0.6\left[1 - \frac{f_{ck}}{250}\right] \ (f_{ck} \ in \ MPa) \quad (5.6)$$

Where:

V_{Rdi} = the design shear resistance at the interface

f_{ctd} = the design tensile strength

f_{ck} = the characteristic compressive cylinder strength of concrete at 28 days

f_{yd} = the design yield strength of reinforcement

f_{cd} = the design value of concrete compressive strength

ρ = A_s/A_i

A_s = the area of reinforcement crossing the interface, including ordinary shear reinforcement (if any), with adequate anchorage at both sides of the interface

A_i = the area of the joint (area of concrete across the interface)

α = the angle of interface shear reinforcement measured from the horizontal interface shear plane

σ_n = the stress caused by the minimum external normal force across the interface that can act simultaneously with the shear force, positive for compression, such that σ_n<0.6 f_{cd}, and negative for tension. When σ_n is tensile f_{ctd} should be taken as 0, MPa.

5.2.4. CSA A23.3-14

The Canadian standards (CSA A23.3-14) Section 11.5 provisions assume a crack and relative displacement to occur along the shear plane which are resisted by cohesion and friction maintained by the shear friction reinforcement crossing the crack. The factored interface shear stress resistance of the interface plane shall be obtained using Eq. 5.7 and Eq. 5.8 and checked by Eq. 5.9 which are stress-based equations.

$$V_r = \emptyset_c \lambda (c + \mu\sigma) + \emptyset_s . \rho_v . f_y . cos\ \alpha_f \quad (5.7)$$

$$\sigma = \rho_v . f_y . sin\ \alpha_f + \frac{N}{A_{cv}} \quad (5.8)$$

$$\emptyset_c \lambda (c + \mu\sigma) \leq 0.25 \emptyset_c . f_c' \quad (5.9)$$

Where:

V_r = the factored shear stress resistance of the interface plane

λ = factor depends on concrete type; 1.0 for normal concrete, and 0.75 for light-weight concrete

ρ_v = A_{vf}/A_{cv}

f_y = the specified yield strength of non-prestressed reinforcement or anchor steel, not more than 500 MPa (72.52 ksi)

α_f = the angle between shear friction reinforcement and shear plane

ϕ_c = The resistance factor for concrete which is 0.65

ϕ_s = the resistance factor for non-prestressed reinforcing bars which is 0.85

σ = the compressive stress on the interface

N = the unfactored permanent load perpendicular to the shear plane

Table 5.1 summarizes the interface shear resistance provisions for CC and associated upper bounds with unified symbols as possible for comparison. Table 5.1 shows that the interface shear is resisted by both concrete cohesion and shear-friction at the interface plane with area (A_{cv}) in all codes except ACI 318-19 that ignores concrete cohesion portion. ACI 318-19, Eurocode-2 (2004), and CSA A23.3-14 provisions consider interface shear reinforcement inclination angle (α) with the perpendicular to the interface in predicting interface shear resistance. In all provisions, the shear reinforcement crossing interface plane is required to be fully developed in both sides of interface plane, and its stress is limited the yield strength. The yield strength should not exceed 60 ksi (420 ksi) in AASHTO LRFD (2020) and ACI 318-19 and 72.52 ksi (500 MPa) in CSA A23.3-14 to control crack width. Also, the compressive strength of weaker concrete layer (f_c') is used in obtaining the interface shear resistance upper bound.

Table 5.2 summarizes the concrete cohesion and shear friction factors stated by the four codes for three different interface surface textures. Two surface textures are recognized by all the codes: (1) smooth texture (clean surface and not intentionally roughened); and (2) highly roughened surface (clean surface and roughened of at least full amplitude of 0.25 in. in AASHTO LRFD and ACI 318-19 or 0.2 in. (5 mm) in Eurocode 2 and CSA A23.3-14. Eurocode 2 is the only code that includes a low roughened interface surface with an amplitude of at least 0.12 in. (3 mm) and estimates the cohesion factor as a fraction of the concrete tensile strength (f_{ctd}). In all the four codes, the friction factors (μ) are the same for smooth surfaces, which is 0.6, and almost the same for highly roughened surfaces (0.9 or 1.0).

Table 5.1

Interface Shear Resistance Prediction Equations between Fresh and Hardened Normal Weight Concrete and Associated Upper Bounds in Different Code Provisions.

Code	Interface Shear Resistance Prediction Equation	Interface Shear Upper Bound
ACI 318-19 (Section 22.9.4), ksi	$\rho . f_y . (\mu \sin \alpha + \cos \alpha)$	$\leq (0.48 + 0.08 f_c') \leq 0.20 f_c' \leq 1.60$
AASHTO LRFD (Section 5.7.4.3), ksi	$c + \mu . (\rho . f_y + \sigma_n)$	$\leq K_1 . f_c' \leq K_2$
Eurocode 2 (Section 6.2.5), MPa	$c' . f_{ctd} + \mu . \sigma_n + \rho . f_y (\mu \sin \alpha + \cos \alpha)$	$\leq 0.5 \upsilon f_{cd}$ $\upsilon = 0.6[1 - (f_{ck}/250)]$
CSA A23.3-14 (Section 11.5), MPa	$\lambda (c + \mu . (\rho . f_y . \sin \alpha + \sigma_n)) + \rho . f_y . \cos \alpha$	$\lambda (c + \mu . (\rho . f_y . \sin \alpha + \sigma_n)) \leq 0.25 f_c'$

α is acute angle between interface shear reinforcement and interface shear plane;
K_1 is the fraction of concrete strength available to resist interface shear;
K_2 is limiting interface shear resistance (ksi);
c' is factor depending on the roughness of the interface;
f_{cd} is the design value of concrete compressive strength (MPa);
f_{ck} is the characteristic compressive cylinder strength of concrete at 28 days (MPa);
f_{ctd} is the concrete design tensile strength (MPa);
λ is the factor of concrete type;
σ_n is the stress caused by the forces normal to the interface plane;

Table 5.2

Cohesion and Friction Factors for Interface Shear Resistance Between Fresh and Hardened Normal Weight Concrete with Different Interface Surface Textures by Different Codes.

Interface Type	Smooth		Low roughened surface (an amplitude of at least 0.12 in.		High roughened surface (an amplitude 0.25 in.	
	c, ksi (MPa)	μ	c, MPa (ksi)	μ	c, ksi (MPa)	μ
ACI 318-19 (Section 22.9.4)	-	0.6	-	-	-	1
AASHTO LRFD (Section 5.7.4.3)	0.075 (0.52)	0.6	-	-	0.28 (1.93) * 0.24 (1.65)	1
Eurocode 2 (Section 6.2.5)	0.20 f_{ctd} **	0.6	0.40 f_{ctd} **	0.7	0.50 f_{ctd} **	0.9
CSA A23.3-14 (Section 11.5)	0.036 (0.25)	0.6	-	-	0.073 (0.5)	1

* in case of cast-in-place concrete slab on clean concrete girder surface

** f_{ctd} is the design tensile strength (MPa)

5.2. Materials

The UNL-UHPC and commercially available pre-bagged UHPC mixes were used in the experimental program and their mechanical properties were presented in Chapter 4. Straight copper coated steel micro-fibers, 0.50 in. long and 0.078 in. in diameter with tensile strength of 400 ksi, were added to the mix at a dosage of 2% by volume. Table 5.3 shows the mix proportions for CC used in the study, which had compressive strength, modulus of elasticity and tensile strength of 6.6 ksi, 4.80 ksi, and 0.6 ksi, respectively. ASTM A615 Grade 60 uncoated black steel rebars were used for all interface shear

reinforcement, which had a minimum yield strength of 60 ksi and minimum tensile strength of 90 ksi.

Table 5.3

Mix Proportions for Conventional Concrete.

Material	Cement (Type 1PF)	Sand	Coarse Aggregate[1]	Water	HRWR[2]	AE[3]
Unit Weight, (Ib/cy)	763	1280	1440	278	5.93	0.13

[1] 1/2 in. nominal maximum aggregate size
[2] High range water reducer
[3] Air entraining admixture

5.3. Model Development

Slant shear tests were conducted to investigate the effect of different interface shear textures on the interface shear capacity of CC-UHPC. The results of these testing combined with the available literature review data are used to obtain interface shear cohesion and friction factors for CC-UHPC.

5.3.1. Slant Shear Testing

A slant shear test was performed according to ASTM C882/C882M to evaluate the interface shear resistance of CC-UHPC. A 4 in. by 8 in. cylindrical composite specimens were used instead of the original 3 in. by 6 in. cylindrical specimens to allow the use of CC substrate instead of mortar (Abo El-Khier et al. 2019). Full CC cylinders were cast, striped out of molds after 24 hours and placed in a curing room for 28 days. Then, hardened CC cylinders were saw-cut diagonally at 60° angle with the horizontal axis to form the CC interface surface of slant shear specimens. Three interface surface textures

were applied to interface surface as shown in Figure 5.1: as-cut (as cut with the wet saw and without additional treatment); shallow grooved (average 1/8 in. depth); and deep grooved (average 1/4 in. depth).

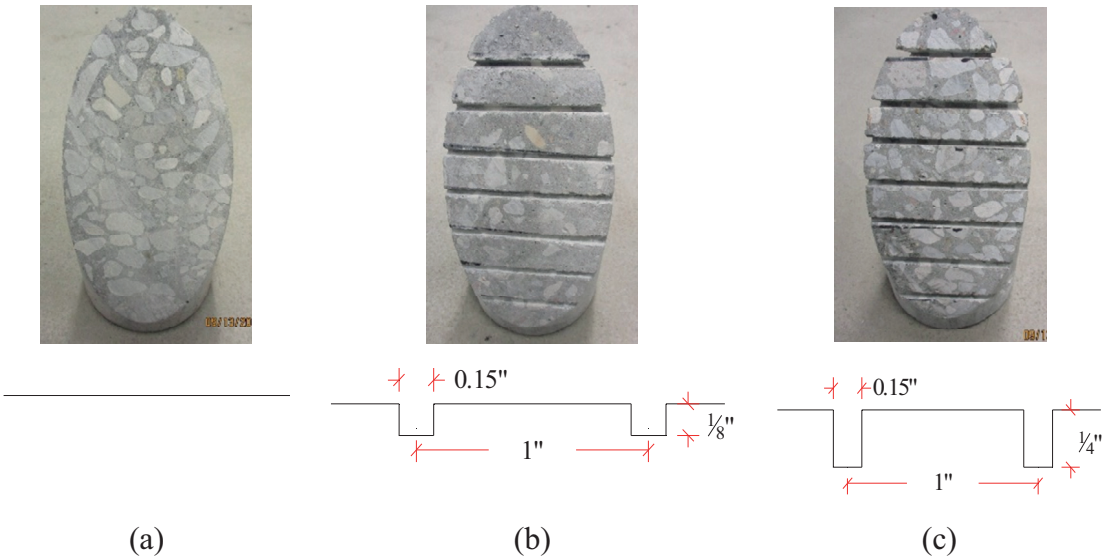

Figure 5.1. Interface Surface Textures of Hardened CC; (a) As-Cut, (b) Shallow Grooved, and (c) Deep Grooved (in.).

The CC specimens were placed back in the plastic molds and their interface surfaces were pre-wetted directly before casting the fresh UHPC. The composite specimens were stripped out of the molds after one day and submerged in lime-saturated water in a room temperature of 73°F until the day of testing. Both ends of composite specimens were mechanically ground and tested as shown in Figure 5.2 using a compression load rate of 300-400 lb/sec until failure according to ASTM C39. A total of 24 slant shear specimens were tested as the UHPC compressive strength (f_{UHPC}) ranged from 17.6 to 27.2 ksi and CC compressive strength was approximately 8 ksi.

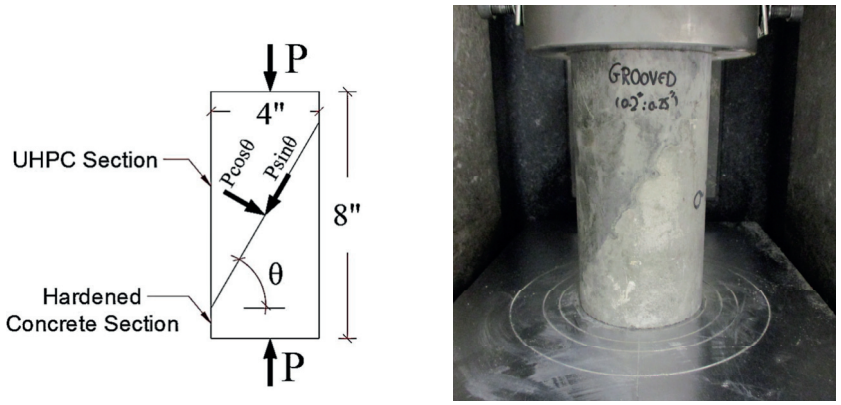

Figure 5.2. Slant Shear Test Specimen Dimensions and Test Setup (in.).

5.3.2. Test Results

Different failure modes were observed for the three interface surface textures as shown in Figure 5.3. Specimens with as-cut surface had interface failure as shown in Figure 5.3(a), while specimens with deep grooved surface had fractured CC as shown in Figure 5.3(c). Specimens with shallow grooved surface had interface failure accompanied with fractured CC as shown in Figure 5.3(b). The interface shear resistance of slant shear specimens (v_{ni}) was calculated as follows:

$$v_{ni} = P.\sin(\theta)/(A/\cos(\theta)) \quad (5.10)$$

Where, P is the maximum applied load, θ is interface shear angle with the horizontal axis, and A is the cross-section area of the cylindrical specimen. Table 5.4 shows the slant shear test results and the associated failure mode at different UHPC compressive strengths for each interface surface texture.

Table 5.4

Slant Shear Test Results

Interface Surface Texture of Hardened CC	f_{UHPC} = 17.7 ksi		f_{UHPC} = 23.4 ksi		f_{UHPC} = 27.2 ksi	
	$v_{ni,}$ (ksi)	Failure Location	$v_{ni,}$ (ksi)	Failure Location	$v_{ni,}$ (ksi)	Failure Location
As-Cut	3.40	Interface	4.27	Interface	4.11	Interface
	3.91	Interface	4.15	Interface	4.24	Interface
	3.46	Interface	3.94	Interface	4.40	Interface
Average	3.59		4.12		4.25	
COV%	7.75		4.08		3.32	
Shallow Grooved	-	-	4.65	Interface & CC	4.44	Interface & CC
	-	-	4.16	Interface & CC	4.69	Interface & CC
	-	-	4.37	CC	4.16	CC
Average	-		4.39		4.43	
COV%	-		5.50		6.05	
Deep Grooved	4.46	CC	4.57	CC	4.48	CC
	4.87	CC	4.30	CC	4.69	CC
	4.84	CC	4.54	CC	4.25	Interface& CC
Average	4.72		4.47		4.47	
COV%	4.94		3.31		4.85	

(a) (b) (c)

Figure 5.3. Slant Shear Specimen Failure Modes; a) Interface Failure, b) Interface Failure and CC Fracture, and c) CC Failure.

5.3.3. Proposed Cohesion and Friction Factors

Slant shear test data collected from the literature were classified into three categories according to the interface surface texture: sandblasted, low-roughened, and high-roughened as shown in Tables 5.5.1 and 5.5.2. Each value in the Table is the average of at least three specimens. This data is used in addition to test data presented earlier to determine cohesion and friction factors for CC-UHPC. The compressive strength of CC and UHPC in this data set ranged from 5.2 ksi to 8.24 ksi and 11.69 ksi to 27.2 ksi, respectively. The low values of UHPC compressive strength represent early age compressive strength at the test day. The sandblasted category includes the specimens with as-cut surface textures. Low-roughened category includes the wire brushed, shallow grooved and form liner (with depth less than 0.20 in.) interface surface textures. Deep grooved, aggregate exposed, and form liners (with depth greater than 0.20 in.) surface textures are included in the high-roughened category. Different specimen shapes, dimensions and interface angles are used to calculate the interface shear resistance as

shown in Eq. 5.10. The normal stress (σ_n) at the interface plane of these specimens is calculated as follows:

$$\sigma_n = P.\cos(\theta)/(A/\cos(\theta)) \quad (5.11)$$

The shear friction model was used to obtain concrete cohesion (c) and shear friction (μ) factors for each category using the following straight-line equation:

$$v_{ni} = c + \mu(\rho f_y + \sigma_n) \quad (5.12)$$

Figure 5.4 and Figure 5.5 show the plots of average interface shear resistance (v_{ni}) and corresponding normal stress (σ_n) at the interface plane for all specimens as well as the trendline of each category and the line plots of the four code provisions presented earlier. The intercept of each line plot represents the cohesion factor, while the slope represents the friction factor. Comparing the trendlines to the code line plots indicate that the proposed UHPC cohesion and friction factors are significantly higher than those of the existing codes provisions for CC.

Table 5.5.1

Interface Surface Texture Categories Based on the Literature of CC-UHPC Interface Shear Resistance

Surface Texture Category	Reference	Surface Preparation	f'_{cc} (ksi)	f'_{UHPC} ksi)	v_{ni} (ksi)	σ_n (ksi)	Failure Location
Sandblasted	Muñoz 2012	Sandblasted	8.11	18.35	3.14	1.79	CC
			8.11	18.35	2.12	0.72	CC
	Tayeh et al. 2012*	Sandblasted	6.50	24.7	2.23	1.29	CC
			6.50	12.00	2.16	1.25	CC
			6.50	12.00	2.16	1.25	CC
	Rangaraju et al. 2013	Sandblasted	6.77	18.52	3.96	2.28	Interface & CC
			6.77	17.92	3.84	2.22	CC
			6.77	22.93	3.58	2.07	CC
			6.77	23.00	4.10	2.37	CC
Low Roughening	Harris et al 2011	Wire Brushed	5.00	15.00	1.82	1.05	Interface & Mortar
	Muñoz 2012	Brushed	6.46	15.29	2.34	1.36	CC
			6.46	15.29	1.76	0.61	Interface
			8.24	12.30	2.59	1.86	CC
			8.11	11.69	2.22	1.22	CC
			8.11	11.69	0.83	0.62	UHPC
			6.67	11.69	0.75	0.54	UHPC
	Tayeh et al. 2012*	Wire Brushed	6.50	24.70	1.60	0.93	Interface & CC
			6.50	12.00	1.44	0.83	Interface & CC
			6.50	12.00	1.46	0.84	Interface & CC
	Aaleti and Sritharan 2017**	Form Liner (0.06 in. deep ribs)	5.20	18.00	2.29	1.72	Interface
			7.46	18.00	3.64	2.73	CC
			6.40	18.00	3.16	2.37	Interface
		Form Liner (0.05 in. deep broom finish)	5.20	18.00	1.87	1.40	Interface
			7.46	18.00	3.17	2.38	Interface
			6.40	18.00	2.59	1.95	Interface
		Form Liner (0.12 in. deep linear pattern)	5.20	18.00	2.71	2.03	CC
			7.46	18.00	3.85	2.89	CC
			6.40	18.00	2.98	2.23	Interface

* UHPC compressive strength was not mentioned. An estimate of 12 ksi was used early-age compressive strength.

** UHPC compressive strength ranged from 15 ksi to 21 ksi. An average of 18 ksi was used.

Table 5.5.2

Interface Surface Texture Categories Based on the Literature of CC-UHPC Interface Shear Resistance

Surface Texture Category	Reference	Surface Preparation	f'_{cc} (ksi)	f'_{UHPC} (ksi)	v_{ni} (ksi)	σ_n (ksi)	Failure Location
High Roughening	Harris et al. 2011	Grooved	5.00	15.00	2.17	1.25	Mortar
	Muñoz 2012	Grooved	6.46	15.29	2.55	1.45	CC
			6.46	15.29	1.63	0.63	CC
			8.11	11.36	1.38	0.45	Interface & CC
		Roughened (Aggregate Exposed)	6.61	17.89	2.47	1.36	CC
			6.61	17.89	1.77	0.62	CC
			7.28	12.30	2.43	1.74	CC
			7.28	12.30	1.40	0.56	CC
			7.28	11.69	0.49	0.17	Interface & UHPC
	Tayeh et al. 2012*	Grooved	6.50	24.70	1.75	1.01	CC
			6.50	12.00	1.74	1.01	Interface & CC
			6.50	12.00	1.74	1.01	Interface & CC
	Aaleti and Sritharan 2017**	Form Liner (0.26 in. deep fluted ribs)	5.20	18.00	2.33	1.75	CC
			7.46	18.00	3.77	2.83	CC
			6.40	18.00	3.58	2.69	CC
		Form Liner (0.2 in. deep round flutes)	5.20	18.00	2.43	1.82	CC
			7.46	18.00	3.56	2.67	CC
			6.40	18.00	4.16	3.12	CC

* UHPC compressive strength was not mentioned. An estimate of 12 ksi was used early-age compressive strength.

** UHPC compressive strength ranged from 15 ksi to 21 ksi. An average of 18 ksi was used.

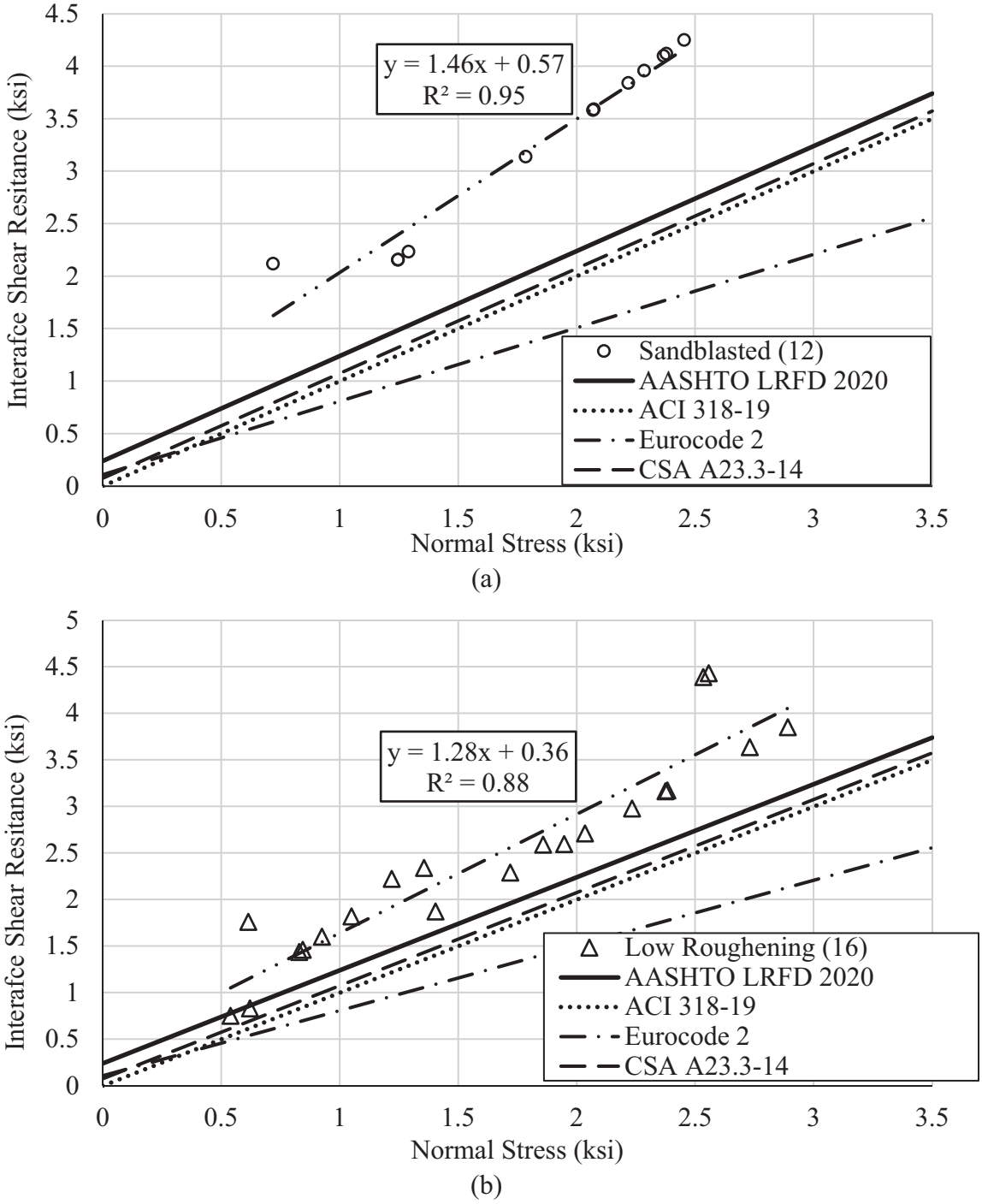

Figure 5.4. Interface Shear Resistance of CC-UHPC with Different Interface Surface Textures; (a) Sandblasted and (b) Low Roughening

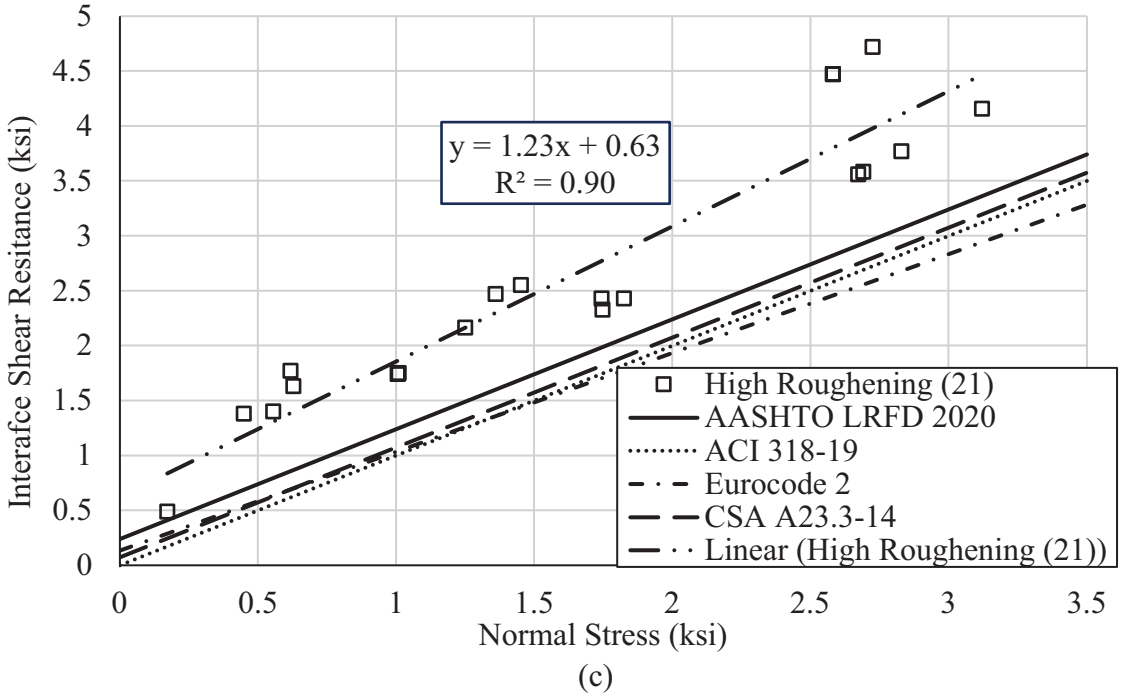

(c)

Figure 5.5. Interface Shear Resistance of CC-UHPC with High Roughening Interface Surface Texture

Table 5.6 summarizes the obtained cohesion and friction factors for each interface surface texture category along with the corresponding coefficients of determination (R^2). The high value of R^2 of each model indicates strong correlation between interface shear resistance and normal stress of CC-UHPC regardless the surface texture. The proposed cohesion factors are two to three times higher than those of CC as the UHPC has higher viscosity that might contribute to its chemical bond with CC. Also, UHPC ability to flow and fill the grooves in the roughened surface achieves a better mechanical interlock with CC substrate, which is evident in the high friction factors for different interface surface textures (23% to 46% higher than CC friction factors of roughened surfaces).

Table 5.6

Proposed CC-UHPC Cohesion and Friction Factors for Different Interface Surface Textures

Interface Surface Texture	Cohesion Factor (c), ksi	Friction Factor (μ)	R^2
Sandblasted	0.57	1.46	0.95
Low-Roughening	0.36	1.28	0.88
High-Roughening	0.63	1.23	0.90

Figure 5.6 shows a plot of the average interface shear resistance grouped by UHPC compressive strength for each interface surface texture. This plot indicates that there is no significant effect of UHPC compressive strength on the interface shear resistance of CC-UHPC with shallow and deep grooved surface textures as the failure occurs at the CC. However, for the as-cut surface texture, where the bond with UHPC is dominant, the interface shear resistance increases with the increase of UHPC compressive strength.

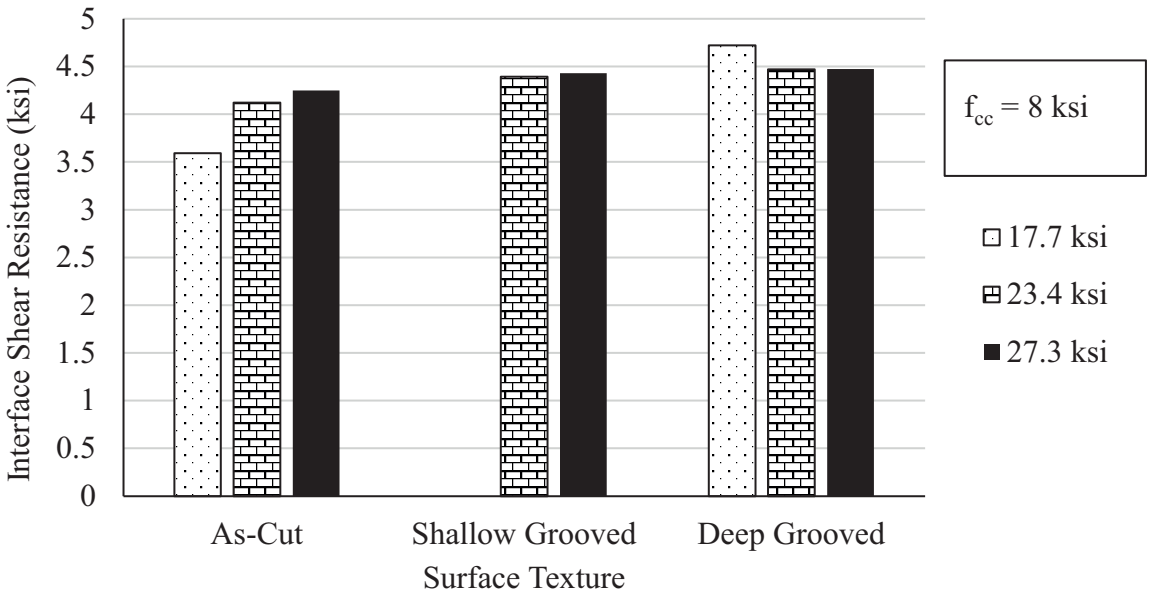

Figure 5.6. Average Slant Shear Test Results at Different UHPC Compressive Strength

5.3.4. Effect of CC compressive Strength on Interface Shear Resistance of CC-UHPC

To study the effect of CC compressive strength, the slant shear data from the literature and experimental investigation were grouped into three categories of CC compressive strength: C1) less than 6 ksi; C2) from 6 ksi to 7 ksi; and C3) greater than 7 ksi. Figure 5.7 shows the average interface shear resistance for each of the three categories in only roughened interface surface textures where CC failure occurred. This Figure indicates that the interface shear resistance increases with the increase of CC compressive strength, however, this trend is not the same among all the three categories. There is insignificant increase in the interface shear resistance between C1 and C2, while there is a significant increase in the interface shear resistance between C2 and C3. More data is needed to determine whether this trend continues for higher compressive strength.

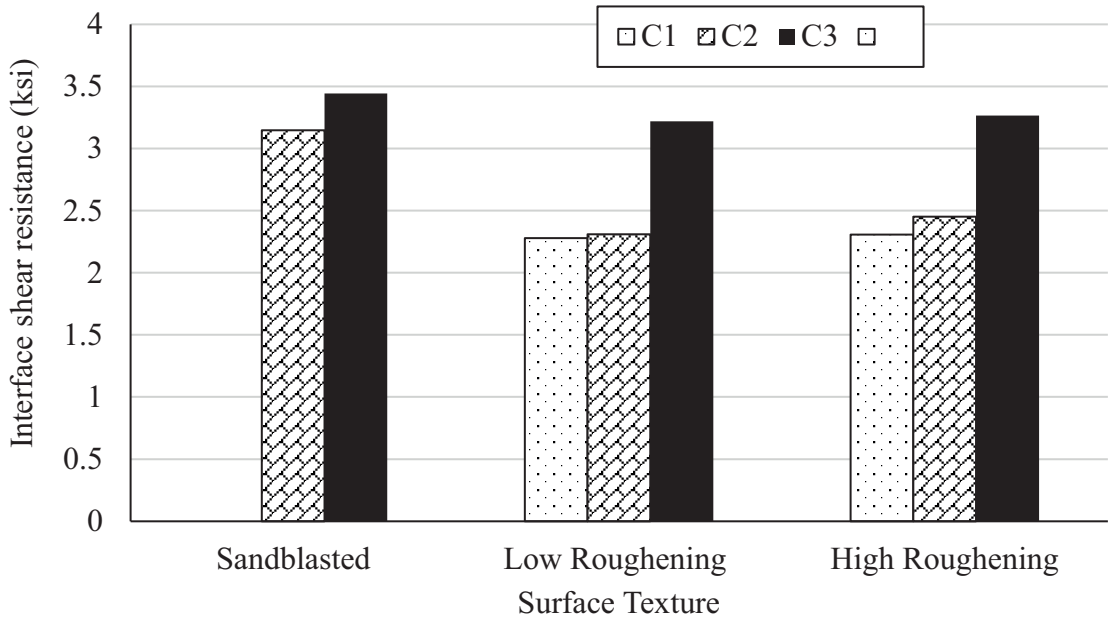

Figure 5.7. Average Slant Shear Test Results at Different CC Compressive Strength

5.3.5. Effect of Fibers on Interface Shear Resistance of CC-UHPC

The effect of steel fibers on the interface shear resistance of UHPC was studied using slant shear testing of two identical groups of specimens with 0.25 in. deep grooves: a) specimens with steel fibers at a dosage of 2% by volume; and b) specimens without steel fibers. Six specimens were tested from each group at two different CC compressive strength and the results are presented in the box-whiskers plot shown in Figure 5.8. This Figure indicates that the presence of fibers does not have significant effect on the interface shear resistance of CC-UHPC. However, it was observed that the specimens without fibers exhibited vertical splitting of the UHPC section without interface failure as shown in Figure 5.9, which could explain the slightly larger interquartile range of this group.

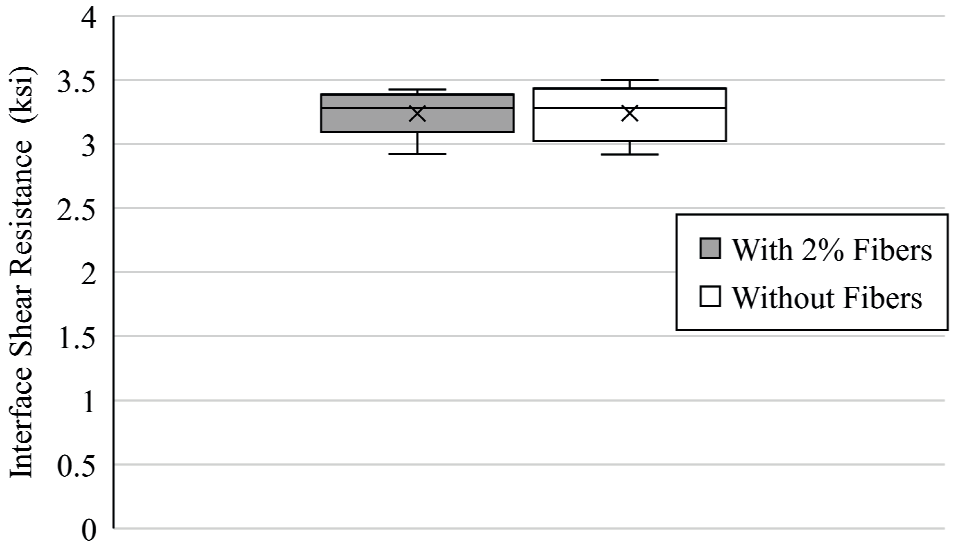

Figure 5.8. Interface Shear Resistance of Slant Shear Specimens with and without Steel Fibers in UHPC

Figure 5.9. Failure Mode for Slant Shear Specimens Using UHPC without Fibers.

5.4. Model Validation

The interface shear reinforcement effect on interface shear capacity of CC-UHPC is studied by conducting L-shape push-off tests. Also, these tests are used to validate the proposed interface shear cohesion and friction factors of CC-UHPC as following.

5.4.1. L-Shape Push-off Test

The L-shape push-off tests were conducted to validate the developed model for CC-UHPC when interface shear reinforcement is used with high roughened surfaces; 0.25 in. deep grooves and shear key with aggregate exposed. Figure 5.10 shows the L-shape push-off specimen dimensions and reinforcement. The shear key dimensions are shown in Figure 5.10 (b). Figure 5.11 shows the test setup and instrumentation. Three different interface reinforcement ratios (0%, 0.44%, and 0.8%) were investigated. A low-slump CC mix was used for casting CC sections to allow for applying ¼ in. deep roughening as shown in Figure 5.12(a). Figure 5.12(b) shows the shear key interface texture as as-cast.

Also, a concrete retarder admixture was applied to the forms at the shear key to allow using a pressure washer, the next day of casting, to have exposed aggregate interface texture as shown in Figure 5.12(c). This procedure of applying aggregate exposed interface is the same used in precast plants. The CC sections of the L-shape specimens were wrapped with plastic sheets for curing after stripping the forms at 24 hours. The fresh UHPC was cast vertically on top of the horizontal hardened roughened CC interface to mimic common construction practices as shown in Figure 5.13(a). For shear key specimens, the UHPC was cast horizontally besides the hardened CC as shown in Figure 5.13(b). The UHPC forms were stripped at 24 hours and the specimens were covered with plastic sheets for curing in room temperature until the day of testing. The average compressive strength of CC was 6.6 ksi and of UHPC were 20.84 ksi and 16.71 ksi for deep grooved and shear key interface textures at the testing day, respectively. The relative displacement in the parallel (slip) and perpendicular (crack width) directions to the interface plane were measured using two LVDTs for each side as shown in Figure 5.11. A hydraulic ram was used to load the specimens at a rate of 600 Ib/sec. using a steel plate and bearing pads to evenly distribute the applied force. Specimens were labeled using the form A-B-C%#D, where A is the first section, B is the second section, C is the interface texture type, D is the interface reinforcement ratio, and E is the specimen number as shown in Table 5.7.

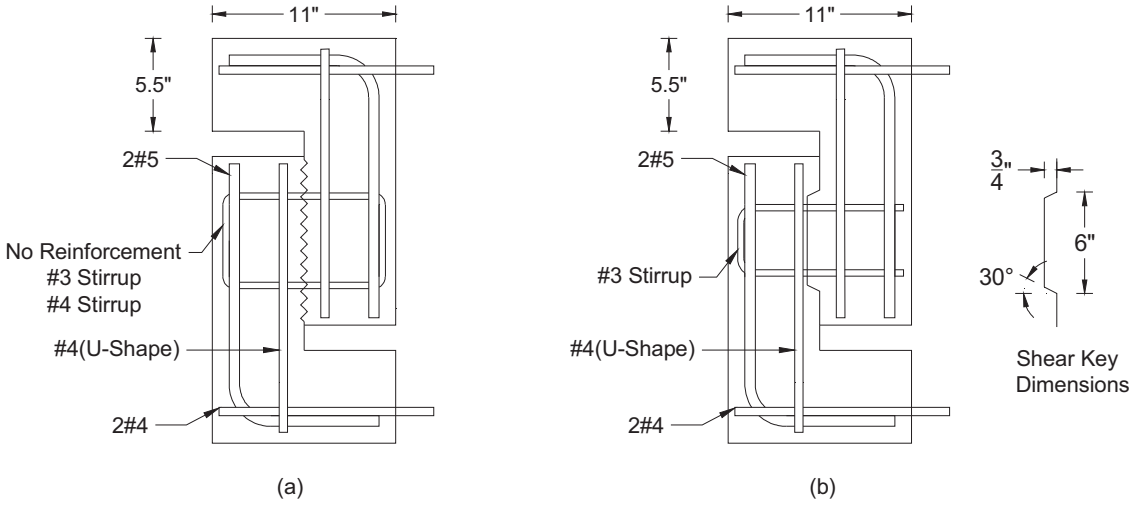

Figure 5.10. L-Shape Push-off Specimen Details and Reinforcement Details (in.); (a) 0.25 in. Deep Grooved Interface Texture and (b) Shear Key Interface Texture.

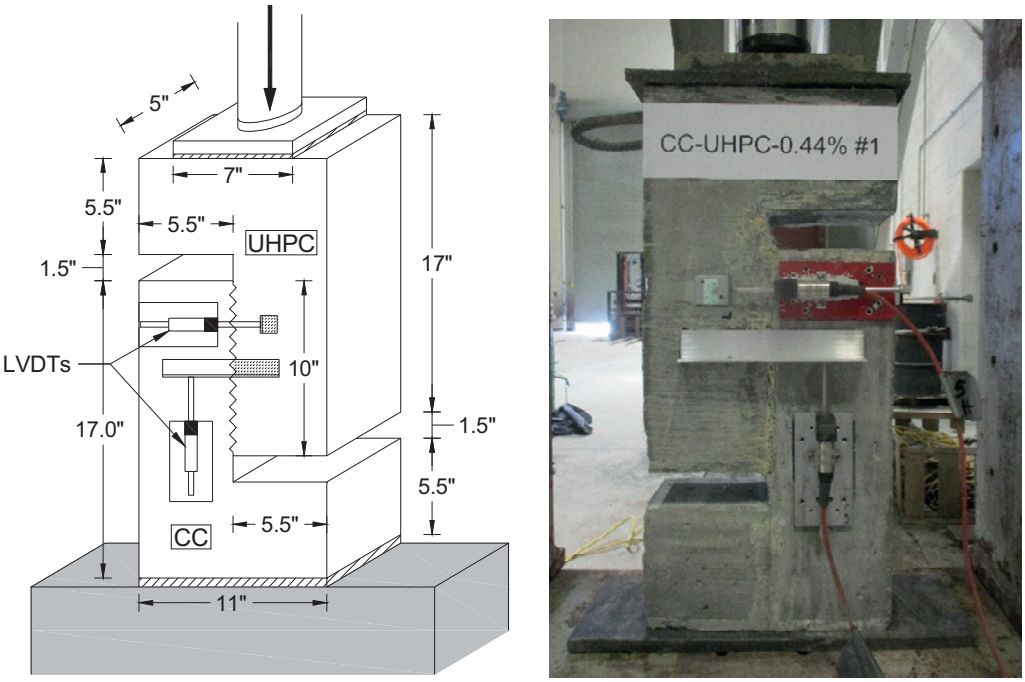

Figure 5.11. L-Shape Push-off Test Setup and Reinforcement Details (in.).

(a)

(b)

(c)

Figure 5.12. Interface Surface Roughening and Reinforcement; (a) No Reinforcement (left), 2leg #3 stirrup (middle), and 2leg #4 stirrup (right), (b) As-cast Shear Key with 2leg #3 stirrup, and (c) Aggregate Exposed Shear Key with 2leg #3

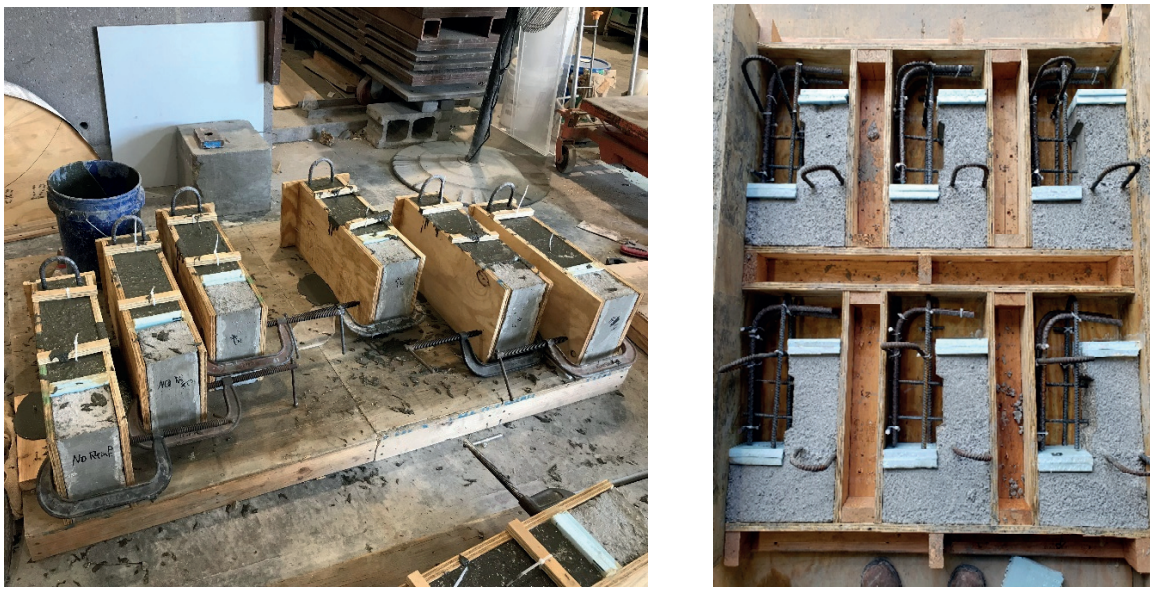

(a) (b)

Figure 5.13. Casting UHPC in L-shape Specimens in Case of Deep Grooved Interface (a) and Shear Key Interface (b)

Table 5.7

L-Shape Push-off Test Specimens

Interface Surface Texture	A_{cv} ($in.^2$)	Interface Reinforcement	Interface Reinforcement Ratio, $\rho = A_{vf}/A_{cv}$ (%)	Label
Deep Grooved (≥1/4 in. deep)	50	None	0.0	CC-UHPC-G-0%
		2-Leg #3 Stirrup	0.44	CC-UHPC-G-0.44%
		2-Leg #4 Stirrup	0.80	CC-UHPC-G-0.8%
As-Cast Shear Key (3/4 in. deep)		2-Leg #3 Stirrup	0.44	CC-UHPC-K-0.44%
Shear Key with Aggregate Exposed (3/4 in. deep)		2-Leg #3 Stirrup	0.44	CC-UHPC-E-0.44%

5.4.2. Analysis of Test Results

Table 5.8 shows the results of testing fifteen L-shape specimens in terms of maximum applied shear stress at failure and failure location. All the specimens with deep grooved interface exhibited failure in the CC section parallel to the interface plane as shown in Figure 5.14. However, all the specimens with shear key interface exhibited failure at interface plane as shown in Figure 5.15. The specimens without interface shear reinforcement exhibited brittle failure at the peak shear load as shown in Figure 5.14(a), while specimens with interface shear reinforcement exhibited ductile failure due to reinforcement yielding as shown in the other specimens.

Table 5.8

L-Shape Push-off Test Results and Comparison to Predicted Resistance

Specimen Label	Maximum Applied Shear Stress (ksi)	Average Shear Stress (ksi)	Predicated Shear Resistance (ksi)	Failure Location
CC-UHPC-G-0% #1	0.82			CC
CC-UHPC-G-0% #2	0.98	0.84	0.63	CC
CC-UHPC-G-0% #3	0.72			CC
CC-UHPC-G-0.44% #1	1.34			CC
CC-UHPC-G-0.44% #2	1.04	1.20	0.95	CC
CC-UHPC-G-0.44% #3	1.21			CC
CC-UHPC-G-0.8% #1	1.32			CC
CC-UHPC-G-0.8% #2	1.26	1.27	1.22	CC
CC-UHPC-G-0.8% #3	1.24			CC
CC-UHPC-K-0.44% #1	0.80			Interface
CC-UHPC-K-0.44% #2	0.87	0.82	0.95	Interface
CC-UHPC-K-0.44% #3	0.81			Interface
CC-UHPC-E-0.44% #1	1.15			Interface
CC-UHPC-E-0.44% #2	1.09	1.13	0.95	Interface
CC-UHPC-E-0.44% #3	1.15			Interface

(a) (b) (c)

Figure 5.14. CC failure modes of L-Shape Specimens with Deep Grooved Interface Texture; (a) no reinforcement, (b) ρ = 0.44%, and (c) ρ = 0.8%.

(a) (b)

Figure 5.15. Interface Failure Modes of L-Shape Specimens with Shear Key Interface Texture with 0.44% Interface Shear Reinforcement; (a) As-Cast, and (b) Exposed Aggregate

Figure 5.16 and Figure 5.17 show the interface shear resistance versus slip and crack width, respectively, at the interface plane of the tested specimens with deep grooved interface (≥1/4 in. deep). The specimens without interface shear reinforcement exhibited brittle failure at the maximum load. However, the presence of interface shear reinforcement led to a ductile failure as evident in the high slip and crack width values after reaching the maximum capacity. Also, these plots show that the peak shear load occurred at very low slip and crack width values (less than 0.01 in.), which indicates the reinforcement contribution in controlling the crack width and interface displacement.

Figures 5.18 and 5.19 show the measured slip and crack width at the interface plane of L-shape specimens with both as-cast shear key and shear key with exposed aggregate. The specimens exhibited interface failure at the shear key with measured slip and crack width of 0.01 in. at the peak load similar to the deep grooved interface. The shear key with exposed aggregate has a higher interface shear resistance of 38% than as-cast shear key. Thus, it is recommended to have aggregate exposed at the shear keys to enhances it performance.

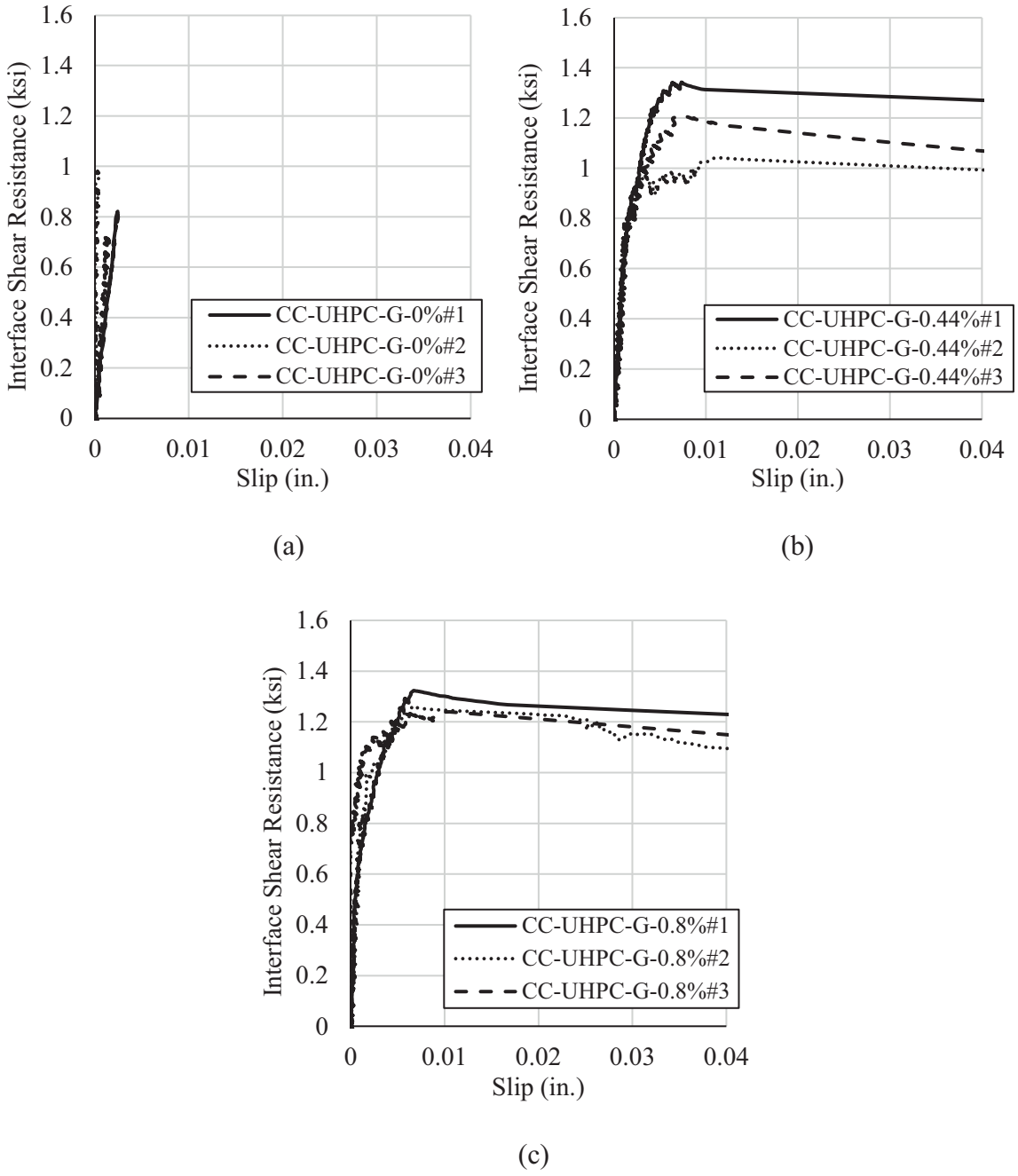

Figure 5.16. Effect of Different Interface Reinforcement Ratios on Slip Measured Between the Two L-Shape Sections in Case of Deep Grooved Interface Texture (≥1/4 in. depth); (a) 0%, (b) 0.44%, and (c) 0.80 %

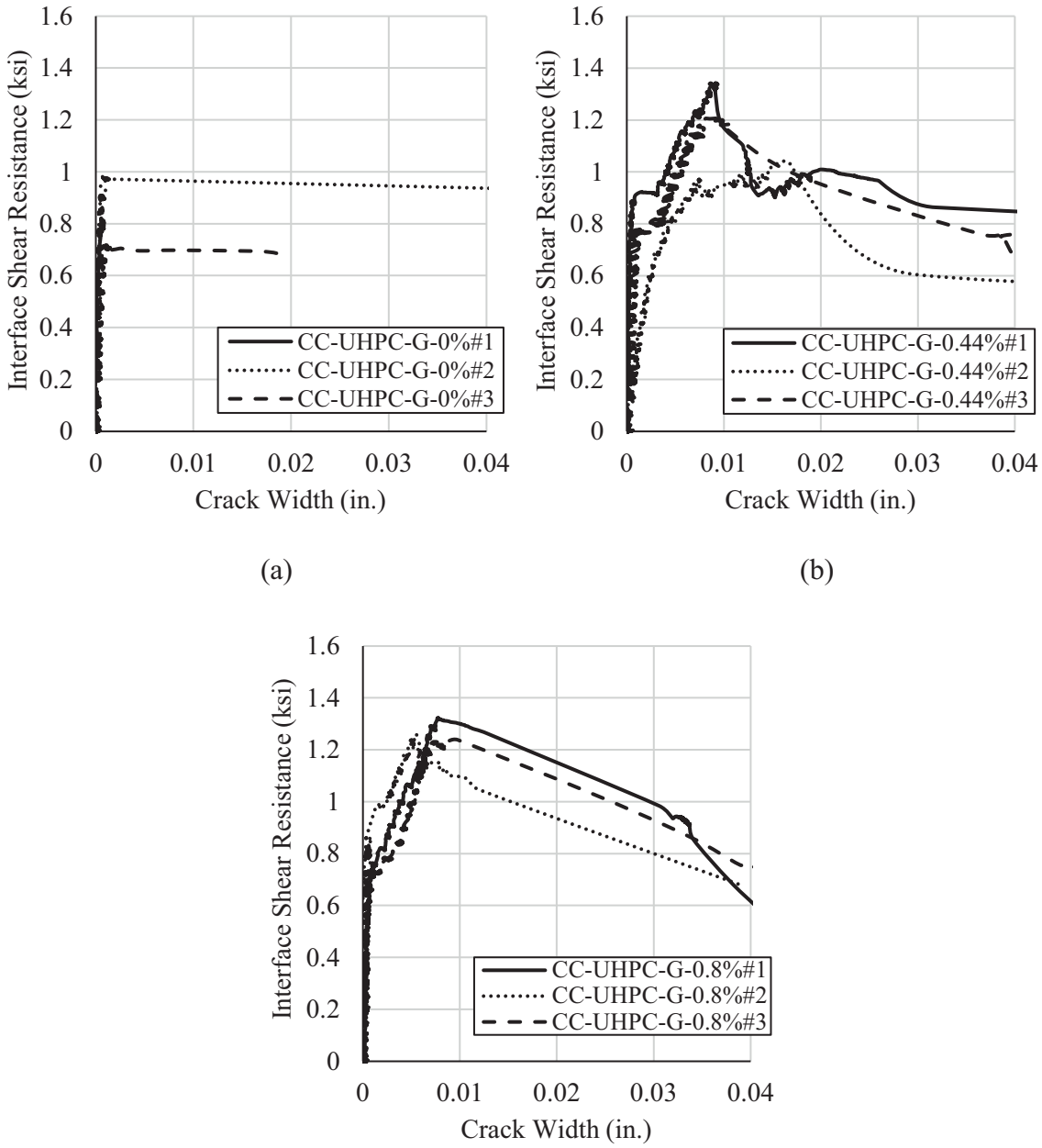

Figure 5.17. Effect of Different Interface Reinforcement Ratios on Crack Width Measured Between the Two L-Shape Sections in Case of Deep Grooved Interface Texture (≥1/4 in. depth); (a) 0%, (b) 0.44%, and (c) 0.80 %

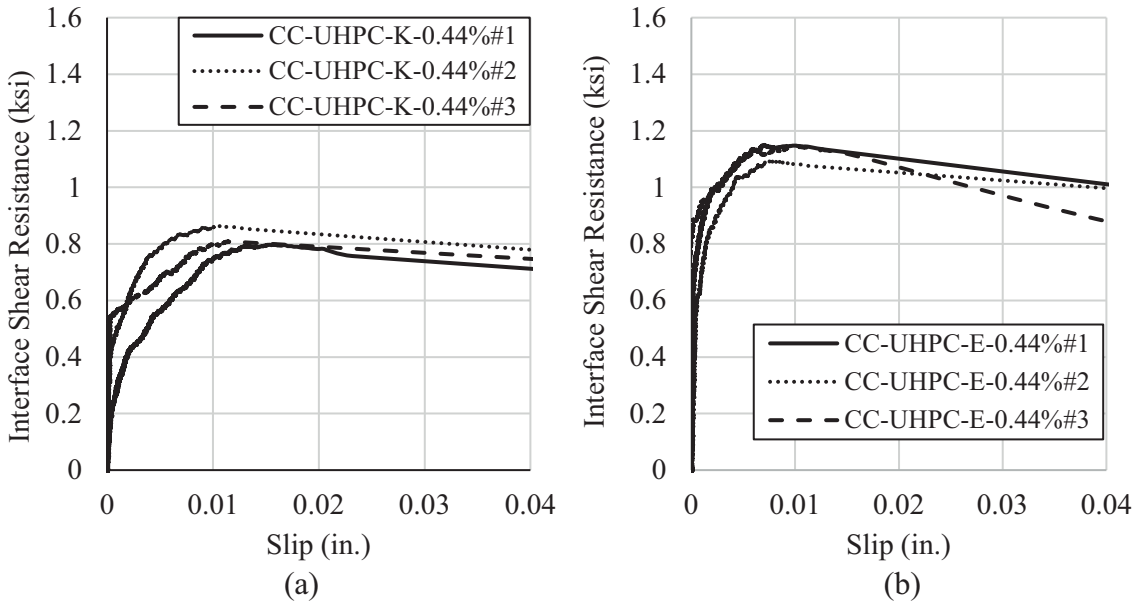

Figure 5.18. Effect of Shear Key Interface Texture on Slip Measured between the Two L-Shape Sections with 0.44% Interface Shear Reinforcement Ratio: (a) As-Cast and (b) Aggregate Exposed

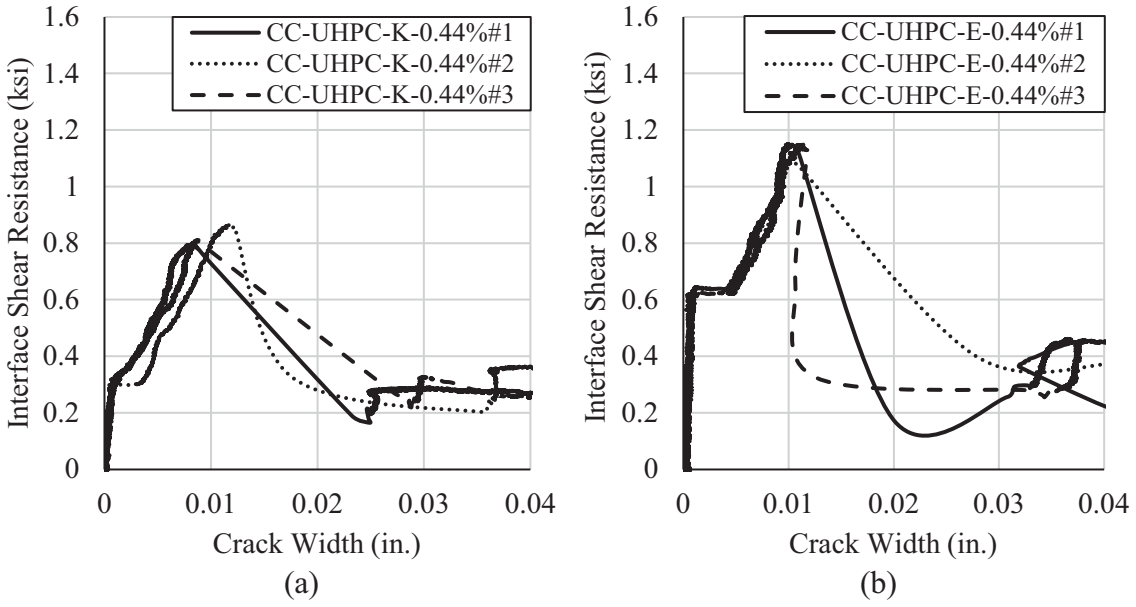

Figure 5.19. Effect of Shear Key Interface Texture on Crack Width Measured between the Two L-Shape Sections with 0.44% Interface Shear Reinforcement Ratio: (a) As-Cast and (b) Aggregate Exposed

The L-shape push-off test results show good agreement with the predicted resistance using the proposed c and μ factors for high-roughened interface surface texture with depth greater than 0.25 in. except the as-cast shear key interface texture as shown in Figure 5.20. This figure also shows that the current code provisions for CC are conservative in predicting interface shear resistance of CC-UHPC of high roughening interface shear textures for both deep grooved interface (≥ 0.25 in. depth) and shear key interface (≥ 0.75 in. depth) as the CC is always the weak link. The proposed interface shear factors are applicable to conventional concrete with compressive strength ranging from 5.2 ksi to 8.24 ksi based on the literature and the experimental program. This CC compressive strength range covers most of the concrete applications. In case of using concrete with higher compressive strength and better mechanical properties, the failure might occur at the interface plane instead.

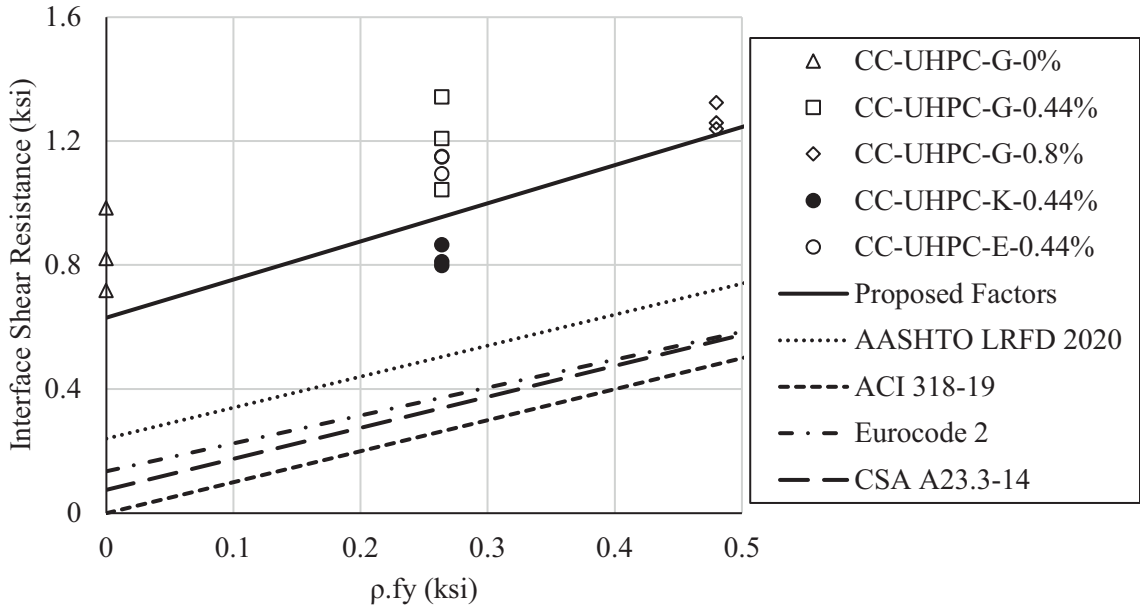

Figure 5.20. L-Shape push-off test results and their comparison with proposed cohesion and friction factors and code provisions.

CHAPTER 6: INTERFACE SHEAR RESISTANCE OF MONOLITHIC UHPC

In this chapter, direct shear, L-shape push-off, and double shear push-off tests were conducted to evaluate the interface shear resistance of monolithic UHPC. Test results were used along with the data obtained from the literature to obtain a cohesion and friction factors for interface shear resistance. Then, A finite element model (FEM) was developed using ANSYS 20 R2 software to perform a parametric study on the shear pocket dimensions and reinforcement size. The UHPC mechanical properties presented in chapter 4 are used to identify the materials models. Finally, a full-scale push-off test for the proposed connection is conducted to evaluate the constructability and structural performance, especially the effect of UHPC stability on the connection performance.

6.1. Interface Shear Resistance Code Provisions

The current code provisions do not have a prediction cohesion and friction coefficient for the case of interface shear resistance of monolithic UHPC. ACI 318-19, AASHTO LRFD 2020, and CSA 2014 interface shear prediction equations were discussed in the previous chapter (Chapter 5). Table 6.1 shows the cohesion and friction factors for monolithic CC as stated in these codes for comparison.

Table 6.1

Cohesion and Friction Factors for Interface Shear Resistance of Monolithic Normal Weight Concrete by Different Codes.

Factors	Cohesion Factor (c), ksi (MPa)	Friction Factor (μ)
ACI 318-19 (Section 22.9.4)	-	1.4
AASHTO LRFD (Section 5.7.4.3)	0.40 (2.76)	1.4
CSA A23.3-14 (Section 11.5)	0.15 (1.0)	1.40

6.2. Experimental Program

Direct shear, L-shape push-off, and double shear push-off tests were conducted to evaluate the interface shear resistance of monolithic UHPC and obtain cohesion and friction factors. The UNL-UHPC and commercially available pre-bagged UHPC mixes were used in the experimental program and their mechanical properties were presented in Chapter 4.

6.2.1. Direct Shear Test

A direct shear test was conducted to evaluate the interface shear resistance of monolithic UHPC without interface reinforcement using 2x2x6 in. prismatic specimens. The specimens were cast from one end in long forms to allow UHPC to flow and align the fiber along the form. The molds were stripped after one day and submerged in lime-saturated water until the day of testing. Then, the specimens were cut using wet saw to the desired length. A steel loading frame was used to apply double shear loading to the specimens as shown in Figure 6.1. A displacement-controlled loading rate of 0.05 in./min. was applied until failure.

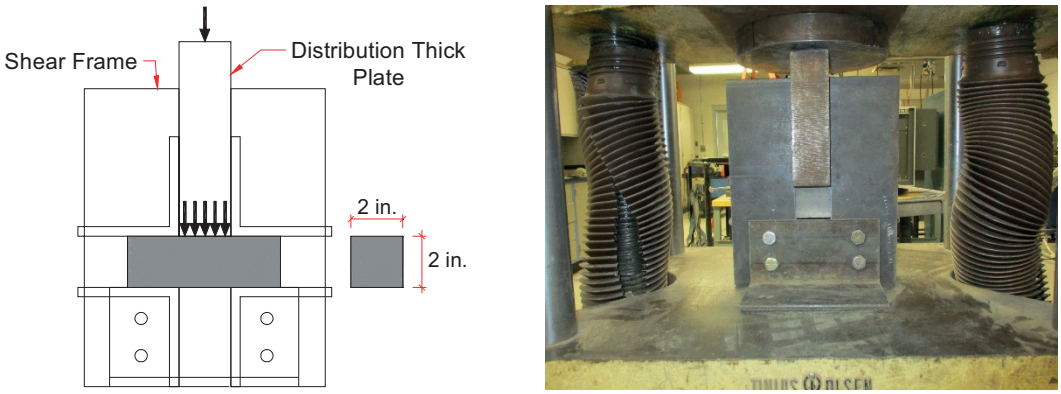

Figure 6.1. Direct Shear Test Setup.

A total of 26 specimens were tested at different compressive strengths of UHPC. All the specimens exhibited double shear failure as shown in Figure 6.2. The obtained direct shear strength was calculated by dividing the applied load by the double shear areas. The average direct shear strength of minimum three specimens ranged from 4.0 to 5.95 ksi as the average compressive strength of UHPC ranged from 11.8 to 23.4 ksi. Figure 6.3 shows the obtained direct shear test results (each point shows an average value) and their comparison to the literature. Detailed testing results are available in Appendix A.

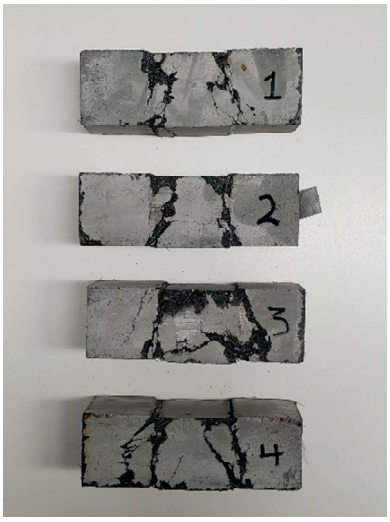

Figure 6.2. Double Shear Failure Mode of Direct Shear Test Specimen.

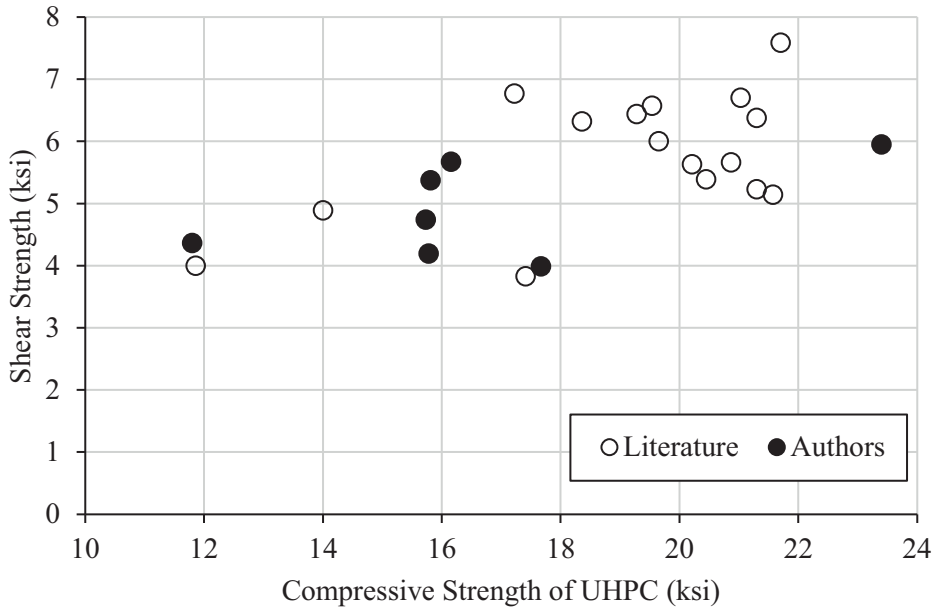

Figure 6.3. Direct Shear Test Results and Their Comparison to the Literature.

Figure 6.4 shows the direct shear strengths with averages of UHPC specimens with different fiber stability: low, medium, and high. The fiber stability of UHPC specimens was determined visually by cutting hardened UHPC cylinders. Specimens with high and medium fiber stability had almost similar direct shear strength, while specimens with low fiber stability had 30% less direct shear strength due to fiber segregation.

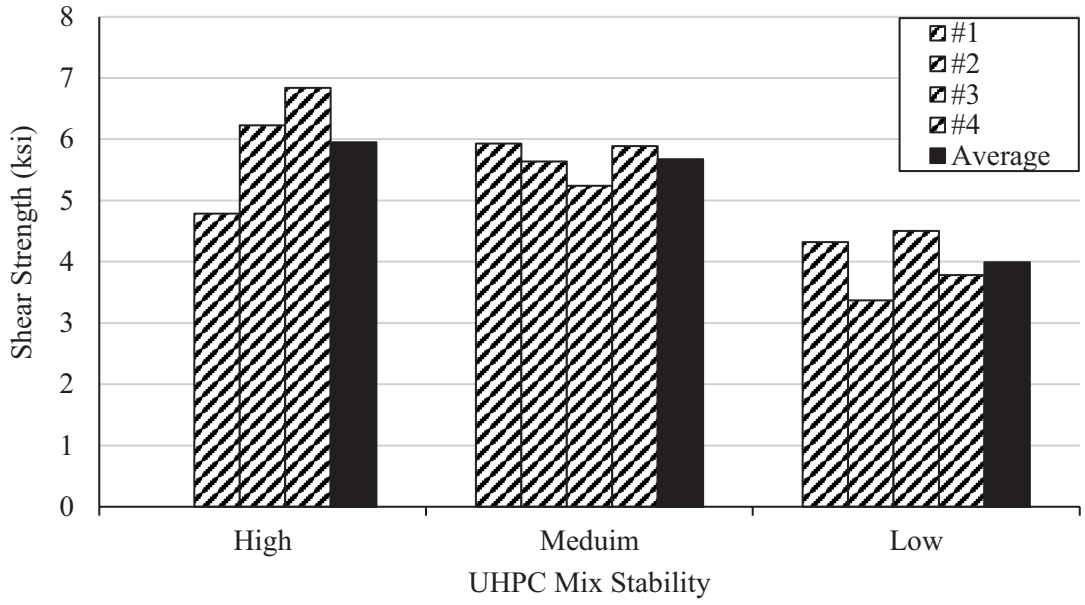

Figure 6.4. Effect of UHPC Mix Stability on Direct Shear Test Results.

It should be noted that direct shear test data shows much higher shear strength than those obtained from L-shape test literature. This difference could be attributed to the small size of the specimens and the presence of a different load path of compression struts from the applied load to the supports, which does not represent the true shear strength of UHPC.

6.2.2. L-Shape Push-off Test

L-shape push-off test was conducted to investigate the interface shear resistance of monolithic UHPC. The L-shape specimens were casted horizontally, stripped out of forms after one day, and covered with plastic until the testing day. Figure 6.5 and Figure 6.6 show the L-shape specimen details and test setup. The relative displacements, parallel (slip) and perpendicular (crack width) to interface plane, between two L-sections were captured using four LVDTs (two LVDTs for each side) as shown in Figure 6.7(a). A

shear load rate of 600 lb/sec. was applied until failure using a hydraulic ram after being aligned with the interface plane. The applied load was measured using a pressure transducer attached to the ram. The specimens were labeled as UHPC-MON-A%#B where MON means monolithic, A is the interface reinforcement ratio, and B is the specimen number.

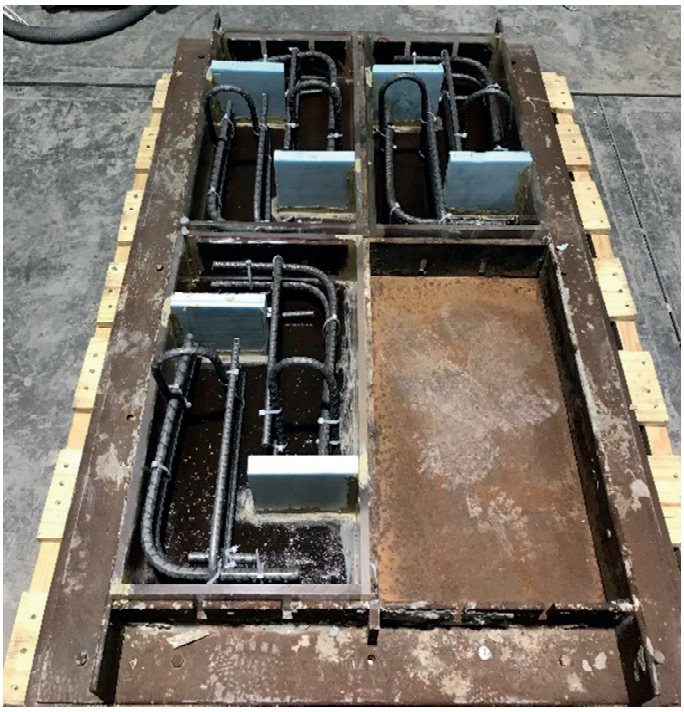

Figure 6.5. L-Shape Push-off Specimen Preparation.

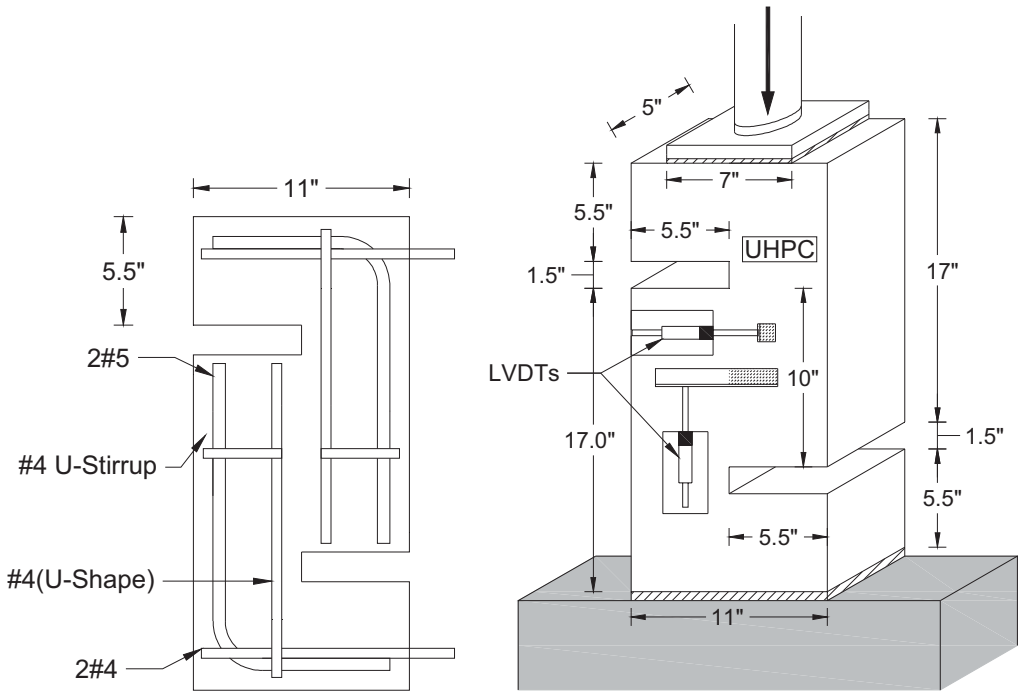

Figure 6.6. L-Shape Push-off Specimen Details and Test Setup and Instrumentation.

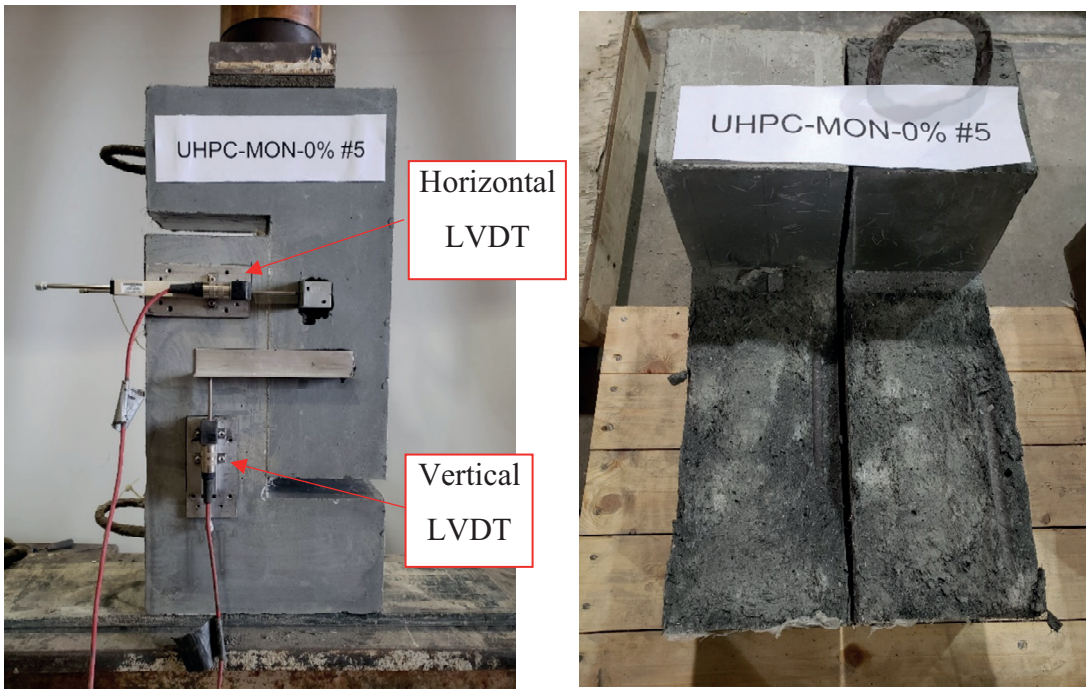

(a) (b)

Figure 6.7. L-Shape Push-off Test; (a) Test Setup, and (b) Failure Mode.

All the specimens exhibited interface shear failure as shown in Figure 6.7(b). The interface shear resistance (v_{ni}) was calculated by dividing the applied load by interface shear area (50 in.^{2}). The specimens #1 to #3 had a compressive strength of 25.3 ksi and specimens #4 and #5 had a compressive strength of 17.1 ksi. The average interface shear resistance of monolithic UHPC is 2.42 ksi and 2.0 ksi at UHPC compressive strength of 25.3 ksi and 17.1 ksi, respectively, as shown in Table 6.2. The measured slip did not exceed 0.01 in. at the peak load as shown in Figure 6.8(a). Figure 6.8(b) shows the effect of fibers crossing the interface that act like stiches and provides ductile behavior at the peak load without interface reinforcement. This ductile behavior mainly controlled by the fiber content in UHPC mix which might change with different fiber content.

Table 6.2

Monolithic L-Shape Push-off Test Results

Specimen Label	f'_{UHPC} (ksi)	Maximum Applied Shear Stress (ksi)	Average Shear Stress (ksi)	COV%
UHPC-MON-0% #1	25.13	2.51	2.42	7.4
UHPC-MON-0% #2		2.54		
UHPC-MON-0% #3		2.22		
UHPC-MON-0% #4	17.13	2.06	2.02	2.8
UHPC-MON-0% #5		1.98		

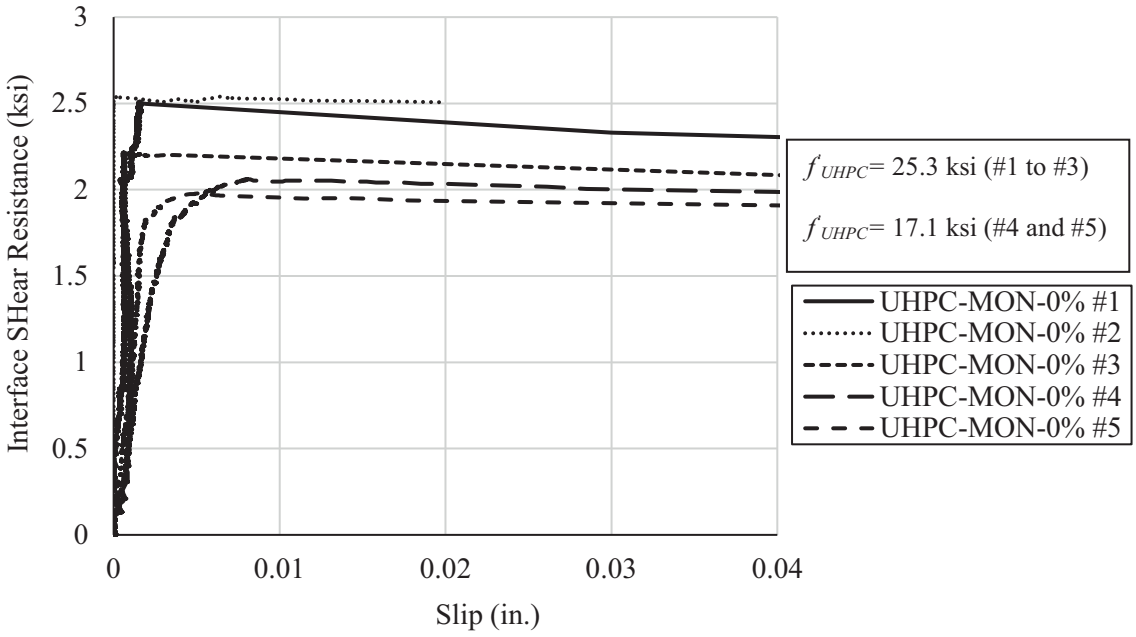

(a)

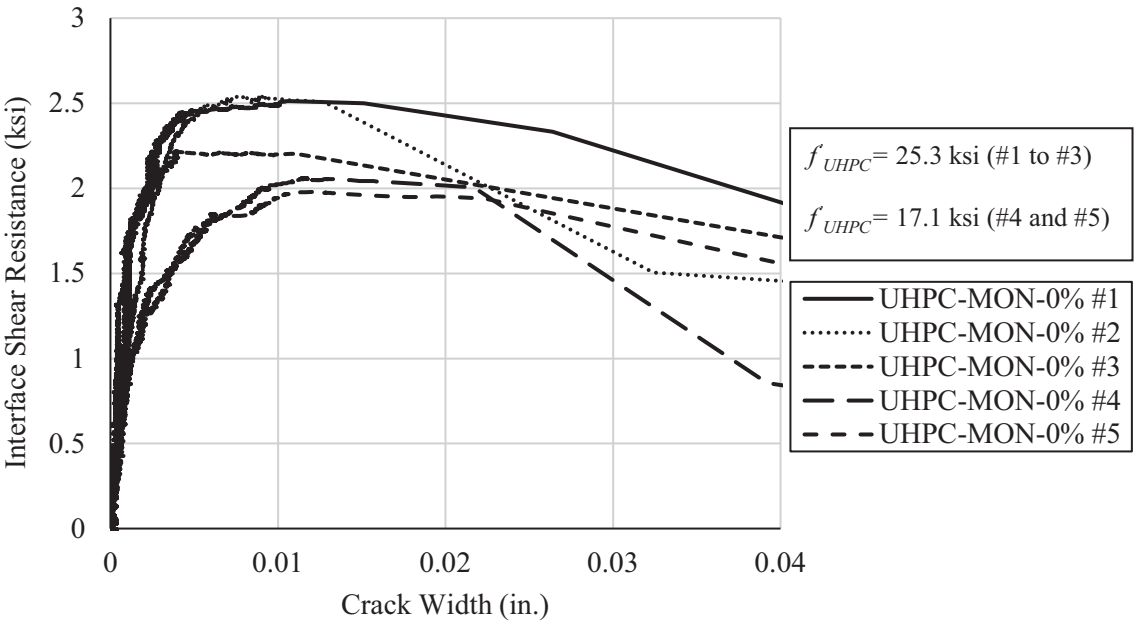

(b)

Figure 6.8. Interface Shear Resistance versus Relative Displacements of Monolithic L-Shape Push-off Test; (a) Slip, and (b) Crack width

Figure 6.9. shows the results of L-shape push-off tests and their comparison with similar testing in the literature (Crane 2010 and Jang et al. 2017). The L-shape test results had better consistency and less scatter than those of direct shear tests. It also shows that the interface shear resistance of monolithic UHPC depends on the compressive strength of UHPC as the trendline gives high correlation, almost 1.0, with the square root of UHPC compressive strength. The high correlation might be attributed to the intersect of the trendline with (0,0) point to obtain the cohesion factor. The interface shear resistance of monolithic UHPC can be predicted using the proposed cohesion factor as follows, which is much higher than that of monolithic CC (0.4 ksi):

$$c = 0.49\sqrt{f'_{UHPC}} \quad \text{(ksi)} \tag{6-1}$$

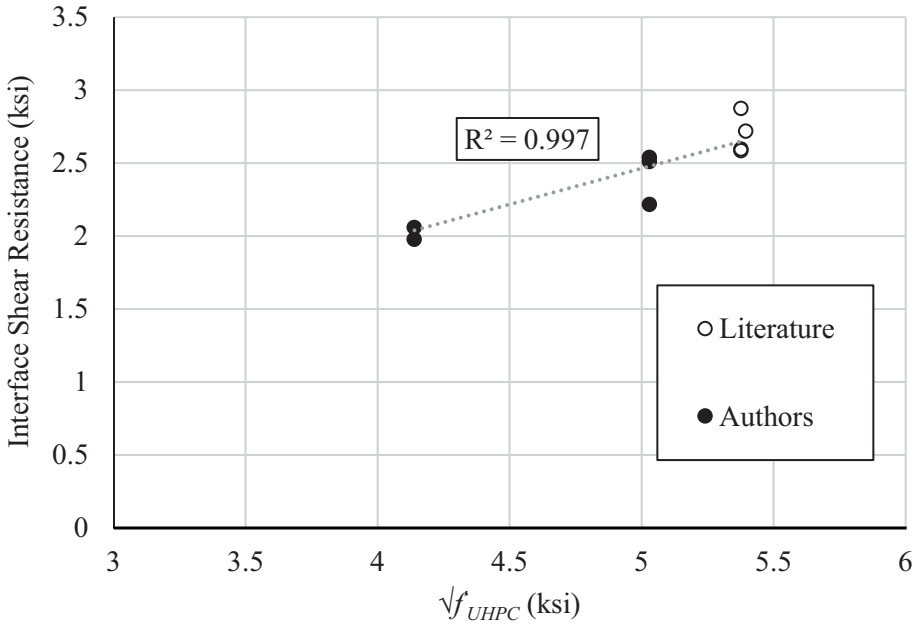

Figure 6.9. L-Shape Push-off Test Results of Monolithic UHPC and their Comparison to the Literature.

6.2.3. Double Shear Test

The interface shear resistance of monolithic UHPC with interface reinforcement was evaluated by performing double shear tests. Double shear specimens were designed to mimic the proposed connection with 6 in. diameter round shear pocket and embedded No. 5 loop bar. Two 20x20x8 in. conventional concrete (CC) slabs, with 6 in. diameter shear pocket in the center, were cast to be used for applying the shear load. Two reinforcement layers (8 #4 each) were used to enhance the capacity of concrete slab. The shear pocket was formed using a corrugated plastic pipe to create 0.25 in. roughened surface between CC and UHPC. Two 16x20x4 in. UHPC slabs were cast on the sides of precast CC slab. Each UHPC slab had two U-shape #4 bars to enhance the slab capacity. A #5 loop bar was added to the shear pocket as shown in Figure 6.10 before casting UHPC. The specimens were labeled similar to the L-shaped push-off specimens.

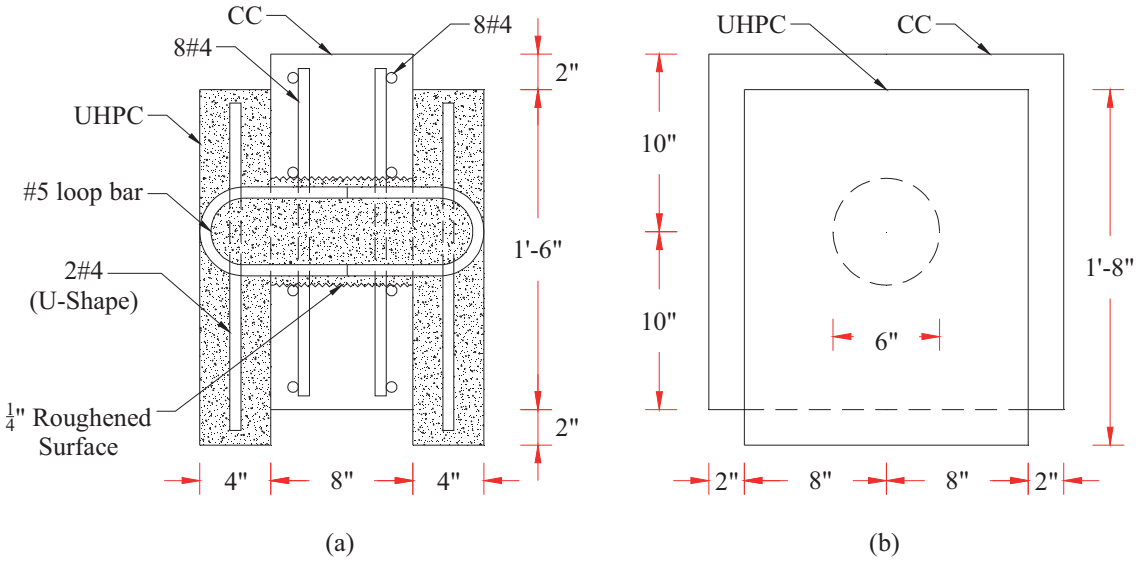

Figure 6.10. Double Shear Test Specimen Details; (a) Section Elevation, and (b) Side View.

- **Specimen Fabrication**

Figure 6.11 shows the fabrication of the CC slab with 6 in. corrugated plastic pipe. The CC slab was cast using self-consolidating concrete and then, was covered with plastic for 28 days to cure. The plastic pipe was removed easily from the shear pocket without damaging the roughening as shown in Figure 6.12(a). In order to eliminate the contact between UHPC and CC, the top and bottom surfaces of CC slabs were covered with wax as shown in Figure 6.12(b). A 2 in. rigid structural foam was used to form the 4 in. UHPC slabs thickness and the No. 5 loop bar was added through the shear pocket as shown in Figure 6.13. The UHPC was cast vertically to fill the slabs and shear pocket. Finally, the top surface of specimens was covered with rigid foam and plastic sheet until the day of testing.

Figure 6.11. Concrete Section of Double Shear Test Specimen.

(a) (b)

Figure 6.12. Concrete Section Preparation of Double Shear Test Specimen; (a) Removed Plastic Pipe, and (b) Applying Wax on Concrete Surfaces.

Figure 6.13. Double Shear Specimen Forming

- **Test Setup**

At time of testing, the compressive strength of CC slab was 6.9 ksi, while the compressive strength of UHPC slabs was 17.7 ksi. The specimen base was ground and placed on structural bearing pads to avoid uneven loading. The shear load was applied using a hydraulic ram and steel plates to distribute the load over an area of 8 in. x 14 in.

Four LVDTs were attached vertically to the specimen (two for each side) to capture the relative vertical displacement (slip) between the CC slab and UHPC (slip) at the two interface shear planes. Figure 6.14. shows the double shear test setup and instrumentation.

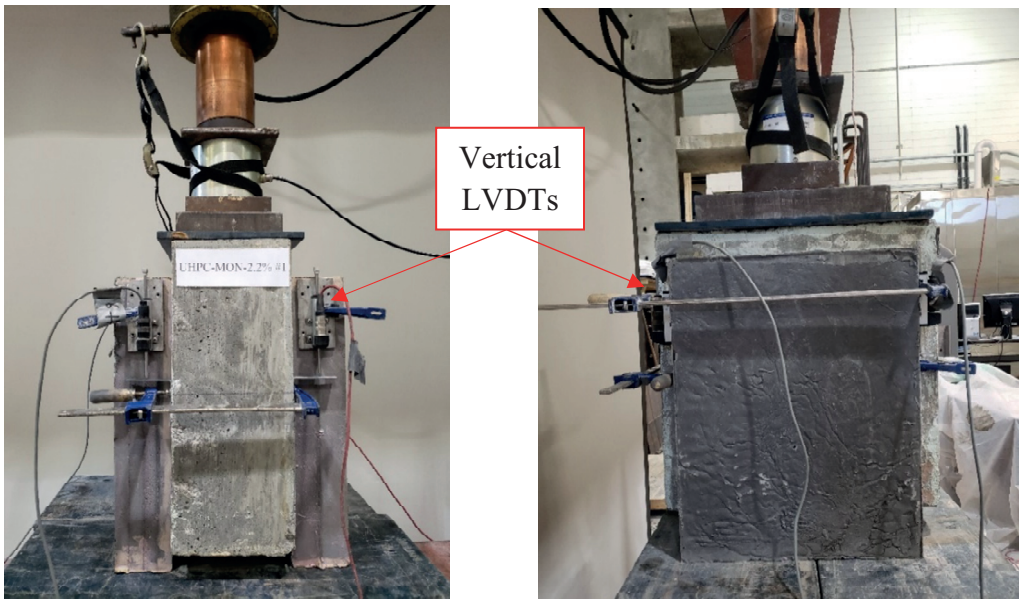

(a) (b)

Figure 6.14. Double Shear Specimen Test Setup; (a) Front View, and (b) Side View.

The two specimens exhibited similar double shear failure at the UHPC shear pocket between CC and UHPC slabs as shown in Figure 6.15(a). Figure 6.15(b) shows the rupture of #5 loop bar at the interface plane. Figure 6.16 shows the average measured slip at the top and bottom interface plane, as the specimens were cast. The average interface shear resistance was 6.77 ksi for monolithic UHPC with 2.2% interface reinforcement as shown in Figure 6.17. The clamping force produced by interface reinforcement provides more ductility to the interface behavior compared to L-shape specimens without interface reinforcement. The average slip recorded by the four LVDTs reached 0.1 in. at the peak load which reflects the effect of clamping forces.

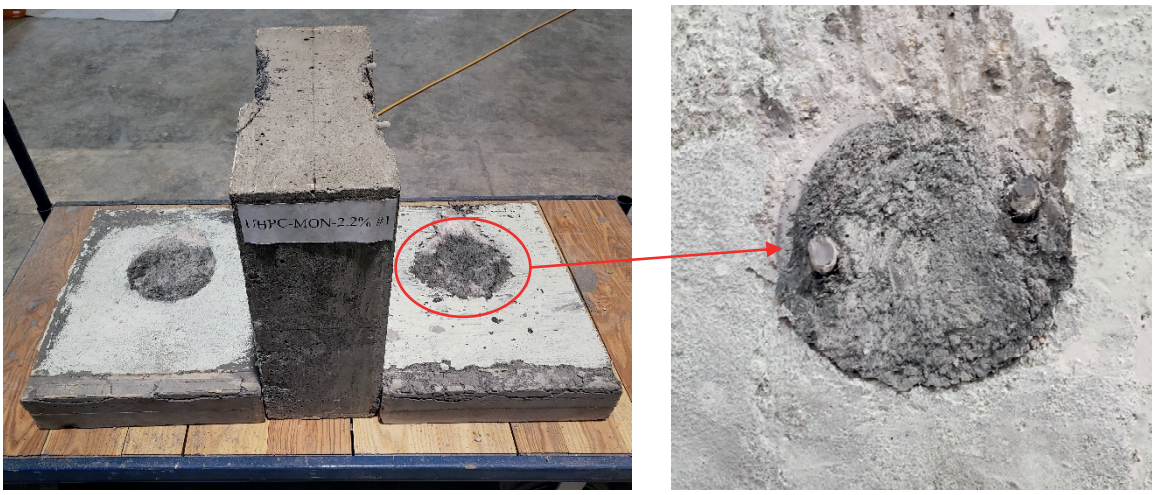

(a) (b)

Figure 6.15. Double Shear Specimen Failure Mode; (a) Double Shear Failure, (b) No. 5 Bar Rupture

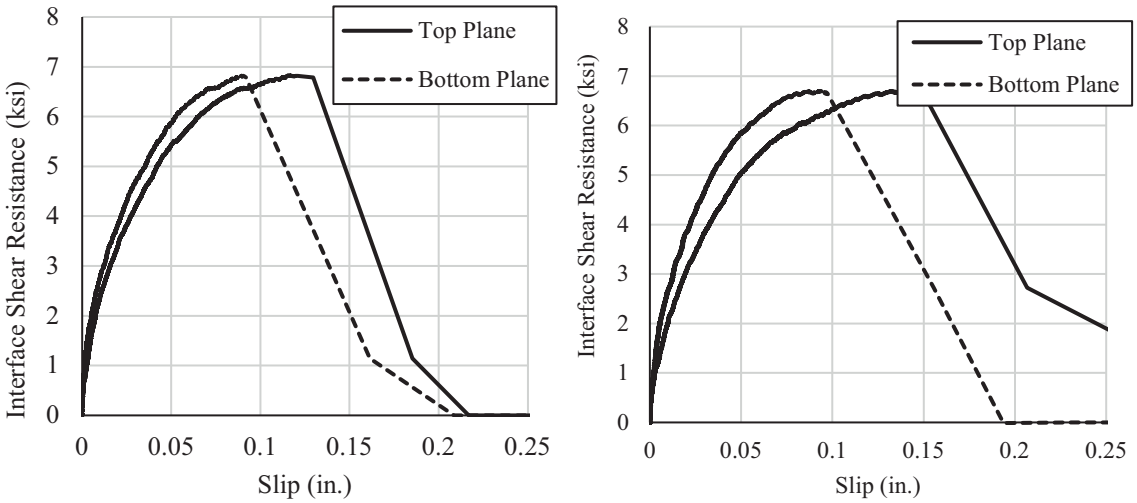

Figure 6.16. Interface Shear Resistance versus Measured Slip at Top and Bottom Interface Planes for Double Shear Specimen #1 (left) and #2 (right)

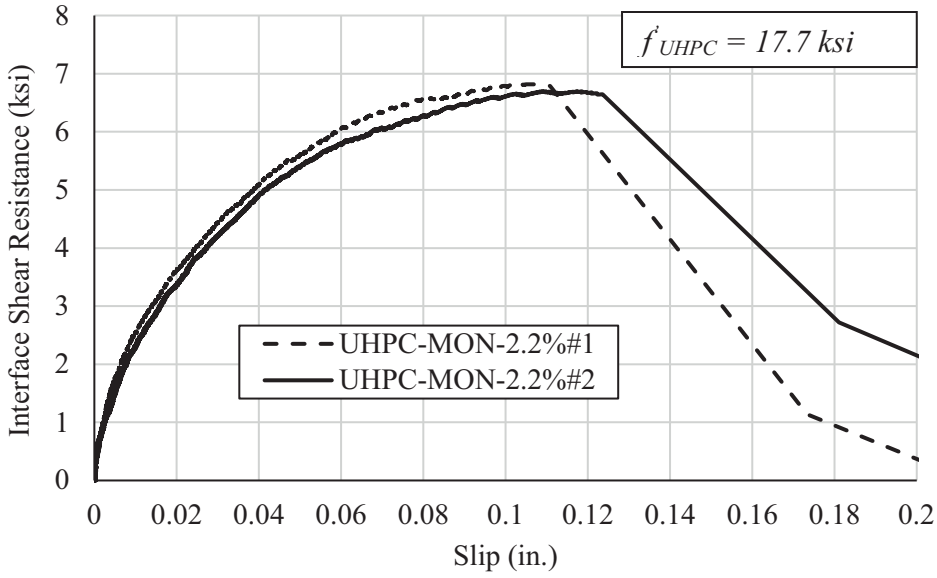

Figure 6.17. Interface Shear Resistance versus Average Measured Slip of Double Shear Test

To develop an equation for predicting the effect of reinforcement clamping force on the interface shear resistance of monolithic UHPC, data obtained from the double shear tests and from the literature (Crane, 2010) were summarized as shown in Table 6.3. The shear friction model of AASHTO LRFD (2020) was used but with considered the effect of UHPC compressive strength on both cohesion and friction factors. Below is the proposed shear friction equation for predicting the interface shear resistance of monolithic UHPC with 2% fiber content:

$$v_{ni} = 0.49\sqrt{f'_{UHPC}} + 0.85\sqrt{f'_{UHPC}} * \rho * f_y \text{ (ksi)} \qquad (6\text{-}2)$$

Table 6.3

Interface Shear Resistance Analysis of Monolithic UHPC with Interface Reinforcement

Specimen ID		ρ (%)	v_{ni} (ksi)		f'_{UHPC} (ksi)	$c = 0.49\sqrt{f'_{UHPC}}$ (ksi)	μ*ρ*fy (ksi)	μ	$\mu/\sqrt{f'_{UHPC}}$		COV %
Authors	#1	2.2	6.83	6.77	17.7	2.06	4.70	3.56	0.85	0.85	1.01
	#2		6.70								
Literature	#1	0.5	3.79	4.02	28.9	2.63	1.39	4.62	0.86		
	#2		4.03								
	#3		4.24								

6.3. Finite Element Modelling (FEM)

This section presents the Finite Element Analysis (FEA) conducted to analyze the proposed connection and perform a parametric study. ANSYS 2020 R2 Software is used to create a finite element model (FEM) simulating the double shear push-off test. The FEM is validated using the double shear test measurements. Then, a parametric study is conducted to better understand the behavior of the proposed connection and study the effect of parameters, such as UHPC shear pocket dimensions and embedded loop bar size and grade on the interface shear capacity of shear pockets. Two challenges face the FEM which are modelling UHPC material and defining interface plane of UHPC.

SOLID65 ANSYS element is used for the three-dimensional modeling of solids with or without reinforcing bars (rebars) as shown in Figure 6.18. The element is capable of cracking in tension and crushing in compression, which is required for modeling UHPC. In concrete applications, the solid element capability may be used to model the concrete while the rebar capability is available for modeling reinforcement behavior. The element is defined by eight nodes having three degrees of freedom at each node: translations in the nodal x, y, and z directions. The most important aspect of this element

is the treatment of nonlinear material properties. The obtained UHPC mechanical properties are used to define the properties of SOLID65 element to simulate UHPC in FEM.

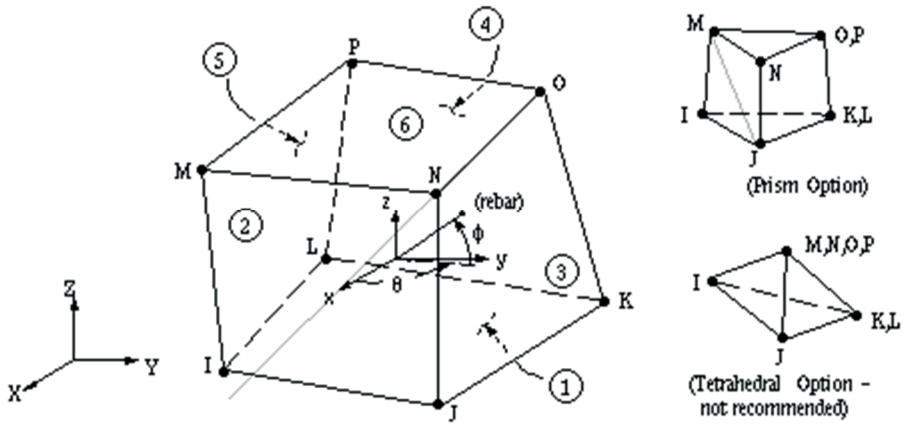

Figure 6.18. SOLID65 3-D Reinforced Concrete Solid (ANSYS Manual).

The second challenge is modeling the interface shear resistance of monolithic UHPC. In the double shear push-off test, the UHPC section is modeled as one unit and the FE model was restricted to force the failure at the interface shear plane as the pocket and haunch (slab in the specimen) are cast as one unit. The loop bar is modeled using Solid 186 element. This element is suitable to model components that has plasticity, large strain capacity with a 3-D quadratic displacement behavior as shown in Figure 6.19.

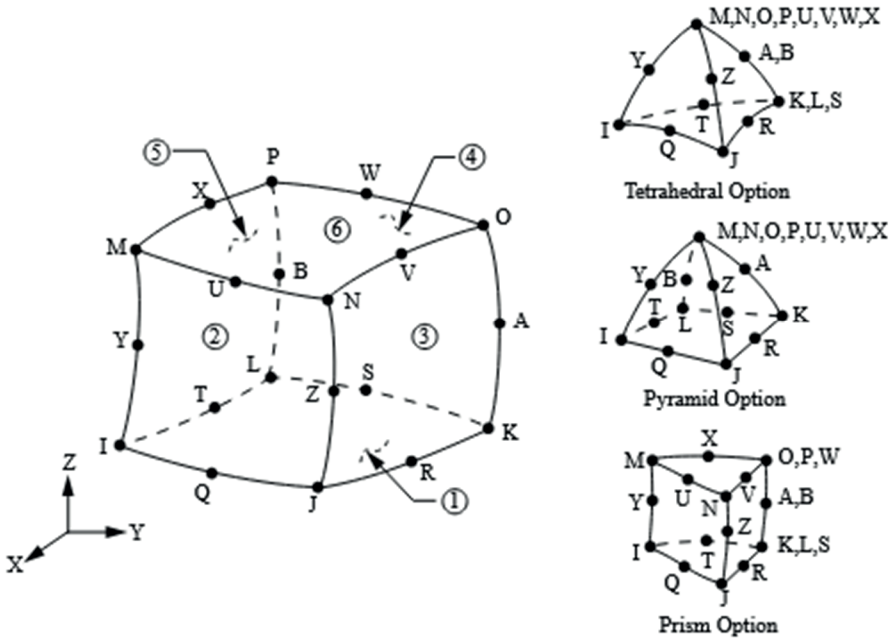

Figure 6.19. SOLID186 3-D Solid Element (ANSYS Manual).

The FE model is created to simulate half of the double shear test specimens at the symmetry axis as shown in Figure 6.20. A symmetry condition is defined at the right end of the FEM. To model the application of the wax at the top of the CC section, a gap is created with a thickness of 0.05 in. to completely separate the two sections and ensure the failure will happen at the shear pocket as shown in Figure 6.20(b). The CC section is modeled using a SOLID65 element, however, a high modulus of elasticity is defined for the CC section to avoid possible failure based on the test observations where the CC section did not fail. The loop bar is modeled as one element that has the equivalent cross-section area at the middle of the shear pocket to reduce the meshing errors as shown in Figure 6.21. The load is applied at the top of the CC section with the same dimensions of the steel plate as point loads acting on the defined nodes shown in Figure 6.21. The FEM is meshed to 1 in. increment to capture good results and because of the specimen

dimensions. The crushing and tension failure limits for the UHPC are defined as 17.7 ksi and 2 ksi, respectively.

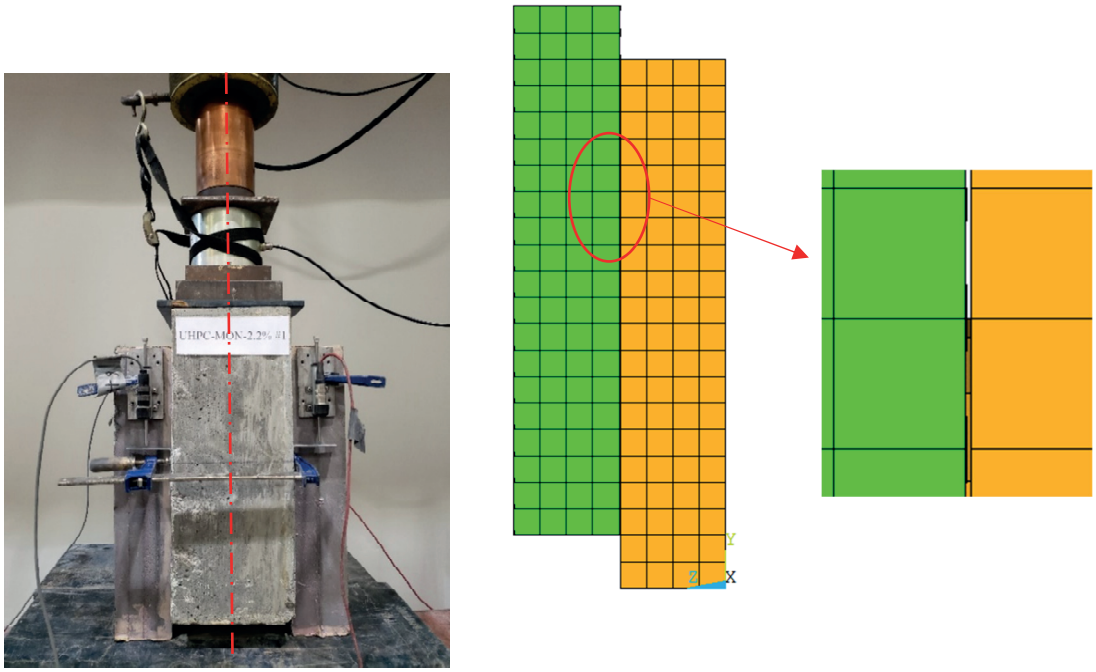

(a) (b)

Figure 6.20. Finite Element Model with the associated test specimen; (a) Double Shear Push-off Test Specimen and (b) Side View of FE Model

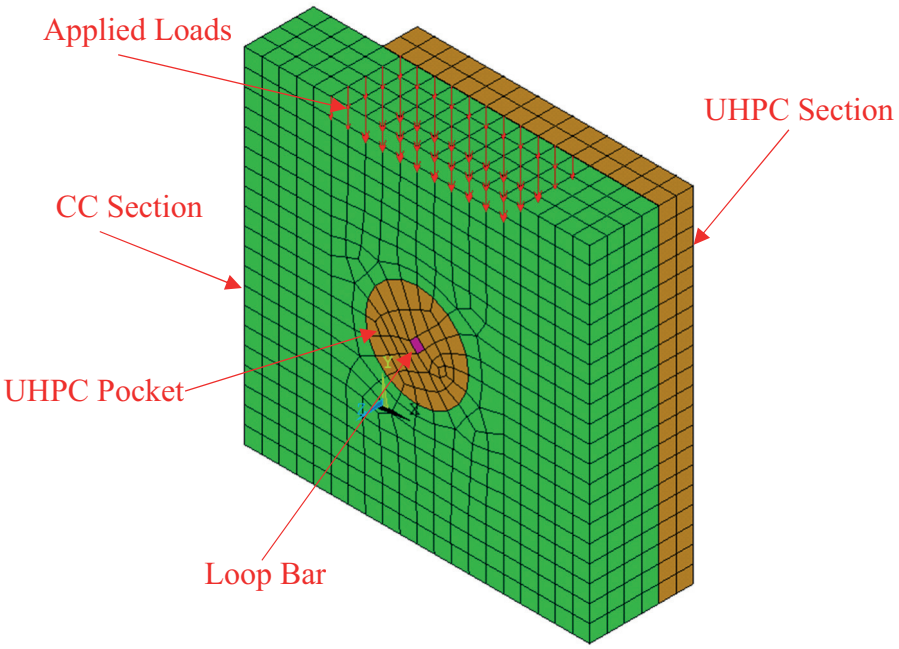

Figure 6.21. 3-D View of Finite Element Model.

Figure 6.22 shows the used boundary conditions in FEM. The UHPC section is resting on hinged supports restricting the movement in X and Y directions. The left side of the CC section is defined as a symmetry line that results in a restriction in the Z direction. The right side of the UHPC section was prevented from movement in the Z direction to reduces the variable dealt with in FEM and for better simulation of a real connection when the UHPC section simulates the haunch which is supposed to be facing the supporting girder (no movement can happen). Using these boundary conditions, the failure is forced to be at the interface shear plane of monolithic UHPC at the shear pocket which is the main goal of this section.

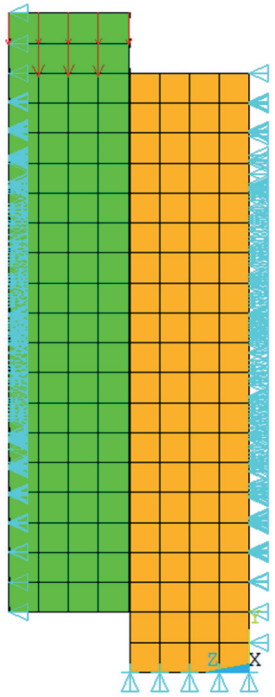

Figure 6.22. Boundary Conditions Used in FEM.

The behavior of UHPC is totally different from that of CC. In CC, the failure is brittle, which allows using the compression stress-strain curve in general with a defined tension cracking limit. On the other hand, when UHPC starts to crack, the first fiber facing the crack acts as a stitch and bridges this crack until it fails in tension. Then, the second fiber starts to engage until its failure and so on. Also, this phenomenon affects the stress-strain curve of UHPC as the more the cracks developed in the section, the less modulus of elasticity it has, and the more strain is gained by the UHPC. Also, simulating the fiber distribution inside the UHPC shear pocket is complicated and cannot be easily achieved. So, a modified UHPC stress-strain curve is used to match the specimen behavior and consider this phenomenon as shown in Figure 6.23. The grade 60 steel was defined as a bilinear curve that is sloped until yield stress and then constant.

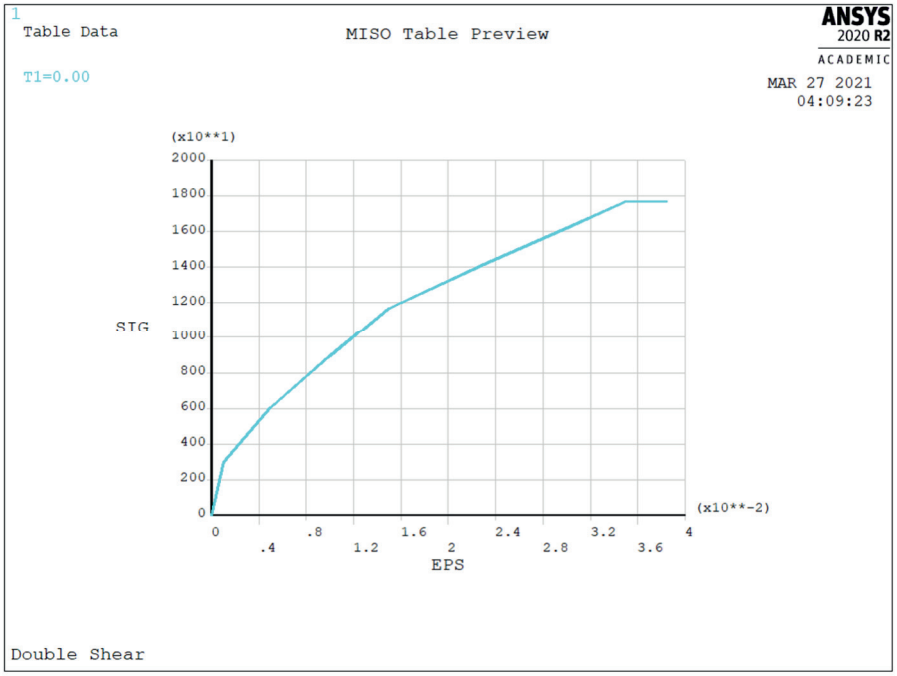

(a)

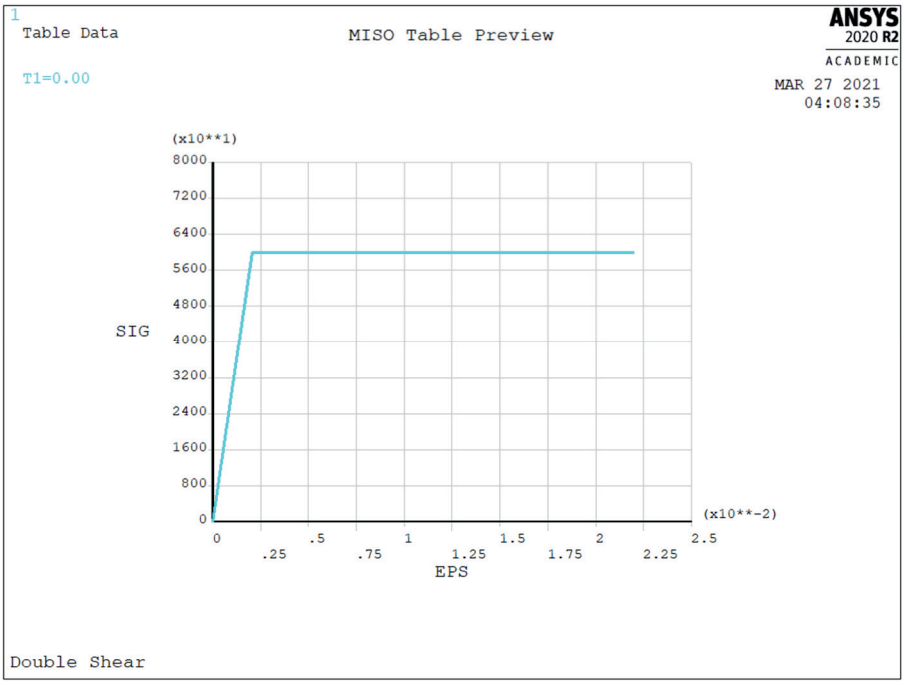

(b)

Figure 6.23. Stress-Strain Curve Defined in FEM; (a) UHPC and (b) Grade 60 Steel

Figure 6.24 shows the FEM model results at the shear pocket and its comparison to the double-shear push-off test results. The FEM shows a matching peak shear value to the test peak load. Figure 6.25 shows the stress distribution and vectors at the shear pocket. This Figure shows that the failure happened at the interface plane when the stress reached 17.7 ksi and the stress vectors are concentrated at the same plane. The interface shear reinforcement exceeded the yield strain, which is 0.00207, as shown in Figure 6.26, that the interface reinforcement fully engaged at the interface plane.

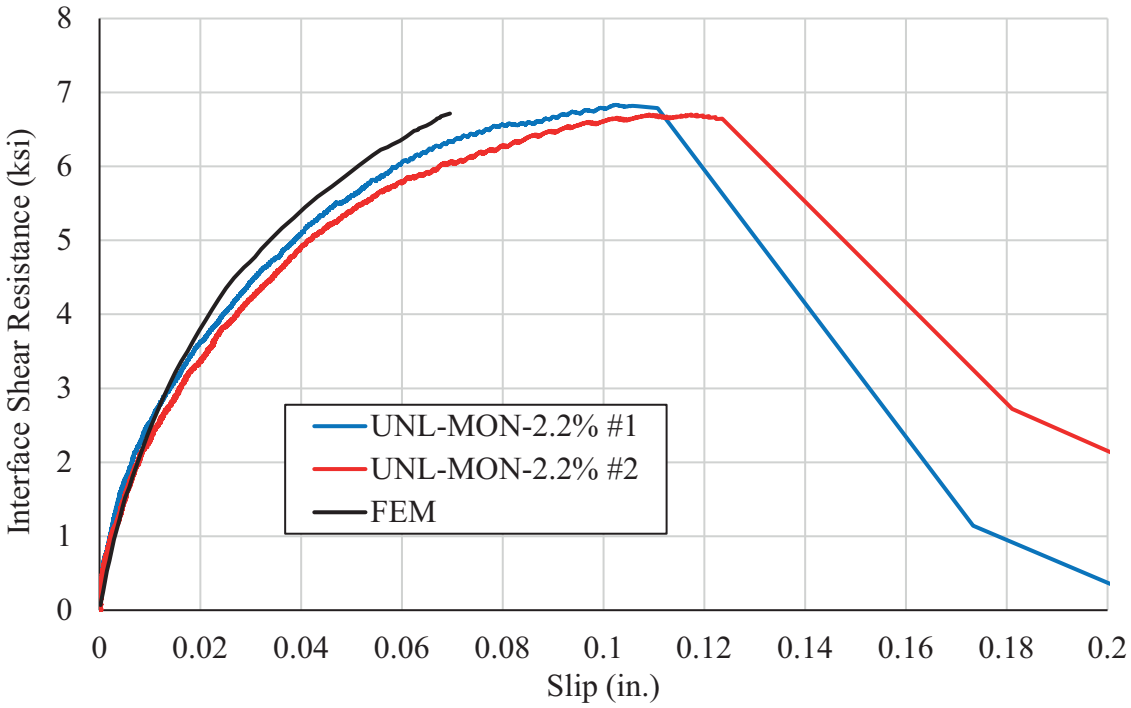

Figure 6.24. Finite Element Model Result and Its Comparison with Double-Shear Test Results.

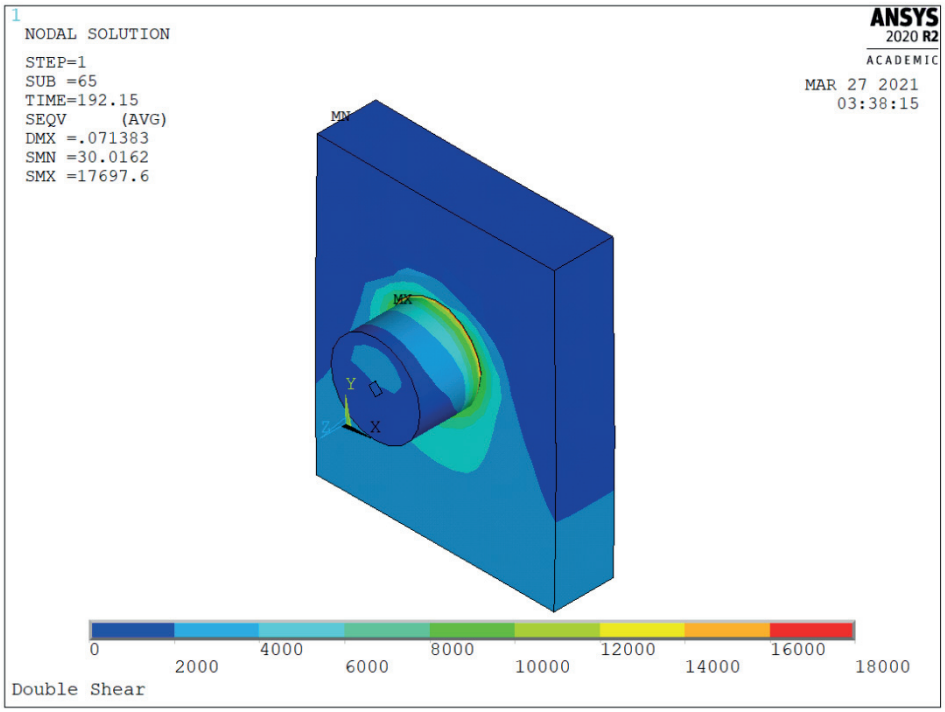

(a)

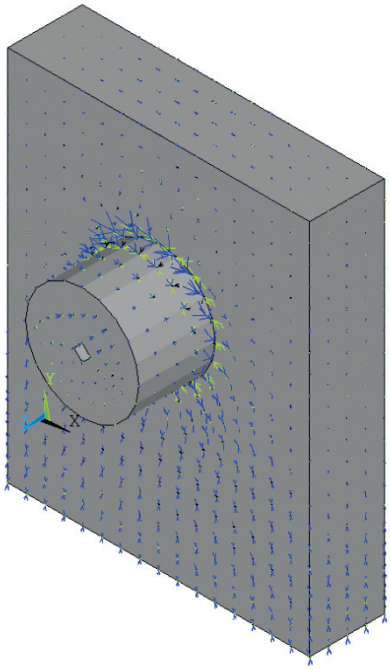

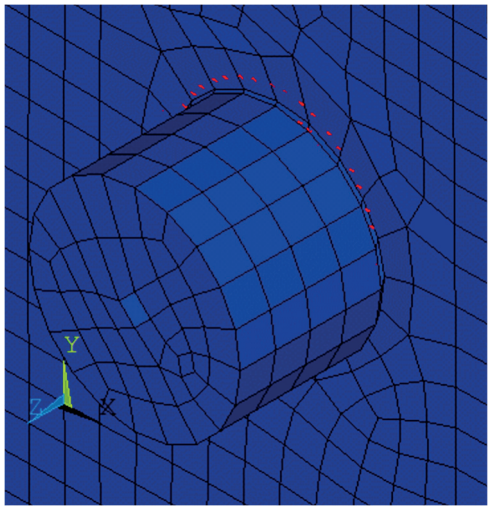

(b) (c)

Figure 6.25. Shear Pocket Results; (a) Stress Distribution, (b) Stress Vectors, and (c) Crack Locations.

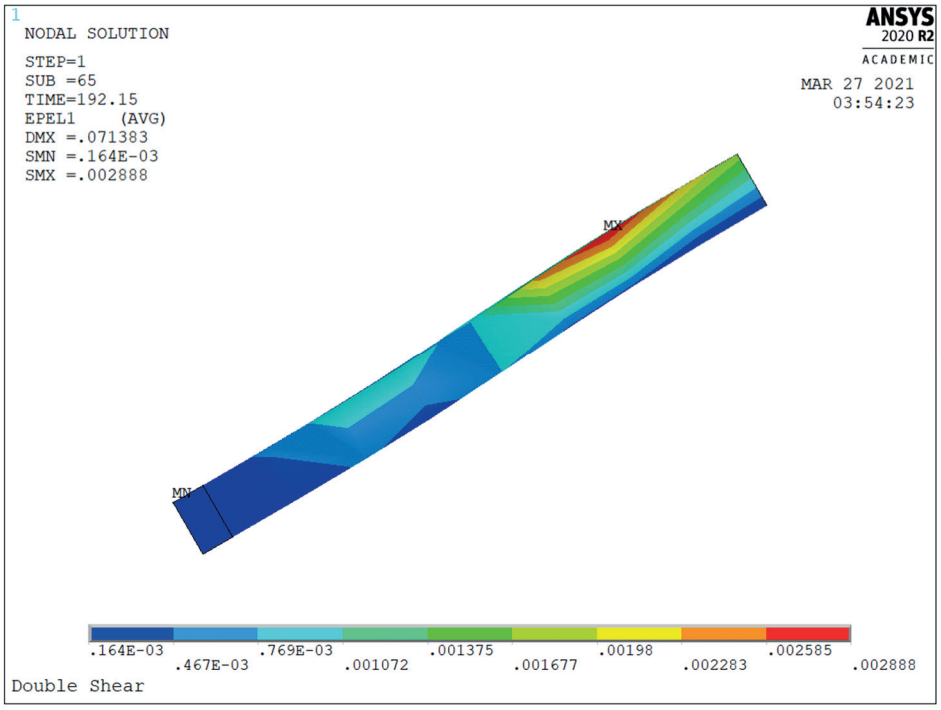

(a)

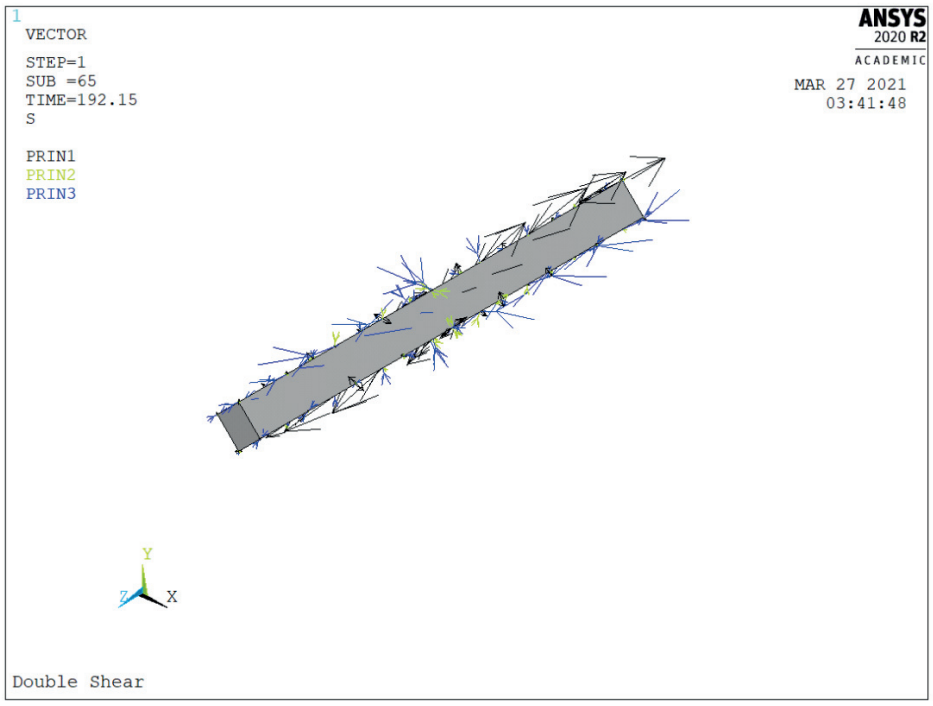

(b)

Figure 6.26. Interface Shear Reinforcement Results; (a) Strain Distribution and (b) Stress Vectors.

6.3.1. Effect of Pocket Diameter

The shear pocket diameter is a key parameter in the interface shear area that controls the cohesion portion of the interface shear resistance. Three different shear pocket diameters are investigated; 4 in., 5 in., and 6 in., using a #4 loop bar that can fit in each of them. As expected, increasing the shear pocket diameter increases the stiffness and interface shear resistance of the shear pocket as shown in Figure 6.27.

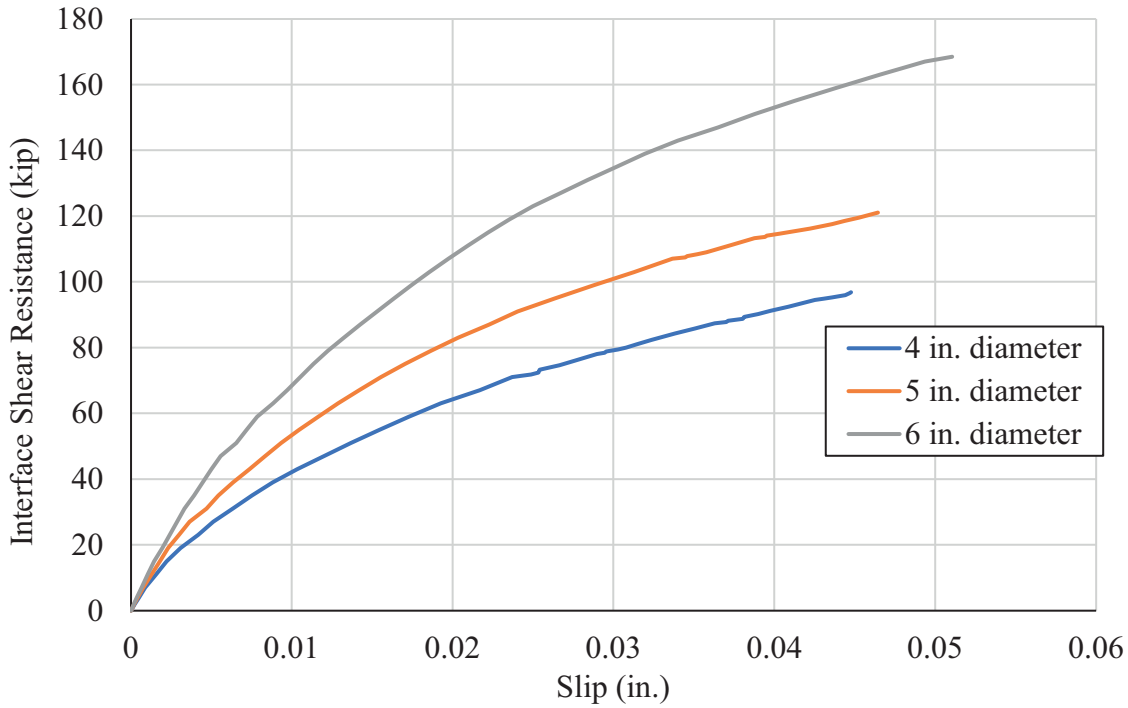

Figure 6.27. Effect of Shear Pocket Diameter on Interface Shear Resistance Using Grade 60 #4 Loop Bar.

6.3.2. Effect of Interface Shear Reinforcement

Adding interface shear reinforcement inside the shear pockets enhances the structural performance of the pockets by increasing the interface shear capacity and provide more ductility to the shear pocket. Two different interface shear reinforcement

are investigated: #4 loop bar and #5 loop bar. These two types of loop bars are the most suitable bars to fit in shear pockets with a diameter ranging from 4 in. to 6 in. The FEM is used to study the effect of interface shear reinforcement using a shear pocket diameter of 5 in. and the proposed two different interface reinforcement. Figure 6.28 shows the FEM results. This figure shows that increasing the interface shear reinforcement not only increases the interface shear capacity but also increases the ductility from 0.05 in. to 0.07 when increasing the bar diameter from 0.5 in, to 0.625 in.

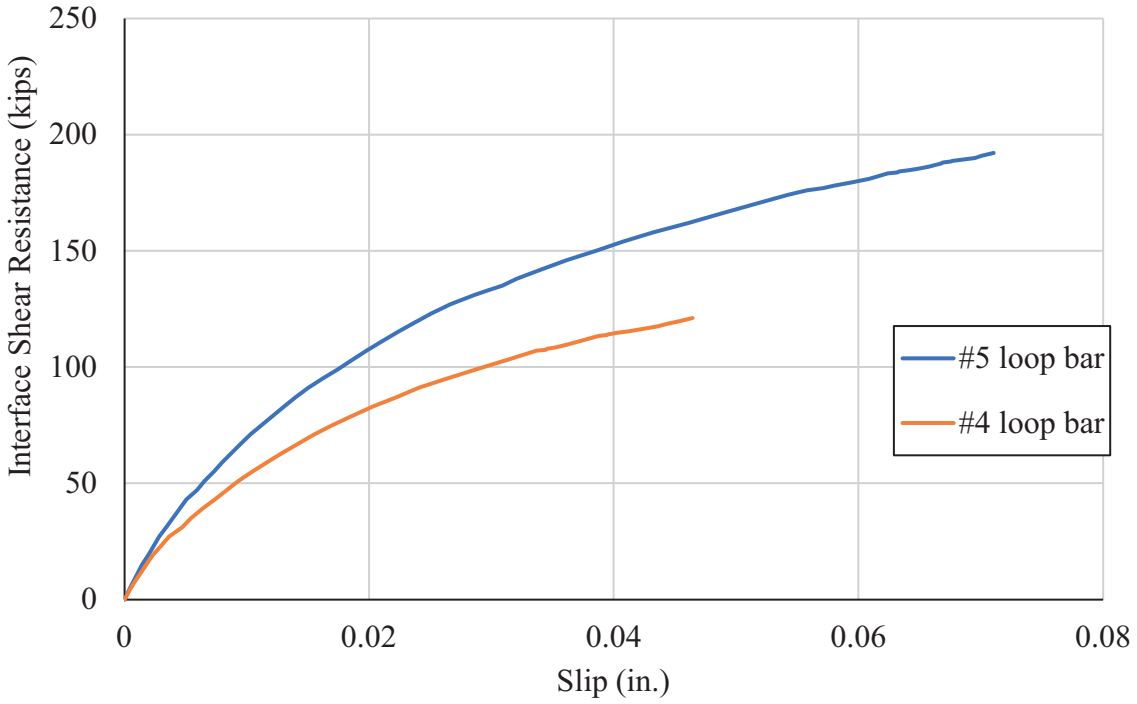

Figure 6.28. Effect of Interface Shear Reinforcement on Interface Shear Resistance Using 5 in. Diameter Shear Pocket.

6.3.3. Effect of Using High Strength Steel

According to AASHTO LRFD, the yield strength of the interface shear reinforcement is limited to 60 ksi even if high-grade steel is used in the case of CC. The

mechanical properties of UHPC are far superior compared to CC in terms of tensile strength and ductile behavior which might eliminate the 60 ksi limit for interface shear reinforcement yield strength. So, high strength steel (ASTM A1035 Grade 100 steel) is evaluated through FEM by using the same loop bar dimensions (#4 loop bar) with the idealized stress-strain the curve of grade 100 steel similar to grade 60. Figure 6.29 shows the results obtained from the FEM for both grade 60 and grade 100 #4 loop bar in a 5 in. diameter shear pocket. This figure shows that grade 100 steel followed the same behavior as grade 60 as both have the same modulus of elasticity with achieving a slightly higher interface shear resistance. This might be attributed to the yield strain of steel that was considered as a bilinear curve with constant relation at the yield stress. Also, this figure shows that the current condition in AASHTO of 60 ksi interface reinforcement yield stress limit is valid when using UHPC. This conclusion is conservative until further experimental studies are conducted as the UHPC is supposed to develop the grade 100 reinforcement better than CC and as a result eliminate this limit.

The finite element analysis shows that the shear pocket size and reinforcement have a high impact on the interface shear resistance of the shear pocket. In addition, increasing interface shear reinforcement increases the shear pocket ductility behavior. However, using high-grade steel (grade 100) slightly increase the interface shear capacity which needs to be validated experimentally.

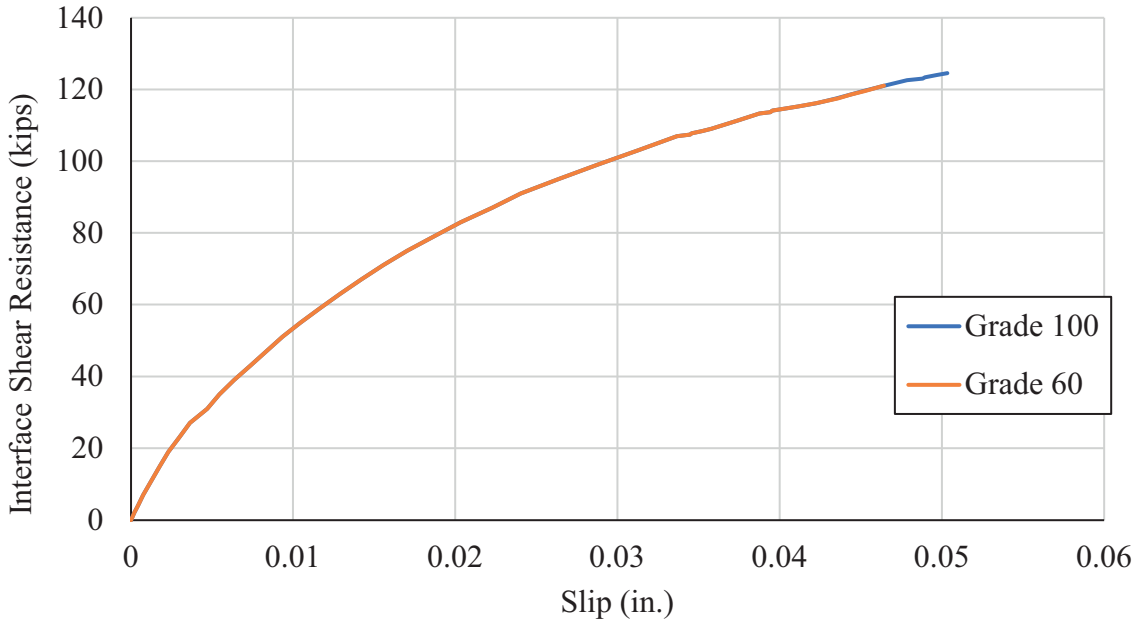

Figure 6.29. Effect of Interface Shear Reinforcement Grade on Interface Shear Resistance Using 5 in. Diameter Shear Pocket.

6.4. Full-Scale Push-off Test

The purpose of full-scale testing is two folds: 1) evaluate the constructability of the new connection especially with the blind casting of a highly viscous material, such as UHPC; and 2) verify the structural performance. Three full-scale push-off specimens were designed and tested using concrete blocks to simulate precast/prestressed concrete girders with 16 in. wide roughened surface. Two #4 bars at 2 ft spacing were used to represent the girder interface shear reinforcement. Two 6 in. diameter shear pockets at 3 ft. spacing were formed using corrugated plastic pipes that provide roughened surface at the sides of the pockets. One #5 loop bar that is 10 in. long was used to reinforce the monolithic UHPC connection and enhance its capacity. Table 6.4 shows the description

of the three full-scale push-off specimens, while Figure 6.30 shows their dimensions and reinforcement details.

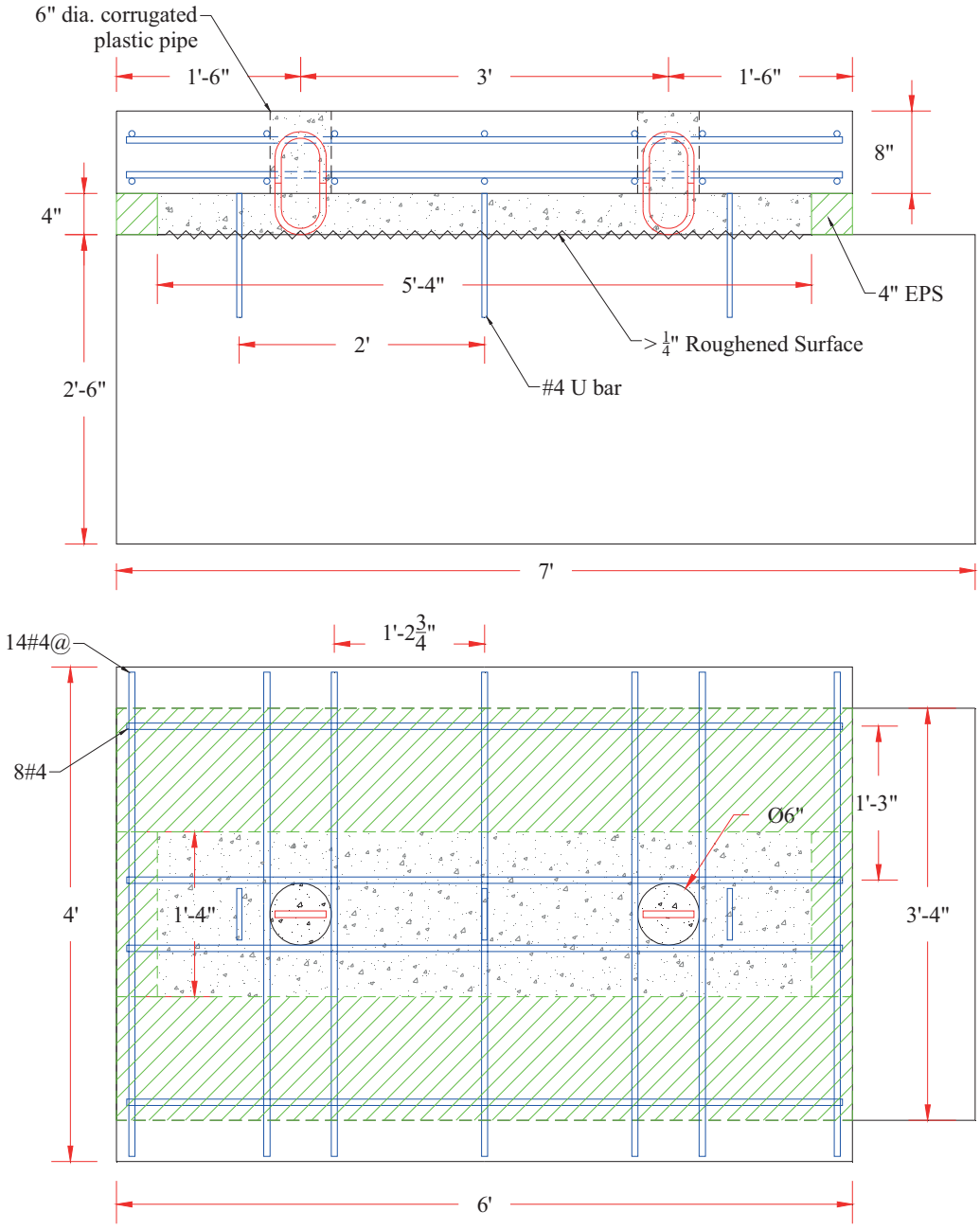

Figure 6.30. Full-Scale Push-Off Specimen Details.

Table 6.4

Full-Scale Push-off Specimens Configuration

Specimen ID	Girder Type	Deck Panel	Shear Pocket
UHPC#1 UHPC#2 UHPC#3	Concrete Block 3'4" x 7' x 2'6"	Precast Concrete 4' x 6' x 8"	Two 6 in. diameter @ 3 ft. spacing

6.4.1. Specimen Fabrication

Each shear pocket was formed using a 6 in. diameter corrugated plastic pipe (known by drain pipe) to provide a roughened surface for the inside surface of the shear pocket. The bottom and top of the pipe were sealed with liquid nails and plastic sheet, respectively, to prevent the leakage of concrete while casting the deck panel. Eight #4 bars (four in each layer) were used to hold the plastic pipe in place and strengthen the area around the shear pockets. Figure 6.31 shows the shear pocket forming and deck panel reinforcement details. The deck panel was cast using self-consolidating concrete (SCC) and then cured for seven days using wet burlap and stored at room temperature.

Figure 6.31. Shear Pockets Forming and Slab Reinforcement Details.

Figure 6.32 shows the interface surface at the top of the concrete block and haunch forming with 2 in. rigid foam boards. The deck slab was placed on the foam boards and was sealed using liquid nail to prevent any leakage of UHPC. The #5 loop bar was bent according to the standard hook specifications, as shown in Figure 6.33, and installed either before or after casting UHPC in the shear pocket. Finally, UHPC was cast to fill the shear pockets and haunch area as shown in Figure 6.34, then, the top of the pocket was covered with plywood for curing. It is worth mentioning that the research team kept adding UHPC to ensure a leveled top surface of the deck as shown in Figure 6.35.

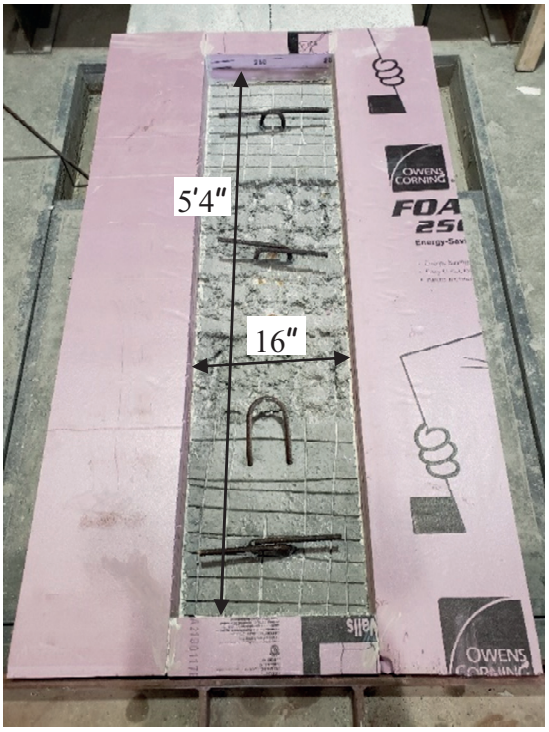

Figure 6.32. CC Interface Shear Area Preparation

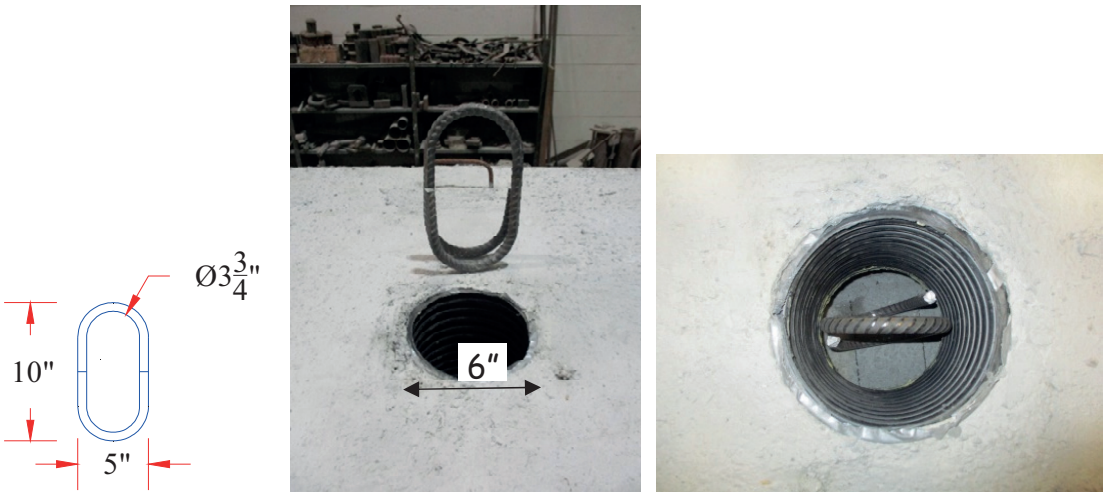

Figure 6.33. No. 5 Loop Bar Details and Installation.

Figure 6.34. UHPC Casting for UHPC#2 Specimen.

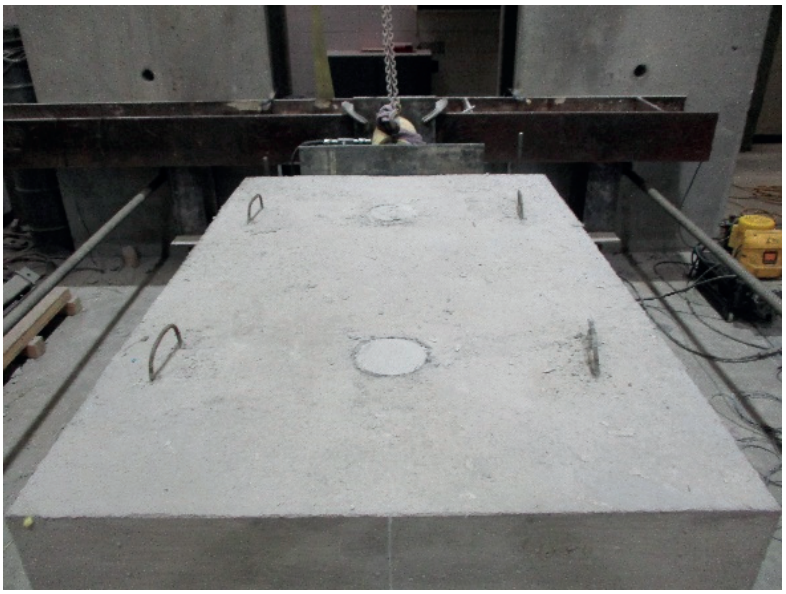

Figure 6.35. UHPC Filled Shear Pockets to Top Surface.

6.4.2. Material Properties

The precast concrete deck panels were made using normal weight self-consolidated concrete (SCC) that has a 28-day compressive strength of 6.6 ksi in the first specimen and 7.34 ksi in the other two specimens. The push-off girder concrete was cast using a ready-mixed SCC with an average slump flow of 22 in and average 28-day compressive strength of 6.8 ksi. For each connection, a total of 3.2 cubic feet of UHPC was grouted to fill the two shear pockets and haunch area. The flowability of UHPC batches were measured, at a temperature of 80˚ F and relative humidity of 50%, using 10 in. diameter flow table according to ASTM C230 as specified by ASTM C1856. The three UHPC batches had three different levels of stability: high, medium, and low for UHPC#1, UHPC#2, and UHPC#3 specimens, respectively. Figure 6.36 shows cross-sections of hardened 3 in. by 6 in. cylinders, cut in half longitudinally using a wet saw, for each of UHPC mixes. The UHPC#1 cylinder had a good distribution of fiber along

the height of the section that indicates high mix stability. UHPC#2 cylinder had good fiber distribution with a minor segregation that can be seen at the top part of the section, medium stability. However, the UHPC#3 exhibited severe fiber segregation that barely had fibers at the top half of the cylinder (low stability). These three conditions were used to study the effect of fiber stability on the performance of proposed connection. The three full-scale push-off specimens were tested at an average UHPC compressive strength of 18 ksi.

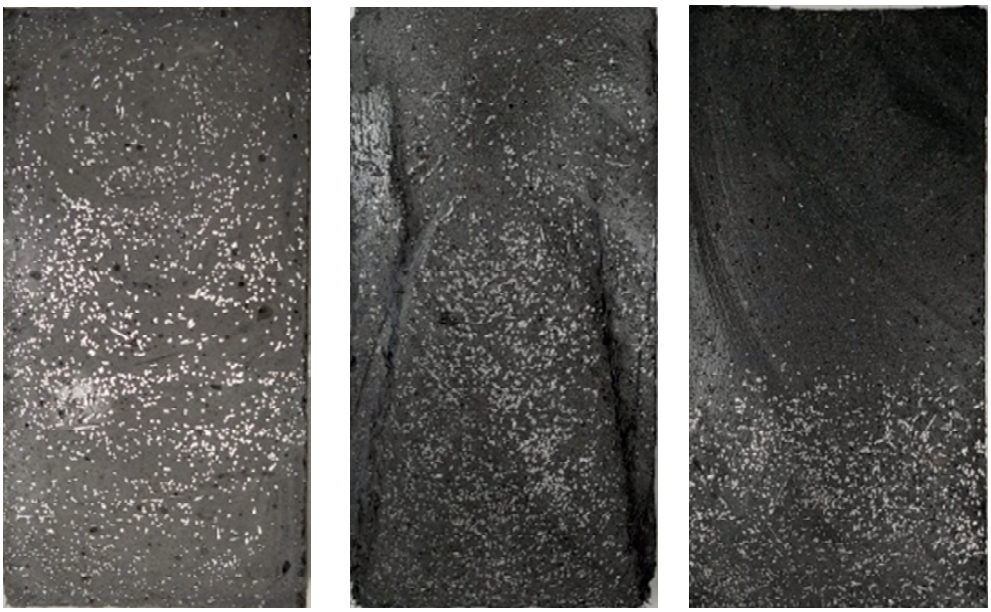

(a) (b) (c)

Figure 6.36. Cross-Section of UHPC Cylinders Obtained from Each Full-Scale Push-Off Specimen; (a) UHPC#1, (b) UHPC#2, and (c) UHPC#3.

6.4.3. Test Setup and Results

After UHPC achieved a compressive strength of 18 ksi, the full-scale push-off specimens were tested by applying a horizontal load to the deck slab using a hydraulic ram as shown in Figure 6.37. A set of steel plates was used to distribute the applied load

over a larger area. The concrete blocks were anchored to the floor by a set of two beams and two threaded rods to prevent their rotation while loading. Also, the concrete blocks were restrained from horizontal movement by a steel beam at the end of the blocks that is tied to a reaction wall by two threaded rods. Four LVDTs (two LVDTs for each side) were used to measure the relative displacements between the deck panel and concrete block, parallel (slip) and perpendicular (crack width) to interface plane. The load was measured using a pressure transducer attached to the ram until failure.

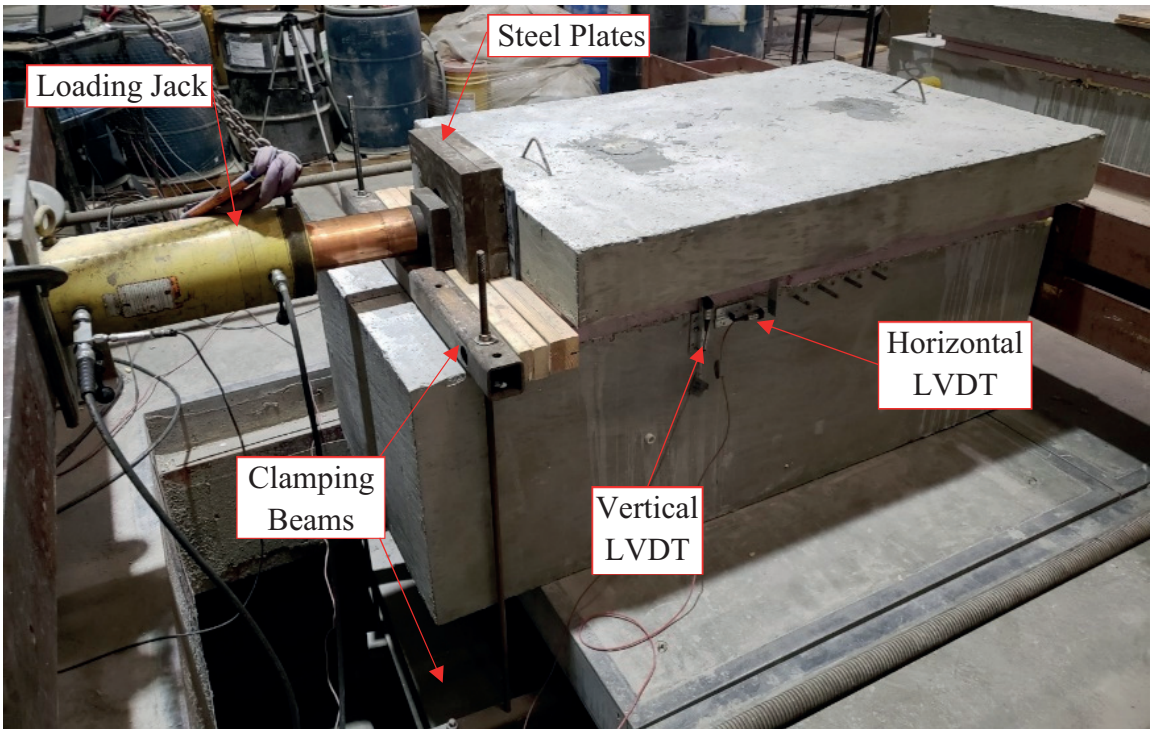

Figure 6.37. Full-Scale Push-Off Specimen Test Setup.

Table 6.5 shows the maximum applied load and the corresponding interface shear force per unit length. Figure 6.38 and Figure 6.39 show the applied load versus measured relative displacements in both parallel (slip) and perpendicular (crack width) directions respectively, for the three full-scale specimens. Despite the differences in the peak load,

the load-slip curves of the three specimens were similar. UHPC#1 specimen exhibited interface shear failure at the first pocket and CC-UHPC at the end of the block as shown in Figure 6.40(a). This CC-UHPC failure can be attributed to the lack of interface reinforcement at the specimen end, which is the same case as real girder, more shear reinforcement at the end. The other two specimens had no interface failure, and the loop bar were pulled out from the UHPC haunch as shown in Figure 6.40(b) and (c). The fiber segregation in these two specimens affected the bond strength between the UHPC and embedded loop bar, which did not happen in UHPC#1 specimen. The three tests showed that the provided side surface roughening of shear pocket was adequate to prevent pull-out of UHPC from the pocket. The effect of UHPC mix stability can be observed in UHPC#3 results as its UHPC mix had the lowest stability that causes fiber segregation despite its high compressive strength. The stability of UHPC mix is a key parameter that highly impact the capacity of the proposed connection. Therefore, it is recommended that field-cast UHPC be tested to ensure adequate UHPC stability and achieve the full capacity of the proposed connection.

Table 6.5

Full-Scale Push-off Test Results

Specimen ID	f'_{UHPC} (ksi)	Maximum Load (kips)	V_{ni} (kips/in.)
UHPC#1	18.40	305	4.24
UHPC#2	17.36	240	3.33
UHPC#3	18.40	192	2.67

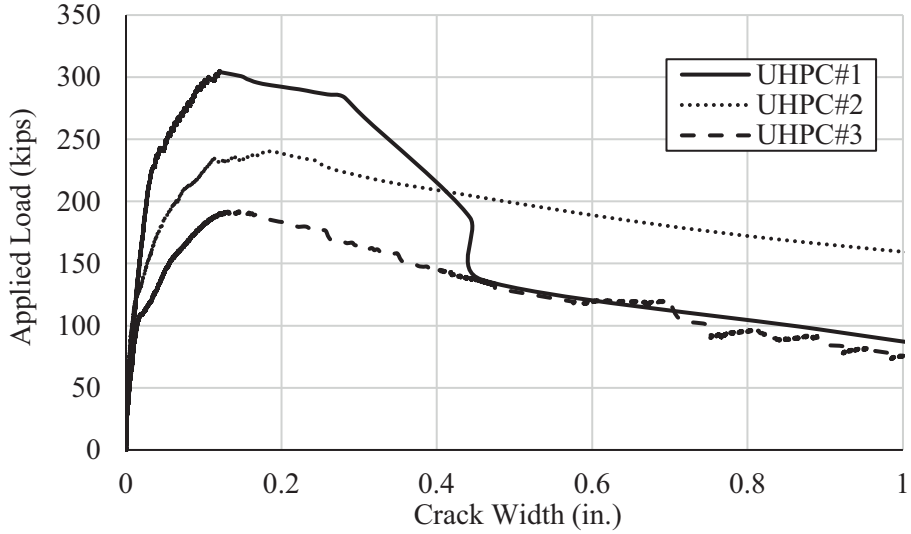

Figure 6.38. Load versus Relative Vertical Displacement of Full-Scale Push-off Specimens.

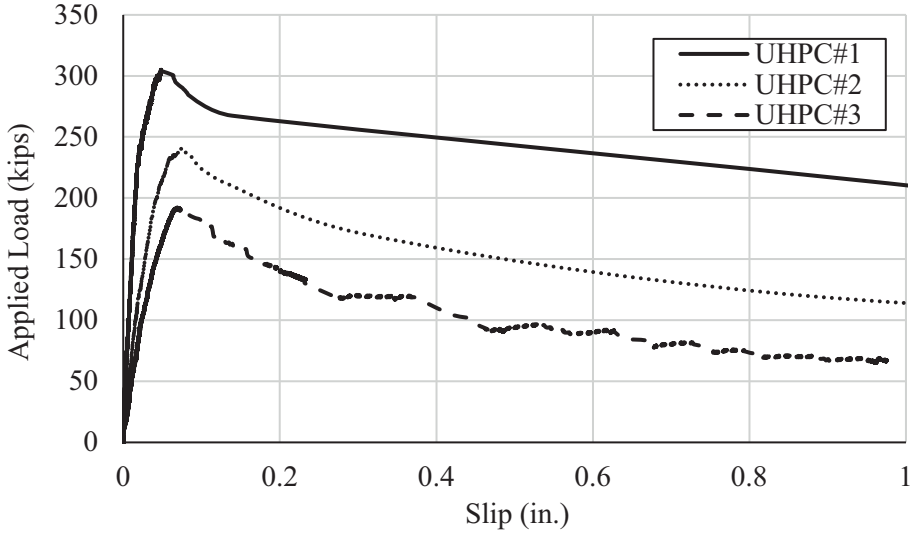

Figure 6.39. Load versus Measured Slip of Full-Scale Push-off Specimens.

(a)

(b)

(c)

Figure 6.40. Full-Scale Specimen Failure Modes; (a)UHPC#1, (b)UHPC#2, and (c)UHPC#3.

CHAPTER 7: DESIGN PROCEDURES, DESIGN AIDS, AND COST ANALYSIS

This chapter presents the design procedure and design aids of the proposed connection. An example bridge from PCI Bridge Design Manual 2014 (PCI BDM Ex. 9.1a) is used to demonstrate the design procedure and the advantage of using UHPC over CC. Finally, cost analysis is conducted to illustrate the benefits of using the proposed connection.

7.1. Design Procedure

The advantage of utilizing the new deck-to-girder connection in precast concrete deck systems are twofold: First, the exceptional mechanical properties of UHPC simplify the design and production of bridge girders and deck panels as they eliminate the need for HSS-formed shear pockets and special connectors; Second, the excellent durability of UHPC eliminates the need for an overlay or other protection systems. The cohesion and friction factors obtained from the experimental investigation are used to design the new connection following the general procedure shown in Figure 7.1.

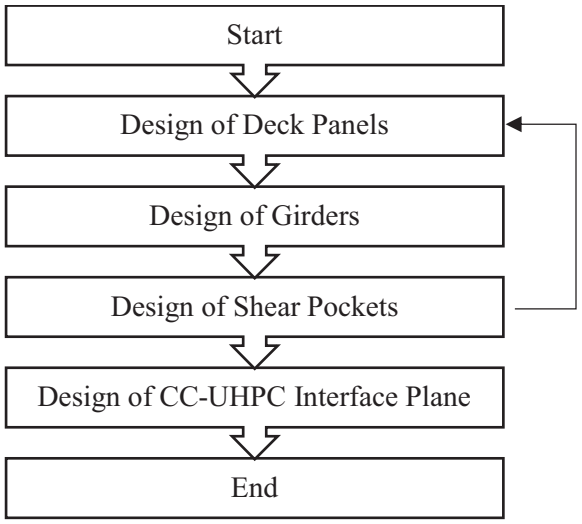

Figure 7.1. Flowchart of General Design Procedures for Proposed System.

The design of shear pocket starts with obtaining the nominal interface shear resistant demand from the different load cases. Then, the spacing between shear pockets is calculated based on preliminary pocket diameter and loop bar size. The spacing between shear pockets is recommended to be from 2 to 4 ft. The obtained spacing is used to predict the minimum UHPC haunch width using the girder shear reinforcement; obtained from the girder shear design. If the minimum UHPC haunch width is greater than the girder top flange width, the interface shear reinforcement needs to be designed based on considering the top flange width as UHPC haunch width. The detailed design procedure is shown in Figure 7.2 to obtain the following outcomes:

- Shear pocket diameter and spacing
- Loop bar embedded in the shear pocket.
- Girder shear reinforcement
- Haunch width

Where:

$A_{cv\text{-}MN}$ = monolithic UHPC interface shear area (in.^{2})

$A_{cv\text{-}CC}$ = CC-UHPC interface shear area (in.^{2})

$A_{vf\text{-}MN}$ = interface shear reinforcement Area across monolithic UHPC plane (in.^{2})

$A_{vf\text{-}CC}$ = interface shear reinforcement Area across CC-UHPC plane (in.^{2})

A_{s1} = loop bar area (in.^{2})

A_{s2} = girder shear reinforcement bar area (in.^{2})

b = girder top flange width (in.)

b_w = UHPC haunch width (in.)

c_{MN} = monolithic UHPC cohesion coefficient (ksi)

c_{cc} = CC-UHPC cohesion coefficient (ksi)

D_p = shear pocket diameter (in.)

f'_c = compressive strength of precast deck slab panel (ksi)

f'_{UHPC} = compressive strength of field cast UHPC (ksi)

f_{yh} = bar yield strength (ksi)

N = Number of interface reinforcement bar legs crossing interface plane

V_{ni} = nominal interface shear resistance per unit length (kips/in.)

$V_{ni\text{-}MN}$ = nominal interface shear resistance of monolithic UHPC plane (kips)

$V_{ni\text{-}CC}$ = nominal interface shear resistance of CC-UHPC plane (kips)

S = girder shear reinforcement spacing (in.)

S_p = spacing between shear pockets (in.)

μ_{MN} = monolithic UHPC friction coefficient

μ_{cc} = CC-UHPC friction coefficient

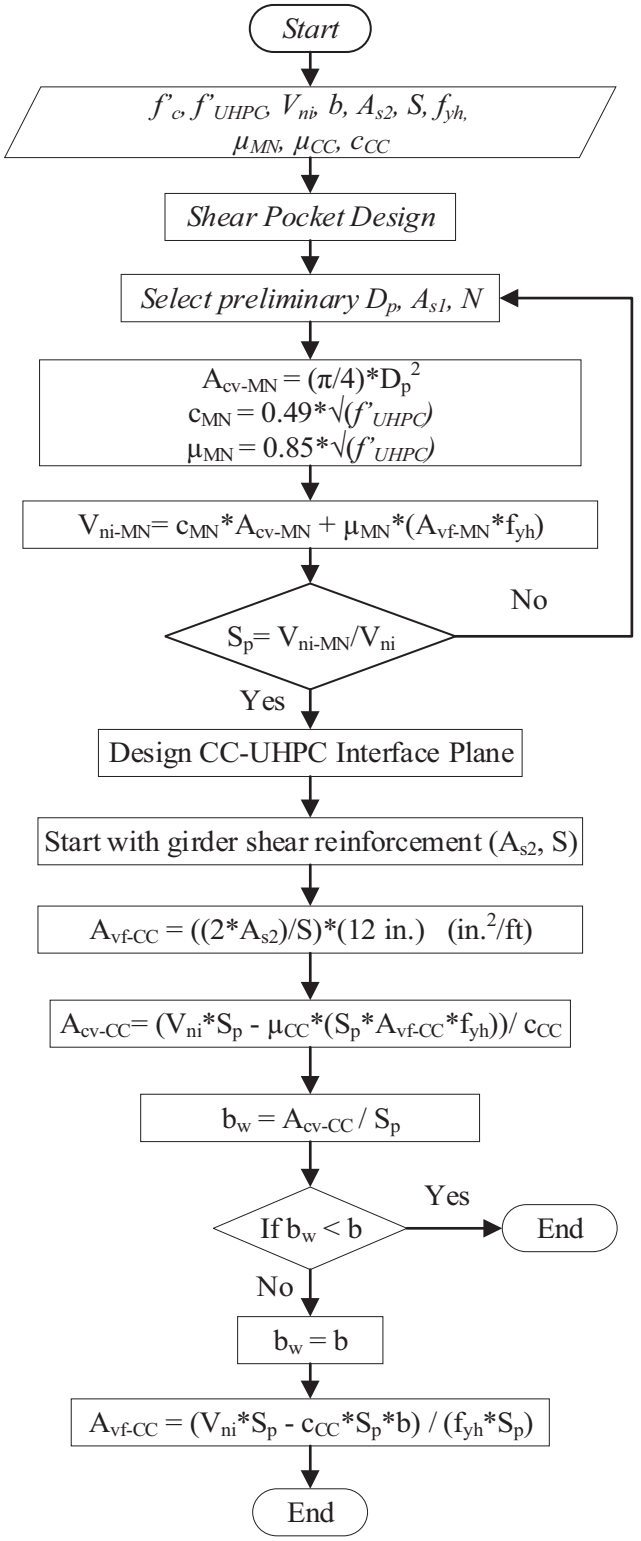

Figure 7.2. Design Procedure flowchart of new connection.

The following calculation demonstrates the design procedure:

Interface Shear Resistance Design for PCI BDM Ex. 9.1a using Proposed UHPC Deck-to-Girder Connection

Material Properties

Deck Panel Concrete Compressive Strength $f'_c := 6\ ksi$

UHPC Haunch Compressive Strength $f'_{UHPC} := 18\ ksi$

Nominal Shear Resistance

According to PCI Bridge Design Manual Example 9.1a Section 9.1a.12:

Factored Interface Shear due to DW and LL at h/2 (DC does not apply to the composite section)

$$V_u := 1.5 \cdot 10.8\ kip + 1.75 \cdot 104.4\ kip = 198.9\ kip$$

Shear Depth $d_v := 75.78\ in - \frac{7.5\ in}{2} = 72.03\ in$

Ultimate Interface Shear at Critical Section $V_{ui} := \frac{V_u}{d_v} = 2.76\ \frac{kip}{in}$

Strength Reduction Factor $\phi := 0.9$

Nominal Interface Shear Resistance per unit length $V_{ni} := \frac{V_{ui}}{\phi} = 3.07\ \frac{kip}{in}$

Preliminary Shear Pocket Dimension and Reinforcement

Pocket Diameter $D_p := 6\ in$ (4 to 8 in.)

Embedded Loop Bar Area (Single Leg) $A_{s1} := 0.31\ in^2$ (#5 bar)

Number of Loop Bar Legs crossing Interface. $N := 2$

Interface Shear Resistance of Monolithic UHPC

Interface Shear Area Per Pocket $A_{cv\_MN} := \frac{\pi}{4} \cdot {D_p}^2 = 28.27\ in^2$

Monolithic Cohesion Coefficient $c_{MN} := 0.49 \cdot \sqrt{f'_{UHPC} \cdot ksi} = 2.08\ ksi$

Monolithic Friction Coefficient $\mu_{MN} := 0.85 \cdot \frac{\sqrt{f'_{UHPC} \cdot ksi}}{ksi} = 3.61$

Monolithic Interface Shear Reinforcement $A_{vf\_MN} := N \cdot A_{s1} = 0.62\ in^2$

Yield Strength $f_{yh} := 60\ ksi$

Nominal Interface Shear Resistance Per Pocket

$$V_{ni\_MN} := c_{MN} \cdot A_{cv\_MN} + \mu_{MN} \cdot \left(A_{vf\_MN} \cdot f_{yh}\right) = 192.9\ kip$$

Spacing Between Pockets $S_p := \frac{V_{ni\_MN}}{V_{ni}} = 5.24\ ft$

Deign Spacing Between Pockets $S_p := 4\ ft$ Choose between 2 to 4 ft. (Recommended)

Girder Dimensions and Shear Reinforcement
(Use the same shear reinforcement obtained from girder shear design)

Width of Girder Top Flange $b := 48\ in$

Girder Shear Reinforcement Bar $A_{s2} := 0.2\ in^2$

Girder Shear Reinforcement Spacing $S := 12\ in$

Interface Shear Resistance of CC-UHPC

CC-UHPC Interface Shear Reinforcement $A_{vf\_CC} := \frac{2 \cdot A_{s2}}{S} \frac{12\ in}{1\ ft} = 0.4\ \frac{in^2}{ft}$

CC-UHPC Cohesion Coefficient $c_{CC} := 0.63\ ksi$

CC-UHPC Friction Coefficient $\mu_{CC} := 1.23$

Yield Strength $f_{yh} := 60\ ksi$

CC-UHPC interface area $A_{cv\_CC} := \frac{V_{ni} \cdot S_p - \mu_{CC} \cdot \left(S_p \cdot A_{vf\_CC} \cdot f_{yh}\right)}{c_{CC}} = 0.3\ ft^2$

Minimum Roughened width of Girder Top Flange $b_{w\_min} := min\left(\frac{A_{cv\_CC}}{S_p}, b\right) = 0.965\ in$

7.2. Design Aids

Design aids were generated using the proposed equations for predicting the interface shear resistance of monolithic UHPC, which controls the connection design. The interface shear resistance was calculated for shear pocket spacing ranging from 2 – 4 ft. using different loop bar sizes. Figure 7.3 and Figure 7.4 show the generated design charts presenting 17 ksi and 21.7 ksi compressive strength of UHPC, respectively and using a reduction factor of 0.9 in accordance with AASHTO LRFD 2020. The design chart legend is labeled using the form DA#B where D is diameter, A is the shear pocket diameter (in.), and B is the embedded loop bar size.

To demonstrate the use of the design charts, the interface shear demand of 2.76 kips/in. of the PCI BDM Example 9.1a bridge is used, as shown in Figure 7.5, to determine the different alternatives in terms of shear pocket spacing, diameter, and reinforcement. An example of these design alternatives is using 4 in. diameter shear pockets at 3 ft spacing and #4 loop bar to satisfy interface shear demand at girder ends. The interface shear demand is significantly reduced towards the middle of the girder and, therefore, the pocket spacing could be increased or pocket size and/or loop bar size could be reduced.

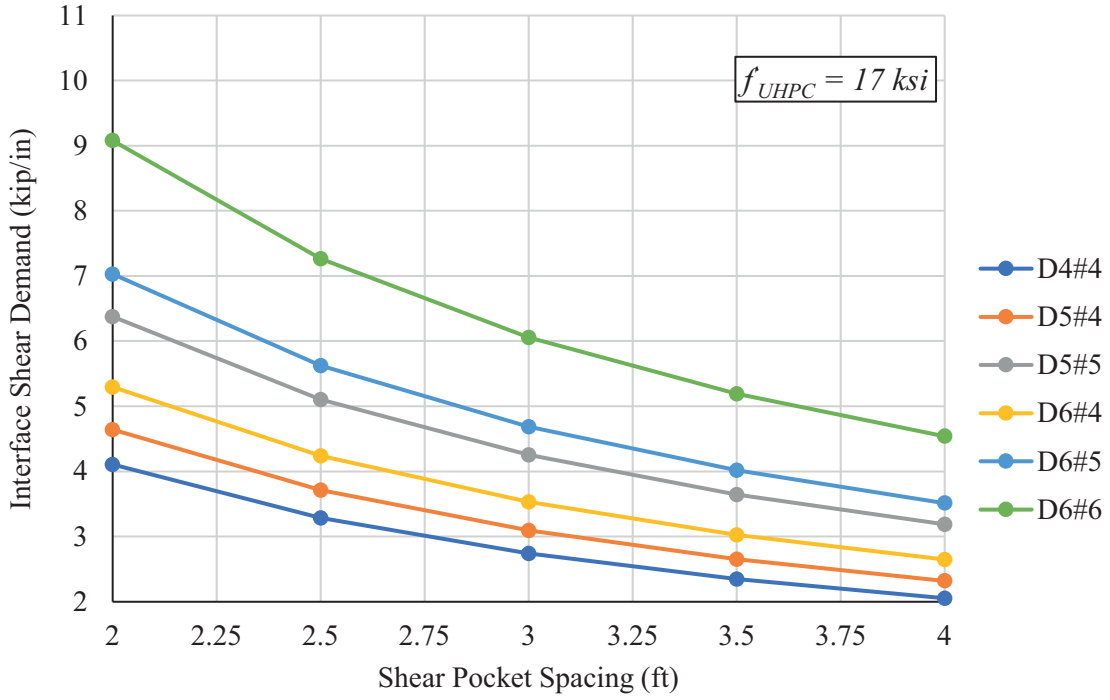

Figure 7.3. Design Chart for UHPC with Compressive Strength of 17 ksi.

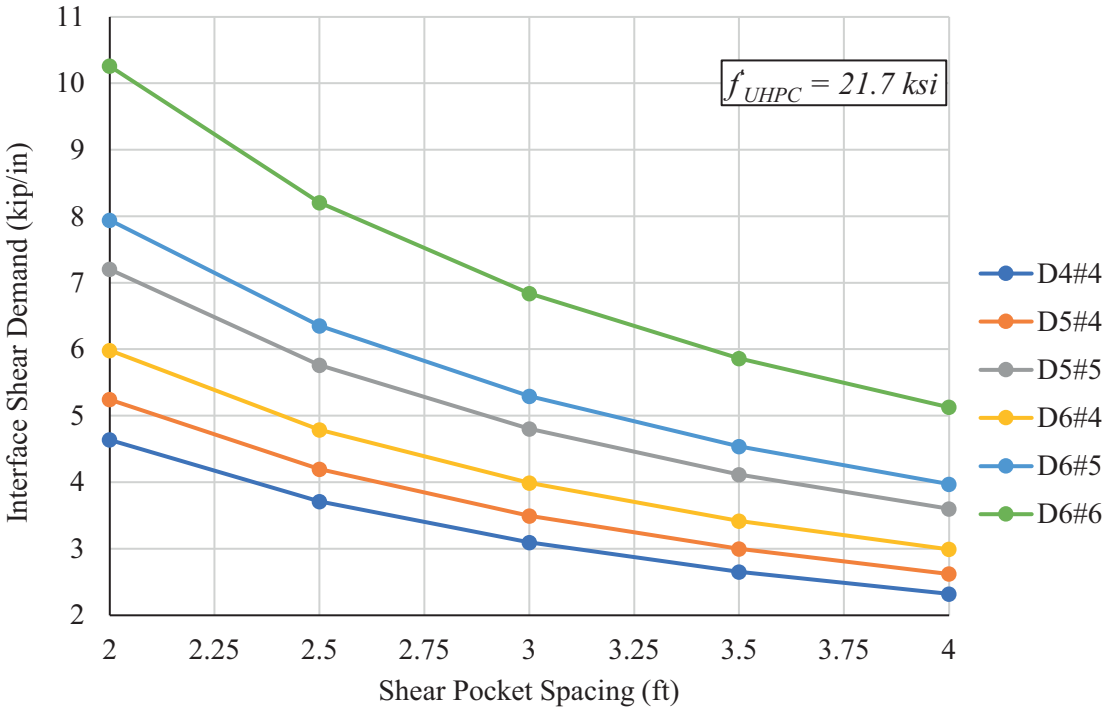

Figure 7.4. Design Chart for UHPC with Compressive Strength of 21.7 ksi.

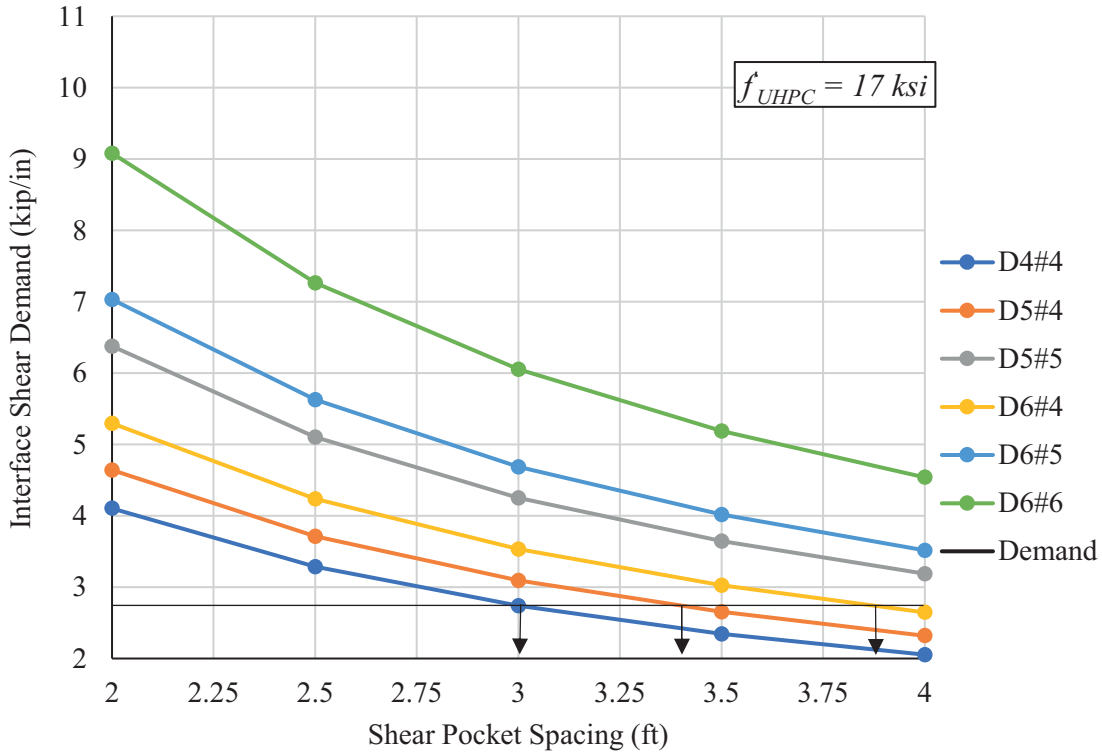

Figure 7.5. Demonstration of Using the Design Aid Chart.

7.3. Cost Analysis

Figure 7.6 show the current precast concrete deck-to-girder connection implemented by Nebraska DOT in the construction of Belden-Laurel bridge in 2018. The bridge is a 130 ft. single span bridge which consists of a 7-NU1100 precast prestressed girder and 22 full-depth deck panels with rails as a replacement of a 3-span steel girder (100 ft long). The connection consists of shear connectors (i.e., threaded rods) extend from the concrete girder into Hollow Structural Section (HSS) steel-formed shear pockets with horizontal shear studs in the deck panels that are filled with self-consolidating concrete to achieve composite action. The deck-to-girder connection was designed to resist the interface shear demand of 155 kips for each pocket at 4 ft. spacing (Morcous

and Tawadrous, 2021). This demand is used to obtain a design for the proposed connection based on the design aids provided in the previous section. The nominal interface shear demand = 155 kip/(4 ft x 12 in.) = 3.23 kip/in. So, 6-in. diameter shear pockets with #5 loop bar spaced at 4 ft. satisfy the demand by a nominal capacity of 3.91 kip/in. For the CC-UHPC interface, a 16 in. wide haunch is enough to satisfy the demand and host the interface shear reinforcement from girder (#4 bars @ 12 in.).

The properties of the deck-to-girder connection in both systems are summarized as following:

- Slab Thickness = 8.0 in.
- Pocket

  D (HSS Pocket) = 14.0 in.

  D (UHPC Pocket) = 6.0 in.

  Spacing = 4.0 ft
- Haunch

  CC width = 48.0 in.

  Average CC depth = 3.0 in .

  UHPC width = 16.0 in.

  Average UHPC depth = 5.0 in.
- Interface Reinforcement
  - For the Belden-Laurel connection, a 1.5 in. diameter A193 coil rod with a nut is used and required to be embedded in the HSS pocket for 5 in. as shown in Figure 7.6.

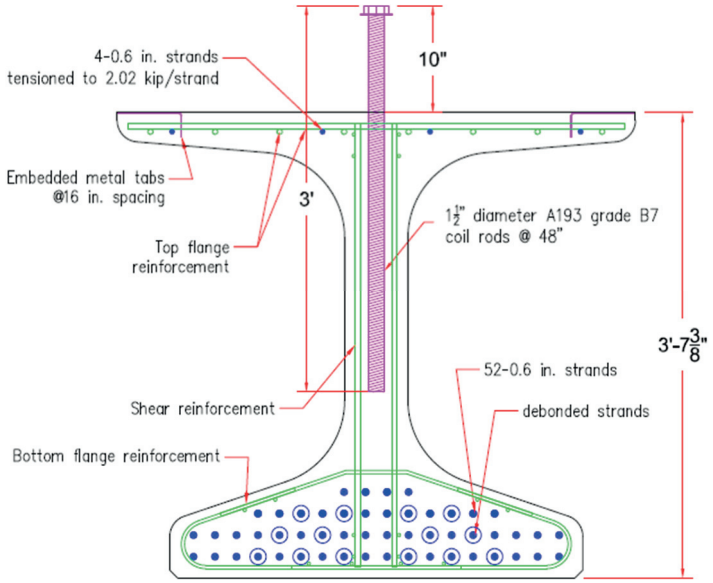

(a)

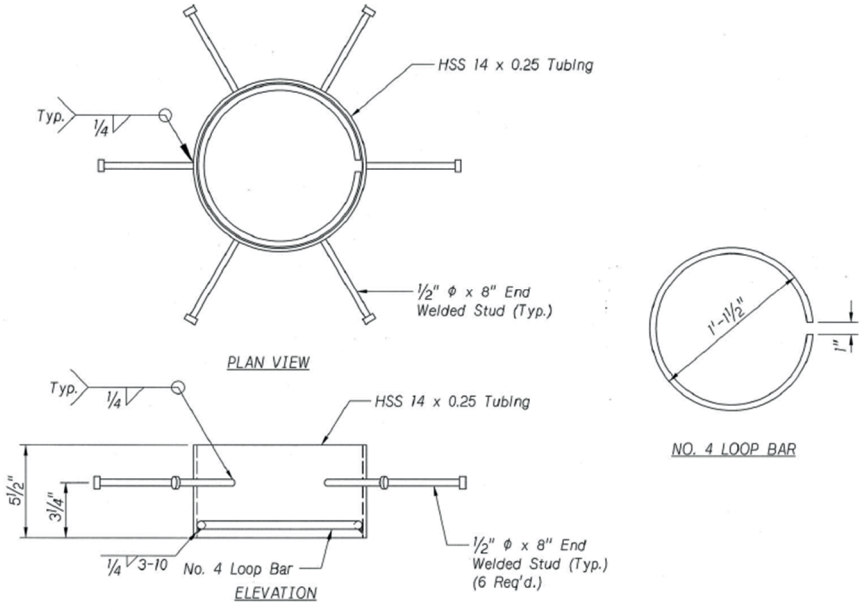

(b)

Figure 7.6. Precast Concrete Deck-to-Girder Connection used in Belden-Laurel bridge, NE by Nebraska Department of Transportation (NDOT) (Morcous and Tawadrous, 2021); (a) Interface Shear Reinforcement in the Girder and (b) HSS Shear Pocket in Precast Deck Panels

- For the proposed connection, No. 4 bar at 12 in. is required which is similar to the regular girder interface shear reinforcement and a #5 loop bar is installed inside the shear pocket.

- Required Concrete Volume to Fill Shear Pocket.

$$CC\ volume\ = \frac{(48)(3)}{144} * 4 + \frac{(\pi)(13.5^2)/4}{144} * \frac{5.5}{12} + \frac{(\pi)(4^2)/4}{144} * \frac{2.5}{12} = 4.47\ ft^3/4ft$$

$$= 1.12\, ft^3/ft$$

$$UHPC\ volume = \frac{(16)(5)}{144} * 4 + \frac{(\pi)(6^2)/4}{144} * \frac{8}{12} = 2.35\ ft^3/4ft = 0.59\, ft^3/ft$$

Table 7.1 shows a cost analysis between the deck-to-girder connection used in the Belden-Laurel bridge and the proposed connection using UHPC shear pockets based on raw material prices. The unit costs used in the analysis were obtained from bidding documents (girder cost and shear pockets) or calculated based on the available materials cost in Nebraska. The proposed connection reduces the cost by 21.8% compared to the Belden-Laurel bridge. Also, it is obvious that the high savings are at the required interface shear reinforcement which is reduced by $88.7/LF without considering the simple installation of the precast deck slab panels compared to the required tolerance with the current connection. In addition, more cost can be added based on the higher-life cycle of UHPC compared to CC and the required curing time for the connection that can be just one to three days for UHPC to achieve 10 to 12 ksi compared to 28 days for CC.

Table 7.1

Cost Analysis between the Belden-Laurel Bridge and the Proposed Deck-To-Girder Connection using UHPC Shear Pockets Based on Raw Material Prices.

Item	Unit	Existing Connection	Proposed Connection
Prestressed Concrete Girder Cost	$/LF	$ 330	$ 260
Pocket Spacing	ft	4.0	4.0
Shear Pocket Cost	$/unit	$ 80	$ 5
Filling Material Unit Cost	$/CY	$ 100	$ 723
Filling Material Quantity per Pocket	ft^3/Pocket	4.47	2.35
Filling Material Cost per Pocket	$/Pocket	$ 16.57	$ 63.05
Total Cost Per Unit Length	$/LF	$ 354.1	$ 277.0
Cost Reduction	%	0.0%	21.8%

CHAPTER 8: SUMMARY, CONCLUSIONS, CONSTRUCTION RECOMMENDATIONS AND FUTURE WORK

8.1. Summary

This dissertation presents a new precast concrete deck-to-girder connection using UHPC. This connection makes advantage of the exceptional mechanical, workability, and durability properties of UHPC to eliminate any changes to the design and production of typical precast/prestressed concrete girders (no special shear connectors are needed). The new connection also simplifies deck panel production by eliminating the need for HSS-formed shear pockets and uses instead 4 – 8 in. in diameter holes every 2 - 4 ft over each girder line. This panel design also simplifies panel reinforcement and achieves composite action by filling the shear pockets and the haunch areas with UHPC. This connection provides adequate production and erection tolerances of precast concrete components and improves the economics of ABC.

Two critical interface shear planes control the design of the new connection. The first plane is at the girder top surface between fresh UHPC and hardened conventional concrete (CC-UHPC), which is usually an intentionally roughened surface. The second plane is at the soffit of the deck panels across the monolithic UHPC. A loop bar is placed in each pocket to cross the second plane to enhance its interface shear resistance. Also, a corrugated plastic pipe is used to form the shear pocket and provide a roughened side surface to bond UHPC with the deck panel concrete.

Current code provisions do not provide guidance on the design of either of the two interface shear planes. Therefore, a non-proprietary UHPC mix was developed using local

materials to be used in the experimental investigation of the interface shear resistance of monolithic UHPC and CC-UHPC.

The interface shear resistance of CC-UHPC is evaluated using slant shear and L-shape push-off shear testing, while the interface shear resistance of monolithic UHPC was evaluated using direct shear, L-shape push-off shear, and double shear push-off testing. Experimental test results and data from the literature were used to develop the cohesion and friction factors of the shear friction model. Finite element analysis was conducted using ANSYS 20 R2 software to perform a parametric study on the shear pocket dimensions and reinforcement. Full-scale push-off testing was conducted to evaluate its structural performance and constructability of the new connection. Prediction equations obtained from the experimental investigation results were used to developed design procedures and design aids for the new connection. Finally, design procedures and design aids were developed, and cost analysis was conducted to illustrate the economics of using the proposed connection.

8.2. Conclusions

Below are the main conclusions made based on the results of the experimental and analytical investigations:

1. The proposed deck-to-girder connection is easy to fabricate, simple to erect, and economical. It can be designed to satisfy interface shear demands in most bridges while using practical pocket size and spacing. The cost analysis has shown a 21.8% reduction in material cost compared to the existing connections.

2. The UNL-UHPC mix shows satisfactory performance compared to commercial mixes, while being more economical as it uses local materials. The UNL-UHPC mix costs approximately $\$723.4/yd^3$ which is 36.2% of commercially available mix. This significant reduction in material cost makes UHPC attractive alternative in bridge construction.
3. The interface shear resistance of UHPC can be predicted using the shear friction model. The cohesion and friction factors of conventional concrete (CC) stated in AASHTO LRFD 2020, ACI 318-19, Eurocode 2, and CSA A23.3-14 provisions are conservative.
4. Interface shear resistance of CC-UHPC with surface roughening of 1/4 in. amplitude, 1/8 in. amplitude, and sandblasted can be predicted using a concrete cohesion factor of 0.63 ksi, 0.36 ksi, and 0.57 ksi and shear friction factor of 1.23, 1.28, and 1.46, respectively. These factors are significantly higher than those used by current codes for CC.
5. The interface shear resistance increases with the increase of UHPC compressive strength for only surfaces that are not intentionally roughened. However, for intentionally high roughened surfaces ($\geq$ 0.25 in. depth), failure occurs in CC. In this case, the interface shear resistance increases with the increase of CC compressive strength. These observations were based on the compressive strength of CC and UHPC ranging from 5.2 ksi to 8.24 ksi and 11.69 ksi to 27.2 ksi, respectively.
6. The presence of fibers in UHPC does not have significant effect on the interface shear resistance of CC-UHPC with surface roughening of 1/4 in. amplitude.

However, applying exposed aggregate texture on shear key interface increases the interface shear resistance of CC-UHPC by 38% compared to as-cast texture.

7. The addition of interface shear reinforcement with ratios of 0.44%, and 0.80% results in higher interface shear resistance and more ductile failure compared to the specimens without interface shear reinforcement, which had brittle failure.
8. Interface shear resistance of monolithic UHPC can be predicted using a cohesion and friction factors that are dependent on UHPC compressive strength as follows: $c = 0.49\sqrt{f'_{UHPC}}$ (ksi) and $\mu = 0.85\sqrt{f'_{UHPC}}$, which provide a cohesion factor of 2.1 ksi and friction factor of 3.6 for 18 ksi UHPC.
9. The UHPC mix stability is the key parameter that significantly affects the UHPC mechanical properties and impact the structural performance of the proposed connection.
10. The finite element analysis shows that the shear pocket size and reinforcement have a high impact on the interface shear resistance of shear pocket. In addition, increasing interface shear reinforcement increases the shear pocket ductility behavior.

8.3. Construction Recommendations

The following construction recommendations can be drawn based on the experience gained throughout the production and testing of full-scale push-off specimens:

1. The flowability of UHPC should be between 8 in. and 10 in. using a flow table test according to ASTM C230, specified by ASTM C1856, to ensure adequate UHPC workability and fiber stability.

2. The loop bars can be either placed before or after casting UHPC. It is preferred to be placed before to ensure adequate embedment and prevent fiber disturbance caused by inserting the loop bar.
3. The shear pockets shall have a roughening surface for its sides with either a minimum amplitude of 1/4 in. or exposed aggregate to bond with UHPC. Corrugated plastic pipe has shown to be an excellent and economical solution to form the shear pocket.
4. The minimum haunch thickness is 4 in. to ensure adequate embedment of the loop bar inside the haunch to achieve composite action. For the same cause, the loop bar should have at least 6 in. embedment inside the shear pocket.
5. The UHPC is highly thixotropic and tends to loss of flowability with time, which is a concern in the construction of this proposed connection. So, the UHPC should be agitated and cast continuously to avoid creating cold joints due to the formation of elephant skin in its surface. The use of workability retaining admixtures is highly also recommended in this application along with reduced time between batches.
6. Use funnel or chimney to cast UHPC with a reasonable hydrostatic head is recommended to allow for faster and longer placements as UHPC is very hard to pump.

8.4. Future work

The present study led to several recommendations for further research:

1. The interface shear resistance of monolithic UHPC could depend on UHPC fiber content, geometry, orientation and grade. Further investigation is needed to determine the effect of different UHPC fiber characteristics on the interface shear resistance of the proposed connection.
2. The UHPC fiber stability is essential for the structural performance of the proposed connection. Therefore, more investigation is needed to develop methods for quality control and quality assurance of fiber stability.
3. The proposed connection can be implemented to precast concrete deck-to-steel girders. Therefore, small and full-scale tests are needed to determine its performance in steel bridges.
4. The proposed connection can be implemented to precast concrete deck-to-UHPC girders. Therefore, small and full-scale tests are needed to determine its performance in UHPC girder bridges.
5. Investigate the feasibility of pumping UHPC for rapid placement.

NOTATIONS

The following symbols are used in this dissertation:

A_{cv} = area of concrete engaged in interface shear transfer (in.^{2});

$A_{cv\text{-}CC}$ = CC-UHPC interface shear area (in.^{2})

$A_{cv\text{-}MN}$ = monolithic UHPC interface shear area (in.^{2})

A_{s1} = loop bar area (in.^{2})

A_{s2} = girder shear reinforcement bar area (in.^{2})

A_{vf} = area of interface shear reinforcement (in.^{2});

$A_{vf\text{-}CC}$ = interface shear reinforcement Area across CC-UHPC plane (in.^{2})

$A_{vf\text{-}MN}$ = interface shear reinforcement Area across monolithic UHPC plane (in.^{2})

b = girder top flange width which is roughened (in.)

b_w = UHPC haunch width (in.)

c = cohesion factor (ksi)

c_{cc} = CC-UHPC cohesion coefficient (ksi)

c_{MN} = monolithic UHPC cohesion coefficient (ksi)

d = cylinder diameter (in.)

D_p = shear pocket diameter (in.)

E_c = modulus of elasticity of precast beam (ksi)

f'_c = the lesser concrete compressive strength out of the two layers (ksi); compressive strength of precast deck slab panel (ksi)

f'_{UHPC} = compressive strength of field cast UHPC (ksi)

f_{cd} = the design value of concrete compressive strength (MPa)

f_{ck} = the characteristic compressive cylinder strength of concrete at 28 days (MPa)

f_{clfk} = characteristic value of the post-cracking strength (MPa)

$f_{clk,el}$ = characteristic value of the tensile limit of elasticity (MPa)

f_{ctd} = the concrete design tensile strength (MPa)

f_y = interface shear reinforcement yield stress (ksi)

I_g = gross moment of inertia of the precast beam (in.^{4})

K = fiber orientation factor, determined by testing

K_1 = fraction of concrete strength available to resist interface shear which is 0.2 and 0.25 for smooth and roughened surface with amplitude of 1/4 in., respectively;

K_2 = limiting interface shear resistance which is 0.8 ksi and 1.5 ksi for smooth and roughened surface with amplitude of 1/4 in., respectively;

L = design span length (ft.); cylinder length (in.)

N = Number of interface reinforcement bar legs crossing interface plane; the permanent load perpendicular to the interface shear plane (kip)

P = maximum applied load indicated by the testing machine (Ibf).

S = girder shear reinforcement spacing (in.)

S_p = spacing between shear pockets (in.)

T = splitting tensile strength (psi)

v_{ni} = nominal interface shear resistance (ksi)

V_{ni} = nominal interface shear resistance per unit length (kips/in.)

$V_{ni\text{-}CC}$ = nominal interface shear resistance of CC-UHPC plane (kips)

$V_{ni\text{-}MN}$ = nominal interface shear resistance of monolithic UHPC plane (kips)

w_c = unit weight of concrete *(kcf)*

w_s = slab weight (kips/ft)

α = acute angle between shear-friction reinforcement and interface shear plane; angle of fiber indentation with the interface shear surface of the hardened UHPC ($45° < \alpha < 90°$); the linearity deviation parameter

γ_c = partial factor for compressed UHPC

ε_c = the concrete compressive strain

λ = factor depends on concrete type; 1.0 for normal concrete and 0.75 for light-weight concrete

μ = friction factor

μ_{cc} = CC-UHPC friction coefficient

μ_{MN} = monolithic UHPC friction coefficient

ρ = interface shear reinforcement ratio, A_{vf}/ A_{cv}

σ_n = the stress caused by the external force normal to the interface plane (ksi)

REFERENCES

Aaleti, S., and S. Sritharan. 2017. "Investigation of a suitable shear friction interface between UHPC and normal strength concrete for bridge deck applications." The Bridge, 515, 294-8103. https://trid.trb.org/view/1470040

AASHTO (American Association of State Highway and Transportation Officials). 2020. "AASHTO LRFD bridge design specifications." 9th Edition, AASHTO, Washington, D.C: AASHTO.

Abo El-Khier, M., and G. Morcous. 2019. "Precast concrete deck-to-girder connection using UHPC." Report No. M085, Nebraska Department of Transportation (NDOT), Lincoln, NE. https://trid.trb.org/view/1690146

Abo El-Khier, M., G. Morcous, and J. Hu. 2019. "Interface shear resistance of ultra-high performance concrete (UHPC)." International Interactive Symposium on Ultra-High Performance Concrete, 1(1). https://doi.org/10.21838/uhpc.9635

ACI (American Concrete Institute) Committee 239. 2018. "Ultra-high-performance concrete: an emerging technology report." ACI 239, Farmington Hills, MI: ACI.

ACI (American Concrete Institute) Committee 318. 2019. "Building code requirements for structural concrete (ACI 318-19) and commentary." ACI 318-19, Farmington Hills, MI: ACI.

AFNOR (Association Française de Normalization). 2016. "P18-710: national addition to Eurocode 2–design of concrete structures: specific rules for ultra-high performance fiber-reinforced concrete (UHPFRC)," NF-P-18-710-UHPC, Paris, France: AFNOR.

ANSYS. Release 20 R2 Documentation for ANSYS, ANSYS help, 2020.

ASTM (American Society for Testing and Materials). 2013. “Standard test method for bond strength of epoxy-resin systems used with concrete by slant shear.” ASTM C882/C882M-13a, West Conshohocken, PA.

ASTM (American Society for Testing and Materials). 2013. “Standard test method for compressive strength of cylindrical concrete specimens.” ASTM C39, West Conshohocken, PA.

ASTM (American Society for Testing and Materials). 2014. “Standard test method for static modulus of elasticity and Poisson’s ratio of concrete in compression.” ASTM C469/C469M, West Conshohocken, PA.

ASTM (American Society for Testing and Materials). 2017. “Standard practice for fabricating and testing specimens of ultra-high performance concrete.” ASTM C1856/C1856M-17, West Conshohocken, PA. www.astm.org

ASTM (American Society for Testing and Materials). 2017. “Standard test method for splitting tensile strength of cylindrical concrete specimens.” ASTM C496, West Conshohocken, PA.

ASTM (American Society for Testing and Materials). 2019. “Standard test method for flexural performance of fiber-reinforced concrete (using beam with third-point loading).” ASTM C1609/C1609M, West Conshohocken, PA.

ASTM (American Society for Testing and Materials). 2021. “Standard test method for flexural strength of concrete (using simple beam with third-point loading).” ASTM C78 / C78M-21, West Conshohocken, PA.

ASTM (American Society for Testing and Materials). 2020. “Standard specification for deformed and plain carbon-steel bars for concrete reinforcement.” ASTM A615 / A615M - 20, West Conshohocken, PA.

Banta, T. E. 2005. “Horizontal shear transfer between ultra high performance concrete and by horizontal shear transfer between ultra high performance concrete.” Master’s Thesis, Virginia Polytechnic Institute and State University, Virginia, USA.

Berry, M., R. Snidarich, and C. Wood. 2017. “Development of Non-Proprietary Ultra-High Performance Concrete.” The State of Montana Department of Transportation, FHWA/MT-17010/8237-001.

Birkeland, P. W., and H. W. Birkeland. 1966. “Connections in precast concrete construction.” ACI J., Proc., 63(3), 345-368.

British Standards Institute. 1999. “Products and systems for the protection and repair of concrete structures-Test methods- Determination of slant shear test.” BS EN 12615

British Standards Institution. 2004. “Eurocode 2: Design of concrete structures - Part 1-1: General rules and rules for buildings.” BS EN 1992-1-1 :2004, London, UK: CEN.

California Department of Transportation. 2015. “Notice to Bidders and Special Provision.” Contract No. 06-0K4604, Project ID 0612000105.

Carbonell Muñoz, M. Á. 2012. "Compatibility of ultra-high performance concrete as repair material: bond characterization with concrete under different loading

scenarios," Master's Thesis, Michigan Technological University, Houghton, Michigan, USA. https://digitalcommons.mtu.edu/etds/225

Crane, C. K. 2010. "Shear and shear friction of ultra-high performance concrete bridge girders." Doctoral Thesis, Georgia Institute of Technology, Georgia, USA.

Culmo, M.P., B. Lord, M. Huie, and B. Beerman. 2011. "Accelerated bridge construction: experience in design, fabrication and erection of prefabricated bridge elements and systems: final manual." Report FHWA-HIF-12-013, Published by the Office of Bridge Technology, Federal Highway Administration (FHWA), McLean, VA.

CSA (Canadian Standards Association). 2014. "Design of concrete structures." CSA A23.3-14, ON, Canada: CSA Group.

District Department of Transportation. 2014. Special provision for ultra high performance concrete. SP60.

El-Tawil, S., Y. Tai, B. Meng, W. Hansen, and Z. Liu. 2018. "Commercial production of non-proprietary ultra-high performance concrete." Michigan Department of Transportation (RC-1670).

Georgia Department of Transportation, Special Provision. 2015. Project No. CSBRG-0007-00(159).

Graybeal, B. A. 2014. "Design and construction of field-cast UHPC connections." FHWA-HRT-14-084, FHWA, Washington, D.C. https://rosap.ntl.bts.gov/view/dot/28283

Haber Z. B., De la Varga, I., Graybeal, B., Nakashoji, B. and El-Helou, R. 2018. "Properties and behavior of UHPC-class materials." Federal Highway

Administration, FHWA-HRT-18-036, U.S. Department of Transportation, Federal Highway Administration, Washington, D.C.

Haber, Z. B., Graybeal, B. A., Nakashoji, B., and Fay, A. 2017. “NEW, simplified deck-to-girder composite connections using UHPC.” 2017 National ABC Conference Proceedings, 1–10.

Harris, D., Sarkar, J., and Ahlborn, T. 2011. “Characterization of interface bond of ultra-high-performance concrete bridge deck overlays.” Transportation Research Record: Journal of The Transportation Research Board, 2240, 40-49.

Hofbeck, J. A., I. O. Ibrahim, and A. H. Mattock. 1969. “Shear transfer in reinforced concrete." ACI J., Proc., 66(2), 119–28.

Iowa Department of Transportation. 2011. “Special provisions for ultra high performance concrete.” SP-090112a.

Jang, HO., H.S. Lee, K. Cho, and J. Kim. 2017. "Experimental study on shear performance of plain construction joints integrated with ultra-high performance concrete (UHPC)," Construction and Building Materials, 152, 2017, 16–23.

Kim, Y., W. Chin, and S. Jeon. 2018. “Interface shear strength at joints of ultra-high performance concrete structures.” International Journal of Concrete Structures and Materials, 12(1), 1-14. Springer Open, https://doi.org/10.1189/s40069-018-0298-8, 14 pp.

Loov, R. E., and A. K. Patnaik. 1994. “Horizontal shear strength of composite concrete beams with a rough interface." PCI J., 39(1), 48–69.

Maroliya, M. K. 2012. “Behaviour of reactive powder concrete in direct shear.” IOSR Journal of Engineering (IOSRJEN), 2(9), 76–79.

Mattock, A. H., and N. M. Hawkins. 1972. “Shear transfer in reinforced concrete recent research." PCI J., 17(2), 55–75.

Mattock, A. H., W. K. Li, T. C. Wang. 1976. “Shear transfer in lightweight reinforced concrete," PCI J., 32(1), 20–39.

Mattock, A. H. 2001. “Shear friction and high-strength concrete." ACI Struct. J., 98(1), 50–59.

Mendonca, F., Abo El-Khier, M., Morcous, G., and Hu, j. 2020. “Feasibility study of development of UHPC for highway bridge applications in Nebraska.” Report No. M072, Nebraska Department of Transportation (NDOT), Nebraska, USA.

Michigan Department of Transportation, Special Provision for Michigan Ultra High Performance Concrete (MI-UHPC) For Field Cast Joints.

Morcous, G. and Tawadrous, R. 2021. “Circular shear pocket connection for full-depth precast concrete deck construction.” J. of Bridge Eng., 26(5).

New York State Department of Transportation. 2013. “Precast concrete deck system construction -option 2”. D262307.

Paulay, T., R. Park, and M. H. Phillips. 1974. “Horizontal construction joints in cast-in-place reinforced concrete.” ACI Special Publication, 42, 599-616.

PCI (Precast/Prestressed Concrete Institute). 1999. “Manual for Quality Control for Plants and Production of Structural Precast Concrete Products.” 4th edition, MNL-116, Chicago, IL: PCI.

PCI (Prescast/Prestressed Concrete Institute). 2014. “PCI bridge design manual.” 3th Edition, 2nd Release, Chicago, IL: PCI.

Rangaraju, P. R., Kizhakommudom, H., Li, Z., and Schiff, S. D. 2013. “Development of high-strength/high performance concrete/grout mixtures for application in shear keys in precast bridges.” FHWA-SC-13-04a. US Department of Transportation.

Roy, M., C. Hollmann, and K. Wille. 2017. “Influence of volume fraction and orientation of fibers on the pullout behavior of reinforcement bar embedded in ultra high performance concrete.” Construction and Building Materials, 146, 582–593.

Russell, H.G., B. A. Graybeal, and H. G. Russell. 2013. “Ultra-high performance concrete: A state-of-the-art report for the bridge community.” FHWA-HRT-13-060. Federal Highway Administration. Office of Infrastructure Research and Development.

Sim, C., M. Tadros, D. Gee, and M. Asaad. 2020. "Flexural design of precast, prestressed ultra-high-performance concrete members." PCI J., 65(6).

Tayeh, B. A., B. A. Bakar, M. M. Johari, and Y. L. Voo. 2012. "Mechanical and permeability properties of the interface between normal concrete substrate and ultra high performance fiber concrete overlay." Constr. Build. Mater., 36, 538-548. https://doi.org/10.1016/j.conbuildmat.2012.06.013

United States Department of Transportation – Federal Highway Administration (FHWA). National Bridge Inventory (NBI) – Count of Bridges by Deck Structure Type, 2016.

Walraven, J. C., J. Frénay, and A. Pruijssers. 1987. “Influence of concrete strength and load history on the shear friction capacity of concrete members," PCI J., 32(1), 66–84.

Yuan, J., and Graybeal, B. A. 2014. “Bond behavior of reinforcing steel in ultra-high performance concrete.” FHWA-HRT-14-090. U.S. Department of Transportation, Federal Highway Administration, Washington, D.C.

APPENDIX A

Testing Results

A.1 Compressive Strength

Table A.1

Compressive Strength Test Results of UHPC Mixes at Different Ages.

Age (Days)			4	7	28	56
Compressive Strength (psi)	UHPC 1450	#1	10,276	11,614	13,705	15,629
		#2	9,789	12,732	14,010	16,260
		#3	-	-	14,192	-
		Avg.	10,033	12,173	13,969	15,944
	UHPC 1700	#1	10,437	13,541	17,063	17,473
		#2	12,149	13,269	16,925	16,922
		#3	-	-	16,475	-
		Avg.	11,293	13,405	16,821	17,198
	UHPC 1900	#1	11,906	13,527	17145	19,380
		#2	12,067	14,712	17771	20,484
		#3	-	-	18,099	-
		Avg.	11,986	14,119	17,672	19,932
	Commercial	#1	11,979	16,667	24,439	27,546
		#2	11,674	16,019	21,344	26,992
		#3	10,754	15,555	24,230	24,307
		Avg.	11,826	16,343	23,338	27,268

A.2 Modulus of Elasticity and Poisson's Ratio

Table A.2

Modulus of Elasticity Test Results from Different UHPC Mixes.

Mix	$f_c^{'}$ (ksi)	No.	MoE (ksi)	Average. MoE (ksi)	COV (%)	FHWA	AASHTO LRFD 2020
UHPC 1450	15.94*	1	6619	6560	1.3	5709	7096
		2	6461				
		3	6602				
UHPC 1700	17	1	6725	6613	2.0	5896	7438
		2	6643				
		3	6470				
UHPC 1900	17.67	1	6385	6331	0.7	6011	7728
		2	6304				
		3	6305				
Commercial	23.34	1	8173	8173	0.8	6908	8687
		2	8238				
		3	8109				

* 56 days compressive strength

Table A.3

Poisson's Ratio Test Results from Different UHPC Mixes

Mix	f'_c (ksi)	No.	Poisson's Ratio	Average Poisson's Ratio	COV (%)
UHPC 1450	15.94*	1	0.266	0.258	3.2
		2	0.258		
		3	0.249		
UHPC 1700	17	1	0.250	0.256	2.2
		2	0.258		
		3	0.261		
UHPC 1900	17.67	1	0.241	0.240	0.5
		2	0.239		
		3	0.239		
Commercial	23.34	1	0.221	0.221	1.3
		2	0.223		
		3	0.217		

* 56 days compressive strength

A.3 Splitting Tensile Strength Test

Table A.4

Splitting Tensile Test Results of Different Mixes

Mix Design	Specimen No.	Maximum Tensile Strength (ksi)	Avg. Tensile Strength (ksi)	COV%
UHPC 1450*	#1	2.26	1.95	16.41
	#2	1.98		
	#3	1.62		
UHPC 1700	#1	2.09	1.88	11.48
	#2	1.66		
	#3	1.89		
UHPC 1900	#1	1.93	1.93	10.28
	#2	1.74		
	#3	2.13		
Commercial	#1	2.08	2.40	11.84
	#2	2.49		
	#3	2.63		

* Tested at 56-day instead of 28-days.

A.4 Direct Shear Test

Table A.5

Direct Shear Test Results of Different UHPC Batches

Batch #1	f'_C (ksi)	Specimen	Max. Load (kips)	Shear strength (ksi)	Avg. Shear strength (ksi)	COV %
1	11.8	1	34.9	4.36	4.36	6.99
		2	31.7	3.96		
		3	36.4	4.55		
2	23.4	1	38.3	4.79	5.95	17.69
		2	49.8	6.23		
		3	54.7	6.84		
3	15.78	1	30.1	3.76	4.19	18.51
		2	40.7	5.09		
		3	29.8	3.73		
4	15.73	1	33.3	4.16	4.74	17.16
		2	42.5	5.31		
5	15.81	1	40.6	5.08	5.37	18.21
		2	51.7	6.46		
		3	36.6	4.58		
6	16.16	1	47.44	5.93	5.68	5.59
		2	45.08	5.64		
		3	41.92	5.24		
		4	47.08	5.89		
7	17.67	1	34.58	4.32	3.99	12.97
		2	26.94	3.37		
		3	36.02	4.50		
		4	30.24	3.78		